

**INVESTIGATION OF PRIMARY PRODUCTION IN THE GERMAN
BIGHT**
- a study on the influence of sea surface temperature -

Dissertation
zur Erlangung des Doktorgrades
der Mathematisch-Naturwissenschaftlichen Fakultät
der Christian-Albrechts-Universität zu Kiel

vorgelegt von
Felipe de Luca Lopes de Amorim
Kiel, 2024

Dekan: Prof. Dr. Frank Kempken

Erster Gutachter: Prof. Dr. Karen Helen Wiltshire

Zweiter Gutachter: Prof. Dr. Birgit Schneider

Tag der mündlichen Prüfung: 29.04.2024

Summary

The German Bight is a shallow region of the North Sea, which is intensely exploited by human activities and under positive temperature trends. A broad-scale investigation of the changes in the surface chlorophyll-a (Chl-a) concentration related to the observed warming of above 1°C since 1962 is vital to understanding the primary production response in the German Bight. This thesis investigates changes in the German Bight primary production associated with increasing temperatures using Chl-a concentration as an indicator. The specific objectives to fulfil this goal are to (1) define the influence of the increasing temperatures at various spatial and temporal scales on the Chl-a concentration, (2) investigate changes in Chl-a temporally and spatially, (3) analyse Chl-a surface concentration fields to estimate the present situation, and (4) evaluate the use of machine learning (ML) algorithms to predict the Chl-a time series.

Chapter 1 provides a general introduction and overview of the importance of marine primary production globally and in shallow seas. It also presents the methodology for the study of the primary production changes based on the literature, and the research gap and research objectives are detailed in this chapter.

In Chapter 2, land temperature and sea surface temperature (SST) are analysed on various spatial scales to investigate warming variability by analysing temperature trends, anomalies, seasonal shifts, and frequency distribution shifts. The SST data from the Helgoland Roads time series (HRTS), a critical and detailed long-term in situ marine ecological time series, is analysed jointly with the Sylt Roads, North Sea, Germany, Europe, North Atlantic, and Northern Hemisphere surface temperatures. Temperature is a primary driver of species diversity and distribution, manifesting on various spatial and temporal scales depending on population growth, life stages, cycles, and habitats. Accordingly, this chapter presents the temperature changes on the appropriate spatiotemporal scales, providing a suitable foundation for studies on the effects of warming on marine ecosystem functioning and biodiversity.

In Chapter 3, the analysis of spatial Chl-a concentrations obtained from remote sensing is presented to investigate the trends and variability of surface Chl-a in the German Bight from January 1998 to December 2020. The results indicate high levels of Chl-a near the coast, demonstrating a decreasing gradient towards offshore waters. A significant long-term positive trend of Chl-a exists close to the Elbe river estuary and the near-coast area under its freshwater

influence. In contrast, about 30% of the German Bight is characterized by a significant negative trend. No significant trends are observed during spring blooms, but the distribution of Chl-a anomalies differs between the period from 1998 to 2009 and from 2010 to 2020, predominantly displaying a shift towards negative anomalies and decreased variability. The Chl-a nonseasonal variability, defined by Empirical Orthogonal Functions, indicates that the first four modes explain around 45% of the variability. The first and second modes are related to the Chl-a inter- and intra-annual variability, respectively, identified by the temporal principal components spectral analyses. Linear trends between Chl-a anomalies, SST, and mixed layer depth (MLD) anomalies are weak and described by opposite signals in offshore and coastal areas. Temperature and Chl-a negatively correlate in offshore areas and positively correlate primarily in coastal areas, whereas the MLD displays the opposite correlation signal. The monthly Chl-a concentration anomalies covaries 45% with the SST anomalies and 23% with the MLD anomalies.

Chapter 4 employs the following three standard ML algorithms from the literature to predict the Chl-a time series from the long-term HRTS dataset: the support vector machine regressor, neural networks multilayer perceptron regressor, and random forest regressor. This chapter evaluates and compares the results with the seasonal autoregressive integrated moving average, a classical statistical method, and assesses the differences. The Chl-a time-series prediction from each of the algorithms is compared, revealing that the support vector machine regressor slightly outperformed other models. The evaluation with a testing dataset and verification using an independent validation dataset for Chl-a concentrations indicate good generalisation capability. As part of the ML preprocessing step, feature selection improved the models significantly. In addition, this chapter demonstrates the importance of SST in Chl-a prediction, along with nutrients and past Chl-a values.

Chapter 5 presents the general discussion, conclusions and future work of this PhD thesis, which gives a comprehensive analysis of chlorophyll-a variability, an indicator of primary production changes, in the German Bight. The observed decrease in chlorophyll-a serves as a base for future research efforts, together with the chlorophyll-a dominant modes of variability described in this thesis. The detailed description of temperature behaviour since 1962 in distinct spatial scales will help researchers on the design of experiments related to climate change and warming, considering real trends and variability. Moreover, innovative machine learning efforts were applied for the first time to the Helgoland Roads time series. Such investigations are expected to contribute to primary production assessments in the German Bight in future

and can be expanded to the greater North Sea. They augment studies on primary productivity already done in other shelf and coastal seas.

Zusammenfassung

Die Deutsche Bucht ist eine flache Region der Nordsee, die durch menschliche Aktivitäten intensiv genutzt wird und einem positiven Temperaturtrend unterliegt. Eine breit angelegte Untersuchung der Veränderungen der Chlorophyll-a-Konzentration (Chl-a) an der Oberfläche im Zusammenhang mit der beobachteten Erwärmung von über 1°C seit 1962 ist für das Verständnis der Reaktion der Primärproduktion in der Deutschen Bucht unerlässlich. In dieser Arbeit werden Veränderungen der Primärproduktion in der Deutschen Bucht in Verbindung mit steigenden Temperaturen anhand der Chl-a-Konzentration untersucht. Die spezifischen Ziele zur Erreichung dieses Vorhabens sind (1) die Bestimmung des Einflusses steigender Temperaturen in verschiedenen räumlichen und zeitlichen Skalen auf die Chl-a-Konzentration, (2) die Untersuchung zeitlicher und räumlicher Veränderungen der Chl-a-Konzentration, (3) die Analyse von Chl-a-Konzentrationsfeldern an der Oberfläche zur Abschätzung der gegenwärtigen Situation und (4) die Bewertung des Einsatzes von Algorithmen des maschinellen Lernens (ML) zur Vorhersage der Chl-a-Zeitreihen.

Kapitel 1 bietet eine allgemeine Einführung und einen Überblick über die Bedeutung der marinen Primärproduktion weltweit und in flachen Meeren. Außerdem wird die Methodik für die Untersuchung der Veränderungen der Primärproduktion auf der Grundlage der Literatur vorgestellt. Darüber hinaus werden die Forschungslücke und die Forschungsziele in diesem Kapitel detailliert beschrieben.

In Kapitel 2 werden die Landtemperatur und die Meeresoberflächentemperatur (SST) auf verschiedenen räumlichen Skalen analysiert, um die Variabilität der Erwärmung durch die Analyse von Temperaturtrends, Anomalien, saisonalen Verschiebungen und Verschiebungen der Häufigkeitsverteilung zu untersuchen. Die SST-Daten aus der Helgoland Reede-Zeitreihe (HRTS), einer kritischen und detaillierten langfristigen marinen ökologischen In-situ-Zeitreihe, werden gemeinsam mit den Oberflächentemperaturen der Sylt Reede, der Nordsee, Deutschlands, Europas, des Nordatlantiks und der nördlichen Hemisphäre analysiert. Die Temperatur ist ein Hauptfaktor für die Artenvielfalt und -verteilung, die sich auf verschiedenen räumlichen und zeitlichen Skalen in Abhängigkeit von Populationswachstum, Lebensstadien, Zyklen und Lebensräumen manifestiert. Dementsprechend werden in diesem Kapitel die Temperaturveränderungen auf den geeigneten räumlichen und zeitlichen Skalen dargestellt,

was eine geeignete Grundlage für Studien über die Auswirkungen der Erwärmung auf die Funktionsweise der marinen Ökosysteme und die biologische Vielfalt bietet.

In Kapitel 3 wird die Analyse der räumlichen Chl-a-Konzentrationen aus der Fernerkundung vorgestellt, um die Trends und die Variabilität von Oberflächen-Chl-a in der Deutschen Bucht von Januar 1998 bis Dezember 2020 zu untersuchen. Die Ergebnisse zeigen hohe Chl-a-Konzentrationen in Küstennähe und einen abnehmenden Gradienten in Richtung küstenferner Gewässer. Ein signifikanter langfristiger positiver Trend von Chl-a besteht in der Nähe der Elbmündung und dem küstennahen Gebiet unter ihrem Süßwassereinfluss. Im Gegensatz dazu sind etwa 30 % der Deutschen Bucht durch einen signifikanten negativen Trend gekennzeichnet. Während der Frühjahrsblüte werden keine signifikanten Trends beobachtet, aber die Verteilung der Chl-a-Anomalien unterscheidet sich zwischen dem Zeitraum von 1998 bis 2009 und von 2010 bis 2020, wobei überwiegend eine Verschiebung zu negativen Anomalien und eine geringere Variabilität zu beobachten ist. Die nicht saisonale Variabilität von Chl-a, definiert durch Empirische Orthogonale Funktionen, zeigt, dass die ersten vier Modi etwa 45 % der Variabilität erklären. Der erste und der zweite Modus stehen im Zusammenhang mit der inter- bzw. intra-jährlichen Variabilität von Chl-a, die durch die zeitliche Hauptkomponenten-Spektralanalyse ermittelt wurde. Lineare Trends zwischen Chl-a-Anomalien, SST und Anomalien der Mischschichttiefe (MLD) sind schwach und werden in küstennahen und küstenfernen Gebieten durch entgegengesetzte Signale beschrieben. Temperatur und Chl-a korrelieren in küstennahen Gebieten negativ und vor allem in küstennahen Gebieten positiv, während die MLD das entgegengesetzte Korrelationssignal aufweist. Die monatlichen Anomalien der Chl-a-Konzentration kovariieren zu 45 % mit den SST-Anomalien und zu 23 % mit den MLD-Anomalien.

In Kapitel 4 werden die folgenden drei Standard-ML-Algorithmen aus der Literatur verwendet, um die Chl-a-Zeitreihen aus dem langfristigen HRTS-Datensatz vorherzusagen: der Support-Vector-Machine-Regressor, der Multilayer-Perceptron-Regressor für neuronale Netze und der Random-Forest-Regressor. In diesem Kapitel werden die Ergebnisse evaluiert und mit dem saisonalen autoregressiven integrierten gleitenden Durchschnitt, einer klassischen statistischen Methode, verglichen und die Unterschiede bewertet. Die Chl-a-Zeitreihenvorhersage der einzelnen Algorithmen wird verglichen, wobei sich zeigt, dass der Support-Vector-Machine-Regressor die anderen Modelle leicht übertrifft. Die Auswertung mit einem Testdatensatz und die Überprüfung anhand eines unabhängigen Validierungsdatensatzes für Chl-a-Konzentrationen zeigen eine gute Generalisierungsfähigkeit. Als Teil des ML-

Vorverarbeitungsschritts verbesserte die Merkmalsauswahl die Modelle erheblich. Darüber hinaus zeigt dieses Kapitel die Bedeutung der SST für die Chl-a-Vorhersage, zusammen mit Nährstoffen und früheren Chl-a-Werten.

Kapitel 5 enthält die allgemeine Diskussion, Schlussfolgerungen und künftige Arbeiten dieser Doktorarbeit, die eine umfassende Analyse der Chlorophyll-a-Variabilität, ein Indikator für Veränderungen der Primärproduktion, in der Deutschen Bucht liefert. Der beobachtete Rückgang von Chlorophyll-a dient zusammen mit den in dieser Arbeit beschriebenen Chlorophyll-a-dominanten Variabilitätsmodi als Grundlage für künftige Forschungsanstrengungen. Die detaillierte Beschreibung des Temperaturverhaltens seit 1962 in verschiedenen räumlichen Maßstäben wird den Forschenden bei der Planung von Experimenten im Zusammenhang mit dem Klimawandel und der Erwärmung helfen, wobei reale Trends und Variabilität berücksichtigt werden. Darüber hinaus wurden erstmals innovative Verfahren des maschinellen Lernens auf die Zeitreihen der Helgoland Reede angewandt. Es wird erwartet, dass solche Untersuchungen in Zukunft zur Bewertung der Primärproduktion in der Deutschen Bucht beitragen werden und auf die gesamte Nordsee ausgeweitet werden können. Sie ergänzen die bereits in anderen Schelf- und Küstenmeeren durchgeführten Studien zur Primärproduktion.

Declaration

I hereby declare that the content and design of the thesis entitled “INVESTIGATION OF PRIMARY PRODUCTION IN THE GERMAN BIGHT - a study on the influence of sea surface temperature -” apart from my supervisor's guidance, is my own work, with no other help than the cited sources. This thesis has not been submitted either partially or wholly as part of a doctoral degree to another examining body. Parts of this work have already been published and submitted to scientific journals and are explicitly stated. This thesis was prepared in accordance with the Rules of Good Scientific Practice of the German Research Foundation (DFG). No academic degree has ever been withdrawn from me.

Bremen, 11.03.2024

Felipe de Luca Lopes de Amorim

Manuscript overview

This dissertation is based on the following manuscripts, prepared by Felipe de L. L. de Amorim (**FA**) in collaboration with other authors:

Manuscript 1

Citation: Amorim, F.L.L*, Wiltshire, K.H*, Lemke, P., Carstens, K., Peters, S., Rick, J., Gimenez, L. and Scharfe, M. (2023). Investigation of marine temperature changes across temporal and spatial Gradients: Providing a fundament for studies on the effects of warming on marine ecosystem function and biodiversity. *Progress in Oceanography*, 216, 103080. <https://doi.org/10.1016/j.pocean.2023.103080>

*joint first authors

Status: Published

Authors contribution: MS and KW initiated this study. KW, **FA**, and PL developed the research ideas, conceptualized and designed the study. **FA** downloaded, compiled and prepared all data. **FA**, PL, KW, and JR performed data analysis. KW, JR, KC and SP provided the Helgoland Roads dataset; quality controlled and validated the in situ data. KW and **FA** wrote the first draft of the manuscript. PL, KW and LG provided the global view. **FA** finalized and edited the manuscript. All authors contributed substantially to revisions.

Manuscript 2

Citation: Amorim, F.L.L., Balkoni, A., Sidorenko, V., and Wiltshire, K.H.: Analyses of sea surface Chlorophyll-a trends and variability in a period of rapid Climate change, German Bight, North Sea, EGU sphere [preprint], <https://doi.org/10.5194/egusphere-2024-311>, 2024.

Status: Submitted

Authors contribution: **FA** conceptualized the study, processed the data, and carried out all data analyses. **FA** wrote the original paper with contributions from AB, VS, and KW. KW supervised the study. All authors reviewed and edited the final paper.

Manuscript 3

Citation: Amorim, F.L.L.; Rick, J.; Lohmann, G.; Wiltshire, K.H. (2021) Evaluation of Machine Learning Predictions of a Highly Resolved Time Series of Chlorophyll-a Concentration. *Appl. Sci.* 11, 7208. <https://doi.org/10.3390/app11167208>

Status: Published

Authors contribution: Conceptualization: **FA**; methodology: **FA**; formal analysis: **FA**; data curation: JR; writing—original draft preparation: **FA**; writing—review and editing: **FA**, GL, JR, and KW; visualization: **FA**; supervision: GL and KW. All authors have read and agreed to the published version of the manuscript.

Acknowledgements

First of all, I would like to thank Prof. Dr. Karen H. Wiltshire for giving me the opportunity to work in my PhD degree. More than an academic supervisor, many times she gave me guidance beyond the subjects of academia. Her support was invaluable for the completion of this thesis, and I express here my gratitude.

I would like to thank my PhD Thesis Committee, composed by Prof. Birgit Schneider, Prof. Hans Burchard, Prof. Gerit Lohmann and Dr. Johannes Rick. A special thank you to Prof. Peter Lemke, Dr. Vera Sidorenko, Dr. Luis Gimenez and Areti Balkoni. They were available when I needed and their expertise in marine and climate sciences and academic support allowed the accomplishment of this work. Thanks to Prof. Achim Wirth for the improvement of the thesis introduction and his moral support.

I would like to express my gratitude to all my colleagues at AWI Bremerhaven and AWI Sylt, always available to help. My gratitude to Dr. Lasse Sander, my first research supervisor in Germany during the NF-POGO program, who became a friend. Thanks to Dr. Daphnie Galvez, who is a friend and always helped me. My appreciation to Dr. Lisa Shama, who took some of her time to help me with the introduction.

I would like to express my thanks to all the great people from Helgoland, and a special thanks to the ones involved in the NF-POGO program, naming Dr. Eva Brodte, Dr. Bärbel Wichmann and Kristine Carstens.

Finally, my deepest thanks to my parents, my brother, relatives and friends in Brazil and around the world, who supported me from far away. To my partner Anna Carstens, thank you so much for your patience and companionship during this journey. Thank you for sharing your family while mine is far away.

Table of Contents

Summary	ii
Zusammenfassung.....	v
Declaration.....	viii
Manuscript overview	ix
Acknowledgements.....	xi
Table of Contents.....	xii
List of Figures	xv
List of Tables	xxi
1 Chapter 1.....	23
Introduction.....	25
1.1 MARINE PRIMARY PRODUCTION	27
1.1.1 Chlorophyll-a Remote Sensing	28
1.1.2 The Helgoland Roads Time Series	29
1.2 PRIMARY PRODUCTION AND TEMPERATURE	31
1.3 MACHINE LEARNING IN ECOLOGICAL STUDIES.....	32
1.4 THE GERMAN BIGHT.....	33
1.5 KNOWLEDGE AND RESEARCH GAPS.....	35
1.6 OBJECTIVES	37
1.6.1 Thesis Outline	37
2 Chapter 2.....	38
Investigation of marine temperature changes across temporal and spatial gradients: Providing a fundament for studies on the effects of warming on marine ecosystem function and biodiversity	38
2.1 INTRODUCTION.....	40
2.2 MATERIALS AND METHODS	42
2.2.1 Data sets	42
2.2.2 Statistical methods	47
2.3 RESULTS.....	48
2.3.1 Overall trends and Cross-Correlation	48
2.3.2 Seasonal patterns.....	53
2.3.3 Temperature variability in first and second half of the Time-Series	56
2.3.4 Long-Term changes in SST distributions	57

2.3.5	Seasonal means and trends.....	60
2.3.6	Seasonal variability	64
2.3.7	Assessment of temperature extremes.....	66
2.3.8	Relationship of the North Atlantic Oscillation (NAO) and temperature	69
2.3.9	Summary of results	72
2.4	DISCUSSION	74
2.4.1	Long-term trends and the role of Indices: Biogeographical shifts over multiple decades and potential regime Shifts	78
2.4.2	Shifts in Seasonality: Local to regional shifts of Succession, competition and phenology	80
2.4.3	Maximum and minimum Temperatures- hot and cold Spells: Physical and behavioural adaptation; competition with neobiota; local species extinction	82
2.4.4	Variability on the Long-Term: Physical and behavioural adaptation; local species Extinction, shifts in growing season and biogeographical species distribution	84
2.5	CONCLUSIONS.....	88
2.6	ACKNOWLEDGEMENTS	88
2.7	SUPPLEMENTARY MATERIAL.....	89
	Link from Chapter 2 to Chapter 3.....	90
3	Chapter 3.....	91
	Analyses of sea surface Chlorophyll-a trends and variability in a period of rapid Climate change, German Bight, North Sea.	91
3.1	INTRODUCTION.....	93
3.2	DATA AND METHODS.....	95
3.2.1	Study Area	95
3.2.2	Chlorophyll-a Concentration Remote Sensing Data.....	96
3.2.3	Sea surface temperature, mixed layer depth and North Atlantic Oscillation (NAO)	96
3.2.4	In situ data.....	97
3.2.5	Data preprocessing.....	98
3.2.6	Evaluation of satellite derived Chl- <i>a</i> data.....	99
3.2.7	Statistical Methods.....	99
3.3	RESULTS.....	100
3.3.1	Evaluation of in situ HPLC and Remote Sensing Chlorophyll-a	100
3.3.2	General findings:.....	102
3.3.3	Seasonal Chlorophyll-a surface concentration.....	104
3.3.4	Month of maximum Chlorophyll-a concentration	107

3.3.5	Chl-a distribution before and after 2009	109
3.3.6	Chlorophyll-a Overall Trends	111
3.3.7	Dominant modes of non-seasonal Chlorophyll-a Variability	113
3.3.8	Chlorophyll-a, Temperature and Mixed Layer Depth relationships	116
3.4	DISCUSSION AND SUMMARY	120
3.5	CONCLUSIONS	122
3.6	ACKNOWLEDGEMENTS	123
3.7	DATA AVAILABILTY	123
	Link from Chapters 2 and 3 to Chapter 4	124
4	Chapter 4.....	125
	Evaluation of Machine Learning Predictions of a Highly Resolved Time Series of Chlorophyll-a Concentration	125
4.1	INTRODUCTION.....	126
4.2	MATERIALS AND METHODS	127
4.2.1	Datasets	128
4.2.2	Data Preprocessing.....	130
4.2.3	Feature Engineering and Selection	131
4.2.4	Model Selection and Hyperparameter Tuning	135
4.2.5	SARIMA Model.....	138
4.3	RESULTS.....	138
4.4	DISCUSSION	143
4.5	CONCLUSIONS	145
4.6	ACKNOWLEDGMENTS.....	146
4.7	SUPPLEMENTARY MATERIAL	147
5	Chapter 5.....	148
	General Discussion and Conclusions.....	148
5.1	SYNTHESIS OF RESEARCH AND GENERAL DISCUSSION	148
5.2	CONCLUDING REMARKS AND SUMMARY	151
5.3	FUTURE WORK	152
6	References	153

List of Figures

Figure 1: Global ocean pelagic and coastal regions, based on General Bathymetric Chart of the Oceans (GEBCO) bathymetry (GEBCO Bathymetric Compilation Group 2023, 2023). White indicates coastal areas. 26

Figure 2: Global mean primary production (PP) from 1998 to 2020 from Copernicus GlobColour (Garnesson et al., 2019). Coastal areas display higher primary production, defined by darker colour. 26

Figure 1.1: Remote-sensing image of the North Sea on March 25, 2020, (left) displaying the different colours during a phytoplankton bloom, and (right) a zoomed-in area at the edge of the German Bight. Composite images combine data acquired by the Moderate Resolution Imaging Spectroradiometer (MODIS) instruments on The National Aeronautics and Space Administration (NASA)'s Terra and Aqua satellites. Modified from NASA Earth Observatory, A Sea of Color and Wind (2020). 29

Figure 1.2: Sampling at the Helgoland Roads station (Aade vessel framed by the black rectangle) with the Düne Island in the background, and entering the harbour at Helgoland Island on December 27, 2023. RV Aade, Alfred Wegener Institute. 30

Figure 1.3: North Sea, German Bight and Helgoland Island, illustrating the study area and the long-term Helgoland Roads time series (HRTS) location (red triangle). DE – Germany; UK – United Kingdom; NL – Netherlands; DG – Dogger Bank; H – Helgoland and D – Düne Island. 34

Figure 1.4: Seasonal mean of depth-integrated ocean currents (0-10 m; m/s) in the German Bight (1993-2022), emphasizing the importance of the English Channel flow and the difference in magnitude among seasons. DJF – December, January and February (winter); MAM – March, April and May (spring); JJA – June, July and August (summer); SON – September, October and November (autumn). Data extracted from Copernicus Marine Service (CMS), product ID NWSHELF_MULTIYEAR_PHY_004_009 (<https://doi.org/10.48670/moi-00059>). 35

Figure 2.1: Regions a) and locations b) analysed in this study. a) 1-Northern Hemisphere, 2-North Atlantic (latitude belt 40°-60°), 3-North Sea, 4-Yellow Sea. b) North Sea area and the two in situ stations – Helgoland Roads (red square) and Sylt Roads (blue circle). UK - United Kingdom; NL - Netherlands; DE - Germany and DK - Denmark. The colour background in a) represents the HadSST3 averaged SST anomalies for the period 1962 to 2019. The temperature anomalies for HadCRUT4 and HadSST3 data are relative to the period of 1961 to 1990 and the

limits used for the seas were defined to be as close as possible to the ones defined by the Limits of Oceans and Seas (IHO, 1953).....	43
Figure 2.2: Sylt Roads SST Time Series – merged from three data sources (solid black line). SR (blue circle), Sylt harbour (orange triangle) and HadISST (black star).....	45
Figure 2.3: Yearly averages of temperature time series (solid red) and their linear trends (dashed black), a) Helgoland Roads and b) Sylt Roads.....	49
Figure 2.4: Anomaly time series (solid blue and solid red) and their linear trends (dashed black). From the top: Northern Hemisphere ST (land + sea surface temperature), Europe SAT, Germany SAT, North Atlantic SST (40°N-60°N belt), North Sea SST, Helgoland Roads SST, and Sylt Roads SST anomalies. Blue lines, except a), are based on surface air data and red lines are based on sea surface data.	50
Figure 2.5: Evolution of the sea surface temperature including seasonality as an example: Helgoland Roads.....	53
Figure 2.6: Probability density function curves of sea surface temperatures at a) Helgoland Roads and b) Sylt Roads calculated using Kernel Density Estimates. For a) and b), the x-axis was limited to 2 °C because lower temperatures are an artefact of the PDF.....	54
Figure 2.7: Seasonal cycles for the SST at HR (blue) and SR (orange) for the entire time series.	54
Figure 2.8: Temporal evolution and trend of the SST anomalies at a) Helgoland Roads and b) Sylt Roads in summer mean (June-August) (solid orange line) and summer linear trend (dashed orange line), winter mean (December-February) (solid blue line) and winter linear trend (dashed blue line).....	55
Figure 2.9: Twelve-month running mean SST anomalies (black curve). Blue, negative anomalies and red, positive anomalies, respectively. a) NS, b) HR, c) SR and d) YS. It is clear the dominant positive pattern after the end of 1980s.....	56
Figure 2.10: Distribution of the sea surface temperature at a) Helgoland Roads and b) Sylt Roads, in terms of probability density function, for the first (blue) and second (orange half) of the time series. The curves show the bimodality originated from seasonality and the shift when comparing early and late years. For a) and b), the x- axis was limited to 2 °C because lower temperatures are an artefact of the PDF.....	58
Figure 2.11: Frequency of occurrence of temperatures at HR and SR. a) HR SST histogram for the period 1962–1990 and b) HR SST 1991–2019. c) SR SST histogram for the period 1962–1990 and b) SR 1991–2019. The bins are defined as 1 °C intervals, except for the edges. Note the difference in temperature intervals for HR and SR.....	59

Figure 2.12: Probability Density Function (PDF) of sea surface temperature anomalies in the first (blue) and second (orange) half of the time series for the a) NA, b) NS, c) HR and d) SR.	59
Figure 2.13: Trends of the summer (dashed orange line) and winter seasons (dashed blue line) mean temperatures at HR for the first half (1962–1990) of the time series.	60
Figure 2.14: Trend of the summer (dashed orange line) and winter seasons (dashed blue line) mean temperatures at HR during the second half (1991–2019) of the time series.	60
Figure 2.15: Trends of the summer (dashed orange line) and winter seasons (dashed blue line) mean temperatures at SR for the first half (1962–1990) of the time series.	61
Figure 2.16: Trend of the summer (dashed orange line) and winter seasons (dashed blue line) mean temperatures at SR during the second half (1991–2019) of the time series.	61
Figure 2.17: The seasonal variation of the standard deviation of the SSTs at a) Helgoland Roads and b) Sylt Roads for the entire time series (grey) and for the first (blue) and second half (orange).	65
Figure 2.18: The seasonal standard deviation (solid blue line) with trend (dashed red line) – a measure of the seasonal amplitude – at a) Helgoland Roads and b) Sylt Roads, calculated per year using monthly SST in situ datasets.	66
Figure 2.19: Number of “cold” and “warm” months for total (grey), early (blue) and late years (orange) of the Helgoland Roads data set.	68
Figure 2.20: Number of “cold” and “warm” months for total (grey), early (blue) and late years (orange) of the Sylt Roads data set.	68
Figure 2.21: First PC Winter mean NAO evolution over time (solid blue line) with linear trend (dashed red line).	70
Figure 2.22: Frequency of occurrence of winter mean (Dec-Feb) NAO index values for the whole period (1962–2019, top), early (1962–1990, middle) and late (1991–2019, bottom) years.	71
Figure 2.23: Temporal and spatial scales of temperature in relation to marine biological systems.	76
Figure 2.24: Results of trends and the direction of increase concerning the different spatial scales for Surface Temperature/Surface Air Temperature anomalies (blue rectangle) and Sea Surface Temperature anomalies (red rectangle).	78
Figure 2.25: The seasonal variation of the standard deviation of the SST in all spatial scales (from Global to local) for the first (blue) and second half (orange) of the time series. a) Global; b) Northern Hemisphere; c) North Atlantic 40°-60°; d) North Sea; e) Helgoland and f) Sylt.	

The y-axis scales are different for top and bottom rows, showing the increase in variability from larger to smaller spatial scales..... 85

Figure 3.1: Bathymetry of the German Bight (GEBCO Bathymetric Compilation Group 2023, 2023). Dot-dashed, solid, and dashed grey lines are 10, 30, and 50 m isobaths respectively. Areas with depths less than 5 m represented by white colour. Black star marks the location that the Helgoland Roads time series have been collected. The acronym DG refer to Dogger Bank; DE to Germany; DK in Denmark; and NL to Netherlands..... 95

Figure 3.2: Evaluation of GlobColour remote sensing surface Chl-a, compared to in situ data from Helgoland Roads. a) Comparison of in situ and remote sensing Chl-a anomalies, with red positive and blue negative anomalies. b) Scatter plot with linear correlation of the time series showed in a). Correlation coefficient is 0.59 and RMSE 1.09 mg m⁻³..... 101

Figure 3.3: a) Boxplots and b) distributions of remote sensing (orange) and in-situ (blue) monthly Chl-a anomalies. 101

Figure 3.4: The a) temporal mean and b) standard deviation of chlorophyll-a concentrations from January 1998 to December 2020. Solid and dashed red lines represent 1 and 2 mg m⁻³, respectively, and the grey and black dashed lines are the 10 and 30 m isobaths. c) Coefficient of variation, in percentage. d) Trends of Chl-a anomalies (mg m⁻³ per year). The shaded areas are significant (p-values <0.05; two-sided Wald test with t distribution)..... 103

Figure 3.5: SST anomalies averaged for the whole German Bight (grey line) and trend from 1998 to 2020 calculated by LOWESS (black line)..... 104

Figure 3.6: Monthly-averaged GlobColour Chl-a, from January 1998 to December 2020 (letters on top right). The Chl-a monthly anomalies are calculated subtracting the monthly-averaged Chl-a from the absolute Chl-a data. It is possible to observe the intra-annual behaviour of Chl-a, with a positive gradient from open waters to coast, and the increase in Chl-a in April and August..... 105

Figure 3.7: Seasonal cycle of Chl-a averaged for areas above the isobath of 30m (coast), areas below 30m (offshore) and HRTS..... 106

Figure 3.8: First and second EOF and PC modes of monthly climatological means of Chl-a. Dashed thin line is the Chl-a spatially averaged at the study area. March-April (green shaded) and August-September (pink shaded)..... 107

Figure 3.9: Month (colour bar from January to December) with maximum Chl-a by pixel from the monthly climatology means of Chl-a (Figure 3.6; mg m⁻³). April (light grey) is the dominant month. 108

Figure 3.10: Spatial averages of Chl-a anomalies in coastal waters (a) and offshore (b) for the months March, April and May. The NAO index winter mean (December, January, February) is the black thin line. 109

Figure 3.11. Probability Density Function estimated from 1998-2009 (blue) and 2010-2020 (orange) for the Chl-a anomalies in March, April and May in the coastal and offshore areas of the German Bight. 110

Figure 3.12: Trend significance of Chl-a anomalies computed with Mann-Kendal trend test. Pixels with p-values <0.05 are considered significant. dec. no sig.= decreasing not significant, inc.no sig. = increasing not significant. 111

Figure 3.13: Sea Surface Temperature time averaged for the study area. The red line marks the 11.1 °C isotherm. 112

Figure 3.14: First four Chl-a anomalies EOF and PC modes. In EOF fields, black solid line is the 0 amplitude contour and black dashed lines are the isobaths of 30m. The amplitude values shown are all max-normalized. Explained variability percentage for each mode are depicted inside parenthesis. 114

Figure 3.15: First four Chl-a anomalies PC. a-d) the PC amplitudes (black) with 6 point rolling means (red solid). e-h) PCs monthly means. i-l) Spectral analysis of PCs time-series. The amplitude values are max-normalized. Explained variability percentages are depicted inside parenthesis. March-April (green shaded) and August-September (pink shaded). 115

Figure 3.16: Correlation maps of Chl-a and SST (a, b), and Chl-a and MLD (c, d). b) and d) lagged correlations with Chl-a lagged one month. Warm colours are positive and cool colours are negative correlations. The dotted areas are significant (p-values <0.05; two-sided Wald test with t distribution). 117

Figure 3.17: MCA results applied to Chl-a and SST anomalies. PC1 is shown as rolling mean of 6 points. 118

Figure 3.18: MCA applied to Chl-a and MLD anomalies. PC1 is shown as rolling mean of 6 points. 119

Figure 4.1: Helgoland Roads monitoring site position (black triangle) in the German Bight, between the Helgoland (H) and Dune (D) islands. 128

Figure 4.2: The train and test partition in chlorophyll-a concentration target (black solid and grey solid lines, respectively), and the HPLC chl-a validation dataset (black dashed). After the split, the testing dataset will remain untouched, to guarantee no leakage of information to the training step. The validation dataset is the independent validation. 131

Figure 4.3: Result of RFECV with Ridge estimator. The black dot represents the maximum value of 17 selected features (predictors) to reach the highest explained variance. After the maximum value, there is an exponential decay/increase in the R^2 /RMSE. 134

Figure 4.4. Boxplot of accuracy in the 10 fold cross-validation training step for the SVR, MLP and RF models, showing the mean and the number of folds (n) or subsets in the training data used to define the best hyperparameters. 140

Figure 4.5: Results of prediction (black dashed) and comparison with the observed test dataset (grey solid). For the three algorithms, R^2 is higher than 0.7 and RMSE lower than $1.2 \mu\text{g L}^{-1}$. (a) SVR, (b) MLP and (c) RF. 141

Figure 4.6: Results of prediction (black dashed) and comparison with the validation dataset (gray solid). For the three algorithms, R^2 is approximately 0.9 and RMSE lower than $0.3 \mu\text{g L}^{-1}$. (a) SVR, (b) MLP and (c) RF. 142

Figure 4.7: Result of SARIMA fit (black dashed) in the test dataset (grey solid). The better fit in extreme values is counter-balanced by the estimation of negative values, decreasing/increasing R^2 /RMSE compared to the ML models results. 143

Figure 4.8: Cross-plots of the modeled and observed chlorophyll values in (a) SVR, (b) MLP and (c) RF. It is possible to notice the deviation in extreme values, showing the limitation of the ML models in deal with these data values. 144

Figure 4.9: Time series of parameters used to predict chlorophyll-a concentration: (a) Secchi disk depth, in meters (m); (b) Sea Surface Temperature, in degrees Celsius ($^{\circ}\text{C}$); (c) Salinity (-); (d) Silicate ($\mu\text{mol L}^{-1}$); (e) Phosphate ($\mu\text{mol L}^{-1}$); (f) Nitrate ($\mu\text{mol L}^{-1}$); (g) Sunlight duration, in hours (h); (h) NAO index (-); (i) Wind Direction, in degrees ($^{\circ}$); (j) Wind Speed, in meters per second (m s^{-1}); and (l) Total zooplankton abundance, individuals per cubic meter (ind. m^{-3}). 147

List of Tables

Table 2.1: Trends in °C/period for the various time series with the associated R ² (Pearson) coefficient.	51
Table 2.2: Cross-correlations calculated from the detrended anomaly time series. All cross-correlation values are significant above 95% confidence level. AMO is added for comparative purposes.	52
Table 2.3: SST anomalies trends in °C/decade in summer and winter. The value in brackets is the associated R ² (Pearson) coefficient.	55
Table 2.4: Annual and seasonal trends of SST in °C/period at Helgoland Roads for the entire period, the first and the second half of the time series for the different seasons. The values in brackets are the associated R ² (Pearson) coefficient, which indicates how much of the variance is explained by the trend.	62
Table 2.5: Mean annual and seasonal SST in °C at Helgoland Roads for the complete period (A 1962-2019), the first half (B 1962-2019) and the second half (C 1991-2019) of the time series. The difference of the late data from the early data (C-B) is presented, as it is significantly positive for all seasons and the whole period.	63
Table 2.6: Annual and seasonal trends of SST in °C/period at Sylt Roads for the entire period, the first and the second half of the time series in the different seasons. The value in brackets is the associated R ² (Pearson) coefficient, which indicates how much of the variance is explained by the trend.	63
Table 2.7: Mean annual and seasonal SST in °C at Sylt Roads complete period (A 1962-2019), the first half (B 1962-2019) and the second half (C 1991-2019) of the time series. The difference of the late data from the early data (C-B) is presented, as it is significantly positive for all seasons and the whole period.	64
Table 2.8: Percentages of the mean number of cold and warm months relative to the total number of months of the late and early time periods at Helgoland Roads (HR).....	69
Table 2.9: Percentages of the mean number of cold and warm months relative to the total number of months of the late and early time periods at Sylt Roads (SR).....	69
Table 2.10: Significance of detrended SST anomalies and NAO correlation (Pearson) for different regions and the stations HR and SR showing all (1962-2019), early (1962-1990) and late (1991-2019) years. Winter mean considers December, January and February months. NA	

- North Atlantic (40°-60° belt); NS - North Sea; HR - Helgoland Roads and SR - Sylt Roads.
.....72

Table 2.11: Overall summary of Results.72

Table 2.12: Comparison of overlapping SST measurements at Sylt harbour and SR sites. Monthly averages, differences with standard deviation (std) and p-values of monthly t-test comparisons.89

Table 3.1: Description of spatial resolution and source of the parameters used in this study. 98

Table 4.1: Statistical description of parameters used as determinants to predict chlorophyll-a concentration (target) after linear interpolation (std, min and max are standard deviation, minimum and maximum values) respectively. 129

Table 4.2: Pearson correlation among predictors and the target chlorophyll-a concentration. 132

Table 4.3: Chosen features after Feature Selection process. The negative numbers represent the number of lags in the original features (t-1,...,t-15). 135

Table 4.4: Hyperparameter tested in GridSearchCV and the ones applied to each ML algorithms. 137

Table 4.5: Comparison of non-optimized (Default) and optimized model performances for predicting Chlorophyll-a concentration during training (train) and testing (test) steps. The linear model serves as a base model. 139

1 Chapter 1

This PhD thesis focuses on the marine primary production represented by chlorophyll-a (Chl-a) concentrations in the German Bight (North Sea) and the changes observed under increasing temperature trends. Marine primary production is the synthesis of organic substances by phytoplankton using inorganic compounds, such as nitrate, phosphate and silica. The marine component accounts for an estimated half of the total global primary production, although the marine biomass responsible for this production is much smaller than the terrestrial biomass component. Marine primary production forms the basis of marine ecosystems, supports the food network, and is a crucial component of biogeochemical cycles and climate regulation, playing a significant role in atmospheric carbon dioxide (CO₂; Sabine et al., 2004; Chavez et al., 2011; Mackenzie et al., 2005; Behrenfeld et al., 2006; Bauer et al., 2013; Sharples et al., 2019). Historically, the Chl-a concentration has been used as a surrogate or indicator of primary production in consideration of the limitations regarding the differences in the amount of carbon and number of pigments (Steele & Baird, 1961; Cullen, 1982; Hayward & Venrick, 1982; Gregg et al., 2003; Boyer et al., 2009).

The German Bight is subjected to changes in primary production due to ongoing climate change, which is expected to result in a reduction in primary production affecting the complex and intrinsic food network, biogeochemical cycles and conversion of inorganic atmospheric CO₂ into organic carbon (carbon fixation), which is essential for climate regulation (Gröger et al., 2013; Capuzzo et al., 2018). However, how temperature directly and indirectly affects phytoplankton and their ability to fix carbon, grow and reproduce in these waters is still unclear. Adequate assessment of the influence of temperature on primary production relies on using long-term temporal and spatial data provided by diverse sources and with various types of analyses (Platt et al., 1997; Sathyendranath et al., 2023).

In this thesis, the overall aim is to investigate the influence of temperature on the Chl-a concentration as a surrogate for primary production in the German Bight, using various data sources and innovative tools to improve the analyses. Specifically, the first aim is to evaluate various spatial scales, from global to local, of temperature changes and the possible effects on the ecosystem. Changes in temperature, seasonal variability, shifts in temperature anomalies, temperature trends, and the distribution of extreme cold and warm temperatures have the potential to alter marine ecosystems, from mass extinctions and species migration to shifts in

phenological traits. This potential serves as the foundation for the second aim: to investigate Chl-a surface trends and variability from 1998 to 2020 in the German Bight using remote-sensing data. The third aim, considering new artificial intelligence approaches, is to employ the Helgoland Roads time series (HRTS) to apply machine learning (ML) algorithms and evaluate their capacity to predict and generalize the Chl-a concentration time series. The use of ML algorithms, combined with a good-quality dataset, indicates that ML is a great tool to predict and analyse the role of predictors for Chl-a in the German Bight.

A general introduction to primary production, Chl-a, the HRTS, and ML is presented to establish the motivation for this thesis and direct the main research questions. The three main chapters, based on published articles and submitted manuscripts, present studies that comprise the core of the thesis. The key findings and general discussion are presented along with an outlook for future work at the end of the thesis.

Introduction

Chapter 5 of the International Panel on Climate Change (IPCC) Special Report on the Ocean and Cryosphere in a Changing Climate (Bindoff et al., 2019) emphasizes that oceans have continuously warmed over the last decades, in keeping with the clear multidecadal ocean warming trends documented in the IPCC Fifth Assessment Report. The warming trend has been further confirmed via improved ocean temperature measurements over the past decades. Due to the warming of the ocean, the global primary production by marine phytoplankton is expected to reduce (Bopp et al., 2013; Cabré et al., 2015). Based on model simulation differences between historical scenarios (1980–1999) and simulations for the end of the century (2080–2099), this reduction could be up to 30%, whereas other scenarios with mitigated warming trends have indicated a 2% decrease (Bopp et al., 2013; Cabré et al., 2015). Regarding the marine coastal ecosystems, the expected responses to this reduction over the 21st century are habitat contraction, migration, and biodiversity and functionality loss. Anthropogenic coastal activities limit natural ecosystem adaptation to climate hazards (Bindoff et al., 2019).

Although shelf coastal seas comprise only about 7% of the world's ocean area (Figure 1), their contribution to global marine primary production is about 10% to 30% (Bauer et al., 2013; Figure 2). Estimates of the annual primary production within shelf seas worldwide are about 11 Gt C a⁻¹ (Jahnke, 2010), which compares with an oceanic total of between 45 and 60 Gt C a⁻¹ (Longhurst et al., 1995; Behrenfeld et al., 2005). The total marine primary production is about half of the total global primary production (Field et al., 1998); thus, this estimation accounts for about one-quarter of the total primary production. The high biological production of the shelf seas also indicates that these areas are essential sources of fixed carbon (Mackenzie et al., 2005; Bauer et al., 2013). Coastal seas play a primary role in the growth of phytoplankton, constituting the primary production of the oceans (Sharples et al., 2019). Globally, shelf seas provide more than 90% of fish production (Pauly et al., 2002).

Currently, coastal seas worldwide are undergoing significant ecological changes driven by human-induced pressures, such as climate change, anthropogenic nutrient inputs, overfishing, and the spread of invasive species (Halpern et al., 2008; Cloern et al., 2016). Approximately 40% of the human population lives within 100 km of the sea, and the coastal zones of continents host many industrial activities (Simpson & Sharples, 2012). In many cases, the changes alter the underlying ecological functions to such an extent that new states are

achieved and baselines are shifted (Lotze et al., 2006; Duarte & Regaudie-de-Gioux, 2009; Kemp et al., 2009; Ehrnsten et al., 2020). The German Bight, a shallow part of the North Sea, has been under significantly increasing temperatures, increasing higher than 1°C since 1962, as indicated throughout this thesis and in the literature (Wiltshire & Manly, 2004; Wiltshire et al., 2010; Amorim & Wiltshire et al., 2023).

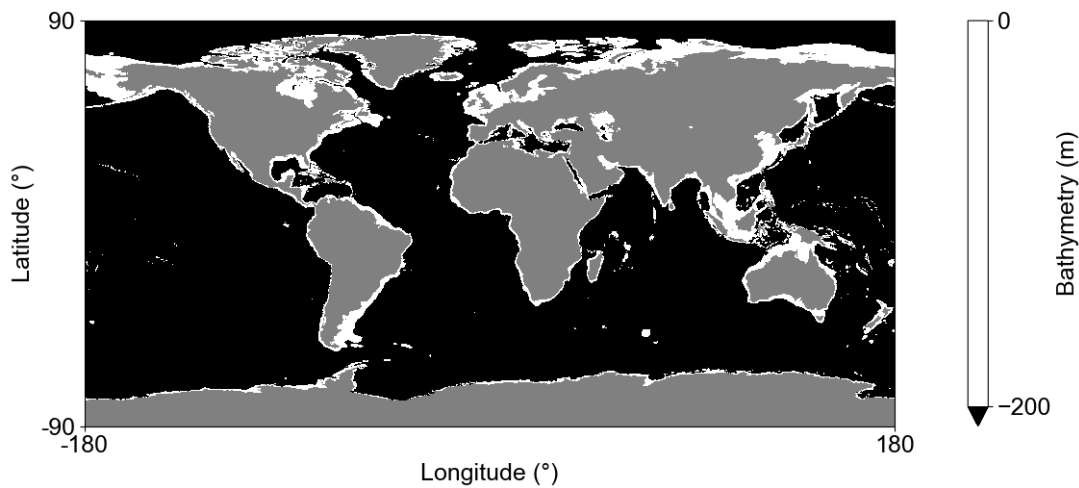


Figure 1: Global ocean pelagic and coastal regions, based on General Bathymetric Chart of the Oceans (GEBCO) bathymetry (GEBCO Bathymetric Compilation Group 2023, 2023). White indicates coastal areas.

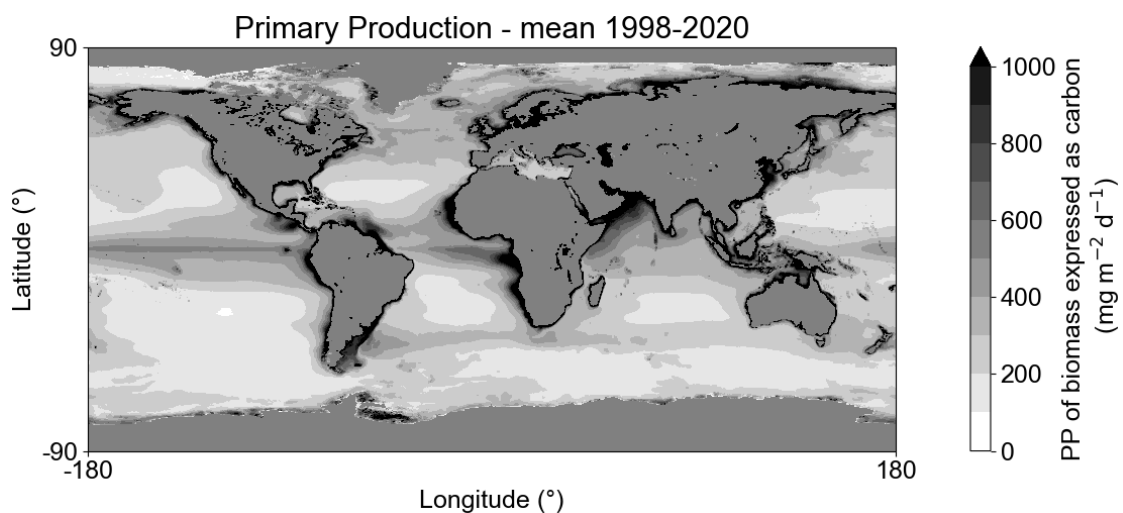
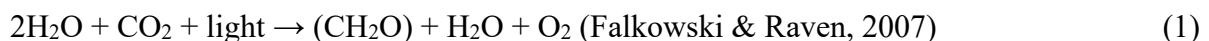


Figure 2: Global mean primary production (PP) from 1998 to 2020 from Copernicus GlobColour (Garnesson et al., 2019). Coastal areas display higher primary production, defined by darker colour.

1.1 MARINE PRIMARY PRODUCTION

Primary production is the synthesis of simple organic compounds by living organisms using inorganic forms of carbon, storing energy within living organisms. Marine primary production supports all life in the oceans, affecting global biogeochemical cycles and the climate by promoting the absorption of CO₂ from the atmosphere in surface waters and sinking it into deeper waters (Sabine et al., 2004; Behrenfeld et al., 2006; Chavez et al., 2011). Phytoplankton conducts marine primary production via photosynthesis in all parts of the ocean where there is sufficient light. Light is a main limiting factor of primary production in high-latitude regions and temperate seas (Harrison & Cota, 1991; Harrison et al., 2008). Almost all ecosystems in the ocean are fuelled by organic carbon and energy, which were initially fixed by photosynthesis. The sea surface layer contains the majority of primary production, with organic carbon and energy transferred to deeper waters via such processes as particle sinking and vertical migration of organisms (Thornton, 2012).

Formally, photosynthesis is defined as the process in which light energy is captured and stored by an autotrophic organism, and the stored energy is used to drive cellular processes (Blankenship, 2008). It can be expressed as an oxidation-reduction reaction in the following form:



Equation 1 is a simplified summary of the overall photosynthesis reaction, which occurs in a number of steps. As Chl-a is the primary pigment responsible for absorbing light for the photosynthesis reaction, it is used as a proxy for the biomass of phytoplankton and serves as a surrogate in marine science for investigating marine primary production (Steele & Baird, 1961; Cullen, 1982; Hayward & Venrick, 1982; Gregg et al., 2003; Boyer et al., 2009).

There are several techniques for measuring the concentration of in situ chlorophyll in seawater. These methods provide information relevant to that particular time and location but are limited when applied at the regional or ocean basin scale. Since 1978, our understanding of the spatial and temporal distribution of phytoplankton biomass has been improved by the measurement of ocean colour from satellite images. Satellite instruments provide

measurements instantaneously over a large area, which is not possible with sampling platforms, such as ships (Thornton, 2012).

High-performance liquid chromatography (HPLC) methods are used for the precise measurement of Chl-a (Wiltshire, 2009), which enables the pigments to be separated using chromatography. Therefore, pure pigments pass through a fluorescence or spectrophotometric detector. Thus, HPLC can be used to estimate phytoplankton biomass in terms of Chl-a. Another option for sampling Chl-a is fluorometers, using various wavelengths to quantify the Chl-a content in water (bbe Moldaenke GmbH, Kiel, Germany; Beutler et al., 2002). The combination of in situ and remote-sensing data is crucial for suitable quality-controlled datasets, producing a vast amount of data to answer research questions concerning processes across a range of temporal and spatial scales (Platt et al., 1997; Sathyendranath et al., 2023).

1.1.1 Chlorophyll-a Remote Sensing

As the primary pigment of phytoplankton, Chl-a uses light as an energy source for photosynthesis. To quantify marine primary production and characterize its variability across spatial scales, frequent measurements with sufficient spatial coverage are necessary. In situ measurements are essential to provide long-term trends and changes, but they usually do not address the spatial component of variability and changes. Remote sensing from satellites allows for spatial and temporal coverage to investigate primary production. The selective absorption of specific wavelengths by Chl-a (peaks at ≈ 440 and ≈ 690 nm) allows the opportunity to quantify marine phytoplanktonic biomass through ocean colour (Figure 1.1). Multi-sensor (multi-satellite) merged products improves the data coverage in both time and space. The Copernicus GlobColour product used in this thesis is obtained by merging data from various sensors: MODIS (Moderate Resolution Imaging Spectroradiometer), MERIS (MEDIUM Resolution Imaging Spectrometer), SeaWiFS (Sea-viewing Wide Field-of-view Sensor), VIIRS (Visible Infrared Imaging Radiometer Suite) and OLCI (Ocean and Land Colour Instrument) (Garnesson et al., 2019). Copernicus GlobColour provides an additional daily 'cloud-free' chlorophyll-a interpolated product that minimizes missing data (Saulquin et al., 2019). A few previous studies have applied the use of Chl-a remote sensing in the North Sea and German Bight, compared with in situ data, to investigate inter- and intra-annual phytoplankton bloom dynamics and long-term trends in Chl-a (Petersen et al. 2008; Su et al.,

2015; Alvera-Azcárate et al., 2021).

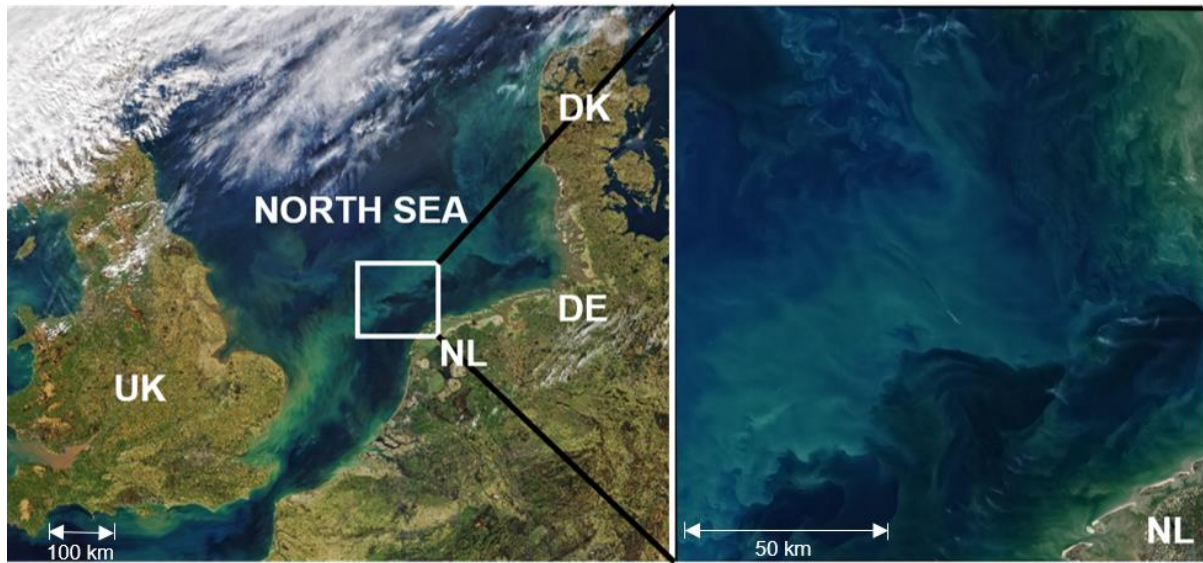


Figure 1.1: Remote-sensing image of the North Sea on March 25, 2020, (left) displaying the different colours during a phytoplankton bloom, and (right) a zoomed-in area at the edge of the German Bight. Composite images combine data acquired by the Moderate Resolution Imaging Spectroradiometer (MODIS) instruments on The National Aeronautics and Space Administration (NASA)'s Terra and Aqua satellites. Modified from NASA Earth Observatory, A Sea of Color and Wind (2020).

1.1.2 The Helgoland Roads Time Series

Time series are the sequential acquisition of data in time. When the series is long enough and well resolved (proper time interval sampling), it allows the separation of short and long-term components, such as seasonal cycles, multidecadal shifts, and long-term changes in variability and trends (Barton et al., 2003; Giron-Nava et al., 2017). The HRTS station ($54^{\circ}11.3' N$, $7^{\circ}54.0' E$) is between the islands of Helgoland and Düne (Figure 1.3, Section 1.4) in the German Bight, North Sea. The Alfred Wegener Institute Helmholtz Centre for Polar and Marine Research has conducted long-term monitoring of various parameters continuously at Helgoland Roads (HR) on a daily basis since 1962 (Figure 1.2), and it is one of the most extended marine datasets available (Wiltshire & Dürselen, 2004). Water samples are collected from a depth of 1 m and preserved for further analysis of Chl-a using fluorometry and HPLC methods. The Chl-a time series, combining both methods, ranges from 2001 to 2020.

Several studies have been conducted analysing the HRTS, focusing on nutrient changes, carrying capacities, plankton phenology and dynamics, and overall changes and system resilience (Wiltshire & Manly, 2004; Wiltshire et al., 2008; Wiltshire et al., 2010; Wiltshire et al., 2015; Sarker & Wiltshire, 2017; Kraberg et al., 2019; Scharfe & Wiltshire, 2019). All related studies collate as one of the best-quality long-term time series available. Although Chl-a has been analysed as a complementary parameter in some of these studies, in the past, no attention was focused on the changes and variability of Chl-a related to warming trends. For example, Wiltshire and Manly (2004) focused on long-term positive trends in the sea surface temperature (SST), relating these trends to the delay or anticipation of spring algal blooms using the phytoplankton abundance long-term series available in the HRTS. In contrast to what is considered normal for temperate coastal systems, they observed delays in the spring blooms instead of an earlier shift. However, due to the limited Chl-a concentration data at that time, they could not include it in their analyses.

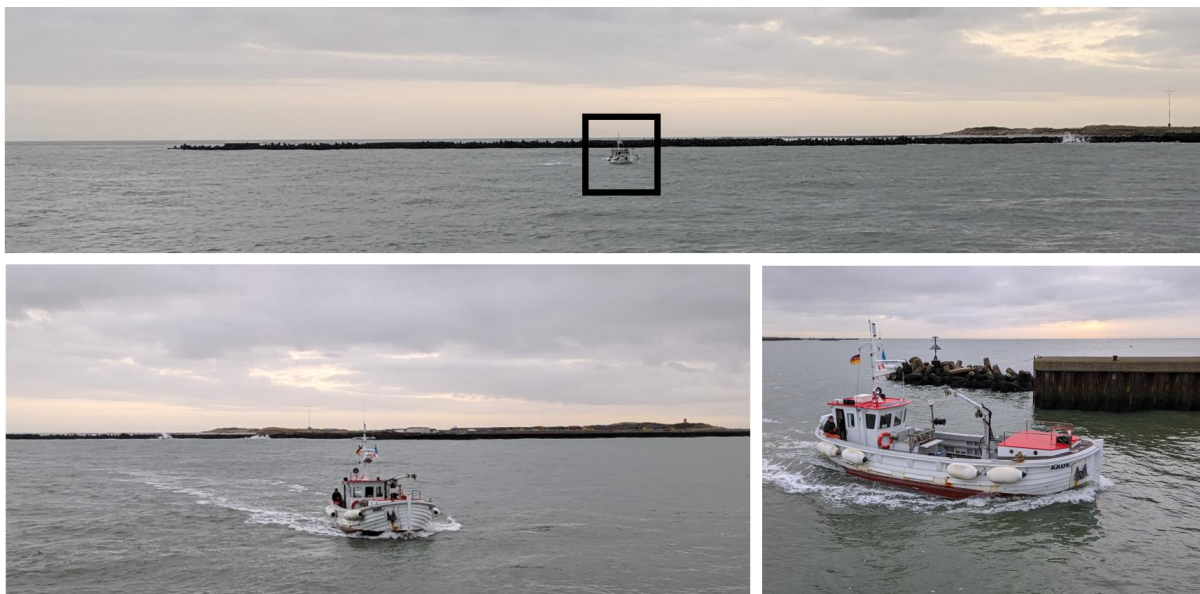


Figure 1.2: Sampling at the Helgoland Roads station (Aade vessel framed by the black rectangle) with the Düne Island in the background, and entering the harbour at Helgoland Island on December 27, 2023. RV Aade, Alfred Wegener Institute.

1.2 PRIMARY PRODUCTION AND TEMPERATURE

Several studies have analysed global changes in marine primary productivity related to warming climates, mostly finding decreasing trends (Gregg et al., 2003; Behrenfeld et al., 2006; Gregg & Rousseaux, 2019). Various parameters, including nutrients, light availability, and temperature, govern primary production. Mechanisms responsible for changes at a regional scale are associated with various hydrographical processes that lead to different productivity regimes on a global scale (Falkowski et al., 1998; Behrenfeld et al., 2006; Henson et al., 2010; Steinacher et al., 2010; Chust et al. 2014). In the low- and mid-latitude oceans and the North Atlantic, a decrease in the net primary production is characterized by reduced inputs of macronutrients into the euphotic zone, related to enhanced stratification, combined with a reduction in the mixed layer depth (MLD) and slowed circulation production. In polar regions, the alleviation of light and temperature as limiting factors is likely to lead to increases in primary production (Chust et al., 2014). Large-scale climate modes, such as the North Atlantic Oscillation (NAO), act on the North Sea through regional climate effects, including increased SST, strong westerly winds (Beaugrand, 2004; Alheit et al. 2005; Weijerman et al., 2005), and an increased inflow of warm, salty water from the Atlantic Ocean (Edwards et al., 2001; Reid et al., 2003; Beaugrand, 2004). In the German Bight, temperature is a critical element in the ecosystem. Plankton dynamics are strongly influenced by temperature (Fromentin & Planque, 1996; Planque & Fromentin, 1996; Dippner, 1997a; Kröncke et al., 1998; Beaugrand & Ibanez, 2004). Temperature can influence trophic interactions in several ways. Temperature determines the geographical distribution of many species (Beaugrand et al., 2002) and affects physiological factors, such as respiration and growth (Desmit et al., 2020).

The relative importance of the factors driving phytoplankton growth in shallow coastal seas depends on water depth, prevailing currents, and riverine inputs to the system, all of which are subject to temporal variation (Wiltshire et al., 2015). Due to a lack of direct observation, whether changes in nutrient levels and light availability in the German Bight, combined with the recent marked temperature increase, have influenced primary production within the bight is currently unclear (Wiltshire & Manly, 2004; Capuzzo et al., 2018; Desmit et al., 2020).

The German Bight is a part of the North Sea, and temperatures have increased by 1.8°C over the last 50 years. Wiltshire and Manly (2004) demonstrated that the average temperature in the North Sea at Helgoland rose by 1.13°C from 1962 to 2002, which agrees with the

warming trends measured in the English Channel (Hawkins et al., 2003), the North Sea (Edwards et al., 2002), and the North Atlantic (Edwards et al., 2001). Following climate model projections, stronger warming is expected to occur at mid- and high latitudes (IPCC Special Report on the Ocean and Cryosphere in a Changing Climate; Bindoff et al., 2019). Amorim and Wiltshire et al. (2023) updated the values described by Wiltshire and Manly (2004) and computed the trends from 1962 to 2020, reaching a 1.8°C increase at Helgoland.

Continental shelves and shelf seas are more productive regions than the open ocean (Gröger et al., 2013); thus, it is critical to study the long-term effects on primary production related to warming trends. Phytoplankton abundance, primary production and the atmospheric CO₂ fixation and fish stocks are expected to be negatively affected by increasing warming trends (Gröger et al., 2013). These claims are supported by the fact that the functioning of the ocean biological pump (Longhurst & Harrison, 1989), which mediates the flux of carbon to the interior of the ocean, is strongly linked to marine primary production. In addition, the central principle that fishery yields are limited by the primary production in the ecosystem (Pauly & Christensen, 1995; Pikitch et al., 2004; Friedland et al., 2012) strengthens the hypothesis of the negative influence of a primary production decrease, along with the possibility that climate change effects are amplified at higher food-web levels than phytoplankton (Lotze et al., 2019).

1.3 MACHINE LEARNING IN ECOLOGICAL STUDIES

As a subfield of artificial intelligence, ML uses techniques such as linear algebra and matrix operations to learn from data and make accurate predictions without being explicitly programmed. Moreover, ML makes minimal assumptions about the input data and can be effective even when the data represent complicated nonlinear interactions (Bzdok et al., 2018). A common difference between classical statistics and ML is that the former provides the theoretical foundation for understanding and interpreting data, whereas the latter provides the tools for automatically learning from data and making predictions and decisions (TAE, 2024).

Oceanography and ecology are in the era of big data (Abbott, 2013). The growth of in situ and remote-sensing data collection at a high frequency and across multiple parameters produces a large quantity of data at diverse multidimensional scales, although often in heterogeneous formats. To deal with large-scale data analyses, traditional statistical tools must be adapted (Durden et al., 2017). Modern ML algorithms with high computational speeds and fewer assumptions about the data, such as assumptions about the structure of the spatiotemporal

covariance and forms of relationships between variables, have great potential for modelling highly nonlinear relationships between variables and for efficient estimation from sparse observations compared to traditional statistical techniques (Giglio et al., 2018).

Many complexities, including historical legacies, time lags, nonlinearity, interactions, and feedback loops, which vary in time and space, of ecosystem datasets are challenged by the need to understand and predict complex ecological processes and patterns. Recent advances in data collection technology, such as remote-sensing and data network centres and archives, have produced large, high-resolution datasets spanning spatial and temporal extents that were, until recently, unattainable (Olden et al., 2008).

1.4 THE GERMAN BIGHT

The German Bight is a shallow marine area located in the southeastern part of the North Sea (Figure 1.3). Its hydrodynamics are dominated by tidal and wind forcing. In coastal areas of the bay, the water column is continuously mixed by tidal and wave forcing, which act against seasonal thermal and haline stratification (density differences due to temperature and salinity), supported by surface buoyancy induced by surface heat fluxes, riverine freshwater fluxes, and tidal straining. In offshore and open areas, stratification occurs due to atmospheric-ocean heat flux. However, the action of wind/tidal mixing and river runoff regulates stratification in the German Bight (Zhao et al., 2019). Considering these characteristics, the German Bight is susceptible to changes due to climate in a number of processes concerning shallow, transitional, and offshore areas (e.g. vertical mixing, stratification, turbulence, and river runoff; see van Leeuwen et al., 2015, for the different underlying physical conditions influencing phytoplankton).

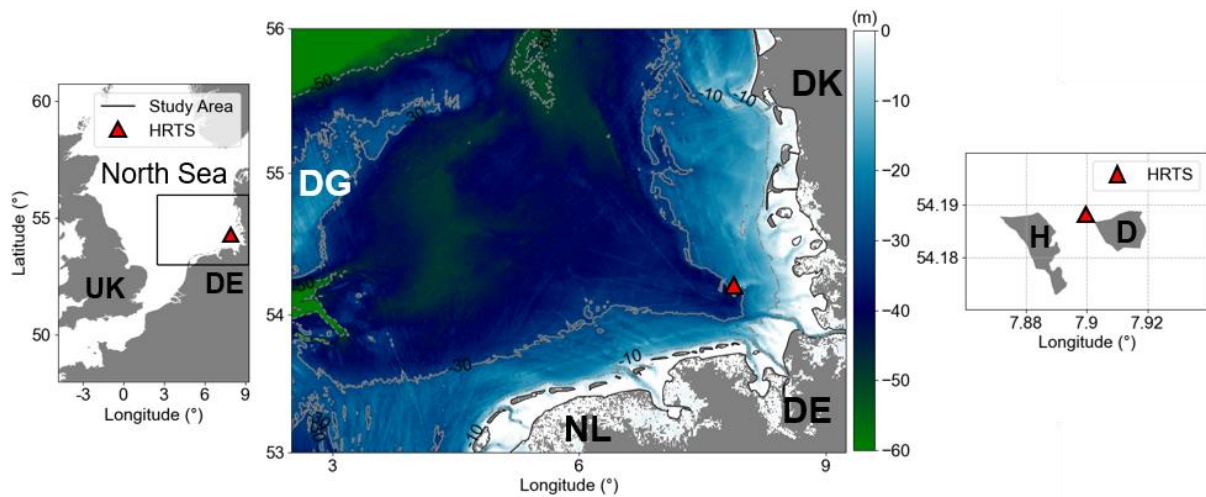


Figure 1.3: North Sea, German Bight and Helgoland Island, illustrating the study area and the long-term Helgoland Roads time series (HRTS) location (red triangle). DE – Germany; UK – United Kingdom; NL – Netherlands; DG – Dogger Bank; H – Helgoland and D – Düne Island.

According to Meyerjürgens et al. (2019), wind conditions have a significant influence on surface currents and transport processes in the German Bight (Huthnance, 1991). The bulk of North Atlantic water enters the German Bight through the English Channel (Burt et al., 2016; Meyerjürgens et al., 2019; Figure 1.4). During transport along the coast, these water masses are influenced by riverine water runoff, decreasing the salinity in coastal waters (Becker et al., 1992). In the eastern part of the German Bight, close to the North Frisian coast, the combination of riverine freshwater and saline water, transported by southwesterly winds into the German Bight, leads to a frontal zone with a strong haline gradient (Becker et al., 1999; Skov & Prins, 2001).

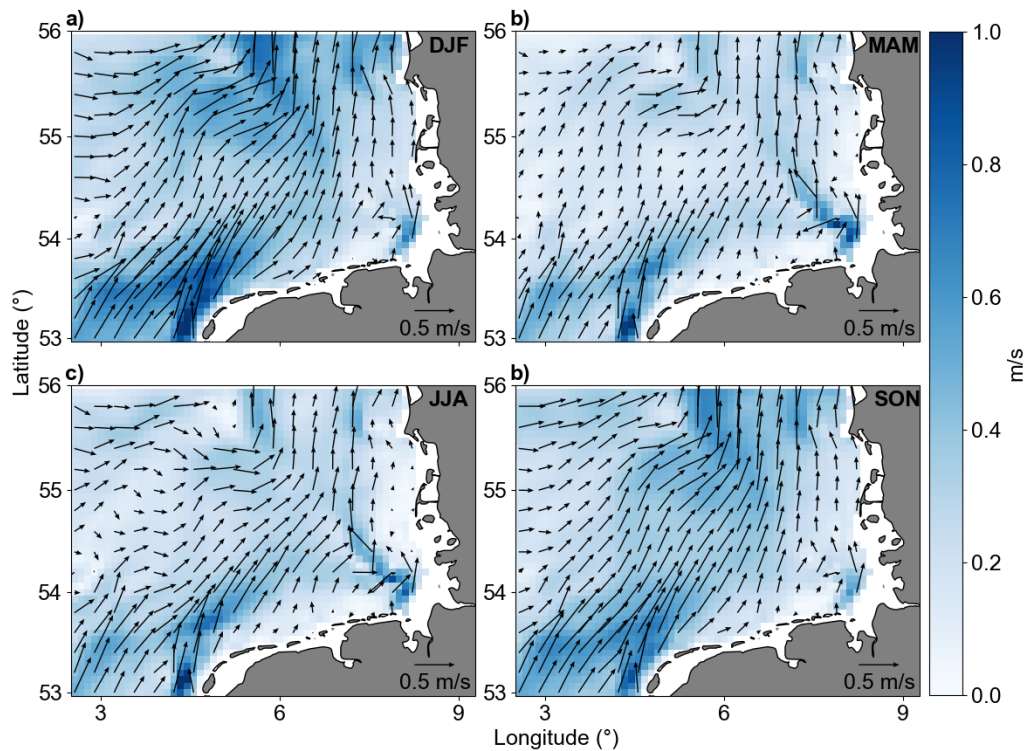


Figure 1.4: Seasonal mean of depth-integrated ocean currents (0-10 m; m/s) in the German Bight (1993-2022), emphasizing the importance of the English Channel flow and the difference in magnitude among seasons. DJF – December, January and February (winter); MAM – March, April and May (spring); JJA – June, July and August (summer); SON – September, October and November (autumn). Data extracted from Copernicus Marine Service (CMS), product ID NWSHELF_MULTIYEAR_PHY_004_009 (<https://doi.org/10.48670/moi-00059>).

1.5 KNOWLEDGE AND RESEARCH GAPS

Considering that primary productivity in the oceans is changing in response to global climate change, with 70% of the productivity decline occurring at high latitudes (Gregg et al., 2003; Boyce et al., 2010), the effect of increasing SSTs is possibly one of the main drivers. In the German Bight, the consequences of the current warming trend in primary production are still unclear, with some studies demonstrating an increase in the past decades and others observing a decrease in primary production (see Desmit et al., 2015). Marine primary production sustains the marine food web and is a crucial component of the biogeochemical cycle in the German Bight; therefore, an understanding of the Chl-a variability and the role of temperature is critical for predictions of future scenarios.

Following the descriptions of marine primary production variability associated with increasing

temperature at various spatial and temporal scales, the central hypothesis of this work is that temperature affects distinct phytoplankton characteristics, such as growth, phenology, and distribution, but so does the environment, by altering wind patterns and frequency, shifting hydrodynamics, and controlling nutrient availability. The combination of temperature effects on phytoplankton and environmental changes is expected to result in decreased primary production.

The following questions are addressed in this thesis:

1. How do SSTs and land surface temperatures correlate from global to local scales? What are the differences in trends and seasonal variability that could be implicated in various responses by ecological systems related to these spatial scales?
2. What are the current trends (from 1998 to 2020) and spatial variability of the surface Chl-a concentrations in the German Bight?
3. How applicable are ML algorithms to the prediction of the Chl-a concentration time series acquired in the German Bight, and what are the best predictors defined by ML analyses? Can ML predict and generalize the results to an independent dataset? Does ML outperform classical statistics?

The core of the problem concerning the effects of warming on marine primary production at the German Bight is that the long-term variability and trends of Chl-a concentrations have only been assessed from (i) in situ records that cover small areas and sometimes irregular sampling intervals or from much larger spatial scales, such as the entire, heterogeneous North Sea, and (ii) model simulations limited by the number of analysed years. In addition, (iii) they have primarily focused on nutrients and light variability, with the temperature only complementing these analyses. Thus, conclusions regarding multidecadal variability and direct temperature effects have either been overlooked or are not yet resolved (Gröger et al., 2013; Wiltshire et al., 2015).

1.6 OBJECTIVES

The general goal of this thesis is to investigate changes in the German Bight primary production associated with increasing temperature using Chl-a concentration as a surrogate. Specifically, this entails the following:

- Analysing the Chl-a surface concentration fields to estimate the present situation,
- Investigating temporal and spatial changes in Chl-a,
- Defining the influence of increasing temperature at various spatial and temporal scales on the Chl-a concentration, and
- Evaluating the use of ML algorithms to predict Chl-a times series.

1.6.1 Thesis Outline

The in situ data from the HRTS were complemented by the German Meteorological Service (Deutsche Wetterdienst: DWD) data, reanalysis datasets from the Hadley Met Office Hadley Centre for various global regions, and remote-sensing and reanalysis datasets from the Copernicus Marine Service (CMS) for the German Bight area to reach these objectives. The three main chapters detail the applied methodologies and results that fulfil the overall objectives.

Chapter 2 assesses different scales of temperature, from global to local, to assess the direct coupling between ocean and land interactions, exploring the trends and variability changes using reanalysis and in situ data and investigating the behaviour of temperature at distinct scales. Next, Chapter 3 describes the present state of superficial Chl-a concentrations. This chapter discusses inter- and intra-annual variability using empirical orthogonal functions (EOFs) and trends, comparing the Chl-a covariance with two physical forcings, SST and MLD, using remote-sensing data from 1998 to 2020. Finally, Chapter 4 employs modern and innovative ML algorithms to predict Chl-a concentrations using the highly resolved, good-quality HRTS. This study is the first to apply ML algorithms to the HRTS.

2 Chapter 2

Investigation of marine temperature changes across temporal and spatial gradients: Providing a fundament for studies on the effects of warming on marine ecosystem function and biodiversity

Published as: Amorim, F.L.L.*, Wiltshire, K.H.*, Lemke, P., Carstens, K., Peters, S., Rick, J., Gimenez, L. and Scharfe, M. (2023). Investigation of marine temperature changes across temporal and spatial Gradients: Providing a fundament for studies on the effects of warming on marine ecosystem function and biodiversity. *Progress in Oceanography*, 216, 103080. <https://doi.org/10.1016/j.pocean.2023.103080>

*joint first authors

Abstract

A current critical issue in climate change studies is how temperature changes and shifts on different spatial and temporal scales can affect organisms in terms of trends, variability and frequency of extremes. In this paper, we analysed marine temperature data on different temporal and spatial scales. We related the sea surface temperature data from the Helgoland Roads Time Series, one of the most important and detailed long-term in situ marine ecological time series, to the Sylt Roads, North Sea, Germany, Europe, North Atlantic and Northern Hemisphere surface temperatures. All time series showed a distinct upwards shift in temperature in the late 1980s, early 1990s, with positive trends in overall for the period between 1962 and 2019 ranging from 1 to 2 °C over 57 years. We quantified changes in temperature variability by comparing the years before and after 1990, on both long-term and seasonal scales. At Helgoland and Sylt, an increase in the number of warmer days in summer and a decrease in extremely cold days in winter are the new characteristics of the temperature pattern after 1990; higher than expected temperatures now also occur earlier during the year. For these locations, we observed the highest trends overall, i.e. of around 0.3 °C/decade. The observed bimodal shape of the probability density functions, characterized by winter and summer modes, had become more heterogeneous, with the cold mode peak moving to higher values and the

steepness to the peak increasing, which is a consequence of a decrease in extremely cold days. North Atlantic Oscillation (NAO) and Multidecadal Oscillation (AMO) large-scale phenomena had no significant correlations or, for the NAO, were limited to the winter season at the regional and local scales. The closest landmass (mainland Germany) temperature was highly correlated with the North Sea sites. Taken together, our results suggest that marine pelagic ecosystems and their species are subject to temperature shifts with similar patterns but with variations in magnitude at the different scales. Temperature is one of the main drivers of species diversity and distribution, and this manifests on different spatial and temporal scales depending on population growth, life stages, cycles and habitat. Accordingly, we here present the temperature changes on the appropriate spatio-temporal scales, and thus provide the suitable and useful fundament for studies on the effects of warming on marine ecosystem function and biodiversity.

2.1 INTRODUCTION

The future of human kind is closely linked to the sustainability of coastal and shelf seas and their ecosystems. Global Ocean warming is fact and the effects of warming on marine ecosystem services presents a threat to long-term coastal sustainability and population stability. (IPCC, 2018; IPCC, 2019). Concomitantly, the vulnerability of human survival and livelihoods on coastal and marine systems becomes ever clearer as climate-related problems such as sea level rise, ocean acidification, loss of economically important species, invasive species and the “race for space” for energy parks, manifest in shelf seas (Barnard et al., 2021; Billé et al., 2022).

The trends from 1962 to 2019 in the whole Global Surface and Global Ocean temperatures is, respectively, given as 0.97 and 0.71 °C/57 years (GISTEMP Team, 2022). These values are based on the compilation of direct measurements at land and sea surface e.g. from simple thermometers, Argo data, ship data and meteorological stations (Lenssen et al., 2019). However, while large-scale projections and especially mean trends values are helpful, especially in the political sense, these alone are not particularly useful when considering direct human and organism responses, food web change and ecosystem disruption issues. More humans will live at, or close to, coasts and shelf seas and, as these populations are dependent on marine ecosystem integrity and ecosystem services, detailed data and information on marine warming, in appropriate time and spatial scales, facilitating mitigation and protection strategies on human and biological time scales are urgently required.

Marine ecosystems and organisms also react to shifts in environments on a variety of time scales. The potential death, fitness, resilience and adaptation of species is dependent on intensity, duration and frequencies of environmental shifts/ events. Predictability and understanding of temperature-related organism health, fitness, and reactions such as heat shock, depend on dense information of maximum temperatures, variability, frequency and duration of periods characterized by specific temperatures (Wiltshire & Manly, 2004).

Detailed long-term data and accompanying statistical information are fundamental for the development of highly flexible regional marine models (Androsov et al., 2019; Baracchini et al., 2020) needed for ecosystem predictability (e.g., for the estimation of warm water entrainment, marine pathogen dispersal, fish deaths in anoxic zones or sea level rise) in a warmer world. Regional management and realistic local decision taking require that these are

operable on very small spatial scales, ranging from 0.5 km to 100 km, also requiring verification and explanatory data on the appropriate scales.

Marine data from ship cruises exist since the 1800 s for some coastal and shelf seas, and impressive large-scale biological change data sets from the continuous plankton survey of Sir Alister Hardy Foundation for Ocean Science's Continuous Plankton Recorder (SAHFOS CPR) are available. However, few continuous and dense time series (i.e., >20 years old) are available for connection with ecological information and biology, even for simple abiotic parameters such as temperature and salinity (Philippart et al., 2003; Wiltshire & Manly, 2004; Ostle et al., 2021). Indeed, dense continuous data from long-term ecological research (LTER) sites are rarely available (Edwards et al., 2010). Without such data, exact changes in environmental drivers are statistically difficult to define and the differentiation of change types including so-called "regime shifts" is often based on poorly defined time scales and system knowledge. Explanatory and predictive models are then difficult and less reliable.

The pressure is on to provide knowledge founded upon detailed real data on appropriate spatial and time scales, in order to predict and understand organism and ecosystem reactions and resilience. It is imperative to relate warming into evinced and graspable effects and consequences, on relevant biological scales. Otherwise, scenario discussions, predictions and management strategies for shelf and coastal seas are difficult/impossible to carry out.

In this paper, we take the sea surface temperature (SST) in situ data from one of the most important and detailed long-term marine ecological time series, the Helgoland Roads Time Series (HR), and relate the data with its nearest neighbour SST time series, the Sylt Roads Time Series (SR). We incorporated to the in situ data spatially averaged SST anomalies time series for the greater North Sea (NS), as well as: Northern Hemisphere (NH) Surface Air Temperature anomalies (SAT), Europe SAT, Germany SAT, North Atlantic (NA) SST anomalies (40°N-60°N belt of latitudes) and the Yellow Sea (YS) SST anomalies time series. These are all spatially averaged and derived from HadCRUT4 and HadSST3 SAT and SST anomalies products, available from the Hadley Meteorological Centre (Kennedy et al., 2011a, 2011b; Morice et al., 2012). The hierarchical and comparative statistical evaluation of all of these time series relative to one another will allow us to relate marine ecosystem change to temperature in terms of time and spatial scales. The objectives are:

1. to investigate the warming in the North Sea in terms of different geographical scales and typical weather indices,
2. to document the different types of changes observed: trends, anomalies and variability
3. to differentiate seasonal shifts,
4. to evaluate anomalies and frequency distributions of temperature over time, and
5. to evaluate hot and cold spells and their variability.

2.2 MATERIALS AND METHODS

2.2.1 Data sets

The data sets were divided into in situ and reanalysis products. Figure 2.1 shows the areas and sites of interest in this article. Not highlighted, but no less important, are the European and German geographical areas, also analysed in terms of spatially averaged temperature anomalies.

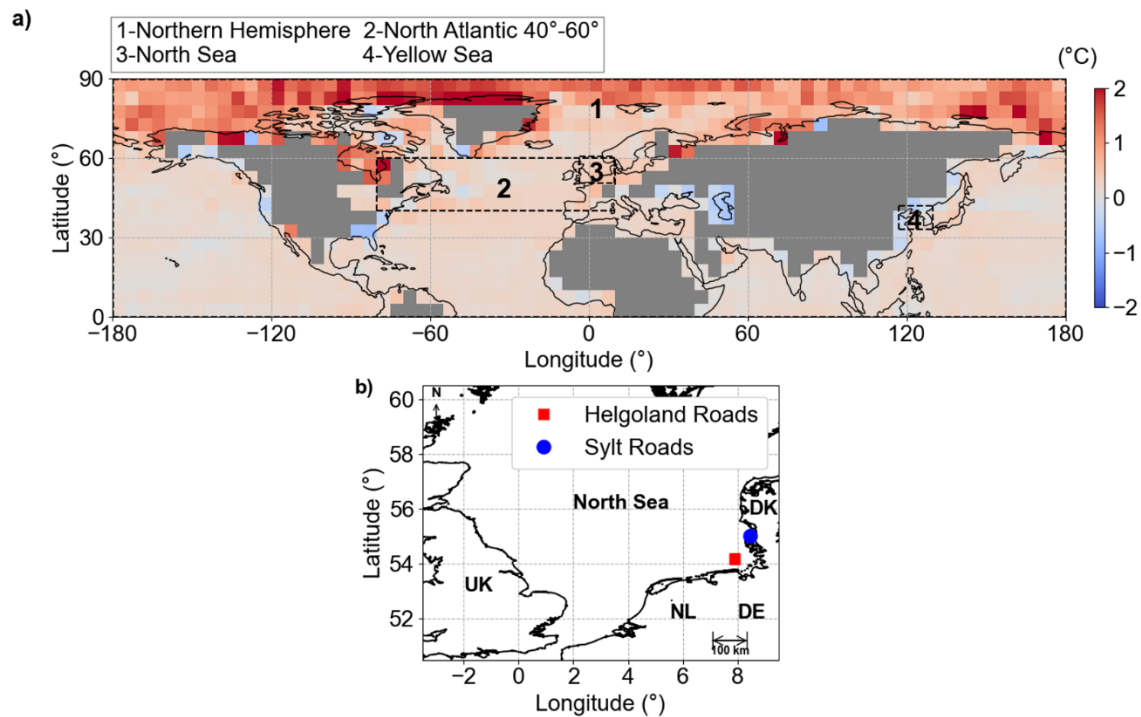


Figure 2.1: Regions a) and locations b) analysed in this study. a) 1-Northern Hemisphere, 2-North Atlantic (latitude belt 40°-60°), 3-North Sea, 4-Yellow Sea. b) North Sea area and the two in situ stations – Helgoland Roads (red square) and Sylt Roads (blue circle). UK - United Kingdom; NL - Netherlands; DE - Germany and DK - Denmark. The colour background in a) represents the HadSST3 averaged SST anomalies for the period 1962 to 2019. The temperature anomalies for HadCRUT4 and HadSST3 data are relative to the period of 1961 to 1990 and the limits used for the seas were defined to be as close as possible to the ones defined by the Limits of Oceans and Seas (IHO, 1953).

2.2.1.1 Helgoland Roads time series (HR)

The renowned Helgoland Roads time series was set up in 1961 with the aim to evaluate change in the North Sea and its pelagic food webs over time. The evaluation scale available is from days to decades. Since 1962, surface water samples have been taken (before 9 a.m.) on working days at the “Kabeltonne” site (54° 11. 3’N, 7° 54. 0’E) between the two islands at Helgoland using a bucket. The data from these samples constitute one of the richest temporal marine data sets available, i.e., a pelagic data comprising of salinity, Secchi disk depth, nutrient analyses, phytoplankton and zooplankton analyses (Wiltshire 2004). The temperature at the sea surface was measured to date using calibrated reversing thermometers (Thomas and Dorey,

1967). The data is archived in PANGAEA (Data Publisher for Earth & Environmental Science). See Wiltshire and Manly (2004) for details on the time series.

2.2.1.2 Sylt Roads time series (SR)

The Sylt Roads time series (55.03° N, 8.46° E) was set up in 1973 to augment Helgoland Roads and German Bight transects with information from a shallow water location. Since 1973, surface water samples have been collected twice a week (except in 1977, 1978 and 1983 when it was suspended), temperature was measured using reversing thermometers and water was analysed for physical, chemical and biological parameters. Data are archived in PANGAEA (Rick et al., 2017a; Rick et al., 2017b; Rick et al., 2020a; Rick et al., 2020b; Rick et al., 2020c; Rick et al., 2020d; Rick et al., 2020e). In order to extend the SR Sea Surface Temperature (SST) time series to cover the same period as the HR series and to fill gaps, the SR data were merged with an additional (until now unpublished) SST data set from a neighbouring station located in List harbour (55.017° N, 8.44° E). This data was provided by Landesbetrieb für Küstenschutz, Nationalpark und Meeresschutz Schleswig-Holstein (LKN.SH, Husum, Germany). The two stations are situated 1.93 km apart in the Sylt-Rømø Bight.

The List harbour data set comprises daily water temperature taken from 1946 to 2003. For the period of overlap (1973–2003) between the two series, the data were compared statistically on a monthly basis applying a double-sided t-test. The overlapping data showed no significant differences (*p* values range 0.22–0.93) and their patterns were well-matched. The harbour data, due to its sheltered position, was insignificantly warmer by an average of + 0.11 °C compared to the SR site. Details on the merged datasets are provided in Supplementary Material (Table 2.12). Using this approach, we managed to assign monthly mean SST data to all but three months (March 1999; April 1999; October 2000). These missing values were filled in with HadISST SST (Rayner et al., 2003) monthly average values from the closest grid point to the Sylt Roads position (<https://www.metoffice.gov.uk/hadobs/hadisst/data/download.html>, downloaded on 20 Jul 2020). The resulting time series is depicted in Figure 2.2, highlighting the different data sources.

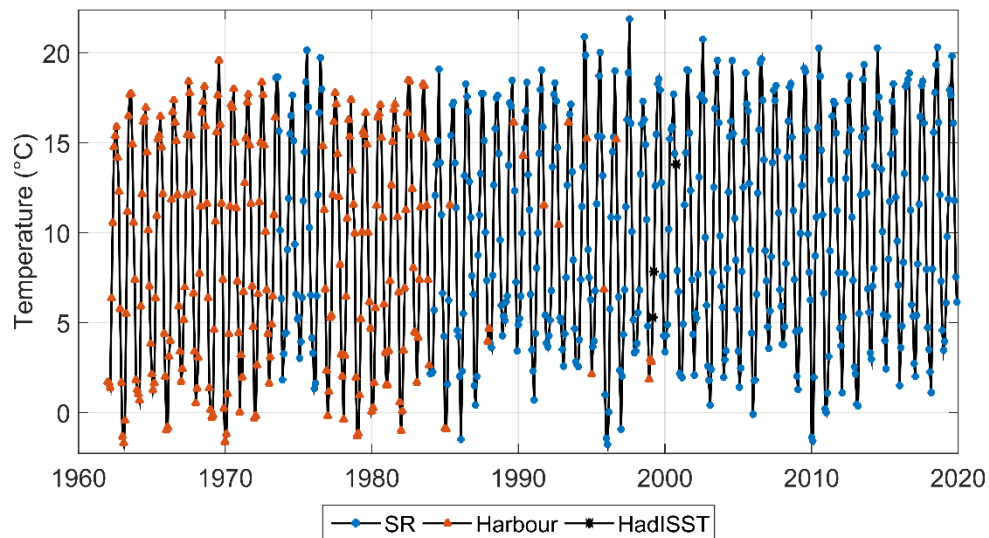


Figure 2.2: Sylt Roads SST Time Series – merged from three data sources (solid black line). SR (blue circle), Sylt harbour (orange triangle) and HadISST (black star).

2.2.1.3 HadCRUT4 and HadSST3 datasets

Land and Sea Surface Temperature anomalies (ST) and Sea Surface Temperature anomalies (SST) were obtained from two products: HadCRUT4 (Morice et al., 2012) and HadSST3 (Kennedy et al., 2011a, 2011b) respectively, provided by Met Office Hadley Centre (<https://www.metoffice.gov.uk/hadobs/>, downloaded on 03/12/2020). Using these two products we ensured consistency with atmospheric and sea surface temperature anomalies. Surface temperature anomalies were spatially averaged for 4 regions: Northern Hemisphere (NH ST), North Atlantic (limited by latitudes 40° and 60°N) (NA SST), North Sea (NS SST) and Yellow Sea (YS SST) (Figure 2.1).

2.2.1.4 European land surface air temperature anomalies

We considered the European land mass temperature connection and scale by using the annual mean European Land Surface Air Temperature Anomalies, provided by the European Environment Agency and downloaded from the website <https://www.eea.europa.eu/data-and-maps/figures/global-left-and-european-land>. As described in the source website, this is a product compiled as the mean of the HadCRUT4, GISTemp v4, and NOAA Tempv5 data sets. The anomalies for this dataset are relative to the pre-industrial period 1850–1900.

2.2.1.5 German surface air temperature anomalies

The nearest landmass temperature data for both Helgoland and Sylt Roads are the annual mean German Surface Air Temperatures, acquired by meteorological stations around Germany. These were taken from the website of the German Weather Service (DWD, <https://www.dwd.de/EN/ourservices/zeitreihen/zeitreihen.html#buehneTop>). The anomalies for this dataset are relative to the 1962–1991 period.

2.2.1.6 North Atlantic Oscillation index (NAO)

The North Atlantic Oscillation Index (NAO) is regularly used to explain variability in temperature and Long-Term Ecological Research (LTER) time series (Becker, 1996; Hurrell et al., 2001; Pozo-Vázquez et al., 2001). According to the National Center for Atmospheric Research (NCAR), the principal component (PC)-based NAO is the time series of the leading Empirical Orthogonal Function (EOF) of Sea Level Pressure anomalies over the Atlantic sector, 20°-80°N, 90°W-40°E, limited by the Icelandic Low and Azores High (NAO, 2022). In this work, we use the PC-based NAO monthly time series to match with the monthly SST time series in frequency.

2.2.1.7 Atlantic Multidecadal Oscillation (AMO)

The Atlantic Multidecadal Oscillation is defined as the spatial average SST anomalies in the North Atlantic over 0°-60°N (Trenberth & Shea, 2006). The AMO time series is provided by the NCAR Climate Data Guide and it was extracted from <https://climatedataguide.ucar.edu/climate-data/atlantic-multi-decadal-oscillation-amo> (AMO, 2021).

2.2.2 Statistical methods

We focused on statistical evaluations of the coastal and pelagic long-term data, considering the period of study from 1962 to 2019, covering a time horizon of 58 years and 696 monthly observations. Statistical analysis was applied to the collection of yearly and monthly surface temperature anomalies time series. Due to the averaging, no missing observations were detected. The methods used were: trend analysis using linear regression; Pearson cross-correlations (significance $p > 0.05$) of detrended time series; variability and seasonality estimated by calculating standard deviation and individual months average; Probability Density Function estimated by Kernel Density Estimate and histograms to observe distribution patterns and changes. All the statistical analyses were performed using the MATLAB® and Microsoft Excel software.

All data were used as anomaly time series, and for the two in situ stations (HR and SR), absolute SST was also analysed. For the in situ SST data, the anomalies were calculated removing the seasonal signal calculated as average of individual months from 1962 to 1991. For yearly time series, the mean temperature from 1962 to 1991 was sub-tracted from the absolute temperature time series. Temperature anomalies were used instead of absolute temperatures because one assumes to first-order that the seasonal cycle is a more or less deterministic consequence of the varying zenith angle of the sun, and all differences from the seasonal cycle (i.e. the anomalies) tell us something about the in-ternal dynamics of the system.

Trends were quantified by fitting linear models through linear regression. We carried out cross-correlation analyses to investigate the statistical inter-relationships between the temperature data from different geographical regions. We computed the cross-correlation of the detrended time series, as the trends occurring in both time series always contributes to the

cross-correlation of two anomaly time series. Seasonal variability was calculated by the standard deviation of specific month temperatures, from January to December.

2.3 RESULTS

The presentation of the results (and also the discussion) is structured as follows:

- Trend and cross-correlation between local Long-Term Observations (LTO) and large-scale time-series in: Northern Hemisphere Surface Temperature (NH ST), Europe SAT (EU SAT), Germany SAT (DE SAT), North Atlantic SST (40°N-60°N belt) (NA SST) and the North Sea SST (NS SST). Here the AMO is also considered.
- Long-term changes in seasonality with focus on LTOs.
- Comparison of seasonal variability between early (1962–1990) and late (1991–2019) years of the time series.
- Means and trends for the above-mentioned periods by seasons, comparing the degree of changes in temperature anomalies related to early and late years.

2.3.1 Overall trends and Cross-Correlation

The data from the two long-term in situ stations at Helgoland Roads and Sylt Roads lend themselves to simple linear calculations of trends based on yearly average (Figure 2.3). The increase in sea surface temperature is clear for both stations. Although the sites are hydrographically completely different, with Helgoland being offshore in the open water of the German Bight and Sylt being a shallow water coastal station in the Wadden Sea, the magnitude of trends are almost the same for both sites.

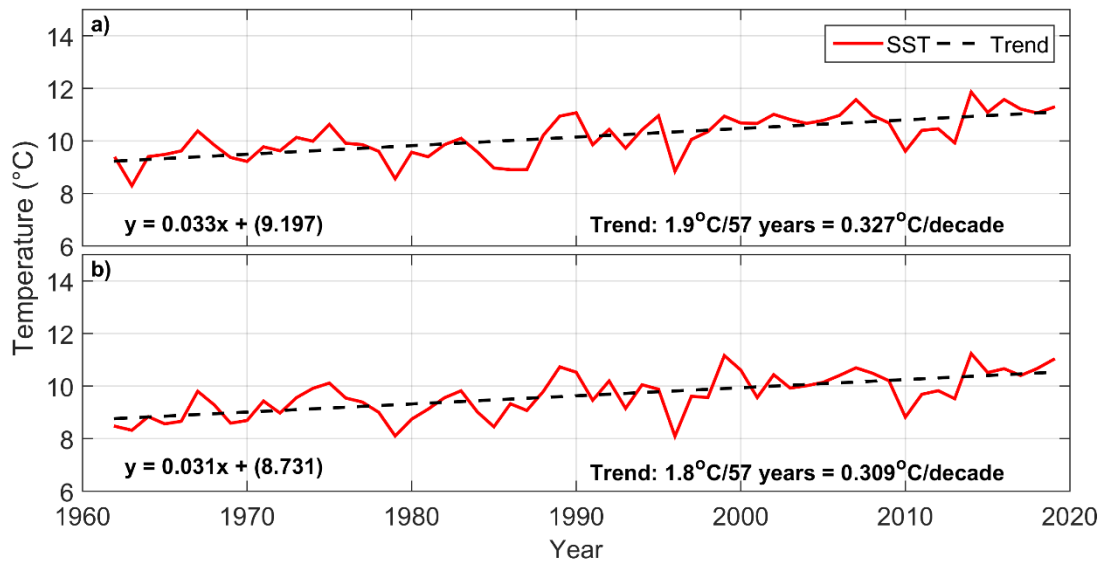


Figure 2.3: Yearly averages of temperature time series (solid red) and their linear trends (dashed black), a) Helgoland Roads and b) Sylt Roads.

Because the HR and SR data are used widely for climate and ecological assessments, it was necessary to evaluate these two local sites into the context of larger geographical regions and especially in the context of the warming of the North Sea and the temperatures of the North Atlantic. To achieve this, we used the temperature anomalies data sets already described and the comparative results are shown in Figure 2.4 and Table 2.1. All the trends were significantly positive and the slopes were larger with decreasing geographical scale (i.e. spatial average) for both surface air temperatures and sea surface temperatures:

- Trend of NH SAT < EU SAT < DE SAT (for the surface/surface air temperature);
- Trend of NA SST < NS SST < HR/SR SST (for the sea surface temperature).

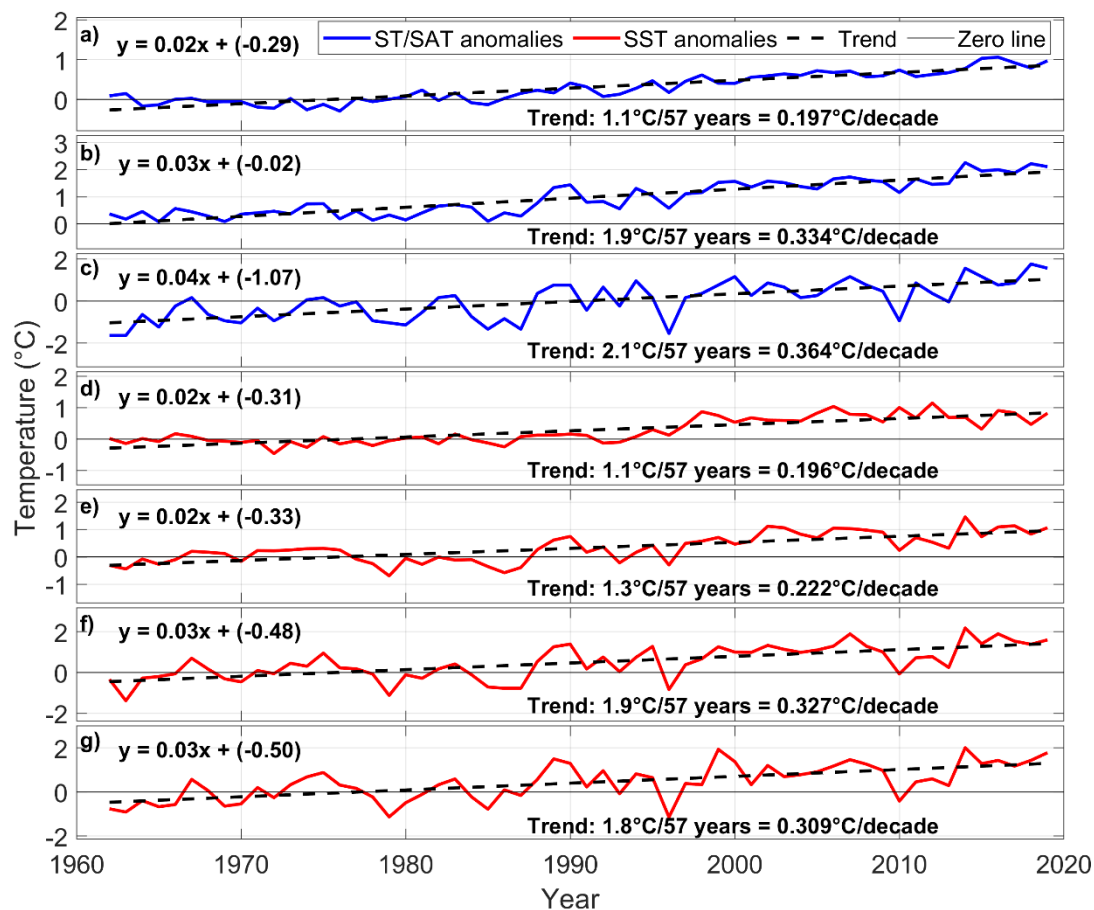


Figure 2.4: Anomaly time series (solid blue and solid red) and their linear trends (dashed black). From the top: Northern Hemisphere ST (land + sea surface temperature), Europe SAT, Germany SAT, North Atlantic SST (40°N-60°N belt), North Sea SST, Helgoland Roads SST, and Sylt Roads SST anomalies. Blue lines, except a), are based on surface air data and red lines are based on sea surface data.

Table 2.1: Trends in °C/period for the various time series with the associated R^2 (Pearson) coefficient.

Temperature Anomalies Time series	Trend per 57 years	Trend per decade	R^2
NH SAT	1.12	0.20	0.82
EU SAT	1.91	0.33	0.80
DE SAT	2.07	0.36	0.49
NA SST	1.12	0.20	0.67
NS SST	1.26	0.22	0.54
HR SST	1.86	0.33	0.47
SR SST	1.76	0.31	0.43

A cross-correlation analysis was carried out to investigate the statistical inter-relationships between the temperature data from different geographical regions. For this, the cross-correlation of the detrended time series was computed, as the cross-correlation of two anomaly time series always has a contribution from the trend occurring in both time series. From Table 2.2, it is clear that the strongest cross-correlations occurred between Germany/Europe and Europe/NH, as was to be expected. The SST of the North Sea was strongly correlated with the European and the German SAT and, to a lesser extent, with the North Atlantic SST and the Northern Hemisphere ST.

Helgoland Roads and Sylt Roads were strongly correlated with the German SAT and to a smaller extent with the European SAT. The stations were highly correlated with each other and also with the SST of the North Sea. This answers the question as to whether both sites can be considered representative with regard to temperature of the overall North Sea.

Table 2.2: Cross-correlations calculated from the detrended anomaly time series. All cross-correlation values are significant above 95% confidence level. AMO is added for comparative purposes.

	NH SAT	EU SAT	D SAT	NA 40-60	NS	HR	SR
NH SAT	1	0.43	0.10	0.55	0.30	0.26	0.09
EU SAT	0.43	1	0.77	0.30	0.73	0.75	0.71
DE SAT	0.10	0.77	1	0.06	0.67	0.83	0.87
NA 40-60	0.55	0.30	0.06	1	0.36	0.24	0.06
NS SST	0.30	0.73	0.67	0.36	1	0.86	0.72
HR SST	0.26	0.75	0.83	0.24	0.86	1	0.87
SR SST	0.09	0.71	0.87	0.06	0.72	0.87	1
AMO	0.48	0.14	-0.11	0.80	0.18	0.06	-0.11

Previous studies considered AMO to be related to e.g. rainfall patterns and fish stocks (Alheit et al., 2014; Frajka-Williams et al., 2017). We also considered the AMO data, and its relationships are presented in the bottom line of the correlation matrix in Table 2.2. Correlations of temperature anomalies with AMO were small, except, unsurprisingly, when related with the NH ST and with the NA SST. The AMO and NA SST data sets overlap, partly consisting of the same data. The correlation between HR SST anomalies and the AMO was smaller than between HR SST anomalies and NA SST. This is because the tropical latitudes below 40° N are not included in the latter. Thus, henceforth we concentrated on the NA SST rather than the AMO in all future comparisons with the Northern Atlantic. All cross-correlation values in Table 2.2 are significant as they are above the 95% confidence levels of uncorrelated white noise.

2.3.2 Seasonal patterns

The temperate climate zone is characterised by clear seasonality, which defines growth periods both in terrestrial and marine systems. Having established the cross-correlative relationships between the data from small to large-scale areas, the next step was to calculate and understand the seasonal cycle and the anomalies. We concentrated on different time scales, starting with seasonality of the in situ LTOs. Thus, we next focused on to understanding variability of the two stations over the past 58 years. Only the results based on the in situ temperature measurements are presented. The sea surface temperature for the data sets were evaluated and show large and variable seasonal evolution (See example in Figure 2.5). The variability of the winter minimum displays a much stronger variability than the summer maximum.

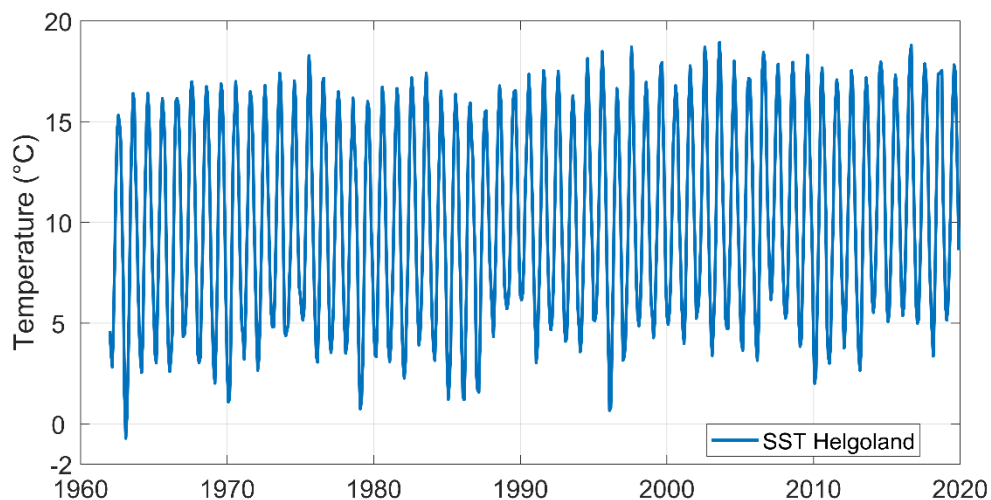


Figure 2.5: Evolution of the sea surface temperature including seasonality as an example: Helgoland Roads.

When the densities/frequencies of the temperature anomalies for all data sets are resolved, two peaks manifest with bunches (=longer duration of SSTs) of cold temperatures around the winter minimum and warm temperatures around the summer maximum (Figure 2.6). These peaks represent the time just before and after the winter minimum and the summer maximum. The density curves suggest that the cold peak around the winter is slightly larger compared with that of the summer for both HR and SR. This reflects the slightly longer winter season compared to summer at these latitudes. The corresponding seasonal cycles of HR and

SR are shown in Figure 2.7. A smaller curvature of the winter minimum values compared to the summer maximum values is apparent. The winter season is clearly longer by approx. half a month. The winter minimum temperatures at Sylt are colder and the summer temperatures are warmer compared with Helgoland. This, also the difference in timing of the start of spring/summer between the two sites, reflects the shallow water coastal site at Sylt, vs. the offshore water site at Helgoland.

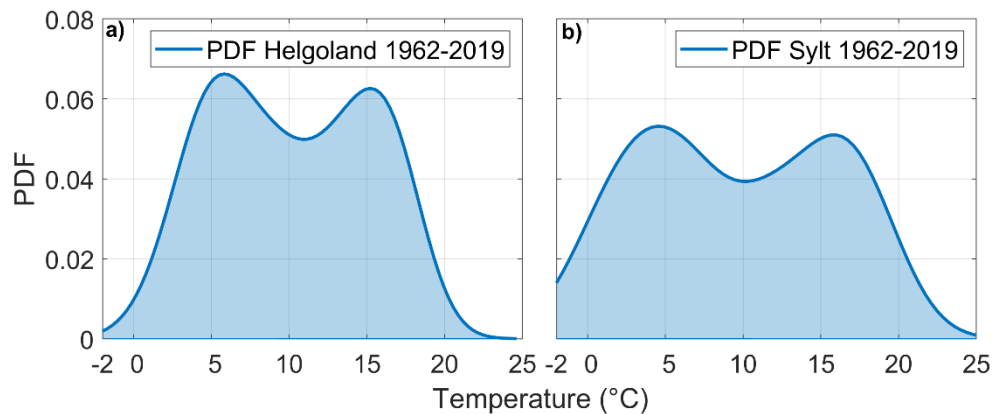


Figure 2.6: Probability density function curves of sea surface temperatures at a) Helgoland Roads and b) Sylt Roads calculated using Kernel Density Estimates. For a) and b), the x-axis was limited to 2 °C because lower temperatures are an artefact of the PDF.

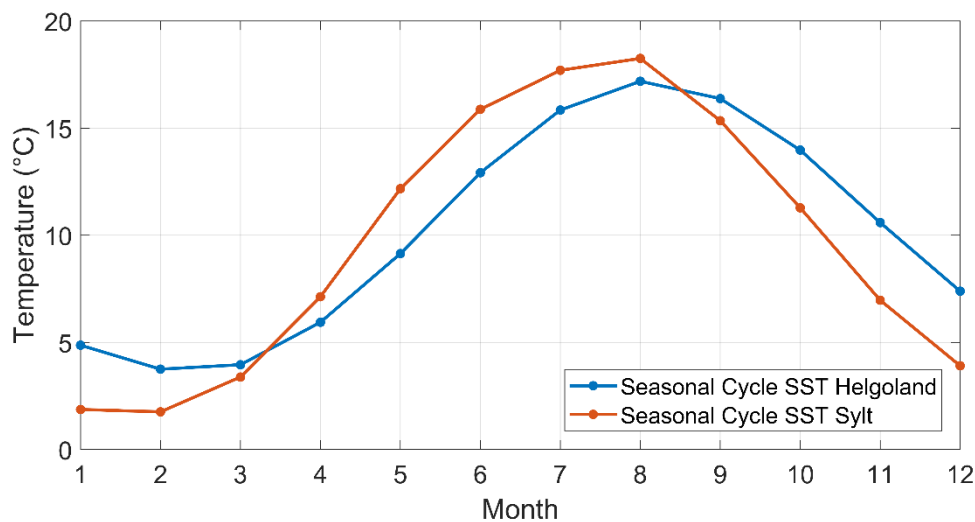


Figure 2.7: Seasonal cycles for the SST at HR (blue) and SR (orange) for the entire time series.

Examination of the NA, NS, HR and SR SST anomalies, and as exemplified by HR and SR in Figure 2.8, indicated positive temperature trends for both summer and winter. The trends for winter and summer were calculated and are presented in Table 2.3 with their associated R^2 (Pearson) coefficient. The analyses revealed that whereas the summer trends are similar in all regions, the winter trends are much larger for the two stations Helgoland Roads and Sylt Roads (reduced cold continental influence in winter) (Table 2.3). A trend of 0.3 °C/decade for both seasons was registered for HR (Figure 2.8a). At the shallow water site SR (Figure 2.8b), the summer warming trend was slightly less than for winter.

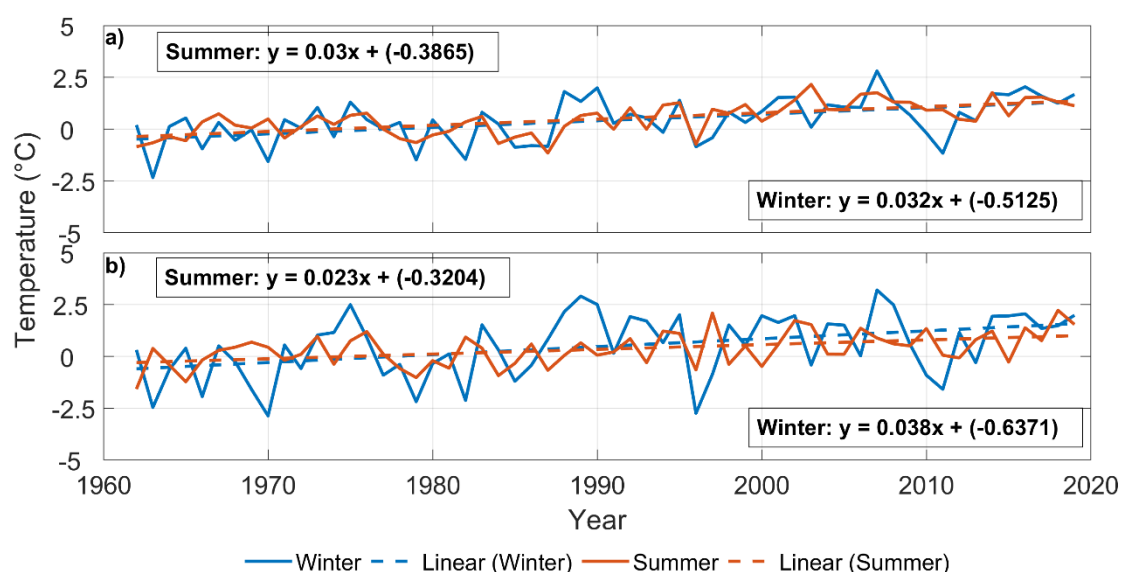


Figure 2.8: Temporal evolution and trend of the SST anomalies at a) Helgoland Roads and b) Sylt Roads in summer mean (June-August) (solid orange line) and summer linear trend (dashed orange line), winter mean (December-February) (solid blue line) and winter linear trend (dashed blue line).

Table 2.3: SST anomalies trends in °C/decade in summer and winter. The value in brackets is the associated R^2 (Pearson) coefficient.

Region	North Atlantic	North Sea	Helgoland Roads	Sylt Roads
Summer	0.26 (0.66)	0.25 (0.40)	0.30 (0.44)	0.23 (0.22)
Winter	0.13 (0.44)	0.17 (0.27)	0.32 (0.26)	0.38 (0.18)

2.3.3 Temperature variability in first and second half of the Time-Series

Having evaluated the seasonality, we next turn again to the analyses of the temperature variability, described by the temperature anomalies time. Again, although we calculated these for all data sets in Section 4.3.1, only the results from NS, HR, SR and YS are depicted here as 12-month running means (Figure 2.9). We kept the y-axis in the same scale for better comparison.

The SST anomalies were mostly negative with a small trend until the late 1980s for NA (not shown), NS, HR, and SR, and mostly positive with a larger positive trend thereafter. Figure 2.9a,b,c clearly shows this for NS, HR and SR and this is also aligned with similar evolution found in the European and German surface air temperature anomalies (Figure 2.4).

In order to check whether this was a phenomenon only related to the Northern Atlantic, we searched for other shelf seas comparable with our focus region. The only comparable one, considering latitude limits and bathymetry, was the Yellow Sea (YS) time series. We found the same pattern, which is depicted in Figure 2.9d below. The overall temperature trend for the YS was calculated $0.16\text{ }^{\circ}\text{C}/\text{decade}$ and $0.9\text{ }^{\circ}\text{C}/57\text{ years}$ for the whole period 1962–2019, with a warming rate of $0.12\text{ }^{\circ}\text{C}/\text{decade}$ vs. $0.13\text{ }^{\circ}\text{C}/\text{decade}$ in winter vs. summer months, respectively.

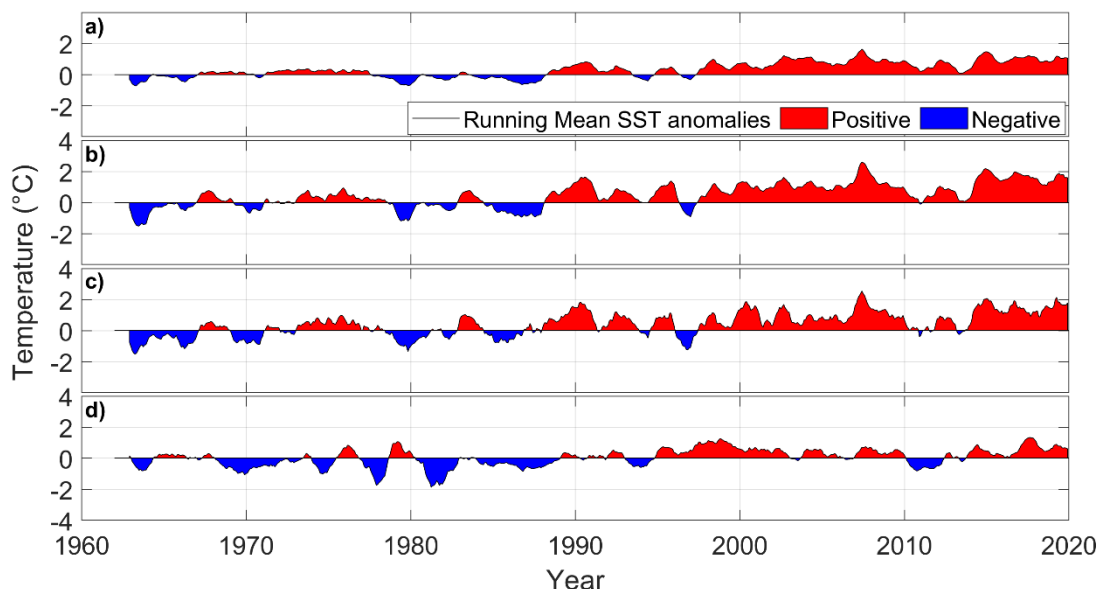


Figure 2.9: Twelve-month running mean SST anomalies (black curve). Blue, negative anomalies and red, positive anomalies, respectively. a) NS, b) HR, c) SR and d) YS. It is clear the dominant positive pattern after the end of 1980s.

The interesting difference between first and second half indicated that an evaluation of the time series in terms of early and recent (late) years separately was necessary. Thus, to avoid bias due to visual interpretation, we simply divided the data series into two halves, from 1962 to 1990 and from 1991 to 2019. We then applied analytical statistics for comparison of early and late years. The anomalies showed distinct differences between these two periods, which were then, examined in detail.

2.3.4 Long-Term changes in SST distributions

Starting with an analysis of the frequency of temperature distribution in the first and second part of the time series, an increase in the occurrence of warmer temperatures during winter was seen in all data sets. In Figure 2.10, we show the temperature distribution by period at HR and SR, showing the dislocation of the two lobes peaks (cold and warm modes) representing winter and summer, towards higher temperatures. For both HR and SR, the first half of the time series shows nearly perfectly symmetric distributions (Figure 2.10a and Figure 2.10b, respectively), with peaks around the mean minimum and maximum. In the second half of the time series, the two modes are still visible, but the cold mode is slightly larger than the warm mode. This must be due to the change in the seasonal cycle: the mean minimum in the second half is a little higher and the curvature is steeper, and the mean maximum is a little lower and the curvature is flatter. Because of this change, more values occur around the cold mode and less values around the warm mode, spreading to higher-than-average values.

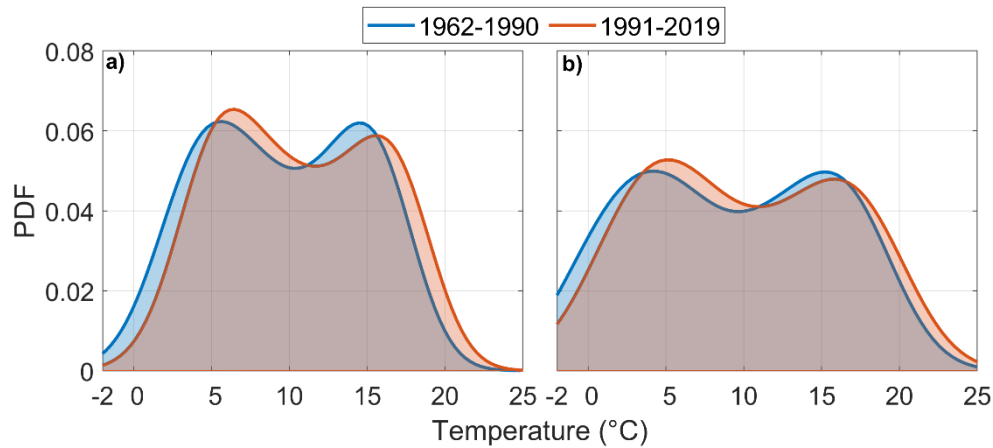


Figure 2.10: Distribution of the sea surface temperature at a) Helgoland Roads and b) Sylt Roads, in terms of probability density function, for the first (blue) and second (orange half of the time series. The curves show the bimodality originated from seasonality and the shift when comparing early and late years. For a) and b), the x- axis was limited to 2 °C because lower temperatures are an artefact of the PDF.

The HR and SR temperature histograms are shown in Figure 2.11 and it is possible to observe that temperature distributions have shifted in the later years for both. At Helgoland the distinctive bi-seasonal bimodal shape is still clear, but the peak intervals in winter and summer increased by 1 °C, showing an increase in maximum temperature values. In the shallow inshore waters around Sylt, the seasonal signal has become more homogeneous, as intermediate temperature intervals became enhanced. The low temperature range peak increased also by 1 °C, with a decrease in the counts for the lowest temperature range. These observations underpin the results on the observed long-term shifts in seasonality as presented in Section 3.2. Consideration of the SST anomalies in the North Atlantic, North Sea, HR and SR showed that the temperature density distribution clearly shifted to higher temperatures in the later years in these areas (Figure 2.12).

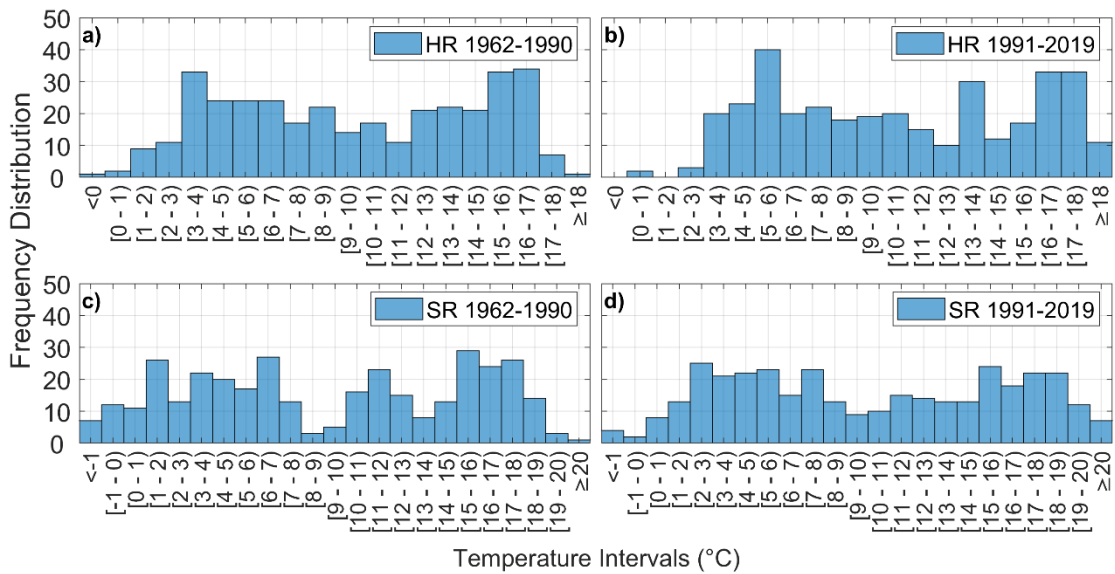


Figure 2.11: Frequency of occurrence of temperatures at HR and SR. a) HR SST histogram for the period 1962–1990 and b) HR SST 1991–2019. c) SR SST histogram for the period 1962–1990 and b) SR 1991–2019. The bins are defined as 1 °C intervals, except for the edges. Note the difference in temperature intervals for HR and SR.

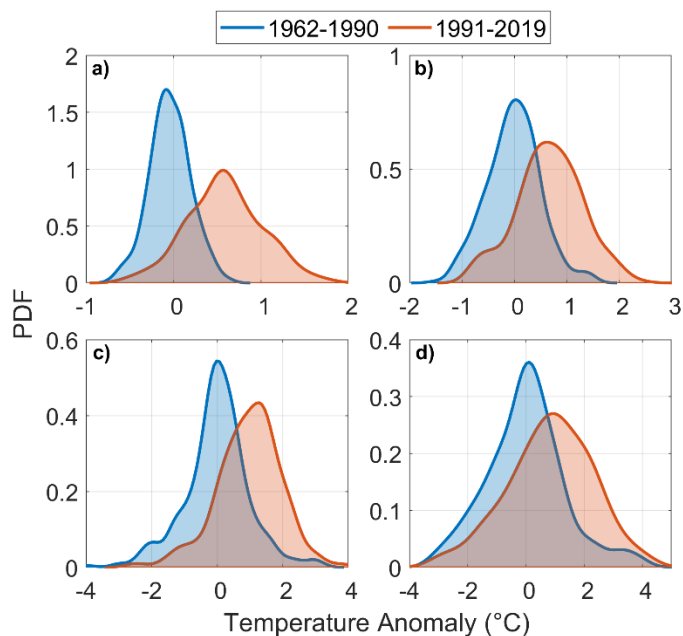


Figure 2.12: Probability Density Function (PDF) of sea surface temperature anomalies in the first (blue) and second (orange) half of the time series for the a) NA, b) NS, c) HR and d) SR.

2.3.5 Seasonal means and trends

It seems that the most pronounced difference between the first and the second half of the time series occurs around the winter minimum and the summer maximum (Figure 2.10). Thus, we examined the seasonal means and trends of the two sections of time series and the analyses showed that actually all seasons are affected. This can be seen in Figure 2.13 to Figure 2.16 and in all the trend values in Table 2.4 (HR) and Table 2.6 (SR).

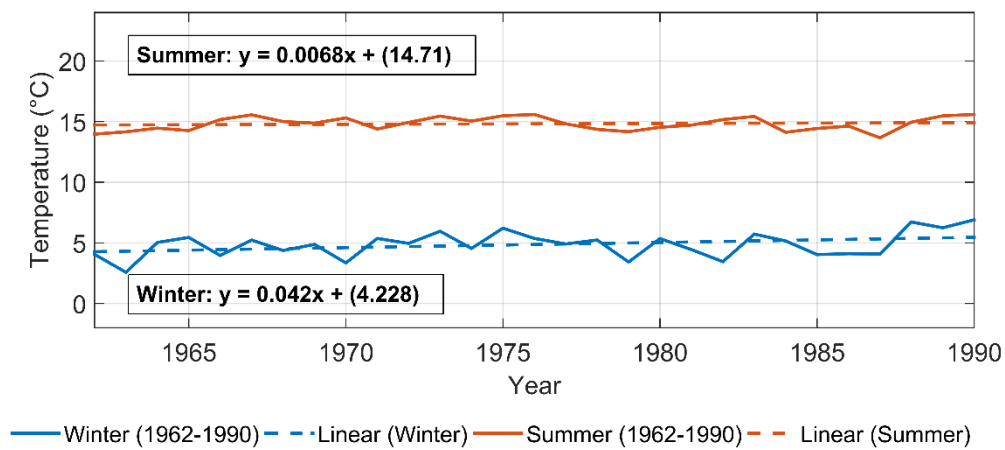


Figure 2.13: Trends of the summer (dashed orange line) and winter seasons (dashed blue line) mean temperatures at HR for the first half (1962–1990) of the time series.

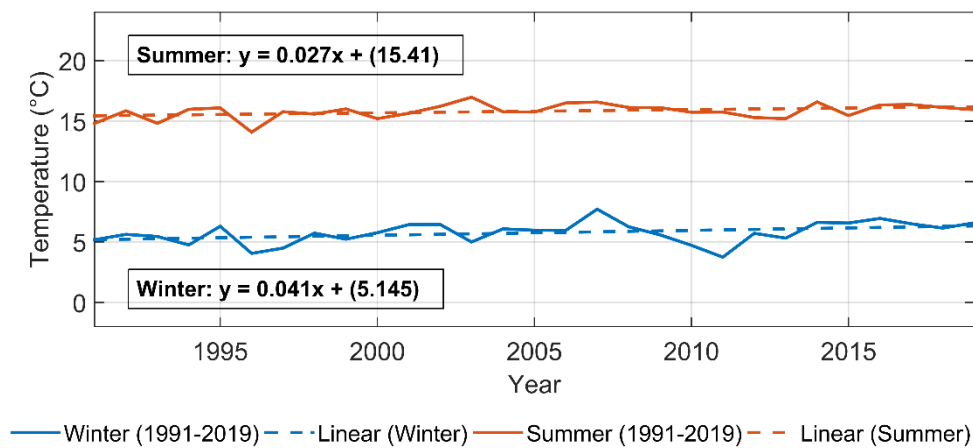


Figure 2.14: Trend of the summer (dashed orange line) and winter seasons (dashed blue line) mean temperatures at HR during the second half (1991–2019) of the time series.

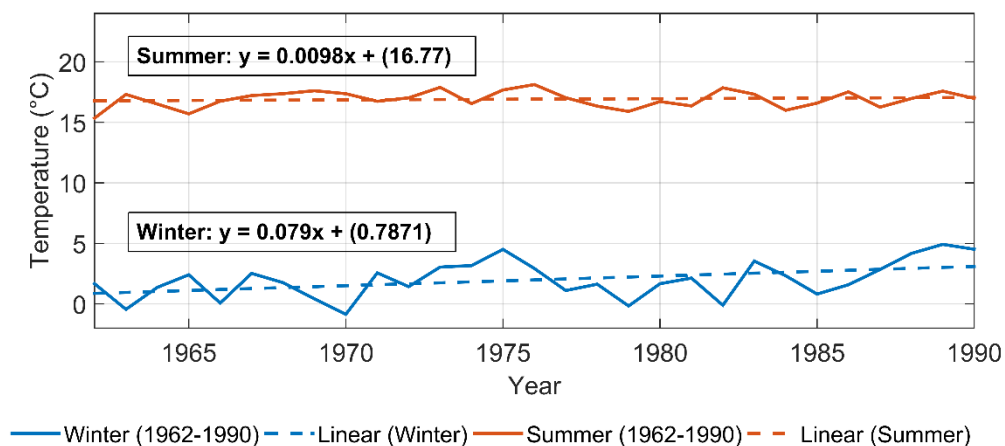


Figure 2.15: Trends of the summer (dashed orange line) and winter seasons (dashed blue line) mean temperatures at SR for the first half (1962–1990) of the time series.

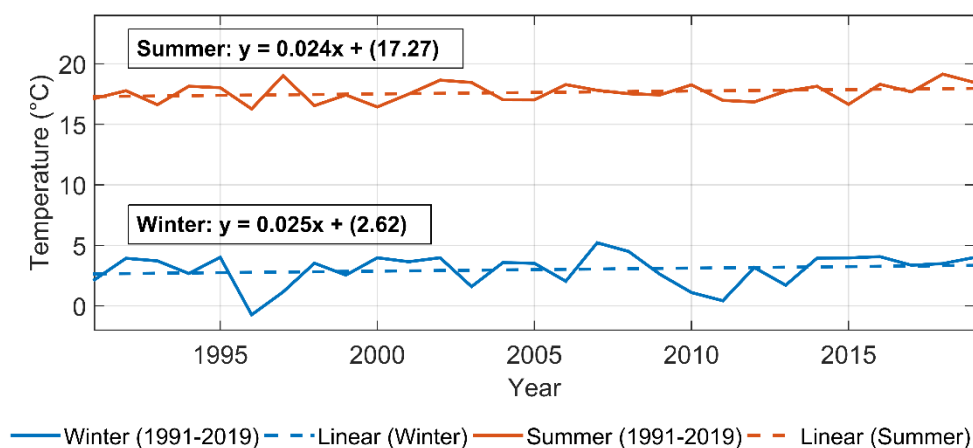


Figure 2.16: Trend of the summer (dashed orange line) and winter seasons (dashed blue line) mean temperatures at SR during the second half (1991–2019) of the time series.

In both Helgoland and Sylt Roads, the summer long-term trends increased after 1990 (Figure 2.13 to Figure 2.16), and the intercepts increased by roughly 1 °C in both winter and summer in the late years, indicating the increase in SST means for these locations. In Table 2.4 and Table 2.5, the changes in the SST trends and means at Helgoland Roads and the difference between the first and the second half of the time series are summarized for all seasons. The associated R^2 (Pearson) coefficient, is also provided. In Table 2.6 and Table 2.7, we summarize

the same results for the Sylt Roads. It is clear from Table 2.5 and Table 2.7 that the mean seasonal SST were significantly higher in late years compared to the early years, especially in spring and summer (>1 °C) at HR and SR. However, when it comes to the trends (Table 2.4 and Table 2.6), these were steeper especially in autumn, compared to the summer period in the late years.

Table 2.4: Annual and seasonal trends of SST in °C/period at Helgoland Roads for the entire period, the first and the second half of the time series for the different seasons. The values in brackets are the associated R^2 (Pearson) coefficient, which indicates how much of the variance is explained by the trend.

Season Period	Spring	Summer	Autumn	Winter	Annual mean
1962-2019	0.405 (0.28)	0.307 (0.45)	0.265 (0.37)	0.335 (0.29)	0.335 (0.48)
1962-1990	0.372 (0.08)	-0.068 (0.01)	-0.006 (0.0001)	0.423 (0.12)	0.243 (0.10)
1991-2019	0.293 (0.05)	0.291 (0.16)	0.541 (0.35)	0.407 (0.15)	0.361 (0.24)

Table 2.5: Mean annual and seasonal SST in °C at Helgoland Roads for the complete period (A 1962-2019), the first half (B 1962-1990) and the second half (C 1991-2019) of the time series. The difference of the late data from the early data (C-B) is presented, as it is significantly positive for all seasons and the whole period.

Season Period	Spring	Summer	Autumn	Winter	Annual mean
A 1962-2019	6.35	15.32	13.63	5.31	10.29
B 1962-1990	5.73	14.82	13.25	4.86	9.79
C 1991-2019	6.97	15.83	14.02	5.76	10.79
Difference: C-B	1.24	1.01	0.77	0.90	1.00

Table 2.6: Annual and seasonal trends of SST in °C/period at Sylt Roads for the entire period, the first and the second half of the time series in the different seasons. The value in brackets is the associated R^2 (Pearson) coefficient, which indicates how much of the variance is explained by the trend.

Season Period	Spring	Summer	Autumn	Winter	Annual mean
1962-2019	0.406 (0.32)	0.228 (0.22)	0.202 (0.16)	0.393 (0.19)	0.307 (0.44)
1962-1990	0.683 (0.28)	0.098 (0.01)	-0.083 (0.02)	0.795 (0.19)	0.365 (0.23)
1991-2019	0.357 (0.08)	0.240 (0.07)	0.611 (0.27)	0.250 (0.03)	0.369 (0.21)

Table 2.7: Mean annual and seasonal SST in °C at Sylt Roads complete period (A 1962-2019), the first half (B 1962-1990) and the second half (C 1991-2019) of the time series. The difference of the late data from the early data (C-B) is presented, as it is significantly positive for all seasons and the whole period.

Season Period	Spring	Summer	Autumn	Winter	Annual mean
A 1962-2019	7.56	17.27	11.20	2.49	9.64
B 1962-1990	7.03	16.92	10.93	1.98	9.22
C 1991-2019	8.10	17.63	11.46	2.99	10.05
Difference: C-B	1.07	0.71	0.53	1.01	0.83

2.3.6 Seasonal variability

In order to assess potential shifts in seasonal variability of temperature at the HR and SR sites, we evaluated the seasonal variability of the standard deviation, i.e. we calculate the standard deviation of all Januaries, Februaries, etc. for the total time series and its early and late halves (Figure 2.17).

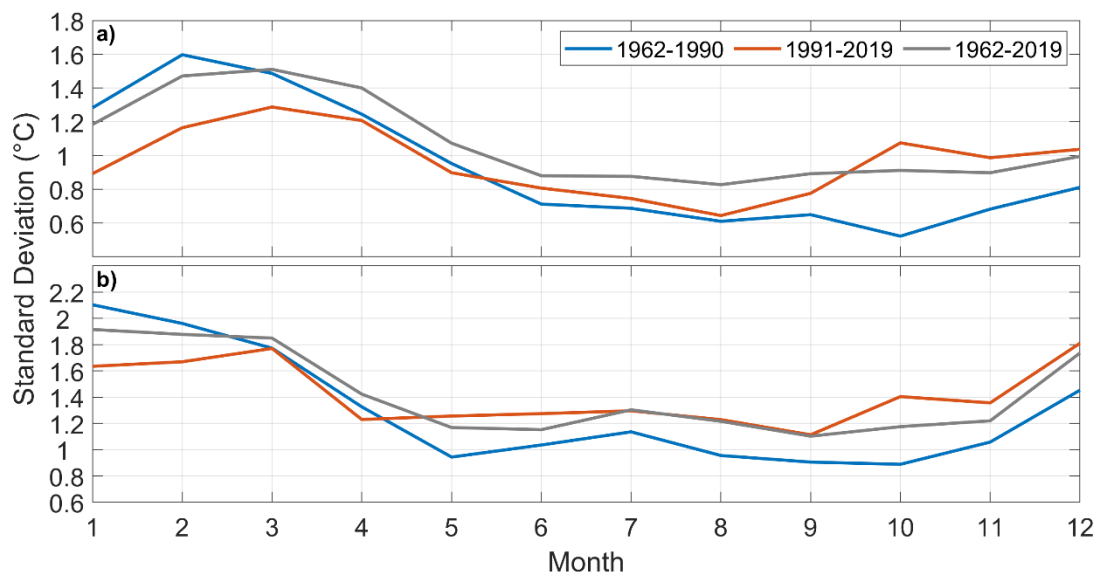


Figure 2.17: The seasonal variation of the standard deviation of the SSTs at a) Helgoland Roads and b) Sylt Roads for the entire time series (grey) and for the first (blue) and second half (orange).

The variability during the winter and spring months was found to be significantly larger than during summer and autumn at both HR and SR. This is especially true for the early half of the time series. In the second half of the time series, the large winter variability has become smaller and the autumn variability has become larger. The same pattern (depicted in Figure 2.25 of the 4.4 Discussion) was found for the North Sea data. However, the data sets for the North Atlantic showed a clear increase in temperature variability for all months since 1991. The Northern Hemisphere and global data sets also show increases in variability in the later years for all months, but with a significantly smaller amplitude.

From Figure 2.17, it is clear that the seasonal variability of temperature is different between the first and the second half of the time series. In order to assess how it changes with time, we computed the standard deviation of all months within each year. With this calculation of the seasonal variance, we obtained a measure of the strength of the seasonal amplitude. The results for HR and SR are shown in Figure 2.18, and indicate a negative trend in the amplitude of the seasonal cycle.

This means that the seasonal cycle became smaller in magnitude over time, also shown in Table 2.4 to Table 2.7. For Helgoland, the difference of the mean between the warm seasons

(summer, autumn) and the cold seasons (winter, spring) is 8.74 °C in the first half of the time series and 8.56 °C in the second half, i.e. a reduction of the seasonal cycle by 0.2 °C (Table 2.5), consistent with the trend indicated in Figure 2.18a. At SR, the reduction of the seasonal cycle between the first half and the second half of the time series is larger at 0.4 °C (Table 2.7). Overall, it is clear that the seasonal variability and, concomitantly, the seasonal amplitude has shifted considerably, becoming less in winter and more in autumn; manifesting especially as a reduction of the definite seasonality, both at the open water site at Helgoland and in the shallow Wadden Sea site of Sylt.

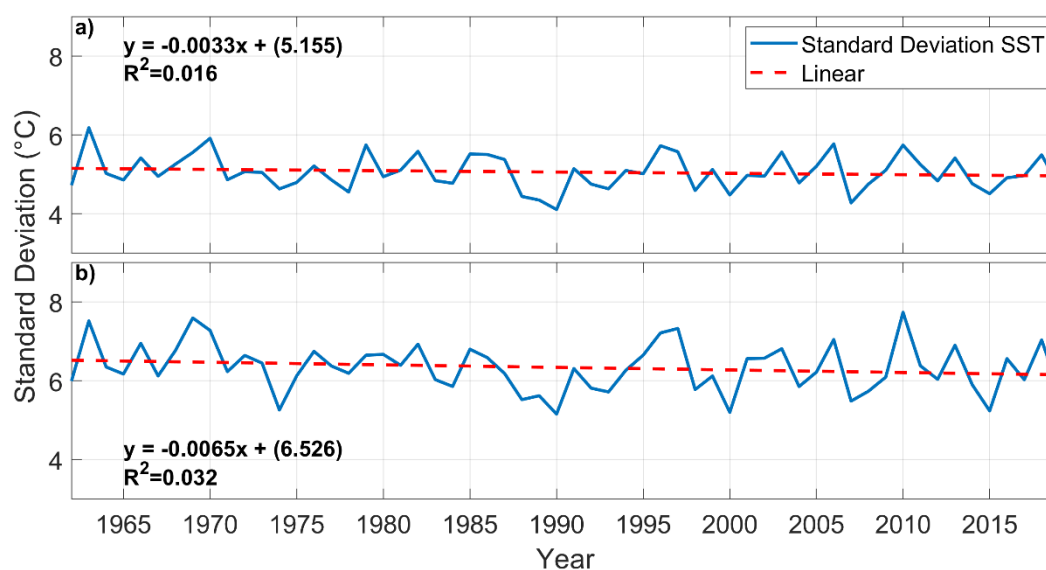


Figure 2.18: The seasonal standard deviation (solid blue line) with trend (dashed red line) – a measure of the seasonal amplitude – at a) Helgoland Roads and b) Sylt Roads, calculated per year using monthly SST in situ datasets.

2.3.7 Assessment of temperature extremes

The determination of the shifts as the occurrence of low and high temperatures is very important for the assessment of ecological conditions. Thus, the data evaluation relative to maximum and minimum temperatures are presented here. The evaluation of the number of “cold” months and “warm” months based on minimum and maximum thresholds shows large change between the early and late years. Helgoland Roads, an exposed open water site, showed minimum cold thresholds of mean monthly temperatures < 2 °C and < 3 °C. The maximum warm thresholds at HR were mean monthly temperatures > 17 °C and > 18 °C. The number of

months with mean values above/below these thresholds is shown in Figure 2.19. It can clearly be seen that there has been a significant shift towards very many warm months with values over 17 °C and 18 °C at Helgoland Roads since 1991. The very cold months (mean values below < 2 °C and < 3 °C) have become significantly less common. The percentages of the mean number of cold and warm months relative to the total number of months of the different time periods are given in Table 2.8. The percentage of months with mean temperatures below 3 °C has gone down from 6.6 % to 1.4% of the total months in the early/ late years, respectively. At the same time, the percentage of months with mean temperatures above 17 °C has gone up from 2.3 % to 12.4 % of the total months in the early/ late years, respectively. Sylt Roads, the shallow water Wadden Sea site, showed minimum cold thresholds of mean monthly temperatures < 1 °C, < 2 °C and < 3 °C. The SR maximum warm thresholds were mean monthly temperatures > 17 °C and > 18 °C. The number of months with mean values above/below these thresholds is presented in Figure 2.20 for SR. It is obvious that there has been a significant shift towards more warm months at Sylt since 1991 and the very cold months (mean values below < 2 °C and < 3 °C) have become significantly less (for percentages of total, see Table 2.9). For example, the percentage of months with mean temperatures below 2 °C has gone from 16.6% to 7.8% of the total months in the early/ late years, respectively. At the same time, the percentage of months with mean temperatures above 17 °C has gone up by over 6% of the total months in the early/ late years at Sylt Roads. It is interesting to note that these data clearly show that the sites at Helgoland and Sylt, because of their different hydrographic situation (i.e. open North Sea vs. shallow Wadden Sea), have different temperature extremes. Sylt water heats up faster and cools down more. On the long run, it may be expected that this difference will become even more pronounced.

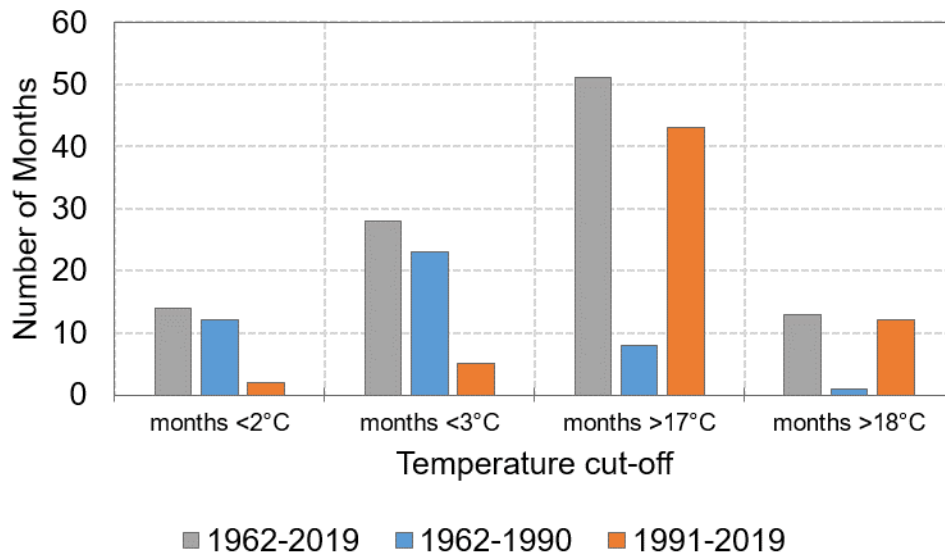


Figure 2.19: Number of “cold” and “warm” months for total (grey), early (blue) and late years (orange) of the Helgoland Roads data set.

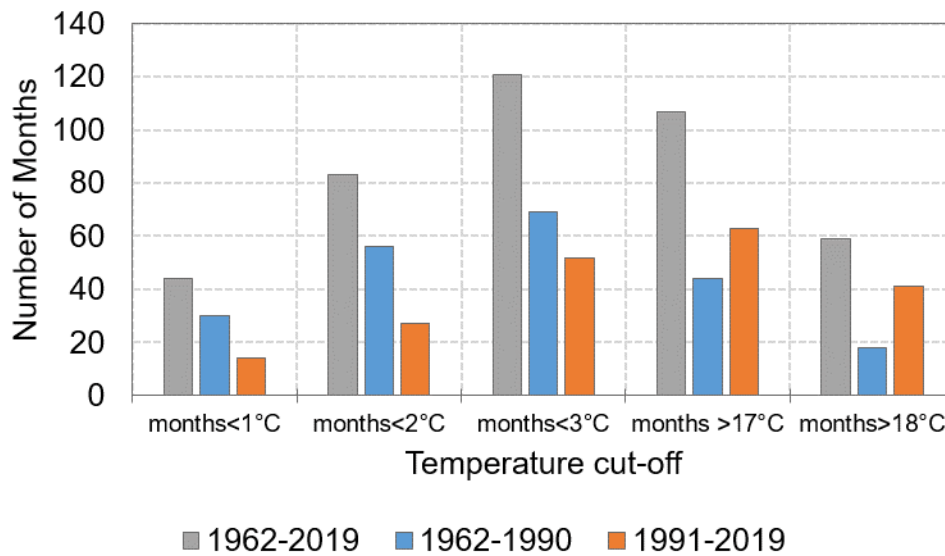


Figure 2.20: Number of “cold” and “warm” months for total (grey), early (blue) and late years (orange) of the Sylt Roads data set.

Table 2.8: Percentages of the mean number of cold and warm months relative to the total number of months of the late and early time periods at Helgoland Roads (HR).

HR %	1962-2019	1962-1990	1991-2019
months <2°C	2.0	3.4	0.6
months <3°C	4.0	6.6	1.4
months >17°C	7.3	2.3	12.4
months >18°C	1.9	0.3	3.4

Table 2.9: Percentages of the mean number of cold and warm months relative to the total number of months of the late and early time periods at Sylt Roads (SR).

SR %	1962-2019	1962-1990	1991-2019
months <1°C	6.3	8.6	4.0
months <2°C	11.9	16.1	7.8
months <3°C	17.4	19.8	14.9
months >17°C	15.4	12.6	18.1
months >18°C	8.5	5.2	11.8

2.3.8 Relationship of the North Atlantic Oscillation (NAO) and temperature

Evaluation of how the NAO relates to temperature data in the Northern Hemisphere is of importance and is often used in the ecological literature. The NAO only relates well to the winter temperatures (December-February) because the difference between the two pressure systems that characterizes the NAO index are more pronounced during winter months (Rodwell et al., 1999). From previous analyses of North Sea data (Wiltshire et al., 2010; Lohmann & Wiltshire, 2012), it was clear that NAO index was also only useful for explaining variability in the North Sea winter temperatures. After checking that indeed the temperature of the summer months at HR and SR barely correlated with the NAO, we concentrated on the winter months.

The analysis of the Hurrell winter NAO index (December to February means) from the first principle component (PC) as per web download, is depicted in Figure 2.21.

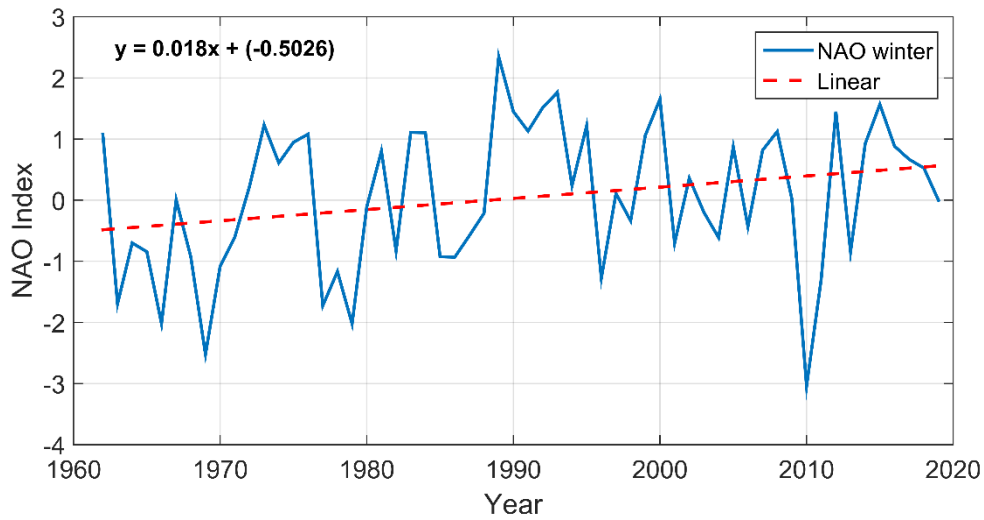


Figure 2.21: First PC Winter mean NAO evolution over time (solid blue line) with linear trend (dashed red line).

In the PC NAO, there is a positive trend toward positive NAO (more frequent westerly winds and warmer temperatures in winter in Europe) (Trigo et al., 2002). As can be seen from the histograms in Figure 2.22, in the first half of the time series there are 7 years with strongly negative values (<-1), and in the second half there are only 3 years with strongly negative values (equivalent to a smaller number of cold winters). The correlation analyses of temperature with the NAO was highly significant for all the data sets except the North Atlantic data set. This was the case for all years and both early and late years (Table 2.10).

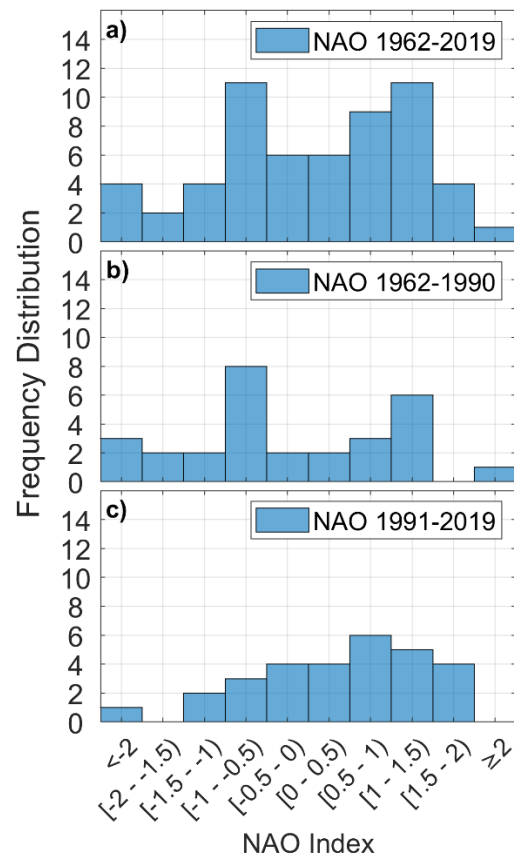


Figure 2.22: Frequency of occurrence of winter mean (Dec-Feb) NAO index values for the whole period (1962–2019, top), early (1962–1990, middle) and late (1991–2019, bottom) years.

Table 2.10: Significance of detrended SST anomalies and NAO correlation (Pearson) for different regions and the stations HR and SR showing all (1962-2019), early (1962-1990) and late (1991-2019) years. Winter mean considers December, January and February months. NA - North Atlantic (40°-60° belt); NS - North Sea; HR - Helgoland Roads and SR - Sylt Roads.

Period	1962-2019				1962 – 1990				1991 – 2019			
	NA	NS	HR	SR	NA	NS	HR	SR	NA	NS	HR	SR
Winter mean	-0.10	0.41	0.54	0.73	-0.13	0.49	0.57	0.78	0.05	0.43	0.54	0.69
Significance		***	***	***		***	***	***		***	***	***
p-values	0.478	0.001	0.000	0.000	0.512	0.008	0.001	0.000	0.788	0.020	0.002	0.000

2.3.9 Summary of results

Table 2.11: Overall summary of Results.

Trends:	Summary
All areas HR & SR	Trends were significantly positive for all surface temperature anomalies data sets examined.
Correlation all areas	Of all, HR and SR showed highest warming trend of 0.3°C/decade.
Correlations HR & SR	All data sets were significantly correlated with each other. HR and SR are most correlated with EU and GE temperature anomalies time series.
AMO HR & SR (early vs late years)	AMO was found to be unsuited for comparisons and was replaced by NA SST. Trends have increased significantly in late years.

Table 2.11: Overall summary of Results, Continued.

<p>Seasonal Analyses:</p> <p>HR & SR Frequency distributions</p> <p>Comparison all areas</p> <p>Winter vs Summer</p> <p>HR SR</p> <p>Variability HR & SR (early vs late years)</p>	<p>Summary</p> <p>Strong seasonal cycle, increased mean in late years (warmer temperatures earlier in time).</p> <p>Bimodal frequency distribution of temperature (cold and warm modes) becoming more heterogeneous, with the cold mode peak moving to higher values and becoming steeper.</p> <p>Summer trends are similar, winter trends much larger for HR & SR (lower thermal inertia compared to deeper and larger areas).</p> <p>Winter peaks larger than summer for both HR & SR = slightly longer winter season.</p> <p>HR seasonal cycle reflects open water situation with modulated winter and summer temperatures.</p> <p>SR seasonal cycle reflects shallow water situation, higher variance between winter and summer.</p> <p>Variability of winter minima displays greater variability than the summer maxima.</p> <p>Late years: winter variability became smaller and autumn variability became larger. For both sites, the seasonal standard deviation (i.e. the seasonal amplitude) decreased with time.</p>
<p>Anomalies:</p> <p>All areas</p> <p>Comparison Yellow Sea (YS)</p> <p>NAO all areas except NA</p>	<p>Summary</p> <p>SST anomalies had a strong positive trend after the 1980s. Clear separation of early and late years. Late years warmer.</p> <p>Clear separation of early and late years. Late years warmer.</p> <p>Winter NAO highly correlated with winter anomalies.</p>
<p>Temperature</p> <p>Extremes:</p> <p>HR & SR warmest months</p> <p>HR & SR coldest months</p>	<p>Summary</p> <p>Highly significant shift towards more warm months with mean values over 17°C.</p> <p>Very cold months (means <2°C and <3°C) decreased frequency.</p>

2.4 DISCUSSION

In this study, we have critically considered long-term temperature data sets on increasing spatial scales: from local, regional, continental, oceanic to hemispheric, in order to investigate the different trends, frequencies, variability and correlations when moving from small to large temporal and spatial scales. We report on analyses carried out relating the sea surface temperature (SST) data from the Helgoland Roads Time Series, one of the most important and detailed long-term in situ marine ecological time series, to the Sylt Roads, North Sea, Germany, Europe, North Atlantic and Northern Hemisphere surface temperatures. The following discussion of these findings is directed to the needs of biologists using long-term data of marine temperature in conjunction with considerations on effects of temperature shifts, events, and variabilities on ecosystems, biodiversity, species adaptation, etc., over many different temporal and spatial scales.

In studies on the effects of changing temperature in temperate marine environments, such as the North Sea, one must consider shifts in a) long-term trends over decades, abrupt regime shift-like and relationships with greater global ocean drivers (e.g., AMO; NAO; b) seasonality; c) shifts in max/min temperatures and frequencies, and d) changes in variability of temperature, which need to be primarily considered in terms of changed biology and ecosystems. Above, we analysed the overall temperature trends, anomalies, seasonal shifts, variabilities and frequency distributions, frequency of occurrence of extremely hot and cold temperatures and the relationship of the temperature measurements with the climate index NAO. For completeness, we also considered the AMO index in the context of the time series.

The impacts of warmer ocean waters on marine organisms are one of the biggest scientific topics of our time and have been subject of many studies over the past two decades (Wiltshire & Manly, 2004; Lima & Wethey, 2012; Gittings et al., 2018; Jorda et al., 2019; Fellous et al., 2022). The need for scenario development and management strategies is pivotal to Earth System sustainability. For this, dense long-term data and an excellent understanding of this data are required; otherwise, modelling of systems and scenarios is impeded. However, most studies on how global warming manifests with regard to marine organisms are laboratory or, more rarely, in situ habitat observations during/after weather extremes. When it comes to direct in situ causal linkage of temperature shifts in the ocean and long-term shifts in ecosystems, this has proven difficult simply because the relevant long-term measurements are not available on the appropriate temporal and spatial scales, and those available are not

temporally and spatially dense enough. Datasets based on LTER at one site can be considered under-representative of a region and the only data sets, which are spatially available, are often interpolative in terms of both space and time. Remote sensing data, with around 40 years of surface temperature measurements, is an efficient option to represent temporal and spatial changes, but it is still constrained by biases in sensors and retrieval algorithms, in addition to the lack of agreement between the products of different satellite missions (Yang et al., 2013). Reanalysis products give robust information combining different observations from multiple sources, including remote sensing, and they are spatially complete, physically consistent and bias adjusted (Dee et al., 2014).

In this study, we place our findings, which are summarised in Table 2.11, in the marine ecological context and deliberate these in terms of time and space, as scale plays a fundamental role when linking drivers to ecosystem function, species distributions and biodiversity (Margalef, 1958). When considering habitat and population resilience in the context of drivers of change, such as temperature and particularly when based on observations, understanding scale in terms of time and space is paramount. Without this, the evaluation of temperature to ecosystem relationships, predictability and for example models of climate with biological relationships are tenuous (Mackas et al., 1985; Addicott et al., 1987; Levin, 1992; Peterson & Parker, 1998; Steele, 2004). With changes in scale, statistical relationships and correlations can change. Variability, at lower scales, can show a lot of noise and at high spatial scales a lack of detail.

Observations, which are made too far apart (in space or time), can result in one missing essential ecosystem detail such as life cycle information or diel vertical migration patterns. Observations, which are too close together (in space or time) might merely, reflect a moment of variability rather than being related to the big picture. Moreover, environmental and ecosystem variables and especially different species with differing adaptations, drivers and niches may not be intercomparable in terms of time and spatial scales. Mackas et al. (1985) showed that in a one-dimensional transect of the North Sea temperature, chlorophyll and zooplankton had very different variabilities and thus, obviously were controlled by different drivers. The complexity of interrelating different species, which have widely different spatial ranges and different patchiness, is well illustrated by Bertrand et al. (2014). The very basis of organism succession, competition and cooccurrence in pelagic temperate environments is based on different scaling in time and space of organisms. Temperature related match-mismatch phenomena (Cushing, 1990) between predators and their prey however, are founded

up on the opposite situation, as the organisms are dependent on the exact timing of their prey. Similarly, diurnal migration of for example zooplankton is also very dependent on timing related to light and stable/ particular triggers on mesoscales. Obviously, there is no one overarching dimension in space or time, which is applicable to all ecosystem questions related to temperature. For example, if scales in time and space in terms of temperature trends are too large, one loses life cycle details (time) or patterns related to local climatic conditions in one's considerations. If, on the other hand, one merely considers effects of temperature on ecosystems and their components, e.g., using short-term or local observations of temperature for future scenarios, these may simply reflect small-scale variability of the system. To paraphrase Levin (1992) "we trade off the loss of detail or heterogeneity within a group for the gain of predictability".

To summarize, marine pelagic ecosystems and their species are subject to temperature on different scales in time and space, with temperature being one of the main drivers of species diversity and distribution. We have summarized the relationships of the biology of marine systems to temperature on different temporal and spatial scales in Figure 2.23, which underpins this discussion.

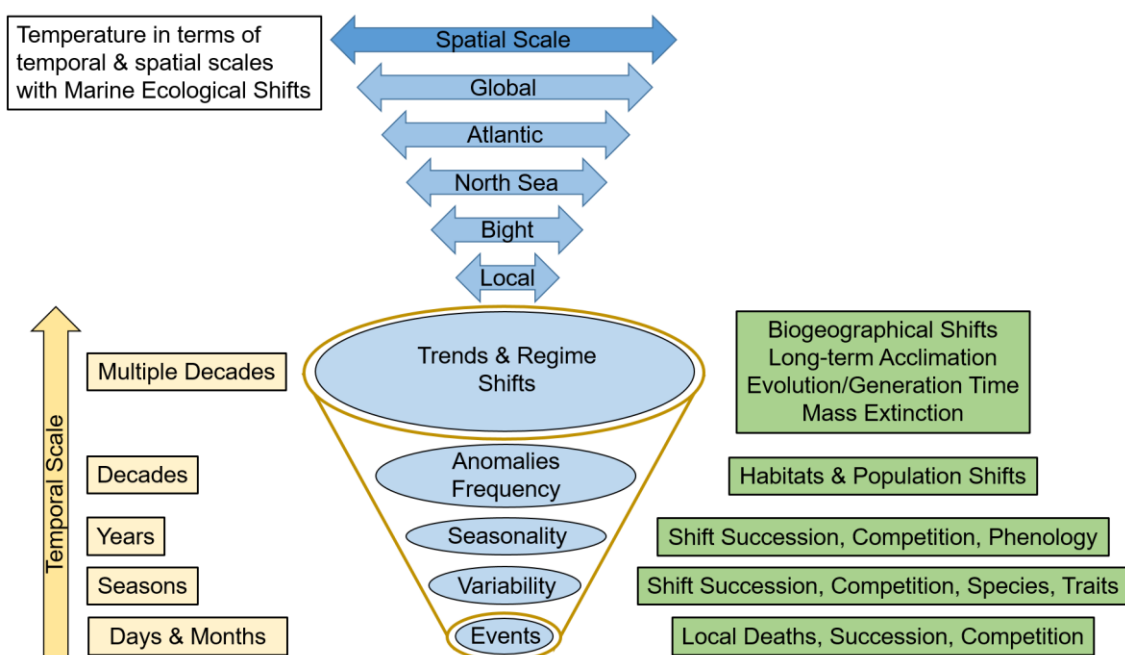


Figure 2.23: Temporal and spatial scales of temperature in relation to marine biological systems.

Depending on the type of reaction and adaptation, and especially if these are required to deal with daily variability (e.g. day-night temperatures) or long-term life cycle shifts and biogeographical changes in habitat, such as movement of organisms to cooler waters, the time scales can range from days to decades. Organisms also react to temperature shifts on time scales of generations, which can be anything upwards from days (e.g. phytoplankton and bacteria) through years and decades (e.g. fish, crustaceans) via epigenetics or evolutionary processes between generations (Cohen, 1967; Wilson and MacArthur, 1967; Slatkin, 1974; Marshall and Burgess, 2015; Shama et al., 2016). The biological distribution of species both in terms of latitude and height/ depth has, since the studies by Humboldt & Bonpland (1805), been accepted to be related to global temperature gradients, and in marine phytoplankton it is not different (Righetti et al., 2019). This is not only the case for terrestrial environments; marine organisms and their habitats are also dependent on the temperature of their environment and its variability. A few excellent studies have shown how life cycles of marine organisms are shifted along biogeographical gradients (e.g., shore crabs and cod) (Perry et al. 2005; Giménez, 2011; Pörtner et al., 2017). The effects of in situ heat shock are well documented for corals and effects of cold winters or sudden cold on exposed marine tidal flats are another example (Büttger et al., 2011; Barceló et al., 2016; Giménez et al., 2021; Hackerott et al., 2021). How marine organisms react and adapt depend very much on their living environment and whether they can move away from stress. Thus, plankton and nekton or sessile benthic organisms will react differently and with different tolerance and long-term resilience (for review on this see Harvey et al. (2022)) dependent on their life cycles. The manner in which marine organisms react to climate shifts and change is diverse. Most papers are interested in fish, however organisms at the bottom of the food web, i.e., plankton, which are at one with the waterbodies, are affected directly and cannot move well/ far in aquatic environments.

2.4.1 Long-term trends and the role of Indices: Biogeographical shifts over multiple decades and potential regime Shifts

In this study, all temperature trends were significantly positive, in agreement with the global literature (IPCC, 2018; IPCC, 2019). The trends were larger with decreasing geographical scale (i.e., spatial average) for both surface air temperatures and sea surface temperatures (Figure 2.24).

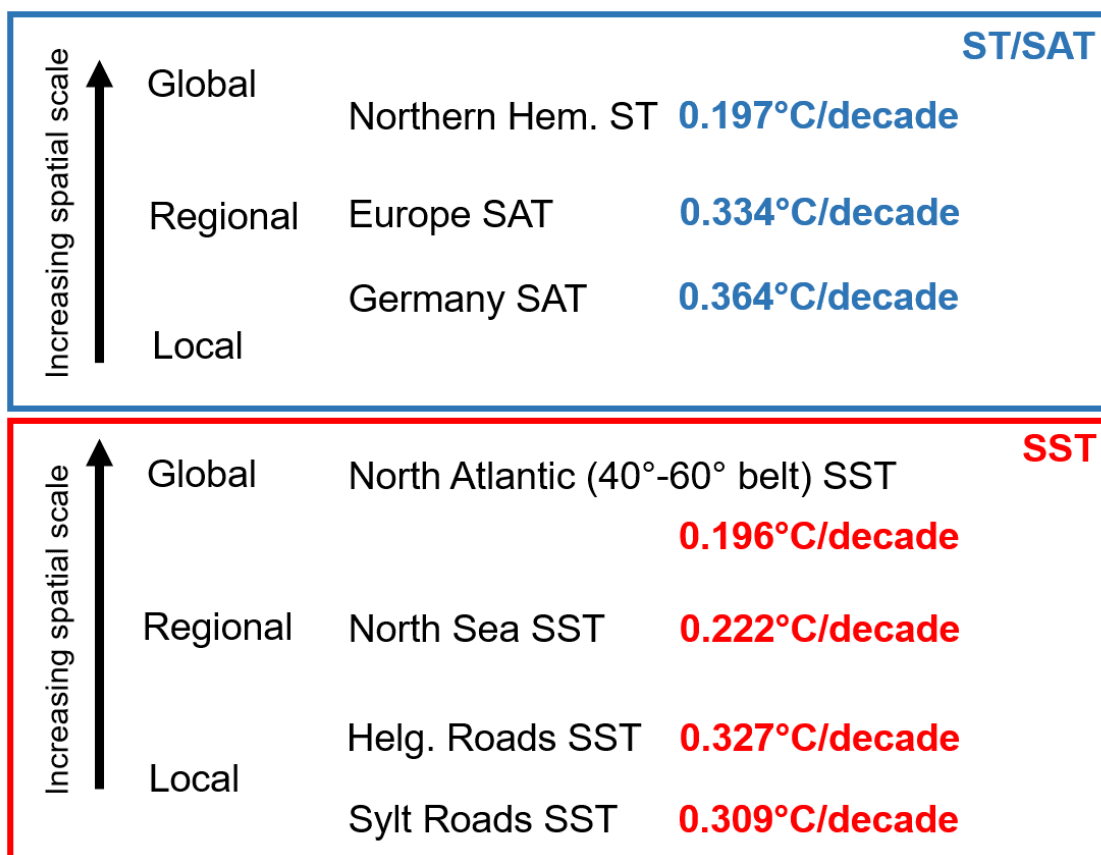


Figure 2.24: Results of trends and the direction of increase concerning the different spatial scales for Surface Temperature/Surface Air Temperature anomalies (blue rectangle) and Sea Surface Temperature anomalies (red rectangle).

When we examined the surface air temperature, it was clear that the strongest cross-correlations occur between Germany/Europe and Europe/NH, as was to be expected. In congruence with the rise in global atmospheric temperatures, the oceans are warming steadily. In addition, as can be seen from Figure 2.24, rise in temperature of the North Sea is considered

especially high. It has repeatedly been shown that, based on long-term data (Edwards et al., 2010) and models (Pierce et al., 2006; Holt et al., 2012; Kjellströmet al., 2018), the North Sea temperatures have been rising steadily in the last decades.

The SST of the North Sea is strongly correlated with the European and the German SAT and, to a lesser extent, with the North Atlantic SST and the Northern Hemisphere SAT. This shows that, like the data for the Dutch Wadden Sea, analysed by van Aaken in 2008, the two LTER sites in the German Bight are more driven by the terrestrial temperature regime than by the Atlantic temperature regime. This can be expected for a shallow sea bounded by land. It also explains why areas in the Southern North Sea are warming faster than the areas in the Northern North Sea (Scottish coast) (see Holliday et al., 2008).

We found that the two stations, Helgoland Roads and Sylt Roads, are strongly correlated with the German SAT and, to a lesser extent, with the European SAT. The stations are highly correlated with each other and also with the SST of the North Sea. This answers affirmatively the question as to whether both sites can be considered representative with regard to temperature of the overall North Sea.

We showed that the NAO index only relates well to the winter temperatures (December-February) in both HR and Wadden Sea SR sites, due to the fact that the Icelandic low pressure system is deeper during winter, showing strong gradient related to the Azores High (Rodwell et al., 1999). Similar results have been found for the western Wadden Sea and Marsdiep area by van Aken (2008), who also pointed out that, since 1982, the NAO does not show any persistent trends. This was also seen here, and previously Wiltshire et al. (2010) showed that the NAO index was also only useful in the winter months for explaining variability at Helgoland Roads. In addition, we speculate that the Atlantic Multidecadal Oscillation (AMO), used to explain biological phenomena in the North Sea and Atlantic (Edwards et al., 2013; Alheit et al., 2014), would not be causal regarding biological shifts in the North Sea at regional and local scales. The AMO, with its broad spatial distribution (0°-60°N, 80°W-0°), was minimally useful for explaining any anomalies or variability in all of our temperature data. Therefore, the driver of biological shifts would rather be the shifts in water masses. The North Atlantic (40°N-60°N) data was more representative for comparisons with the North Sea and HR and SR time series. The AMO was considered to be an oscillatory index in the past, however its validity is currently being questioned, based on recent literature by the original authors (Mann et al., 2021).

We have avoided discussion of so-called regime shifts in ecosystem drivers (temperature) here, because of the temporal tenuousness of such identifications in time series of merely a few decades. However, other authors have identified temporal shifts in the 1960s, 1980s and during the period 1996 to 2003 in the North Sea (Siegismund & Schrum, 2001; Edwards et al., 2002; Beaugrand et al., 2008; Beaugrand et al., 2014). Beaugrand et al. (2014) suggests that these three shifts impacted 40% of the plankton species or taxa considered in a study of data of the CPR in the North Sea.

We highlight that in all of the temperature time series analysed for the Northern Hemisphere, a distinct upwards shift in temperature trend can be seen in the late 1980s. One explanation for this could be found in a decrease in cold spells and an increase in heat waves due to blocking systems (Brunner et al., 2018).

Our comparisons of the temperature trends from local through to hemispheric scales, showed comparable trends/ patterns over large spatial scales. We showed overall warming, which is highest in the southern North Sea at HR. These trends will result in new biogeographical gradients and redistribution of species, with cold adapted species moving further north, as is currently being seen with for example cod (Drinkwater, 2005). This is where it becomes important to link up with such spatial data sets as the CPR provides, where indeed, strong evidence of species shifts on large spatial scales have been found (Beaugrand, 2004; Heath, 2005; Weijerman et al., 2005). However, data is exceedingly rare on species diversity overall, and daily LTER data are non-existent. Therefore, we can only make the links through statistical comparison of the drivers and shifts on different spatial scales and then add the knowledge we have on organisms also via models.

2.4.2 Shifts in Seasonality: Local to regional shifts of Succession, competition and phenology

Overall, the daily variability has declined at HR and SR. Wiltshire et al. (2010) showed that the number of growth days (defined as days with temperatures over 5°C) have increased significantly at HR. This was also found in the present study for both HR and SR. When subtracting the annual minimum from the annual maximum, we found a negative trend, indicating that the difference between cold and warm days of the year has become smaller, meaning that the strong seasonality of our regions has weakened. The positive temperature trend in the cold season (winter and spring) was also larger than the positive trend in the warm

season (summer and autumn), i.e., again evidence that the seasonal cycle has become smaller with time. Because the overall trend is a warming trend, with extension of warmth into the cooler months, the growing period has become longer. This affects the timing and succession of particularly microalgae (phytoplankton) and their predators (zooplankton). Investigations of seasonal shifts in temperature, in units of days, weeks, months and seasons are required to understand how temperature drives marine ecosystems. Growth rates, number of growth days, phenology, enrichment of new species may then be related to long-term changes (Wiltshire et al., 2010; Beaugrand et al., 2014; Scharfe and Wiltshire, 2019; Chivers et al., 2020). The complex nature of the wind, tide and current interactions at Helgoland and Sylt result in large daily variability of water conditions, both at HR and SR. We had no means of comparing marine daily data with other regions, because unfortunately this is currently unavailable. It would be interesting to compare our results with data from the Dutch Wadden Sea (van Aken, 2008) and with the compilation of data for the Baltic Sea (Mackenzie & Schiedek, 2007) where it seems that variability in the systems may have shifted considerably in the past 50 years. It is often precisely this variability which results in growth triggers and controls (e.g. turbulence, resuspension of sediments and nutrient recycling) and which are associated with seasonal shifts (Philippart et al., 2003; Wiltshire & Manly, 2004; Scharfe and Wiltshire, 2019).

Wiltshire et al. (2015) have shown how the timing of the spring bloom of phytoplankton at HR has shifted based on daily values and that this could be related to the continued overwintering grazing of herbivorous zooplankton. Based on these works, Sommer and Lengfellner (2008) carried out experiments in mesocosms with a modelling backdrop, to demonstrate how temperature regulated the interaction of microzooplankton, zooplankton and phytoplankton growth. Scharfe and Wiltshire (2019), in an analysis of key phytoplankton species, showed that the timing, in days, of late winter/early spring (e.g. *Skeletonema spec.*), spring (e.g. *Ditylum brightwellii*) and early summer species (e.g. *Rhizosolenia setigera*) have shifted forward in the last 50 years, also often evincing longer periods of occurrence. However, the timing of others, for example *Odontella sinensis* and *Thalassionema nitzschioides*, late summer/ autumn species respectively, shifted towards central winter reflecting longer warm periods in autumn, as shown in the temperature analyses of this paper. The work by Scharfe and Wiltshire (2019) and some work by the CPR groups of SAHFOS (Hinder et al., 2012) have shown that the reaction of species is specific to their enrichment time. Based mostly on weekly data, Beaugrand et al. (2014), Greve et al. (2004) and Heath (2005) provide evidence that the phenology and succession of species of zooplankton (copepods) have shifted at HR

and in the greater North Sea. As the timing of zooplankton and its life cycle stages are very dependent on the available phytoplankton food, shifts in phytoplankton timing and species composition can be detrimental to food web function, as proposed in the match-mismatch hypothesis by Cushing (1990). As with the timing of land plants and the occurrence of pollinating insects or pests (Solga et al., 2014) such timing relationships are often just as narrow in marine systems; in the order of days or maximally weeks.

Whether or not shifts in phenology based on days and weeks are spatially ubiquitous/transferable to wider areas across the northern latitudes depends on the species ranges and the adaptability of organisms. Plants driven by photosynthesis adapt differently to animals. The link to greater spatial areas is given when, as shown in this study, trends/ shifts observed in detailed long-term data can be related to the same trends/ shifts at other spatial scales.

2.4.3 Maximum and minimum Temperatures- hot and cold Spells: Physical and behavioural adaptation; competition with neobiota; local species extinction

We found that there was a significant shift towards much more presence of very warm months with values over 17 °C and 18 °C at HR and SR since 1991, while the very cold months (mean values below < 2 °C and < 3 °C) have become significantly less common. An associated study (Gimenez et al., 2022), based on HR, showed that the frequency of marine heatwaves has increased, especially after the 1990 and that the major heatwaves coincide with large atmospheric European summer heatwaves or mild winter spells. Hence, different forms of data analyses highlight the increasing prevalence of warm periods for the German Bight.

Maximum and minimum temperatures and the number of days with specific temperatures are very important to the adaptation, (both on the short term and longer term over generations) and survival of species in marine systems. Heat waves and their consideration are currently very important in the literature (Frölicher & Laufkötter, 2018; Ainsworth et al., 2020). Marine heatwaves in particular have led to a number of changes in marine ecosystems, ranging from mass mortality of foundation species to changes in the food web (Arias-Ortiz et al. 2018, Hayashida et al. 2020). The latitudinal or climatic temperature regime which organisms are acclimatised to will also make a big difference in how they react to heat (Boersma et al., 2016). Minimum temperatures can regulate the difference between survival and non-survival of

indigenous vs. neobiota (Lenz et al., 2011). When it gets too warm, the thermal tolerance will indicate species vulnerability to climate warming (Madeira et al., 2012). The majority of species found in the German Bight, whether they are plankton, fish, crustaceans or mammals have very large ranges of occurrence and for example, many phytoplankton have been around for millennia (see fossil records, Dale, 2001).

Based on this data for the increased number of months/days with maximum temperatures plus the evinced trends for HR, SR, the North Sea and North Atlantic it is clear that “warm waters are the new normal”. Species, no matter when they occur, will have to cope with warmer waters and many more days with much warmer maximum and minimum temperatures. Brunner et al. (2018) have examined the cold spells and especially the increase in warm spells in Europe and related these to blocking systems. They found that over 80% of cold spells in southeastern Europe occur during blocking and that warm spells are correlated with blocking mostly in northern Europe. They suggest that, in future, cold snaps are likely to become even more important in these new warmer normal, as they seem to be associated to each other.

However, marine organisms are not merely enriched between maximum and minimum temperatures or the number of days making a heat wave or cold snap. The frequency with which organisms are confronted by a specific temperature will be central to its acclimatization and range of occurrence (Boersma et al., 2016). Thus, it is incorrect to assume that species adjustment to temperature has mostly to do with maximum and minimum temperatures of the system where the organism is enriched. It is also not realistic to simply project a line between min and max temperatures and use this for experimental evaluations of temperature acclimation. Unfortunately, due to the lack of frequency distribution analyses many studies, which have been carried out on how organisms react to temperature change, both on the short and long-term, may be based on false assumptions on distributions of temperature in nature (Pörtner, 2002; Thomas et al., 2012; Boyd et al., 2013). Instead, we should consider experiments that manipulate realistic temperature scales and levels of intensity, defined accordingly to empirical temperature distributions.

Interestingly, the frequency distributions of temperature over the years have changed substantially in the later years. At Helgoland and Sylt, the homogeneous bimodal shape, besides the shift of the two distinct lobes peaks to higher temperature values, has flattened in the warm mode and got steeper in the cold mode. This indicates that more values occur around

the cold mode and less so around the warm mode. Especially, autumn and winter months have become warmer and the number of very hot days/ months has increased significantly.

Plots of the frequency distributions of the temperature anomalies for the North Atlantic, North Sea and HR and SR (Figure 2.12) showed that the anomalous temperature density distribution clearly shifted to higher temperatures in the later years in all spatial areas. Interestingly, especially in the North Atlantic, the maximum and minimum values of the anomalies have moved significantly further apart, indicating that the variability of the anomalies has become higher. The shape of the distribution of the temperature anomalies has also flattened considerably for the North Atlantic data, much more so than the other regions. This may reflect the very large spatial area considered in the North Atlantic and the wide range of temperatures, which have different shifts and because of the high spatial variability of temperature evinced across the different latitudes.

2.4.4 Variability on the Long-Term: Physical and behavioural adaptation; local species Extinction, shifts in growing season and biogeographical species distribution

The variability during the winter and spring months was found to be significantly larger than during summer and autumn at both HR and SR, particularly for the early half of the time series. In the later part of the time series, the large winter variability became smaller and the variability of temperature in the autumn became larger (Figure 2.17 and Figure 2.25e,f). The same pattern, but slightly smaller in amplitude, was found for the North Sea data (Figure 2.25d). The North Atlantic showed a significant increase in temperature variability for all seasons since 1991 (Figure 2.25c). In comparison, the Global and Northern Hemisphere datasets show a smaller increase in variability in the later years for all months (Figure 2.25a,b).

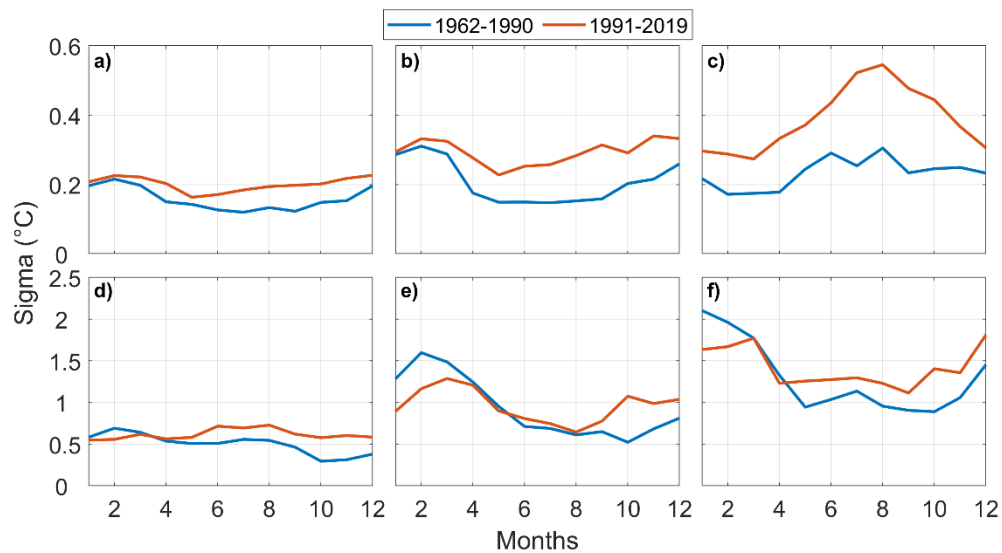


Figure 2.25: The seasonal variation of the standard deviation of the SST in all spatial scales (from Global to local) for the first (blue) and second half (orange) of the time series. a) Global; b) Northern Hemisphere; c) North Atlantic 40°-60°; d) North Sea; e) Helgoland and f) Sylt. The y-axis scales are different for top and bottom rows, showing the increase in variability from larger to smaller spatial scales.

Aquatic ecosystem variability can be considered a driver of species diversity, thus, it is important to evaluate the magnitude of variability changes in climate change studies (Flöder & Sommer, 1999; D’Odorico et al., 2008; Dornelas, 2010; Borics et al., 2013). Indeed, explanation of species diversity as a function of ecosystem variability is subject of a long-term discussion in the literature (e.g., Grime, 1973; Connell, 1978; Robinson & Minshall, 1986; Collins, 1990). Sarker et al. (2018) describe the 1980s as the period of high ecosystem variability at the Helgoland Roads Time Series station, with a considerably less variable period identified after the 1990s. They also showed that both diversity and species occurrence probability declined with the increase of ecosystem variability. The occurrence of more species was seen at low ecosystem variability without a loss of rare species already in the system. This implies a high level of niche differentiation, reducing interspecies competition and lack of exclusion and this directly increases species diversity. Indeed, increasing species diversity and the co-existence of neo biota and indigenous species has been going on in the North Sea and especially the German Bight for the past 20–30 years (Greve et al., 2004; Buschbaum & Gutow, 2005; Wiltshire et al., 2010; Reise et al., 2017). This reflects the ecosystem theory that the

warming of a cold temperate sea will allow for more species. Beaugrand et al. (2008) also showed that the 1980s overall were a period of high variability, whereas the 1990s were identified with a low variability in the North Atlantic region. Conversi et al. (2010) observed similar change in the late 1980s in long-term records of Mediterranean ecological and hydro-climate variables.

Temperature variability induced by shifts in larger weather patterns, including storm patterns such as El Nino and Blocking Systems, can be translated to shifts in hydrography, turbulence, stratification and, in coastal systems, freshwater input from rivers. Such shifts affect e.g., primary productivity, fish distribution, spawning timing and species distribution of planktonic organisms (Dippner, 1997b; Root et al., 2003; Stenseth et al., 2004; Mackenzie and Schiedek, 2007). Here, we also considered the indicator indices of large Northern Hemisphere climate patterns, namely the NAO and the (in the meantime questionable) AMO (Mann et al., 2021). These indices are often used in the literature to explain events and as links to organism distribution e.g. fish, bivalves and copepods (Dippner, 1997b; Philippart et al., 2003; Reid et al., 2003; Alheit et al., 2014). It is not logical to link the large-scale climate indices such as NAO to marine organisms directly, as these are not drivers in themselves. Rather, it is the effect of the large-scale weather patterns on hydrography and temperature, which can be drivers of the pelagic distribution and species life cycles (van Aken, 2008). For example, it is not the NAO that drives the shift of *Calanus helgolandicus* vs. *Calanus finmarchicus*, but rather the inflow of the Atlantic Ocean into the North Sea, which transports the Atlantic species *C. finmarchicus* more or less into the North Sea. This inflow is related to large-scale weather pattern fluctuations of which the NAO is an indicator (Heath et al., 1999). This can also be seen in the study on timing of spawning of *Limecola (Macoma) baltica*, by Philippart et al. (2003) and van Aken (2008). Phillipart et al. (2003) postulated that this was related to the NAO index, but later it was found by van Aken (2008) that it is not likely that the NAO is directly related to spawning and it is certainly as an index, not the trigger. They consider the long-term trend in temperature to be the reason for earlier triggering and not zonal winter winds reflected by the NAO pressure index.

Boersma et al (2016) have shown that it is also very important to understand the frequency distributions of temperature which organisms are subjected to rather than max/ min curves only. As the frequency distributions for temperature data and their anomalies have shifted considerably over the past 20 years on all the special scales we examined, we can

assume that especially animals, which have tight temperature adaptations, will have to move or acclimate in all examined areas.

Animals will react differently to temperature changes than plants. Plants, including marine phytoplankton and macroalgae, moving further north or indeed into cooler deeper waters will also have to adjust their photosynthesis apparatus to deal with different light regimes (Falkowski, 1984; Jorda et al., 2020). The highly significant shifts in seasonality and the associated very much warmer winters and autumns are much more visible at the Wadden Sea (SR) and German Bight (HR) sites than in the North Atlantic, due to the higher heat capacity larger and deeper water bodies, like the latter, present. Even in the North Sea, this is not so pronounced. Such local to regional effects can result in shifts in the phenology, spawning time and/or life cycles of bivalves and other species, and result in match-mismatch food web situations (Edwards and Richardson, 2004).

We have taken one of the densest data series in the world, the Helgoland Roads time series, and we described the statistical and comparative analysis on different scales, from local to hemispheric context, in order to make its data sensibly and accurately available, especially to biologists. With this, we also have demonstrated the usefulness of point-source temperature time series in the North Sea and showed their representativeness to overall temperature time series.

2.5 CONCLUSIONS

Marine ecosystem function is governed by the scale-dependent nature of physical processes. These are also reflected in both coupling and differences among processes occurring in the ocean, the coastal zone and land, requiring reliable temperature data and assessments of this data. Here, we provided a study on how temperature behaves on different spatial scales, the magnitude of changes in trends and variability and the representability of local scales in larger scales and vice-versa. From global to local, all temperature trends are positive, corroborated by the significant positive correlations among the analysed areas and sites. For the local and regional scales, the highest correlations observed between the sea sites and the closest land mass is an important result. This allows us to understand the variability mechanisms of temperature change in the North Sea. The large-scale phenomena such as AMO and NAO which are often considered important do not necessarily have a significant influence on regional and local scales. Evaluations and the observed changes in variability, seasonal as well as inter-annual, cannot be ignored in temperature considerations, as they are part of the significant changes occurring in temperature affecting ecological systems. We provide this information as a basis for marine biological and ecological research, and especially for considerations of responses in organisms and environments to temperature shifts and changes on diverse scales. We thus provided the necessary information to increase the robustness of predictability and assessments of future climate risk to biological systems.

2.6 ACKNOWLEDGEMENTS

We acknowledge the immense effort of the Aade and Mya II crews to collect the Helgoland and Sylt Roads data and the Landesbetrieb für Küstenschutz, Nationalpark und Meeresschutz Schleswig-Holstein for the complementary Sylt SST data. We thank the Met Office Hadley Centre, the European Environment Agency, the German Weather Service (Deutscher Wetterdienst) and NOAA National Center for Atmospheric Research (NCAR) for making available the datasets used here.

2.7 SUPPLEMENTARY MATERIAL

Table 2.12: Comparison of overlapping SST measurements at Sylt harbour and SR sites. Monthly averages, differences with standard deviation (std) and p-values of monthly t-test comparisons.

Month	Harbour SST (°C)	Harbour SST std (°C)	SR SST (°C)	SR SST std (°C)	Delta (°C)	std Delta (°C)	n	p- value
January	2.87	1.83	2.90	1.93	-0.03	0.76	111	0.92
February	2.74	2.00	2.69	2.06	0.05	0.70	111	0.86
March	3.77	1.93	3.67	1.99	0.10	0.75	134	0.68
April	7.10	1.92	7.24	2.08	-0.14	1.06	121	0.58
May	12.18	2.10	12.15	1.99	0.03	1.03	105	0.93
June	15.83	1.87	15.65	2.05	0.18	1.10	141	0.43
July	17.79	1.76	17.72	1.78	0.07	0.86	164	0.73
August	18.72	2.03	18.74	1.86	-0.02	0.92	151	0.90
September	15.08	1.86	14.84	2.03	0.24	0.98	130	0.32
October	10.79	2.07	10.47	2.07	0.32	0.94	103	0.28
November	6.48	1.95	6.19	2.04	0.29	0.90	143	0.22
December	3.97	1.89	3.91	1.81	0.06	0.95	97	0.82

Link from Chapter 2 to Chapter 3

After analysing the trends and variability of land temperature and SST, considering the global and local spatial scales, the next step was to investigate the current situation regarding the Chl-a concentration in the German Bight and quantify the covariability between Chl-a and SST, exploring the possible direct and indirect effects of temperature on the observed negative Chl-a trends. Considering that the properties of temperature are different for various spatial scales, the effects of temperature in ecological systems cover a range of consequences, from biogeographical shifts and long-term acclimation to short-term events of local depth and competition.

3 Chapter 3

Analyses of sea surface Chlorophyll-a trends and variability in a period of rapid Climate change, German Bight, North Sea.

Submitted to Ocean Science: de Luca Lopes de Amorim, F., Balkoni, A., Sidorenko, V., and Wiltshire, K. H.: Analyses of sea surface Chlorophyll-a trends and variability in a period of rapid Climate change, German Bight, North Sea, EGU sphere [preprint], <https://doi.org/10.5194/egusphere-2024-311>, 2024.

Abstract

Satellite remote sensing of ocean colour properties allows observation of the ocean with high temporal and spatial coverage, facilitating the better assessment of changes in marine primary production. Ocean productivity is often assessed using satellite derived chlorophyll-a concentrations, a commonly used proxy for phytoplankton concentration. We used the Copernicus GlobColour remote sensing Chl-a surface concentration, comparing with the Helgoland Roads Chl-a in situ data, to investigate seasonal and non-seasonal variability, temporal trends, changes in spring bloom Chl-a magnitude and the relationship with sea surface temperature (SST) and mixed layer depth (MLD) in the German Bight (GB) from 1998 to 2020. Empirical Orthogonal Functions and Multi Covariance Analysis were employed, in order to investigate dominant spatial and temporal patterns (modes) related to the main processes of Chl-a variability and to extract the dominant structures that maximize the covariance between Chl-a and SST|MLD fields. High levels of Chl-a were found near the coast, showing a decreasing gradient towards offshore waters. A significant long-term positive trend was observed close to the Elbe estuary and adjacent area, while 30% of the GB was characterized by a significant negative trend. No significant trends were observed during spring blooms, but the distribution of Chl-a anomalies changed when periods from 1998 to 2009 and 2010 to 2020 were compared, mostly showing a shift towards negative anomalies and decrease in variability. The Chl-a non-seasonal variability showed that the first four modes explained around 45% with the first and second modes related to inter and intra-annual variability, respectively, observed in the temporal principal components spectral analyses. Linear trends between Chl-a anomalies

and SST and MLD anomalies were weak and described by opposite signal in offshore and coastal areas, with negative correlation between Chl-a and temperature in offshore areas and positive in mostly coastal areas, while for MLD was the contrary. The monthly chlorophyll-a concentration anomalies covaried 45% with sea surface temperature anomalies and 23% with mixed layer depth anomalies. This study demonstrated that the Copernicus Global Ocean Colour chlorophyll-a concentration product can assess mostly of the known processes connected to chlorophyll-a surface variability in the German Bight. The monthly averages were suitable to investigate long-term trends and variability for SST, but for MLD, higher frequency should be used. The causes for the significant negative trends in most of the central German Bight cannot be solely explained by the direct effect of warming. However, the rising water temperature, combined with its indirect effects on other variables, can partially explain these observed trends.

3.1 INTRODUCTION

Long-term ocean productivity serves as a crucial indicator of planetary change, with direct ties to shifts in ecosystem functionality and the decline of higher trophic levels (Henson et al, 2010; Stock et al, 2014). Marine ecosystems, particularly those in shelf seas, are subject to both natural variability and the increasing stress from anthropogenic climate change. The German Bight, a highly dynamic region of the North Sea, has undergone significant changes over the past sixty years. Pronounced shifts in seawater nutrient concentrations and stoichiometry are well reported (Raabe and Wiltshire 2009; van Beusekom et al. 2019; Balkoni et al. 2023). In parallel, Sea Surface Temperature (SST) has been on a steady rise since 1962 (Amorim & Wiltshire et al., 2023). Changes in nutrient concentrations have profound impacts on phytoplankton productivity and species composition (Hickel et al., 1993; Topcu et al., 2011; Burson et al, 2016). However, the role of increasing temperature remains unclear.

Increasing SST can affect phytoplankton biomass both directly, by influencing species physiology and ecosystem structure, and indirectly, by altering the hydrographic conditions of a region. For example, increasing SST can enhance phytoplankton cell division rate (Hunter-Cevera et al. 2016). However, if the optimum temperature is exceeded, the growth rate and primary production may decrease (Baker et al., 2016). Indirect effects include changes in regional hydrographic conditions, as rising temperature can increase water column stratification and reduce the Mixed Layer Depth (MLD), thereby affecting light and nutrient availability to primary producers. Understanding the drivers of phytoplankton biomass variability in coastal waters is crucial for gaining insights into the dynamics and fluctuations of higher trophic level populations (Marrari et al, 2017), and for assessing the ecological status of the coastal environment (European Environment Agency, 2022).

Chlorophyll-a (Chl-a) is commonly used to estimate the phytoplankton biomass in the water column (Eisner et al., 2016; Huot et al., 2007). However, acquiring accurate spatial and temporal data on Chl-a concentration can be a challenge due to data scarcity in one or both domains. While extensive time series data can be collected at a single geographical point, this approach lacks spatial resolution. Satellite data offers a solution to this problem by providing comprehensive spatial and temporal coverage, enabling the assessment of Chl-a spatiotemporal variability. The detection of phytoplankton via remote sensing relies on the unique properties of chlorophyll, which absorbs and reflects sunlight in the visible-near infrared part of the electromagnetic spectrum.

Surface Chl-a remote sensing products have long been an effective observational

methodology in both coastal and open ocean environments (Henson et al., 2009; Henson et al., 2010; Fernández-Tejedor et al., 2022). In open ocean waters, remote sensing measurements allow for accurate determination of ocean colour. However, in coastal waters, the detection of ocean colour is complicated by the presence of suspended particulate and dissolved matter, making the retrieval of Chl-a concentration more complex in these systems (Pahlevan et al., 2020). One limitation of satellite-derived Chl-a is that it restricts the accurate depiction of the entire system due to the absence of a vertical dimension (Zhao et al., 2019). Despite this, it enables a spatially dynamic description of surface chlorophyll. For shallow seas like the German Bight, remote sensing provides a good representation of the chlorophyll in the water column, as the first optical depth, ranging from 1 to 12 m in the region of interest, is sampled (Doerffer & Fischer, 1994). Turbulent mixing induced by storms, tides, and internal waves redistributes chlorophyll to near-surface depths (Zhang et al., 2019; Becherer et al., 2022). Overall, remote sensing, despite the limitations, remains a valuable tool for studying phytoplankton biomass in both space and time (Blondeau-Patissier et al., 2014).

In this study, we investigated the long-term trends and variability of Chlorophyll-a (Chl-a) in the German Bight, considering the rapid increase in SST in the region over the past two decades. We retrieved the Copernicus GlobColour-merged Chl-a product, spanning from January 1998 to December 2020, and compared it with in-situ Chl-a measurements. We also examined the spatial and temporal covariability of Chl-a in relation to SST and MLD. Our specific objectives were to understand the following:

- (i) The differences between in-situ and satellite-derived Chl-a.
- (ii) The seasonal variability of Chl-a.
- (iii) The long-term trends of Chl-a.
- (iv) The dominant modes of Chl-a variability.
- (v) The relationship between Chl-a, SST, and MLD in the region.

By addressing these points, we aim to provide an updated perspective on Chl-a trends and variability in the German Bight (Figure 3.1), as well as a comprehensive understanding about its relationship with SST and MLD in the study area.

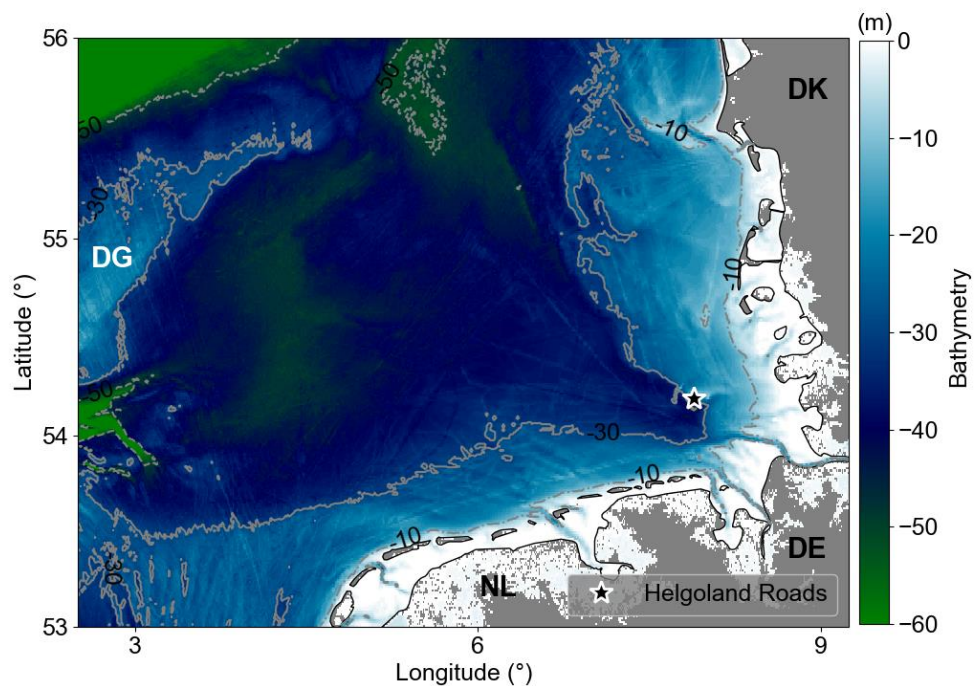


Figure 3.1: Bathymetry of the German Bight (GEBCO Bathymetric Compilation Group 2023, 2023). Dot-dashed, solid, and dashed grey lines are 10, 30, and 50 m isobaths respectively. Areas with depths less than 5 m represented by white colour. Black star marks the location that the Helgoland Roads time series have been collected. The acronym DG refer to Dogger Bank; DE to Germany; DK in Denmark; and NL to Netherlands.

3.2 DATA AND METHODS

3.2.1 Study Area

The German Bight is a coastal area in the south-eastern North Sea bounded by the Netherlands (NL), Germany (DE), and Denmark (DK) (Figure 3.1). The area defined in this work ranges from $2.5\text{-}9.25^{\circ}\text{N}$ and $53\text{-}56^{\circ}\text{E}$. It extends from the Elbe estuary to the northwest and passes the Dogger Bank (DB) and it has a maximum depth of about 50 m (Figure 3.1). A 30 to 40 m deep funnel-like feature, defined by the deep Elbe valley, crosses the area in a diagonal direction from southeast to northwest (Stanev et al., 2014). The hydrodynamics of the region are very complex due to the interactions of riverine discharges, central North Sea water, Atlantic water (which is inserted into the region through the English Channel), and the tidal

and atmospheric forcing (Becker et al., 1992; Kerimoglu et al., 2020).

The productivity in the German Bight is linked to its hydrographic conditions and bathymetric features (Emeis et al. 2015; Capuzzo et al., 2018). In regions where the depth is less than 20 m, the vertical concentration of Chl-a is largely homogenized throughout the year, primarily due to the mixing effects of tidal currents and wind. However, in areas where the depth exceeds 20 m, the vertical Chl-a concentration exhibits significant variability in terms of its extent, duration, and intensity (Schrum, 1997; Zhao et al, 2019). This variability is largely attributed to stratification and biogeochemical processes, such as the slow decomposition rates of organic matter (van Beusekom et al., 1999), which result in a distinct vertical Chl-a distribution when compared to shallower regions (Zhao et al, 2019).

3.2.2 Chlorophyll-a Concentration Remote Sensing Data

In this study, we downloaded the Copernicus Marine Service (CMS) GlobColour. daily interpolated cloud-free surface Chl-a concentration product, ranging from January 1998 to December 2020. This product was available for download at the time of access on 20 October 2021 from <https://resources.marine.copernicus.eu/> under the product described as OCEANCOLOUR_ATL_CHL_L4_REP_OBSERVATIONS_009_098. This Chl-a dataset was produced using multiple sensors (multi-sensor product), multiple Chl-a algorithms and a daily space-time interpolation scheme, with a 1 km² spatial resolution (Garnesson et al, 2019).

3.2.3 Sea surface temperature, mixed layer depth and North Atlantic Oscillation (NAO)

Daily fields of sea surface temperature (SST) and mixed layer depth (MLD) were obtained from CMS (ESA SST CCI and C3S reprocessed sea surface temperature analyses; <https://doi.org/10.48670/moi-00289>), spanning from January 1998 to December 2020. The SST dataset is gap-free maps of daily average SST at 0.05deg. horizontal grid resolution, using satellite data from the Advanced Along-Track Scanning Radiometer (AATSR), Sea and Land Surface Temperature Radiometer (SLSTR) and the Advanced Very High Resolution Radiometer (AVHRR) (Lavergne et al., 2019; Merchant et al., 2019; Good et al., 2020).

Daily mixed-layer depth data (≈ 7 km horizontal resolution) were obtained from CMS, as part of the Atlantic-European North West Shelf-Ocean Physics Reanalysis product (<https://doi.org/10.48670/moi-00059>). The MLD was defined as the depth where the density increase compared to density at 3m depth corresponds to a temperature decrease of 0.2°C in local surface conditions (Kara, 2000; PUM, 2021).

The NAO winter index data was obtained from the Climate Analysis Section, National Center for Atmospheric Research (NCAR). It is calculated as the leading Empirical Orthogonal Function of sea level pressure anomalies considering the gradient between the Icelandic low and Azores high (Hurrell et al., 2003). The winter NAO index is the mean of the index for the December, January and February months.

3.2.4 In situ data

In-situ Chl-a concentrations, measured with a high-performance liquid chromatography (HPLC) on a work-daily basis since 2004 at Helgoland Roads (see black star in Figure 3.1 for the data site) (Wiltshire et al., 2008), were used for the evaluation of the satellite derived product. Helgoland Island is located in the German Bight approximately 60 km of the German coast and since 1962, surface water samples have been collected at the Helgoland Roads site, between the Helgoland and Düne Islands ($54^{\circ} 11.3' \text{ N}$, $7^{\circ} 54.0' \text{ E}$). The samples are representative for the whole water column due to the well-mixed conditions (Wiltshire et al., 2010). The Helgoland Island is in a transition zone in the German Bight, influenced by offshore (higher salinity) and coastal waters (lower salinity) (Wiltshire et al., 2015).

3.2.5 Data preprocessing

As we were interested in long-term trends and variability, Chl-a, SST and MLD daily fields were monthly averaged, also avoiding problems with spatial missing data. We computed monthly anomalies by subtracting the monthly means absolute values by the climatological averages, which are the mean of monthly absolute values over the 1998 to 2020 period.

All spatial datasets were remapped to the grid of lowest spatial resolution (Table 3.1) using the bilinear method in the Climate Data Operators (CDO; Schulzweida. 2022). We excluded areas with bathymetry shallower than 5 m to circumvent dynamics related to intertidal zones. For analysis, coastal and offshore areas were defined as areas with bathymetry above and below 30 m, respectively. The Dogger Bank was considered in the offshore region.

The Chl-a in situ data was monthly averaged and monthly anomalies were calculated. We extracted the nearest grid point from the Helgoland Roads location in the remote sensing gridded data (hereby referred to as HRsat) and used monthly anomalies for comparison and validation of the GlobColour Chl-a dataset.

Table 3.1: Description of spatial resolution and source of the parameters used in this study.

Variable	Spatial Resolution	CMS Product ID
Chl-a	1 km	OCEANCOLOUR_ATL_CHL_L4_REP_OBSERVATIONS_009_098
SST	0.05°	SST_GLO_SST_L4_REP_OBSERVATIONS_010_024
MLD	0.111° × 0.067°	NWSHELF_MULTIYEAR_PHY_004_009

3.2.6 Evaluation of satellite derived Chl-*a* data

We compared the HRsat monthly anomalies time series with the in situ (HPLC) Chl-*a* monthly anomalies from the Helgoland Roads Time Series (HRTS) from 2004 to 2020. In this case, only the matching days were used for the calculation of the monthly anomalies, in both HRsat and HRTS. Our primary focus was on trends and monthly variability to assess the degree of coherence between the in situ and remote sensing datasets. For the evaluation of trends, we applied the Mann-Kendall trend test (Mann, 1945; Kendall, 1975) and we made use of a boxplot for the variability assessment. The coefficient of correlation (r) and root mean squared error (RMSE) were computed to evaluate the goodness of fit between in situ and remote sensing data. Differences in distribution between Chl-*a* in situ and remote sensing were verified by the two-sample Kolmogorov-Smirnov test.

3.2.7 Statistical Methods

As a pre-analysis, we calculated temporal mean and standard deviation (std) of the Chl-*a* anomalies. Using the mean and std, we computed the coefficient of variation (CV), calculated as $CV = \frac{mean}{std} \times 100$, in % (Morel et al., 2010). Additionally, we examined linear trends in Chl-*a* anomaly fields. The significance of the linear trends was determined using a two-sided Wald test with t distribution. For more robust identification of significant positive and negative trends, we applied the Mann-Kendall trend test to the Chl-*a* anomalies. This was done on a pixel-by-pixel basis using the Python “pyMannkendall” library (Hussain et al., 2019). We calculated the Probability Density Function to investigate the changes occurring in the distribution of Chl-*a* anomalies.

We examined the relationship between the Chl-*a* anomaly fields with SST and MLD anomalies applying linear correlations in the direct anomaly fields and in 1 time step lagged Chl-*a* in relation to SST and MLD. For the analysis of dominant modes of Chl-*a* variability and covariability with SST and MLD, we used Maximum Covariance Analysis (MCA), a statistical technique that identifies prominent patterns of covariation (Bretherton et al. 1992) to maximize the covariability of associated parameters. MCA was designed to find patterns in two space-time data sets that explain the maximum fraction of the covariance between them. This can provide insight into the physical processes leading to the spatial and temporal variations

exhibited in the fields being analysed. Given the known significance of SST and MLD forcing in inducing chlorophyll changes (de Mello et al., 2022), this technique is particularly suited for our purpose. In essence, MCA extracts the singular vectors of the cross-covariance matrix of two fields, in order of importance. These singular vectors, also referred as structures or modes of variability, are extracted. When MCA was calculated using only one field, such as the Chl-a anomalies, we obtained the Empirical Orthogonal Functions (EOFS), which represented the leading modes of Chl-a variability. We utilized the Python package “xmca” (Rieger 2021) to apply EOFS and MCA. For the EOFS analysis, we used the monthly climatological Chl-a concentrations and the Chl-a anomalies, normalized during the analysis. For the MCA, the Chl-a, SST and MLD anomalies were employed.

3.3 RESULTS

3.3.1 Evaluation of in situ HPLC and Remote Sensing Chlorophyll-a

Figure 3.2a illustrates the comparison of HRTS and HRsat Chl-a monthly anomalies time series. Both time series showed significant negative trends, evaluated by the Mann Kendall trend test. While satellite observations accurately reproduced the intra- and inter-annual frequency, there was a discrepancy, with remote sensing tending to overestimate chlorophyll at low concentrations (Figure 3.2b). In fact, satellite products tend to overestimate Chl-a values when they are less than 1 mg m^{-3} (Alvera-Azcárate et al., 2021). When comparing the in situ HRTS and HRsat anomalies (Figure 3.2a), we found a correlation coefficient (r) of 0.59 ($p\text{-value} < 0.05$) and root mean squared error (RMSE) of 1.09 mg m^{-3} (Figure 3.2b). These values are in the range of values described in other works and considered acceptable for case-2 waters (Silva et al., 2021; Pramlall et al., 2023), in which the remote sensing product is defined by other constituents besides chlorophyll, such as coloured dissolved organic matter and non-algal particles (Doerffer & Schiller, 2007).

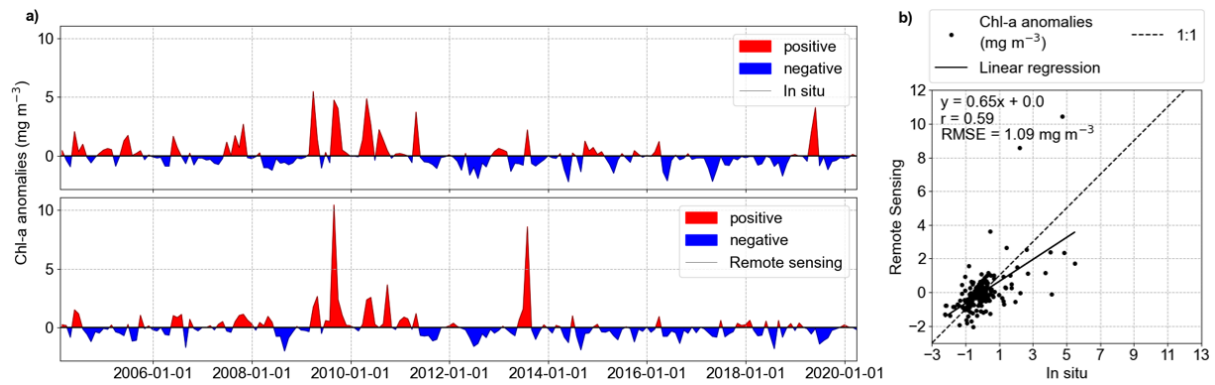


Figure 3.2: Evaluation of GlobColour remote sensing surface Chl-a, compared to in situ data from Helgoland Roads. a) Comparison of in situ and remote sensing Chl-a anomalies, with red positive and blue negative anomalies. b) Scatter plot with linear correlation of the time series showed in a). Correlation coefficient is 0.59 and RMSE 1.09 mg m⁻³.

In the boxplot (Figure 3.3a), we observe that the in situ data has higher variability than the remote sensing data in April and May, months characterized by the phytoplankton spring bloom (Wiltshire et al., 2008). A rigorous assessment using the two-sample Kolmogorov-Smirnov test revealed no statistically significant differences between the anomaly distributions (p-value=0.83; Figure 3.3b). The differences between in situ and remote sensing data were mitigated by using monthly mean anomalies. As a comparison, the evaluation using daily matchup Chl-a anomalies time series were $r=0.35$ and $RMSE=2.64$ mg m⁻³.

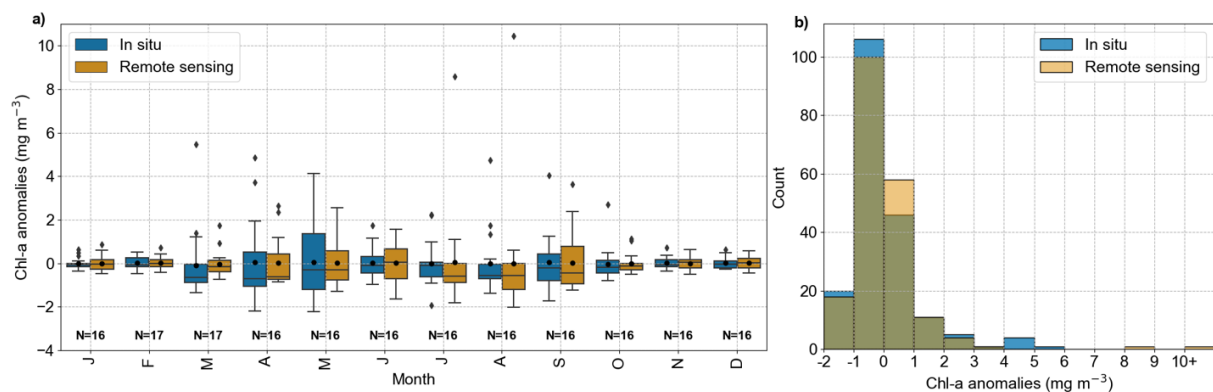


Figure 3.3: a) Boxplots and b) distributions of remote sensing (orange) and in-situ (blue) monthly Chl-a anomalies.

3.3.2 General findings:

The average of Chl-a (Figure 3.4a) showed that higher concentrations ($> 2 \text{ mg m}^{-3}$) were generally found near the coast, in areas with bathymetries less than approximately 30 m. This excludes the shallow region of Dogger Bank (Figure 3.1). Areas with higher standard deviation ($\text{sd} > 1 \text{ mg m}^{-3}$) were also found in shallow areas, with a depth less than 30 m. The increased variability in these shallow areas is primarily due to larger seasonal differences compared to the offshore waters (see Amorim and Wiltshire et al 2023 on temperature and seasonal variability comparisons for shallow and offshore sites). The standard deviation reflects the inter-pixel variability. Therefore, the coefficient of variation (CV) provided a measure of the spatial heterogeneity within the study area (Morel et al., 2010). The CV showed that 60% of the studied area is between 40 and 60%, a medium term between stable and large fluctuations. Two areas with larger CVs are in the north, around the Dogger Bank and the Danish coastal zone where there is a large bathymetry gradient; another area with high CV was found in the southern shallow waters of the Dutch coast, which is influenced by the water inflow from the English Channel. In the central region of the GB, we have identified significant negative linear trends with values ranging around from -0.01 to -0.03 (mg m^{-3}) per year. In contrast, the south-eastern corner of the study area, which is influenced by fresh water runoff from the river Elbe, exhibited positive significant linear trends (up to about 0.02 (mg m^{-3}) per year).

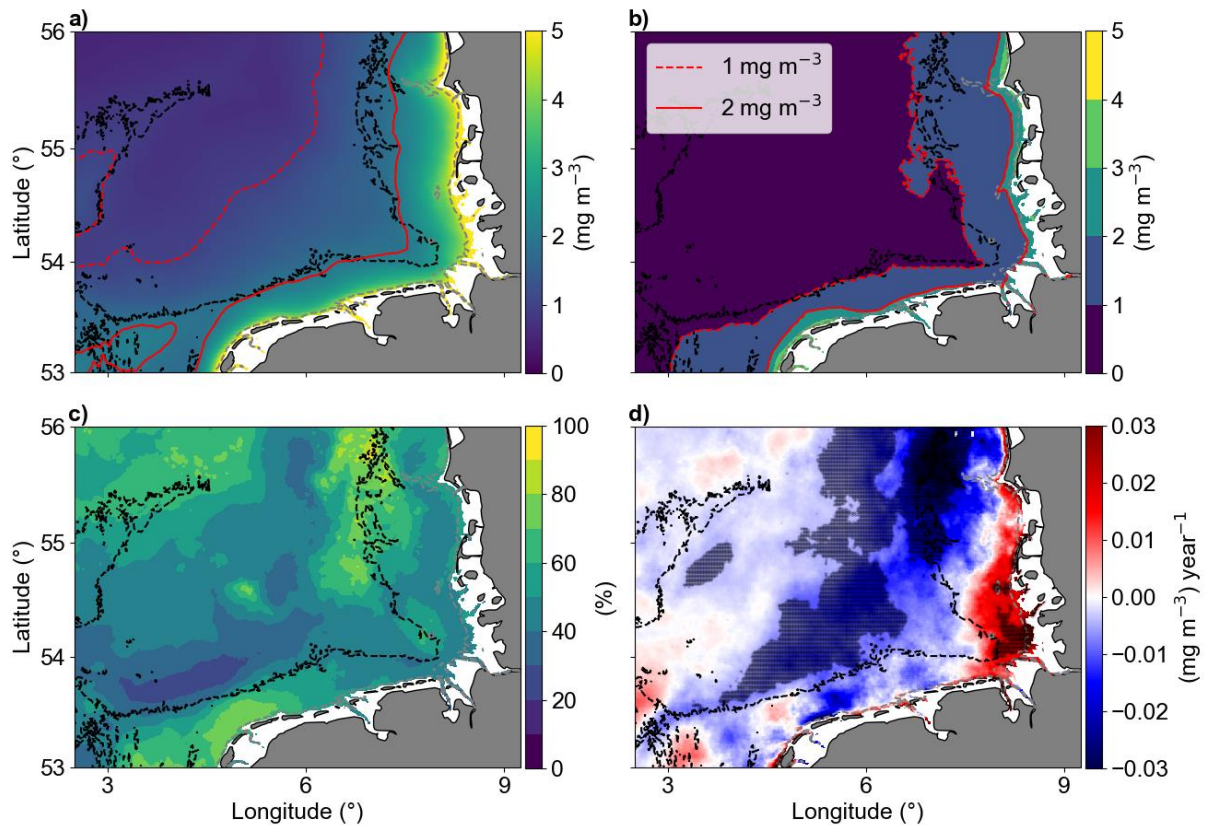


Figure 3.4: The a) temporal mean and b) standard deviation of chlorophyll-a concentrations from January 1998 to December 2020. Solid and dashed red lines represent 1 and 2 mg m⁻³, respectively, and the grey and black dashed lines are the 10 and 30 m isobaths. c) Coefficient of variation, in percentage. d) Trends of Chl-a anomalies (mg m⁻³ per year). The shaded areas are significant (p-values < 0.05; two-sided Wald test with t distribution).

Since 1962 there has been a notable SST increase in the North Sea, a trend that persists to the present (Amorim and Wiltshire et al., 2023). Specifically within the German Bight, the mean SST anomaly trend, as estimated by the locally weighted scatterplot smoothing method (LOWESS; Cheng et al., 2022) indicated an increase of 0.77°C from 1998 to 2020 (Figure 3.5). This was further confirmed by the Mann-Kendall trend test, which showed a significant positive trend (p-value < 0.001). However, when it comes to the averaged MLD, no significant trend was observed.

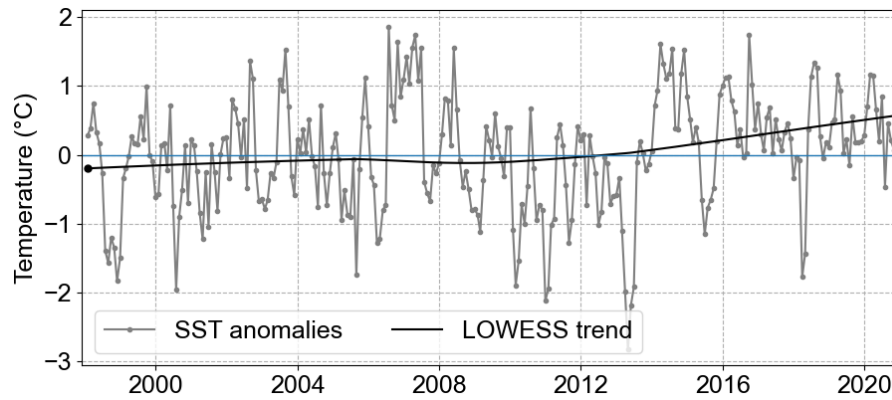


Figure 3.5: SST anomalies averaged for the whole German Bight (grey line) and trend from 1998 to 2020 calculated by LOWESS (black line).

3.3.3 Seasonal Chlorophyll-a surface concentration

The monthly climatological means (Figure 3.6) were characterized by decreasing concentrations from coast towards offshore areas. The months of April and May exhibited elevated chlorophyll concentrations, a result that aligned with existing literature on the spring blooms of diatoms (Wiltshire & Manly, 2004; Wiltshire et al 2010; Neumann et al., 2021). A slight increase was observed in August, indicative of the late summer/autumn bloom of dinoflagellates (Yang et al., 2021).

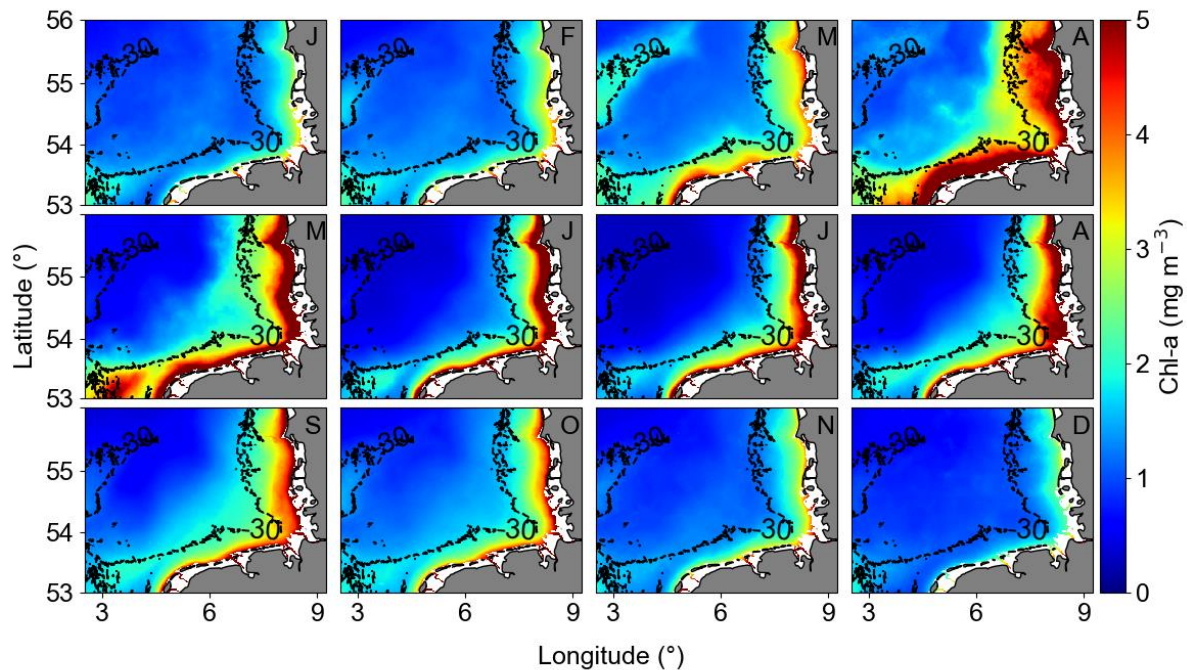


Figure 3.6: Monthly-averaged GlobColour Chl-a, from January 1998 to December 2020 (letters on top right). The Chl-a monthly anomalies are calculated subtracting the monthly-averaged Chl-a from the absolute Chl-a data. It is possible to observe the intra-annual behaviour of Chl-a, with a positive gradient from open waters to coast, and the increase in Chl-a in April and August.

Figure 3.7 illustrates the seasonal cycle of Chl-a remote sensing, spatial averaged for coastal and offshore areas, and HRTS in situ. Both coast and offshore were defined by a larger Chl-a peak in April, describing the phytoplankton spring bloom. Higher variability was observed in the coastal area, and a smaller peak, representing the late summer/autumn bloom, was observed in August. Values below 2 mg m^{-3} were observed from November to February. The offshore area second peak was more perceptible compared to coastal areas, and it was observed in September/October. The summer Chl-a decrease was more accentuated in relation to the second peak in offshore areas, characterizing the period of lowest Chl-a, below 1 mg m^{-3} . The in situ HRTS acquired in the transitional zone of the German Bight, between coastal and offshore areas, aligned well with the spatial averages of Chl-a remote sensing, although the spatial averaged Chl-a remote sensing was overestimated during winter months, and the second bloom peak was delayed in offshore areas.

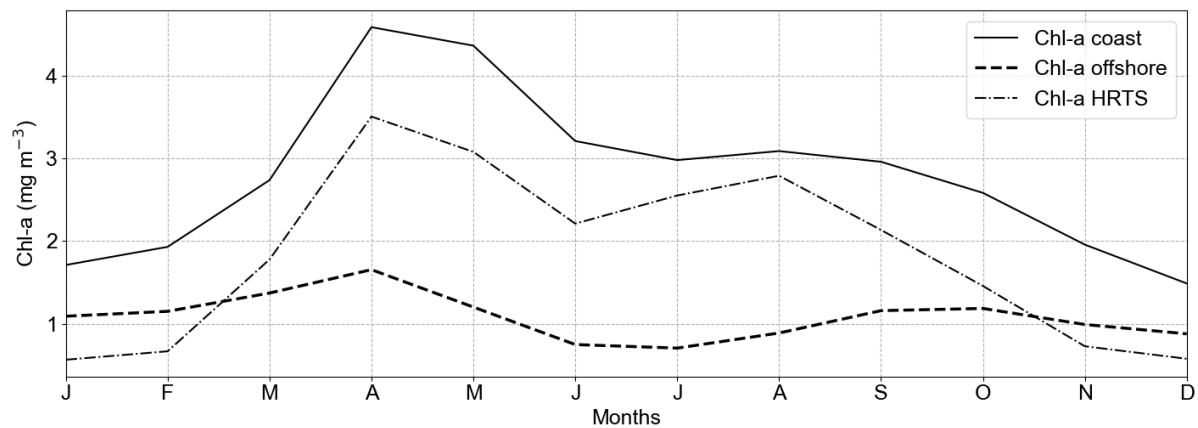


Figure 3.7: Seasonal cycle of Chl-a averaged for areas above the isobath of 30m (coast), areas below 30m (offshore) and HRTS.

The Empirical Orthogonal Functions (EOFS) applied to the climatological Chl-a values in Figure 3.6 revealed a dominant seasonal variation. This variation was represented by the first and second modes, which together explained 88% of the total variance in the annual cycle of Chl-a in the region (Figure 3.8). For interpretation, we made use of the variability signals in the spatial modes/structures (EOF) defined by the red and blue colours (positive and negative, respectively) together with the signal of the associated principal component (PC). The first spatial mode (EOF1) accounted for 53% of the annual Chl-a variability, exhibiting a positive signal across the entire German Bight. The first principal component (PC1) showed the two bloom signals, the spring bloom, in April, and the late-summer bloom, in September. Overall mode 1 described the maximum positive Chl-a variability during the spring bloom and, to a lesser extent, the late summer/autumn bloom (same signal in the spatial and PC temporal pattern), in contrast with winter and summer months, described by negative variability (opposite signals). The second spatial mode (EOF2) explained 35% of the Chl-a variability, dividing the GB in two regions based on the variability between cold and warm months. The coastal/transition region was defined by maximum negative variability during the winter months and positive during summer months, according to the signals of EOF2 and PC2. Opposite, the offshore region showed negative variability during summer and positive variability during winter. This matched with the seasonal cycle of Chl-a shown in Figure 3.7, which represented the minimum Chl-a months in coastal areas during winter, but during summer in the offshore region.

Following EOFs mode 1 explained variability, we determined April and September as the most contrasting months for explaining the positive Chl-a variation in association with the environmental and biological/ecological drivers, and winter and summer as the negative variability months.

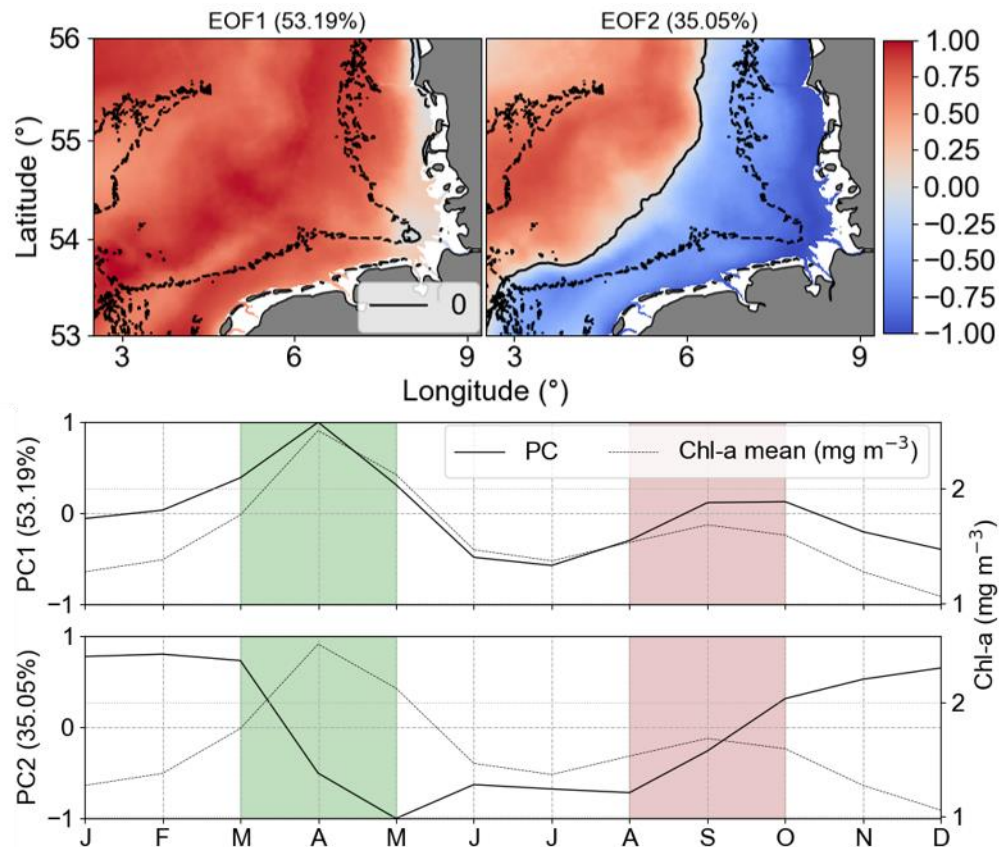


Figure 3.8: First and second EOF and PC modes of monthly climatological means of Chl-a. Dashed thin line is the Chl-a spatially averaged at the study area. March-April (green shaded) and August-September (pink shaded).

3.3.4 Month of maximum Chlorophyll-a concentration

96% of the German Bight area here analysed had a maximum climatological chlorophyll-a observed in March, April and May (20%,63% and 13%, respectively), representing the main months of primary production, and mainly related to diatom blooms (Wiltshire et al, 2008).

One interesting result for the remote sensing assessments was the month with maximum chlorophyll concentration (Figure 3.9). Around Helgoland Roads position, August was,

according to the remote sensing data, the month with maximum chlorophyll. However, this is not consistent with the HRTS HPLC dataset. This might be an influence of the suspended matter dynamics (Fettweis et al., 2012) and/or the different pigmentation in phytoplankton species. Considering the two blooms occurring in the area, the spring bloom is characterized by dominant abundance of diatoms while the late summer/autumn bloom has also high abundance of dinoflagellates, more prone to develop in stratified periods and with different pigment compilations (Shang et al., 2014; van Leeuwen et al., 2015). There is a defined difference between the reflectance spectra of diatoms and dinoflagellates due to the distinct amounts of pigment types in each species (Shang et al., 2014) and such enhanced chlorophyll-a could be associated with cellular motility and the ability to regulate position in the water column, resulting in enhanced near-surface aggregation of flagellated cells (Franks, 1992). The Dogger Bank area was characterized by an early maximum in March, whereby could be that the shallower bathymetry allows the development of the spring bloom earlier due to light availability and enough nutrients for the growth of phytoplankton (Moll, 1997; Los et al., 2008).

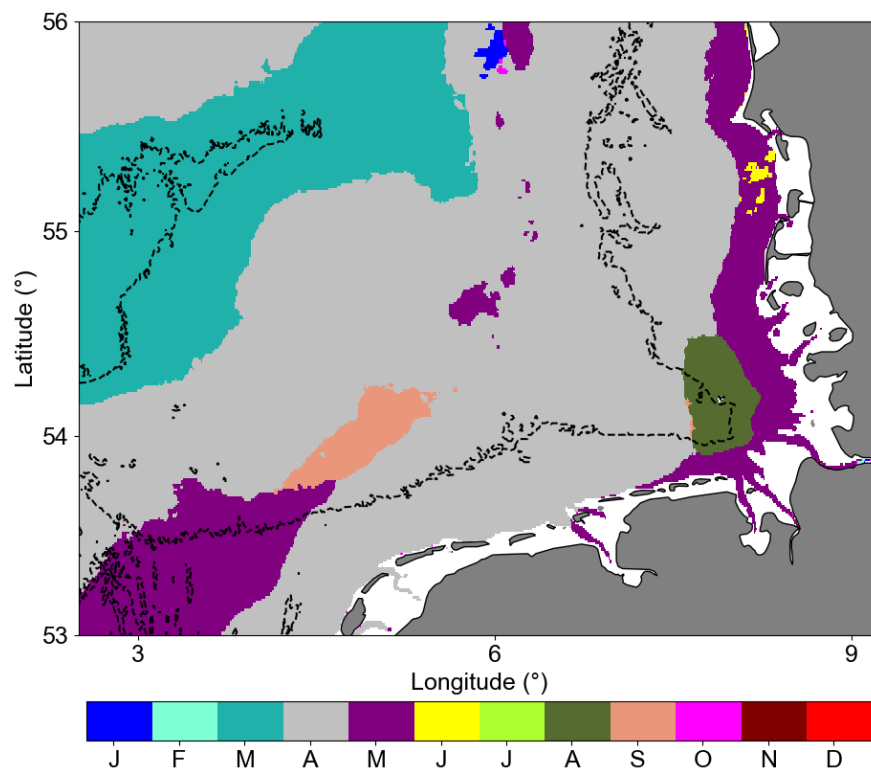


Figure 3.9: Month (colour bar from January to December) with maximum Chl-a by pixel from the monthly climatology means of Chl-a (Figure 3.6; mg m^{-3}). April (light grey) is the dominant month.

3.3.5 Chl-a distribution before and after 2009

We examined the Chl-a anomalies spatial averages for the months of March, April and May over the 1998-2020 period to visually identify any potential increase or decrease of Chl-a, assessing interannual variability in coastal and offshore areas (Figure 3.10). As the Mann Kendal trend test did not point any significant trends in the averaged Chl-a anomalies, we analysed the changes in Chl-a anomalies distribution, splitting the time series based in the April peak observed in 2008 for both coastal and offshore areas (Figure 3.10). The peak in Chl-a anomalies in 2008 was related with a positive peak of North Atlantic Oscillation index winter mean (NAO) (Figure 3.10). In 2010, negative Chl-a anomalies peak was observed in April and May in the offshore area and, in coastal area, in May, coinciding with an also negative peak of NAO. After 2010, a positive NAO winter trend was observed. Considering these observations, we defined two periods to analyse Chl-a anomalies distribution: until 2009 and after 2009.

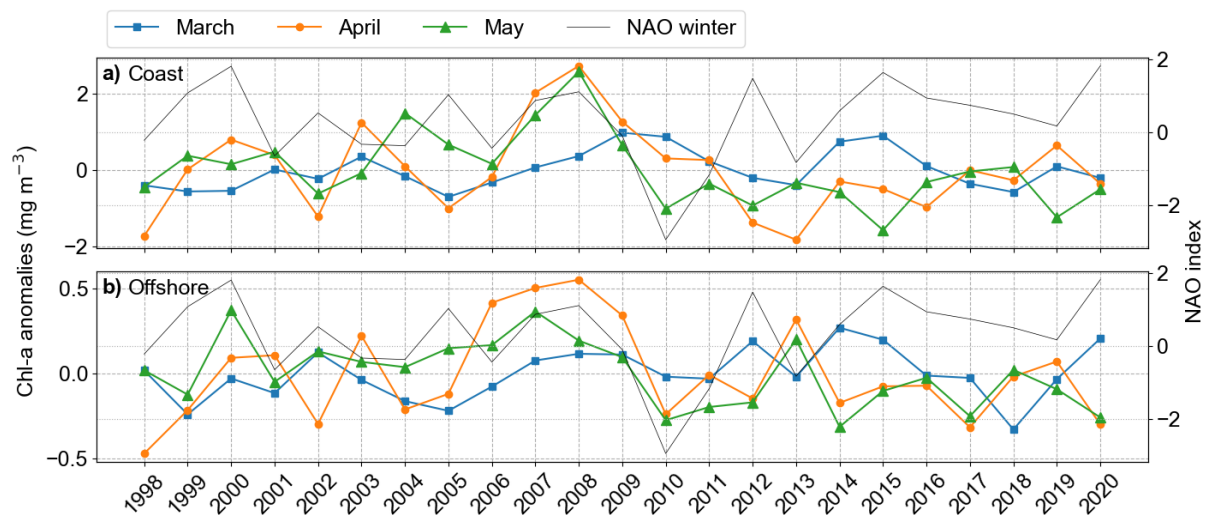


Figure 3.10: Spatial averages of Chl-a anomalies in coastal waters (a) and offshore (b) for the months March, April and May. The NAO index winter mean (December, January, February) is the black thin line.

We calculated the Probability Density Function of the two periods to investigate the changes occurring in the distribution of Chl-a anomalies (Figure 3.11). For the coastal area, March showed a shift from slightly normal to a bimodal distribution, with a small negative bias related to the mean. The bimodal distribution was still dominated by Chl-a negative anomaly values but with a lower second peak in positive values, indicating years with positive Chl-a

anomalies. The offshore area distribution described an increase in variance and increase of positive anomaly values. These results could be the response of earlier spring blooms in the period 2010-2020 compared to the years before. April showed the highest variance change, decreasing from the first period (1998-2009) to the second period (2010-2020). The decrease in positive anomaly values was evident and it can be considered as part of the negative trend observed in the German Bight, together with the shift in May, moving completely from positive to negative anomalies (Figure 3.11).

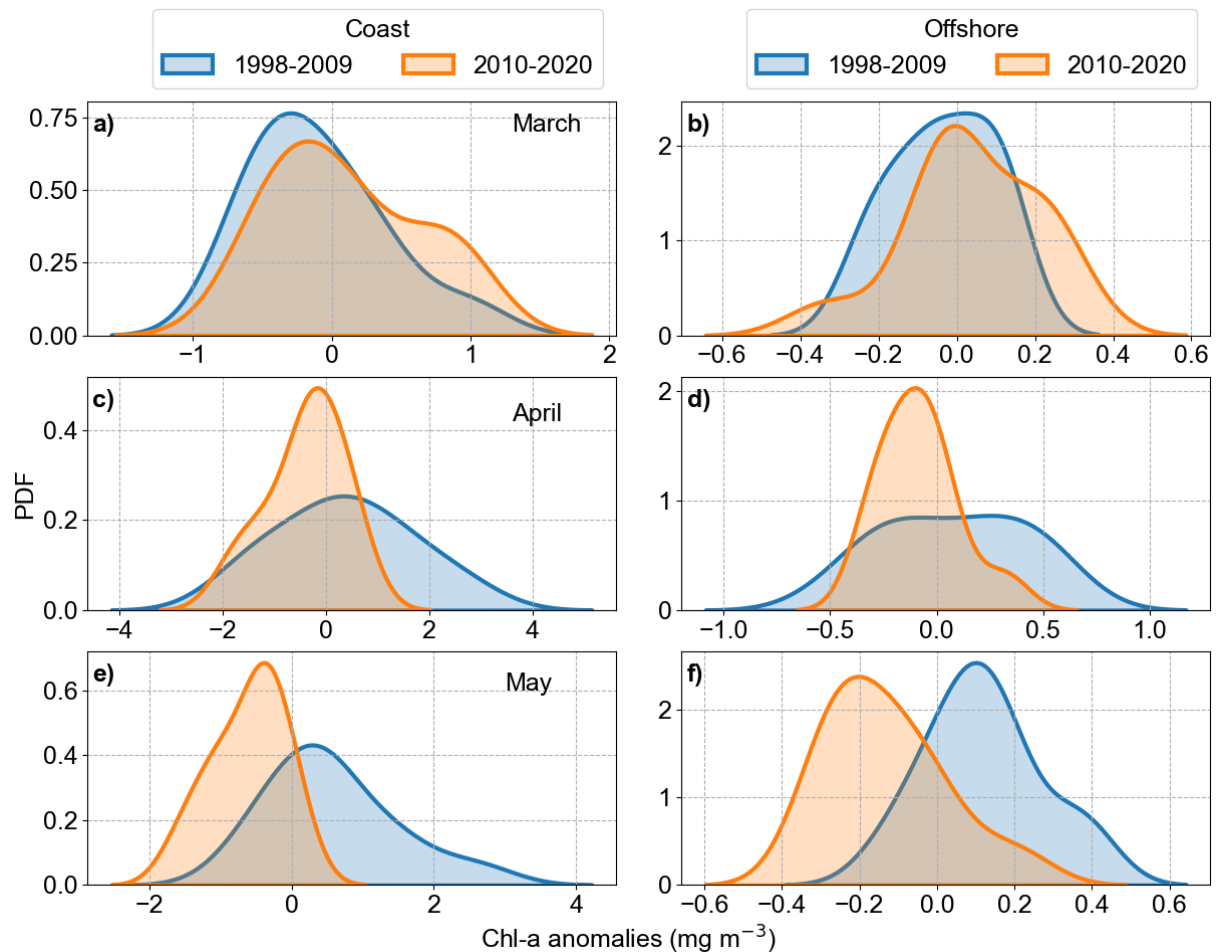


Figure 3.11. Probability Density Function estimated from 1998-2009 (blue) and 2010-2020 (orange) for the Chl-a anomalies in March, April and May in the coastal and offshore areas of the German Bight.

3.3.6 Chlorophyll-a Overall Trends

Figure 3.12 shows the trends of Chl-a anomalies in the GB. Mann-Kendall trend test showed that Chl-a anomalies significantly decreased in 31% of the analysed area ($p < 0.05$). In the coastal area, mostly defined in the south-eastern corner of the study area, we found significant positive trends, covering 4% of the analysed area. In this region, there are available nutrients because of continued river input. Even with the turbid characteristic waters due to the river plumes influence, light availability is not a limitant (Fichez et al., 1992; Kerimoglu et al. 2017).

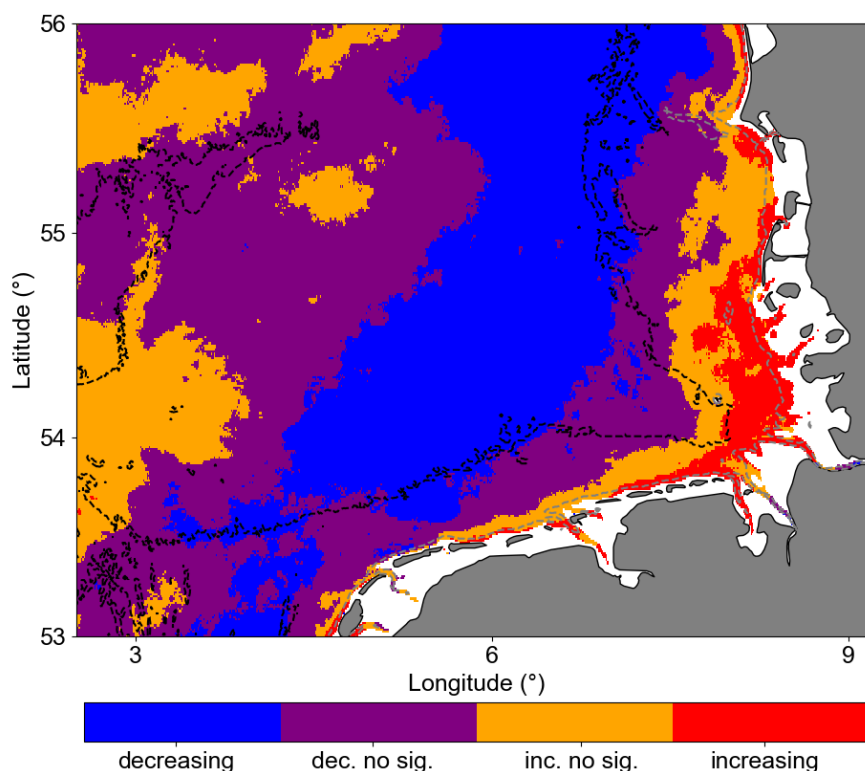


Figure 3.12: Trend significance of Chla-a anomalies computed with Mann-Kendal trend test. Pixels with p -values < 0.05 are considered significant. dec. no sig.= decreasing not significant, inc.no sig. = increasing not significant.

Most of the central German Bight showed significantly negative trends. Associating the observed overall trends with the observed distribution changes, Amorim and Wiltshire et al (2023) examined the winter mean NAO index and computed a positive trend. Also, the period after 2010 is characterized by long phases of a positive NAO index (Figure 3.10, thin black line). Naturally, the positive NAO phase is associated with strong and frequent westerly (W)

and southwesterly (SW) winds during winter and spring. In addition, also localized cyclonic systems over the British Isles can generate such winds (see Rubinetti et al., 2023). As expected, there is a positive trend within the 21st century in a frequency of W-SW winds (Rubinetti et al., 2023). Due to the Ekman transport, SW and W winds suppress the spreading of coastal waters from the south of the German Bight, offshore, and intensify counter-clockwise wind-driven circulation in the German Bight (Schrum, 1997; Chegini et al., 2020). In addition, NAO in its positive phase characterizes strong Atlantic wind-driven inflow through the English Chanel, increasing mean temperatures in the North Sea (Pingree, 2005). In the spatial SST average (Figure 3.13), we can see a tongue with North Atlantic water temperature characteristics, i.e. warmer than the characteristic German Bight surface water. This means that negative and positive trends in Chl-a offshore and coast, respectively, can partly be explained by the wind pattern and in particular by increasing frequency of W-SW winds during winter and spring, which leads to limited offshore spreading of rich nutrient coastal waters, and increases the warm Atlantic water inflow into the North Sea.

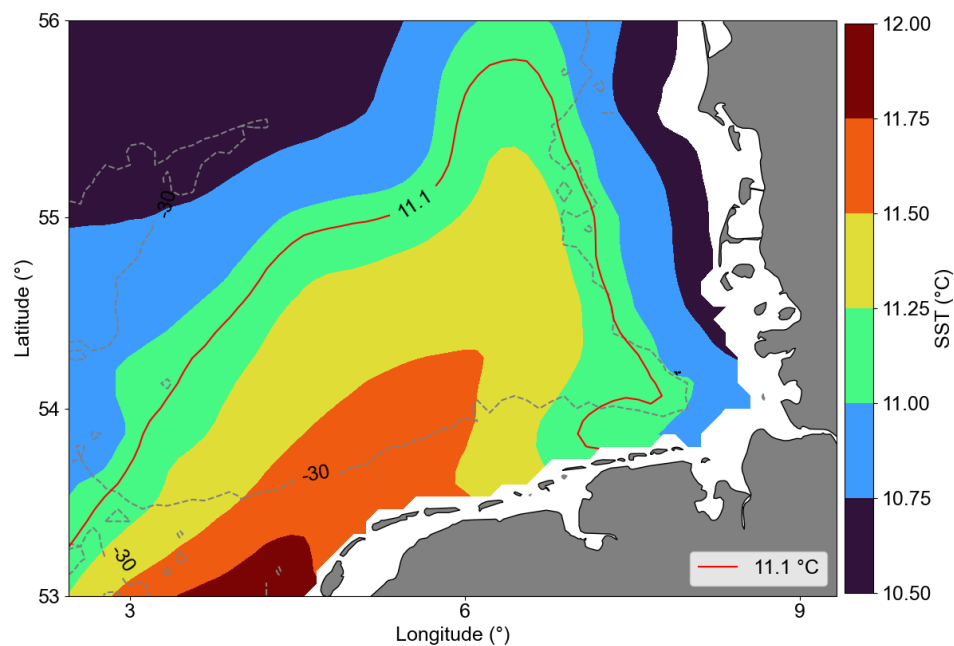


Figure 3.13: Sea Surface Temperature time averaged for the study area. The red line marks the 11.1 °C isotherm.

3.3.7 Dominant modes of non-seasonal Chlorophyll-a Variability

EOFS analysis was applied to examine the long-term non-seasonal variability in more detail. Recent studies have used this type of analysis on chlorophyll remote sensing and model simulation spatial data to detect the influence of environmental/oceanographic processes on phytoplankton biomass time/space variability (Daewel & Schrum, 2017; Alvera-Azcárate et al, 2021). Results of our EOFS analyses showed that the first four modes accounted for 45% of Chl-a non-seasonal variability in the study area. The percent variance explained by each mode was 19.02% (mode 1), 11.79% (mode 2), 8.36% (mode 3) and 5.54% (mode 4). Figure 3.14 shows the spatial patterns for the EOFS modes 1–4 which are associated with dominant long-term non-seasonal features, since seasonal frequency cycles have been removed by the climatological monthly means subtraction procedure. The normalized amplitude time series (principal component, PC) corresponding to the spatial patterns (EOF) and the monthly means are shown in Figure 3.15a-d and Figure 3.16e-h, respectively. The PCs represent the time evolution of all pixels in the corresponding mode spatial pattern. If a pixel in the spatial pattern and its associated temporal amplitude have the same sign, it means a positive chlorophyll deviation for that pixel at that time, in relation to the zero value in the spatial map. Conversely, when pixels in the spatial pattern and associated temporal amplitude show opposite signs, it means a negative deviation from zero. Therefore, pixels that show similar signs and values in the spatial pattern (Figure 3.14) have similar behaviour in time and represent coherent features (Garcia & Garcia., 2008).

In terms of the spatial variability of Chl-a, we show that there were distinct spatial and temporal variability in the German Bight concerning the modes of variability. EOF1 showed the same signal for the whole German Bight i.e. a decreasing variability from coast to offshore regions and, as indicate by the PC1, it is mostly related with interannual variability during spring blooms and positive peaks after the late summer/autumn bloom. EOF2 split the area into offshore (northwest region) and transitional/coastal waters from southwest to northeast. EOF3 was characterized by a positive signal in the southwest region, possibly related with the English Channel inflow, bringing warmer waters to the German Bight. EOF4 can probably be related to stratification for a relatively long time mediated by the wind forcing and river forcing associated with Elbe and Weser fresh water discharges (Chegini et al., 2020). It is important to point that the modes or structures of variability contain information about the variability of the dataset that is not necessarily related directly to physical features. The interpretation of the

EOFS modes just aims to relate the data modes with physics (Olita et al., 2011). The temporal amplitudes associated with the spatial patterns are also object of physical interpretation. To facilitate the interpretation of the PCs, we applied the spectral analysis information (Figure 3.15i-l).

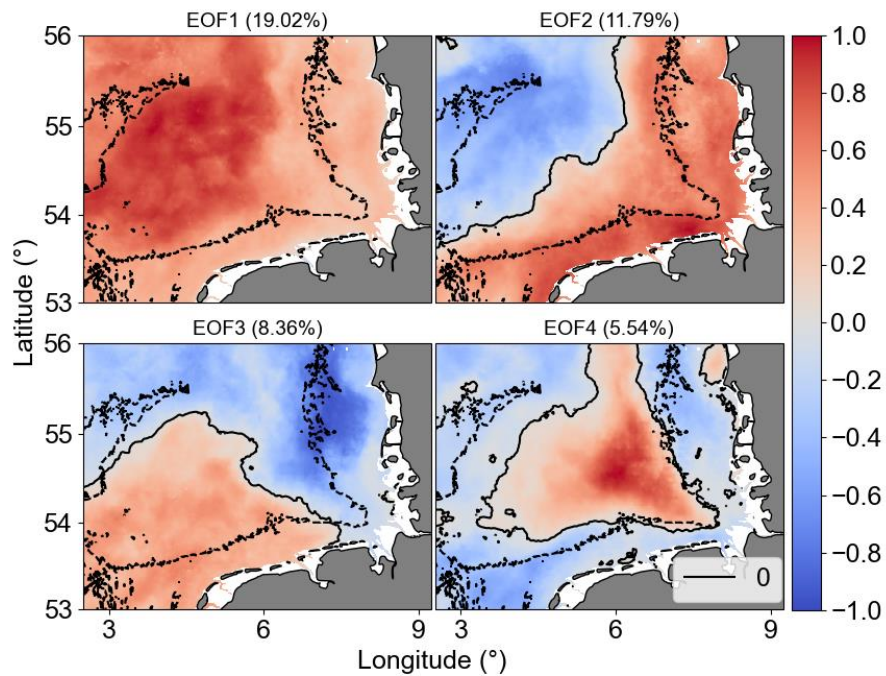


Figure 3.14: First four Chl-a anomalies EOF and PC modes. In EOF fields, black solid line is the 0 amplitude contour and black dashed lines are the isobaths of 30m. The amplitude values shown are all max-normalized. Explained variability percentage for each mode are depicted inside parenthesis.

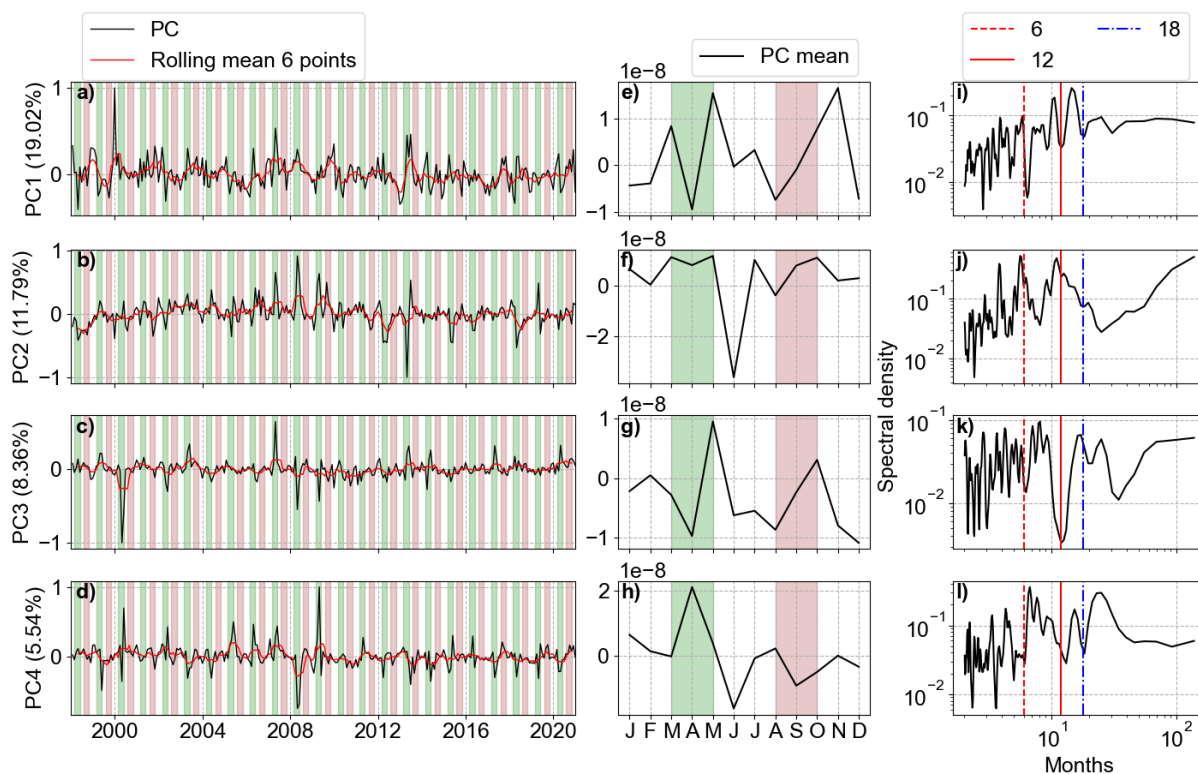


Figure 3.15: First four Chl-a anomalies PC. a-d) the PC amplitudes (black) with 6 point rolling means (red solid). e-h) PCs monthly means. i-l) Spectral analysis of PCs time-series. The amplitude values are max-normalized. Explained variability percentages are depicted inside parenthesis. March-April (green shaded) and August-September (pink shaded).

The spectral analysis of the Chl-a anomalies PC1 identified the highest peak of energy around 15 months and another high peak at 11 months, related to interannual variability, mostly at the spring bloom April month, while PC2 has peaks at 4, 6 and 12 months, linked to the intra annual variability. In the averaged PCs, we can see that PC1 accounted for the variability of the two blooms, while PC2 was related with the decrease of Chl-a during summer months, happening mainly in deeper areas due to nutrients depletion during the spring blooms and the zooplankton grazing. PC3 and PC4 together accounted for approximately 14% of the variability and seemed to be characterized by extreme values occurring in sporadic periods due to the English Channel and Elbe river inflows, as observed in the EOFs.

3.3.8 Chlorophyll-a, Temperature and Mixed Layer Depth relationships

Linear correlations revealed significant but not strong relationships between Chl-a anomalies variability and SST or MLD anomalies at the study area (Figure 3.16). For Chl-a and SST correlations, the southern coastal area (along Germany and Netherlands border) was characterized by significant positive correlation, while a patch of negative correlation was observed close to the Dogger Bank area. For Chl-a and MLD, most offshore areas showed significant positive correlations, indicating that positive MLD anomalies were correlated to positive Chl-a anomalies. The correlations between Chl-a and MLD close to the coast and around isobaths of 30 m were negative. Lagged correlations between Chl-a and the two parameters (SST and MLD) did not provide higher correlations, indicating that the Chl-a variability possibly responds in time scales shorter than monthly periods or longer time scales. Focusing in the areas with significant correlation in Figure 3.16, Chl-a and SST anomalies lagged correlations were negative around the Dogger Bank, where bathymetry changes from around 50 m to shallower than 30 m in the bank area. The southern coastal area of the German Bight is described by positive correlations, a result not aligned with the Chl-a overall trends, indicating an indirect effect of temperature on Chl-a. The Chl-a and MLD correlations are positive in most of the deeper parts of the GB, where higher Chl-a values were found and connected with deeper MLD. In most of the areas shallower than 30 m, Chl-a and MLD anomalies were negatively correlated.

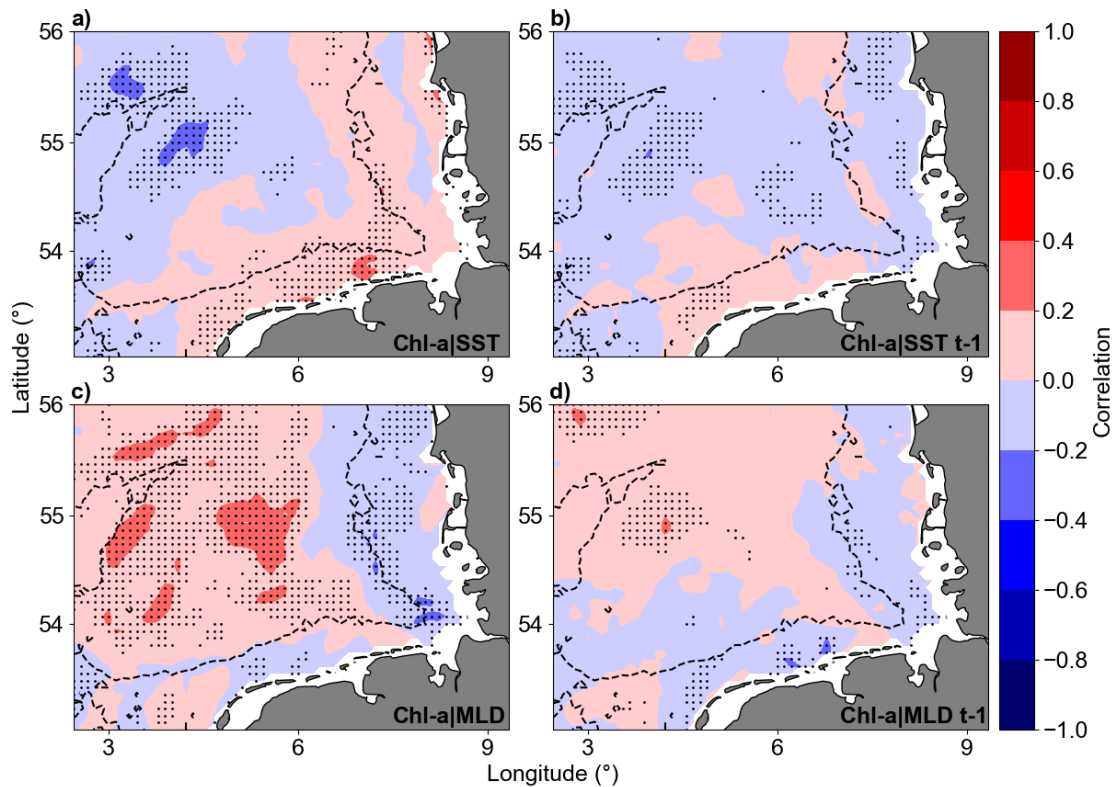


Figure 3.16: Correlation maps of Chl-a and SST (a, b), and Chl-a and MLD (c, d). b) and d) lagged correlations with Chl-a lagged one month. Warm colours are positive and cool colours are negative correlations. The dotted areas are significant (p-values < 0.05; two-sided Wald test with t distribution).

Maximum Covariance Analysis (MCA) was carried out on Chl-a anomalies and SST and MLD anomalies to identify spatial patterns. With this we hoped to explain as much as possible of the mean-squared temporal covariance between the two fields (Bretherton et al., 1992). MCA produces two sets of singular vectors along with a set of singular values. The relevant property of these singular vectors is that they maximize covariance (Storch & Zwiers, 1999; Martínez-López & Zavala-Hidalgo, 2009). The correlation coefficient between the “same mode” principal components of the two fields quantifies the strength of the coupled maximum covariance described by that mode (Martínez-López & Zavala-Hidalgo, 2009). This possibly tells us about how strong the processes are directly connected or if there are other indirect processes involved, and about the time scale coherence between the variables (Fukutome et al., 2003; Rieger et al., 2021)

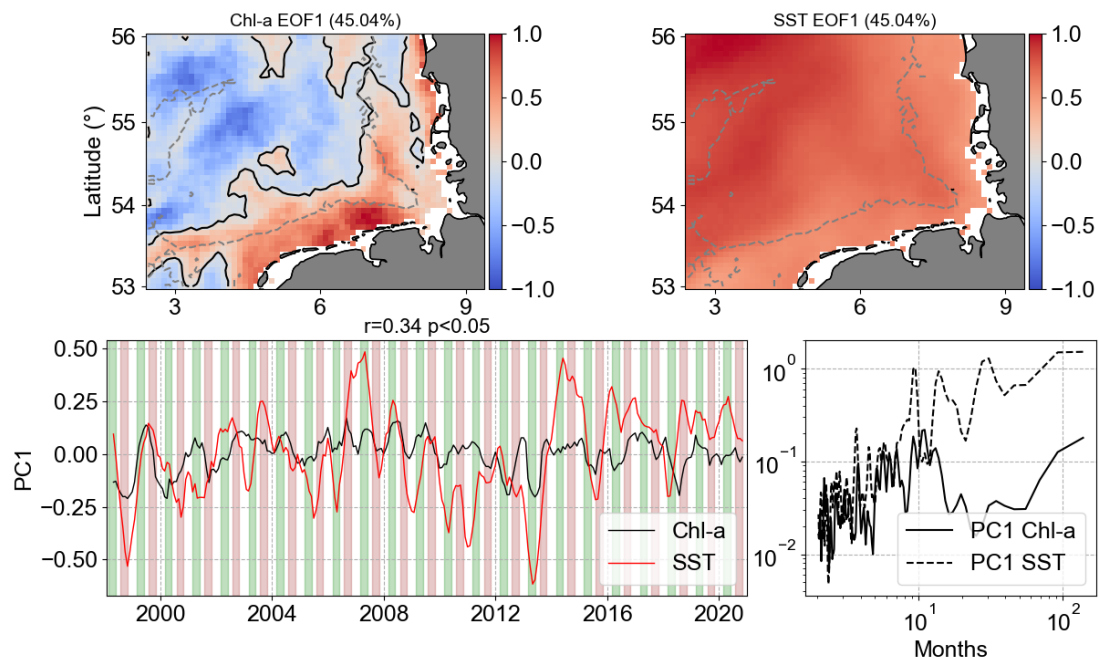


Figure 3.17: MCA results applied to Chl-a and SST anomalies. PC1 is shown as rolling mean of 6 points.

The MCA Chl-a|SST anomalies first mode (Figure 3.17) presented positive anomalies covering the whole German Bight for SST, while the Chl-a showed negative anomalies in the deeper offshore area, far from the coast, and positive anomalies in the depths around 30 m and shallower. The largest negative Chl-a anomalies in mode 1 were in areas surrounding the Dogger Bank, and the positive ones in the coastal southern part of the German Bight. This pattern was already visible in the Chl-a|SST anomalies correlation presented in Figure 3.16. The first mode explained 45% of the covariance between Chl-a anomalies and SST anomalies, the non-seasonal variability. The result of MCA mode 1 was more or less what was observed in the spatial Chl-a correlation, with positive correlation in offshore waters and negative correlation in the coastal areas. In the offshore region, we assume this is the role played by the critical depth theory (Sverdrup, 1953; Tian et al., 2011) and the weakening of turbulence after winter (Wiltshire et al., 2015). The PC1 showed a significant weak correlation of 0.34, meaning weak coupling between the two PCs. The spectral analysis of PC1 did not show connected peaks, indicating that intra-annual variability in Chl-a covariates with lower frequencies of SST. The mode 2 of Chl-a|SST anomalies MCA explained much less, only 9.2% (not shown).

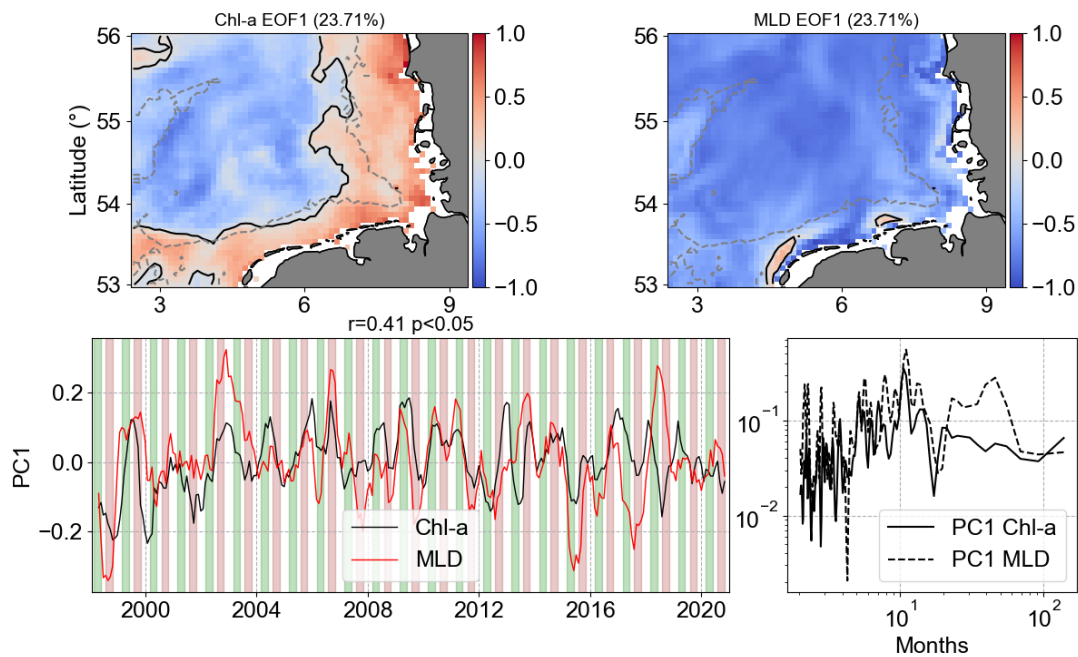


Figure 3.18: MCA applied to Chl-a and MLD anomalies. PC1 is shown as rolling mean of 6 points.

The MCA mode 1 of MLD anomalies had the same signal in the majority of the analysed spatial domain, but Chl-a mode 1 had a clear separation between coast and offshore (Figure 3.18). MLD and SST work in opposite ways for these two regions. Even though mode 1 of Chl-a and MLD anomalies accounted for approximately 23% of covariance, less than the Chl-a|SST, the Chl-a|MLD PC1 spectral analysis showed slightly higher coherence, with non-seasonal changes in MLD affecting Chl-a in the same temporal scale.

3.4 DISCUSSION AND SUMMARY

The use of the Copernicus GlobColour chlorophyll-a surface concentration allowed a comprehensive analysis of Chl-a long term trends and variability (23 years) in the German Bight. The evaluation of the GlobColour remote sensing dataset using a long HPLC Chl-a time series from the Helgoland Roads showed good agreement in trends and variability. The seasonal intra-annual variability in coastal and offshore areas of the GB was defined by two Chl-a peaks, characterizing the spring and late summer/autumn phytoplankton blooms. Higher variability in coastal waters was observed between winter and bloom periods, while in offshore areas, the higher variability was between summer and the bloom periods. The distribution of coastal and offshore area averaged Chl-a, before and after 2009, was characterized by clear changes in April and May Chl-a anomalies, with decrease of variance and the distribution peaks moving to negative values. Following the distribution changes, the overall trends in the German Bight were described by a large area in the centre of the GB with significant negative trends, with only a limited area close to the Elbe river influence showing significant positive trends. The dominant modes of the non-seasonal Chl-a variability defined spatial and temporal components, associated to interannual variability of Chl-a during the bloom periods and a distinction between coastal/transitional and offshore areas. The English Channel and river inflows accounted for a small fraction of the explained Chl-a variance. The covariability of Chl-a anomalies with SST and MLD anomalies, assessed by Maximum Covariance Analysis, showed higher covariability between Chl-a and SST, but the spectral analysis and the lower PC correlation indicated distinct time scales of variability. In the case of Chl-a and MLD covariability, the value was almost half of the one observed for SST, but occurring in the same time scales. The low linear correlation between Chl-a and SST could mean that there are indirect effects caused by temperature changes. The direct positive influence of increasing temperature is limited and can be outweighed by negative indirect effects and other factors, such as nutrient availability.

It is important to point that the changes and variability in Chl-a cannot be assumed to happen only due SST or MLD, but as a combination of factors that can compensate or amplify each other (Xu et al., 2020). The relationship between SST and MLD together with the availability of light, nutrients and turbidity controls mostly of the primary production variability in the German Bight. Changes in ocean surface temperature are associated with changes in other variables, including biological variables such as Chl-a, primary productivity,

species physiological responses and species distributions (Dunstan et al 2018, SST and Chl-a). Potentially, warming can either affect directly and indirectly the Chl-a variability. Higher temperatures can alter the species physiological responses and species distributions (Dunstan et al., 2018). Wind patterns and fresh water discharge are impacted by climate change, and phytoplankton predation are enhanced by the increase in temperature due to accelerated metabolism of zooplankton. The mechanism of influence becomes intricate as temperature modifies the physiology of species, species composition, river runoff, and other factors (van Beusekom & Diel-Christiansen, 2009; Capuzzo et al, 2018; Dunstan et al., 2018). Although there is a direct positive influence of increasing temperature, it is limited and can be outweighed by negative indirect effects and other factors, such as nutrient availability.

Balkoni et al (in prep.) estimated nutrients decadal changes in the German Bight and the results point out that there is a decrease in nutrients. Capuzzo et al (2018) pointed that observed decrease in primary production in the North Sea from 1988 to 2013 are attributed to increasing temperature and decrease in nutrients, corroborated by Desmit et al. (2020) analysis in the southern North Sea. van Beusekom and Diel-Christiansen (2009) identified that higher temperatures favours zooplankton growth and grazing during the spring blooms, decreasing the intensity of phytoplankton growth. Alvera-Azcárate et al. (2021) observed decreasing trends and slight increase of Chl-a in the last 12 years for the whole North Sea, together with early onset of spring blooms and positive trends in bloom duration, indicating the high variability and heterogeneity in the different regions of the North Sea. A combination of factors is the most likely scenario under climate change for the primary production in the German Bight, but it is important to assess the individual consequences to better understanding the whole.

3.5 CONCLUSIONS

The utilization of GlobColour Chlorophyll-a surface concentration enabled the identification of the primary modes of variability in the German Bight. Overall, the comparison between remote sensing and in situ data demonstrated consistent results in evaluating Chl-a surface variability. Specifically, when comparing the in situ HRTS and remote sensing monthly anomalies, a correlation coefficient (r) of 0.59 and a root mean squared error (RMSE) of 1.09 mg m^{-3} were determined. The analysis of surface chlorophyll-a concentration trends and variability was conducted in conjunction with anomalies in sea surface temperature and mixed layer depth. Spatial Chl-a trends reveal a significant decrease in concentration in the central region of the German Bight over the past 23 years. In contrast, the near-coastal zone influenced by the Elbe River discharge exhibits a notable increase in chlorophyll-a. Concurrently, a positive temperature trend is observed throughout the German Bight. It can be concluded that its direct positive influence on chlorophyll-a concentration is limited and can be outweighed by negative indirect effects and other factors, such as nutrient availability and wind conditions. Over the last 23 years, a positive trend in the frequency of south-westerly and westerly winds during the winter/spring season has been observed, attributed to a prolonged positive NAO phase during the considered period. Such winds prevent the offshore spreading of nutrient-rich coastal waters from the southern German Bight and enhance the warm Atlantic water inflow into the central North Sea. This, in part, can explain the contrasting Chl-a trends in offshore and inshore zones. The EOFs analyses of the chlorophyll-a concentration showed the most variability in the intra-annual blooms (first mode) and the decrease in Chl-a during summer in offshore areas and in winter months on the coast (mode 2), totalling around 88% of seasonal explained variance. For the Chl-a non-seasonal EOFs results, the first mode (19%) was defined by inter-annual variability, with a peak of energy in the spectrum at 11-months and 15-months cycle frequencies. This can be explained by the negative inter-annual variability in the spring blooms and positive variability after late summer/autumn blooms. The first four modes explained 45% of variability, defined by the division into offshore and transitional/coastal waters and intra-annual variability, the English Channel inflow, and the presence of fresh water stratification. The MCA analysis showed higher covariability between Chl-a and SST anomalies than Chl-a and MLD anomalies. The first mode of Chl-a|SST was represented by 45%, and the first mode of Chl-a|MLD by 23%. For next steps, we suggest the analysis of nutrients in the German Bight, relating possible changes with winds and stratification. A

combination of remote sensing Chl-a coupled with vertical in situ data would give even more insight about the 3D variability of Chl-a in the German Bight.

3.6 ACKNOWLEDGEMENTS

This study has been conducted using E.U. Copernicus Marine Service Information (<https://doi.org/10.48670/moi-00289>; <https://doi.org/10.48670/moi-00169>; <https://doi.org/10.48670/moi-00059>). We acknowledge the immense effort of the Aade crew to collect the Helgoland Roads data and the people who carried out the chemical analyses.

3.7 DATA AVAILABILITY

North Atlantic Chlorophyll (Copernicus-GlobColour) from Satellite Observations: Daily Interpolated (Reprocessed from 1997) replaced on July 2022 by the Atlantic Ocean Colour (Copernicus-GlobColour), Bio-Geo-Chemical, L4 (daily interpolated) from Satellite Observations (1997-ongoing), E.U Copernicus Marine Service Information (CMEMS), Marine Data Store (MDS), DOI: <https://doi.org/10.48670/moi-00289> (Accessed on 12 Dec 2021).

ESA SST CCI and C3S reprocessed sea surface temperature analyses. E.U. Copernicus Marine Service Information (CMEMS). Marine Data Store (MDS). DOI: <https://doi.org/10.48670/moi-00169> (Accessed on 23-Mar-2023).

Atlantic- European North West Shelf- Ocean Physics Reanalysis. E.U. Copernicus Marine Service Information (CMEMS). Marine Data Store (MDS). DOI: <https://doi.org/10.48670/moi-00059> (Accessed on 20-Apr-2023).

Link from Chapters 2 and 3 to Chapter 4

Investigations of Chl-a and surface temperature trends and variability demonstrated that these two parameters are linked, with temperature affecting Chl-a directly and indirectly through other variables. In the next chapter, a data-driven approach based on ML algorithms is employed to evaluate the prediction capacity of the Chl-a time series, comparing three ML algorithms and a classical statistics seasonal autoregressive integrated moving average (SARIMA) model. As part of the ML process, the best predictors of Chl-a are defined, testing whether temperature is one of them.

4 Chapter 4

Evaluation of Machine Learning Predictions of a Highly Resolved Time Series of Chlorophyll-a Concentration

Published as: Amorim, F.L.L.; Rick, J.; Lohmann, G.; Wiltshire, K.H. (2021) Evaluation of Machine Learning Predictions of a Highly Resolved Time Series of Chlorophyll-a Concentration. *Appl. Sci.* 11, 7208. <https://doi.org/10.3390/app11167208>

Abstract

Pelagic chlorophyll-a concentrations are key for evaluation of the environmental status and productivity of marine systems, and data can be provided by in situ measurements, remote sensing and modelling. However, modelling chlorophyll-a is not trivial due to its nonlinear dynamics and complexity. In this study, chlorophyll-a concentrations for the Helgoland Roads time series were modelled using a number of measured water and environmental parameters. We chose three common machine learning algorithms from the literature: the support vector machine regressor, neural networks multi-layer perceptron regressor and random forest regressor. Results showed that the support vector machine regressor slightly outperformed other models. The evaluation with a test dataset and verification with an independent validation dataset for chlorophyll-a concentrations showed a good generalization capacity, evaluated by the root mean squared errors of less than $1 \mu\text{g L}^{-1}$. Feature selection and engineering are important and improved the models significantly, as measured in performance, improving the adjusted R^2 by a minimum of 48%. We tested SARIMA in comparison and found that the univariate nature of SARIMA does not allow for better results than the machine learning models. Additionally, the computer processing time needed was much higher (prohibitive) for SARIMA.

Keywords: time series regression; artificial intelligence; Helgoland Roads time series; support vector machine; multi-layer perceptron; random forest; productivity; SARIMA

4.1 INTRODUCTION

Pelagic chlorophyll-a concentrations (chl-a) are a common indicator of primary production and key to evaluation of the health and productivity of marine and freshwater systems (Huot et al., 2007; Terauchi et al., 2014). It is therefore of crucial importance to accurately measure/predict chlorophyll from proxy parameters in such systems (Luo et al., 2019). Accelerated global warming is exacerbating climate change and unsettling ecosystems' processes, while the impacts of this are directly affecting marine primary production and triggering an upwards transfer of effects that reach humans. Thus, the importance of modelling chlorophyll is emphasized in environments undergoing change resulting from global warming (Botkin et al., 2007).

Prediction of chlorophyll-a time series data is a challenge due to their complexity and nonlinearity, and indeed, conventional approaches show limitations with prediction of unobserved data (Shamshirband et al., 2019; Shin et al., 2020). To date, all conventional approaches, including factors based on single measurements, are limited with regard to prediction accuracy of chlorophyll-a concentrations (Kwiatkowska et al., 2003). A few previous studies have tried to implement various machine learning techniques to predict chlorophyll concentrations, mainly in fresh water systems, with a few in marine regions (Cho et al., 2018; Keller et al., 2018; Krasnopolsky et al., 2018; Liu et al., 2019). Machine learning (ML) techniques constitute a set of tools belonging to the fields of computer science and artificial intelligence. The versatility of these techniques allow the successful application in many fields of science and to a great variety of problems. The focus is often placed on tackling pattern recognition problems and on the construction of predictive models to make data-driven decisions (Lo et al., 2019). According to Brownlee (2020), the general benefits of ML algorithms for time series prediction over classical methods include the ability of supporting noisy features, noise and complexity in the relationships between variables and in the handling of irrelevant features. State-of-the-art ML algorithms for time series regression include random forest regressor (RF), support vector machine regressor (SVR) and neural networks multi-layer perceptron regressor (MLP). All of these have been used to some degree in the literature for the prediction of chlorophyll-a concentrations in aquatic systems, and have achieved significantly accurate results in both error and goodness of fit metrics (Park et al., 2015; Liu et al., 2019; Luo et al., 2019). These are studies based in chl-a time series either with short length and daily frequency or long-term, low frequency sampling time series, using different ML

methods to best predict chl-a behaviour. The features applied as predictors in these studies are limited to just a few, but it must be considered that the dynamics in lacustrine systems are distinct from those presented in marine systems. Here we extend these ideas and test these methods on a good quality long-term time series, the Helgoland Roads time series, evaluating the prediction using unseen data. With the purpose to compare ML methods with a classical statistical regression model, we included an improved autoregressive integrated moving average (ARIMA) model, called seasonal ARIMA (SARIMA), which includes seasonal parameters to support data with a seasonal component (Box & Jenkins, 1976).

The objective of this work is to evaluate the accuracy of machine learning algorithms for the estimation of chlorophyll-a concentration, using in situ high-resolution long-term datasets. We (1) assess three ML algorithms—random forest, support vector regressor and neural networks multi-layer perceptron regressor—for chlorophyll-a concentration estimation; (2) examine the importance of feature selection and engineering in the different models; (3) compare with, and evaluate, a univariate SARIMA classical regression model.

4.2 MATERIALS AND METHODS

All the ML models used in this study were implemented applying the “Scikit-Learn package”, which is an open-source Python module project that integrates a wide range of common ML algorithms (Pedregosa et al., 2011; Buitinck et al., 2013), while the SARIMA model was implemented with the statsmodels package (McKinney et al., 2011). The preprocessing was also implemented in the Python environment, using the well-known packages Pandas, NumPy and SciPy (Lemenkova, 2019).

4.2.1 Datasets

The Helgoland Roads is a long-term pelagic monitoring site ($54^{\circ}11.3' \text{ N}$, $7^{\circ}54.0' \text{ E}$) about 60 km off the German coast and represents a marine transition zone between coastal waters and open sea (Figure 4.1) (Wiltshire & Dürselen, 2004). Since 1962, surface water samples have been collected on working days, taken with a bucket lowered from a research vessel. Secchi depth and water temperature (SST) are measured in situ and the water samples analyzed in the laboratory for nutrients (nitrate, phosphate and silicate) and salinity. Chlorophyll-a concentration measurements were started at the end of 2001, acquired in laboratory by FluoroProbe (bbe Moldaenke GmbH, Kiel, Germany) (Beutler et al., 2002) and, since, 2004 have been complemented with high-performance liquid chromatography analysis (HPLC) (Wiltshire et al., 2008; Raabe & Wiltshire, 2009). Sunshine duration, wind speed and direction (Deutsche Wetterdienst (DWD) Climate Data Center (CDC)), North Atlantic Oscillation (NAO) daily index (NOAA ESRL Physical Sciences Laboratory, Boulder, CO, USA, 2020) and zooplankton abundance (Greve et al., 2004), were added to the Helgoland Roads parameter matrix for this work (Table 4.1). As indicated in the literature (Irwin & Finkel, 2008; Capuzzo et al., 2018; Scharfe & Wiltshire, 2019), and also from working experience, the included parameters are environmental variables which determine algal verdure and, thus, modulate chlorophyll-a concentrations in marine systems.

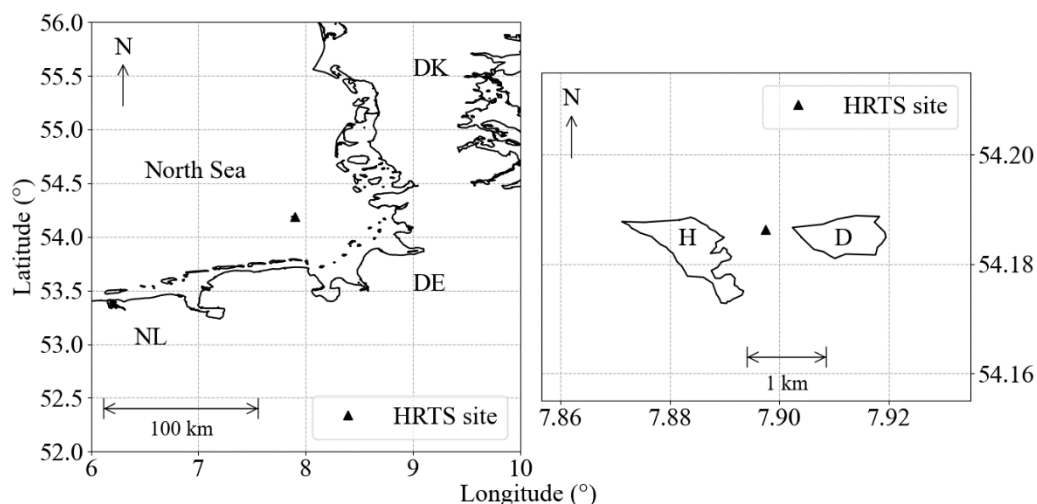


Figure 4.1: Helgoland Roads monitoring site position (black triangle) in the German Bight, between the Helgoland (H) and Dune (D) islands.

Table 4.1: Statistical description of parameters used as determinants to predict chlorophyll-a concentration (target) after linear interpolation (std, min and max are standard deviation, minimum and maximum values) respectively.

Parameters	Units	Counts	Mean	std	min	max	Median
Secchi depth	m	4920	3.70	1.80	0.20	12.00	3.67
SST	°C	4920	10.64	5.00	1.10	20.00	10.30
Salinity	–	4920	32.31	1.06	26.71	36.11	32.42
SiO ₄	μmol L ⁻¹	4920	6.49	5.04	0.01	37.20	5.26
PO ₄	μmol L ⁻¹	4920	0.56	0.41	0.01	3.98	0.53
NO ₃	μmol L ⁻¹	4920	10.19	9.82	0.10	77.38	7.12
Sunlight Duration	h	4920	4.78	4.52	0.00	16.60	3.60
NAO index	–	4920	-9.44	121.5 5	-564.29	351.95	-0.52
Wind Direction	Degrees [°]	4920	203.09	74.71	20.00	353.00	212.00
Wind Speed	m s ⁻¹	4920	8.23	3.28	1.60	20.80	7.80
Zooplankton Abundance	individual s m ⁻³	4920	3164.7 0	4450. 64	5.00	75364. 50	1676.21
Chlorophyll-a	μg m ⁻¹	4920	2.40	2.86	0.00	45.45	1.48

4.2.2 Data Preprocessing

The raw data of Helgoland Roads are characterized by long-term measurements on work-daily frequency, with missing values during weekends and extreme bad weather days. When merged with date of other features such as zooplankton abundance, it ends with approximately 40% of missing data in the time series. To fill the missing data and creating a regular sampled daily time series, a number of imputation methods were tested in sunlight duration, a feature added to the Helgoland Roads from an external source, with no missing values. After creating a synthetic missing values dataset with sunlight duration, we calculated root mean square error (RMSE) and coefficient of determination (R^2) between the original and interpolated data. Minimum changes in frequency distribution between missing data and interpolated variables, lowest RMSE and highest R^2 , were the basis for the decision to use a linear interpolation, supported by (Scharfe & Wiltshire, 2019). After the interpolation, we have daily datasets of parameters in Table 4.1 comprising approximately 13 years, from 2 November 2001 to 22 April 2015, and presented in Supplementary Material, Figure 4.9.

In this study, to validate the performance of the ML models, the dataset was split in 80% ($n = 3940$) for model training, and 20% ($n = 980$) for model testing, so we could investigate the model generalization ability (Mao et al., 2019). To eliminate the dimensional differences of the data and improve the prediction ability of the models, we used the StandardScaler method from the Scikit-Learn package, which standardizes features by removing the mean and scaling to unit variance.

The training dataset, the sample of data used to fit the model, dates from 2 November 2001 to 15 August 2012 (~11 years), while the test set is from 16 August 2012 to 22 April 2015 (~2.5 years) and it is used for model evaluation (Figure 4.2). For independent validation, we used a linear interpolated time series of HPLC estimated chlorophyll data (05 May 2015 to 27 November 2018, $n = 348$).

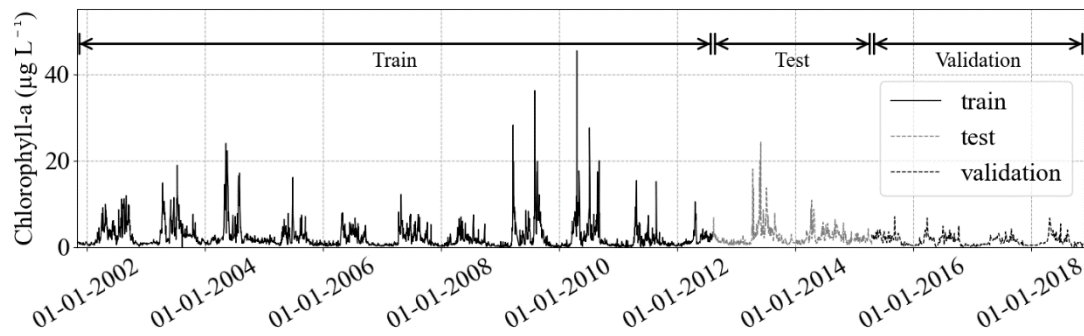


Figure 4.2: The train and test partition in chlorophyll-a concentration target (black solid and grey solid lines, respectively), and the HPLC chl-a validation dataset (black dashed). After the split, the testing dataset will remain untouched, to guarantee no leakage of information to the training step. The validation dataset is the independent validation.

4.2.3 Feature Engineering and Selection

The Pearson correlation coefficients were calculated to investigate linear relationships between chlorophyll-a concentration and the other variables (Table 4.2). All correlation coefficients were lower than 0.5, indicating no strong linear correlation between chlorophyll-a and any other variable.

Table 4.2: Pearson correlation among predictors and the target chlorophyll-a concentration.

Predictors	Code	Correlation
year	year	-0.05
sin(days)	sin(days)	0.04
cos(days)	cos(days)	-0.46
Secchi depth	SD	0.15
Sea Surface Temperature	SST	0.27
Salinity	Salinity	-0.22
Silicate	SiO4	-0.31
Phosphate	PO4	-0.29
Nitrate	NO3	-0.09
Sunlight duration	Sunlight	0.31
NAO index	NAO	0.06
sin(wind direction)	sin	0.02
cos(wind direction)	cos	0.10
Wind Speed	Speed	-0.20
Zooplankton Abundance	Abundance	0.22
Chlorophyll-a	Chl	1.00

Prediction is a major task of time series data mining, which uses known historical values to estimate future values, and feature selection and engineering is essential and crucial for accurate predictions (Tsai & Hsiao, 2010). To seek improvement, 15 days lagged predictors were generated, totalizing 211 features (Lee et al., 2020). The choice of lags was based in a two-week period where all the predictors supposedly influence chlorophyll-a concentration, including chl-a past values, i.e., the lagged target values were used as predictors ($t - 1, \dots, t - n$; with t as the current time and $n = 15$). As there are significant seasonal differences, e.g., summer and winter nutrients uptake, the definition of two weeks seemed reasonable for this work to input information, considering that the machine learning algorithms are data-driven and they are not mechanistic models (Saberioon et al., 2020). Additionally, date features were generated, namely, namely, “year” and “day of year” from 1 to 365 or 366. The cyclic variables “day of year” and “wind direction” were transformed with

$$\sin \left[\frac{2\pi (\text{day of year})}{(\text{number of days in year})} \right] \quad (1)$$

$$\cos \left[\frac{2\pi (\text{day of year})}{(\text{number of days in year})} \right] \quad (2)$$

$$\sin \left[\frac{2\pi (\text{wind direction}(\text{°}))}{(360)} \right] \quad (3)$$

$$\cos \left[\frac{2\pi (\text{wind direction}(\text{°}))}{(360)} \right] \quad (4)$$

to ensure that the last day of a year was understood to be in sequence with the first day of the next year and 0 degree in direction was equal to 360° (Tang et al., 2019).

A large number of features in the dataset drastically affects both the training time as well as the accuracy of machine learning models. One means to limit model complexity from multiple variables is to reduce the model by selectively eliminating predictors. Feature selection procedure was conducted applying a combination of Recursive Feature Elimination. We used Scikit-Learn module Recursive Feature Elimination with cross-validation (Scikit-Learn `feature.selection RFECV` module) and Ridge estimator, to estimate the best number of features balanced with accuracy (Figure 4.3). After the best number of features were defined with the Ridge cross-validation method, we applied Recursive Feature Elimination (Scikit-Learn `feature.selection RFE` module) with SVR linear estimator, this way selecting the 17 best parameters to model chl-a in a robust manner (Table 4.3) (Lenert & Walsh, 2018).

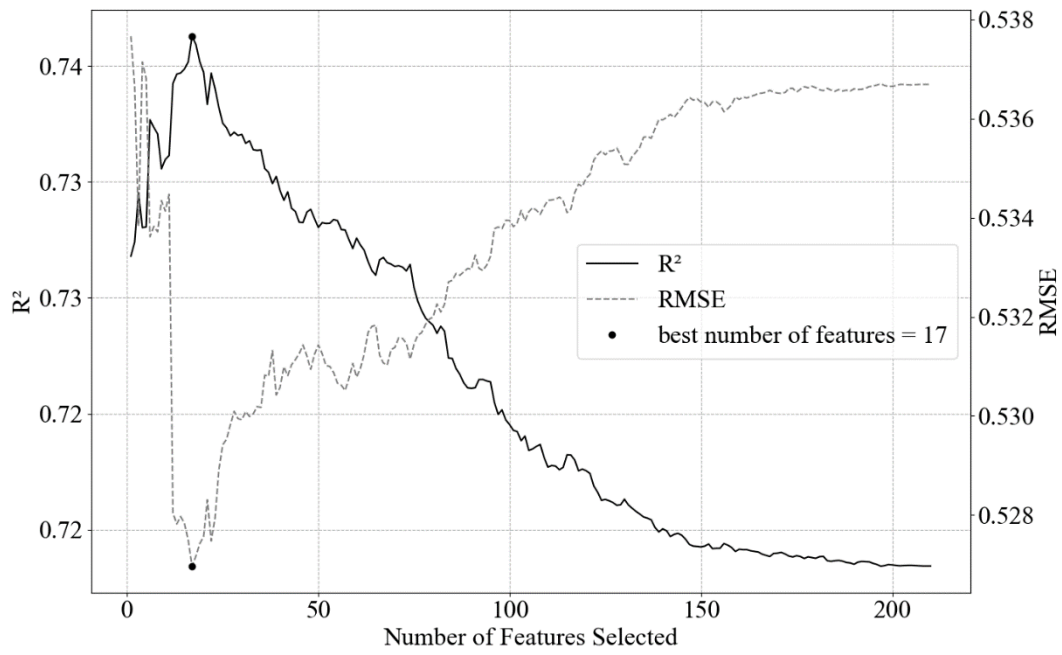


Figure 4.3: Result of RFECV with Ridge estimator. The black dot represents the maximum value of 17 selected features (predictors) to reach the highest explained variance. After the maximum value, there is an exponential decay/increase in the R²/RMSE.

Table 4.3: Chosen features after Feature Selection process. The negative numbers represent the number of lags in the original features (t-1,...,t-15).

Features
SD
SST
Salinity
SD_-1
SST_-1
SST_-2
SST_-9
SST_-12
SST_-13
SST_-14
SST_-15
Salinity_-1
Chl_-1
Chl_-4
Chl_-5
Chl_-7
Chl_-8

4.2.4 Model Selection and Hyperparameter Tuning

The algorithms evaluated in this study are random forest regressor (RF) (Breiman, 2001), support vector machine regressor (SVR) (Cortes & Vapnik, 1995) and multi-layer perceptron regressor neural network (MLP) (Hornik et al., 1989; Gardner & Dorling, 1998). These were chosen to be widely used and to present available information that allows the easy application in any level of knowledge concerning ML. Compared with deep learning approaches, traditional machine learning does not need large amounts of data to train and the computer processing can be performed in low-end machines without a GPU (Graphics Processing Unit) (Phung & Rhee, 2019).

SVR is a kernel-based nonlinear regression method. It transforms the original input data space into a high-dimensional input space (hyperplanes) and performs linear regression in the

high-dimensional space by defining a maximum margin separator, which minimizes expected generalization error instead of the prediction error in the training dataset. The kernel functions, which take as input the dot products of pairs of input points, allows the SVR to map the inputs efficiently compared to calculating the corresponding points of each input in the high-dimensional space. Basically, SVR finds hyperplanes that minimize the errors and maximize the margins of continuous data (Shin et al., 2020).

RF is a machine learning technique that utilizes an ensemble of decision trees for regression tasks. It randomly takes subsets of the data and input variables, and the results of all trees are averaged to achieve a better result than individual trees. The use of random samples of the training data for multiple decision trees reduces overfitting compared to using the entire training set with a single decision tree (Ooi et al., 2021).

MLP is an artificial neural network and it consists of connected nodes, resembling the neurons in a biological brain. It consists of at least three layers of nodes: the input layer, hidden layer and output layer. Excluding the input layer nodes, each node receives inputs from the other nodes, and the outputs are calculated using a nonlinear activation function. The learning process for MLP involves continually adjusting weights in the network to minimize the error rate using backpropagation. Backpropagation computes the gradient of the loss function with respect to the weights and updates the weights in the network using methods such as stochastic gradient descent (Ooi et al., 2021).

Depending upon the study cases, different ML algorithms usually require some adjustments. These are often crucial for the development of a successful application. Each ML algorithm has parameters, so-called hyperparameters, which define the setup of the machine to modelling the target function. For each model, a search range of hyperparameters was tested. In cases where a value was selected at the edge of the search range, a new cross-validation was conducted including more values.

All hyperparameter tuning of the models (Table 4.4) is based on GridSearchCV in the Scikit-Learn package, which can evaluate all possible given combinations of hyperparameter values using 10-fold cross-validation. This procedure determines the best combination of hyperparameters of the model that gives the best accuracy, in terms of coefficient of determination (R^2). Cross-validation is a model validation technique for obtaining reliable and stable models. The use of multiple models in the evaluation removes possible biases of some models with some data sets. We used the training dataset to search for the best parameters, and reported the prediction performances on the test dataset using these parameters (Sun et al.,

2015). The mentioned grid search was performed independently for each model on the training subset.

Table 4.4: Hyperparameter tested in GridSearchCV and the ones applied to each ML algorithms.

Model	Hyperparameter	Selected value	Default
SVR	kernel	rbf	rbf
	C	3	1
	gamma	0.01	0.1
	Epsilon	0.1	0.0001
MLP	max_iter	90	200
	hidden_layer_sizes	80	100
	activation	logistic	relu
	solver	adam	adam
	Alpha	0.5	0.0001
	warm_start	True	False
RF	bootstrap	True	True
	max_depth	11	None
	max_features	14	auto
	min_samples_leaf	13	1
	min_samples_split	2	2
	n_estimators	100	100

R^2 , adjusted coefficient of determination ($\text{adj } R^2$) and RMSE were the metrics used in this work to evaluate the predictions. The use of $\text{adj } R^2$ in multiple regression is important because it increases only when new independent variables that increase the explanatory power of the regression equation are added; this makes it a useful measure of how well a multiple regression equation fits the sample data. A linear base model, available in Scikit-Learn, was used to observe the improvements using the more sophisticated algorithms.

4.2.5 SARIMA Model

For the SARIMA model, the univariate chl-a data was used, while maintaining the partitions in the training and test dataset. To test stationarity, the Augmented Dickey–Fuller test (ADF) was applied indicating significant stationarity ($p < 0.05$) in the train and test datasets. To fill the model $(p, d, q) \times (P, D, Q)_{365}$, where 365 represents the seasonality, the best autoregressive (p, P) and moving average (q, Q) parameters were selected using an iterative method in the train dataset. The parameters ranged from 0 to 4 in the nonseasonal parameters (p, q) and 0 to 2 in the seasonal parameters (P, Q), selecting the combination with lowest Akaike information criterion (AIC). The difference order parameters d and D were 0, due to the stationarity results of the ADF test. The best parameters selected using the training dataset were $(4, 0, 1) \times (2, 0, 1)_{365}$, and this SARIMA model was used to fit the test dataset.

4.3 RESULTS

For this study, the best R^2 , adj R^2 and RMSE achieved for predicting chlorophyll-a using support vector machine regressor, random forest regressor, and neural network multilayer perceptron regressor are presented in Table 4.5. In a combination of hyperparameters tuning and feature selection, the models showed improvement compared with the default models (no feature selection, no tuning) for the test datasets. Comparing the algorithms, SVR reached the best R^2 (0.78) and RMSE ($1.113 \mu\text{g L}^{-1}$), however, these were only slightly better results (MLP = 0.76; $1.144 \mu\text{g L}^{-1}$ and RF = 0.75; $1.189 \mu\text{g L}^{-1}$). The algorithms presented good performances for the subsets of training dataset during the cross-validation step (Figure 4.4). In addition, the predicted values were close to the observed data (Figure 4.5). All the ML algorithms were better than the linear base model.

Table 4.5: Comparison of non-optimized (Default) and optimized model performances for predicting Chlorophyll-a concentration during training (train) and testing (test) steps. The linear model serves as a base model.

Default						
	train			test		
	adj R ²	R ²	RMSE ($\mu\text{g L}^{-1}$)	adj R ²	R ²	RMSE ($\mu\text{g L}^{-1}$)
SVR	0.81	0.82	1.255	0.63	0.71	1.273
RF	0.96	0.96	0.23	0.15	0.33	1.929
MLP	1	1	0.04	0.02	0.23	2.068
Optimized						
	train			test		
	adj R ²	R ²	RMSE ($\mu\text{g L}^{-1}$)	adj R ²	R ²	RMSE ($\mu\text{g L}^{-1}$)
SVR	0.77	0.77	1.424	0.77	0.78	1.113
RF	0.81	0.81	0.495	0.74	0.75	1.189
MLP	0.75	0.75	0.56	0.76	0.76	1.144
Linear (base model)						
	train			test		
	adj R ²	R ²	RMSE ($\mu\text{g L}^{-1}$)	adj R ²	R ²	RMSE ($\mu\text{g L}^{-1}$)
	0.74	0.76	1.47	0.65	0.73	1.227

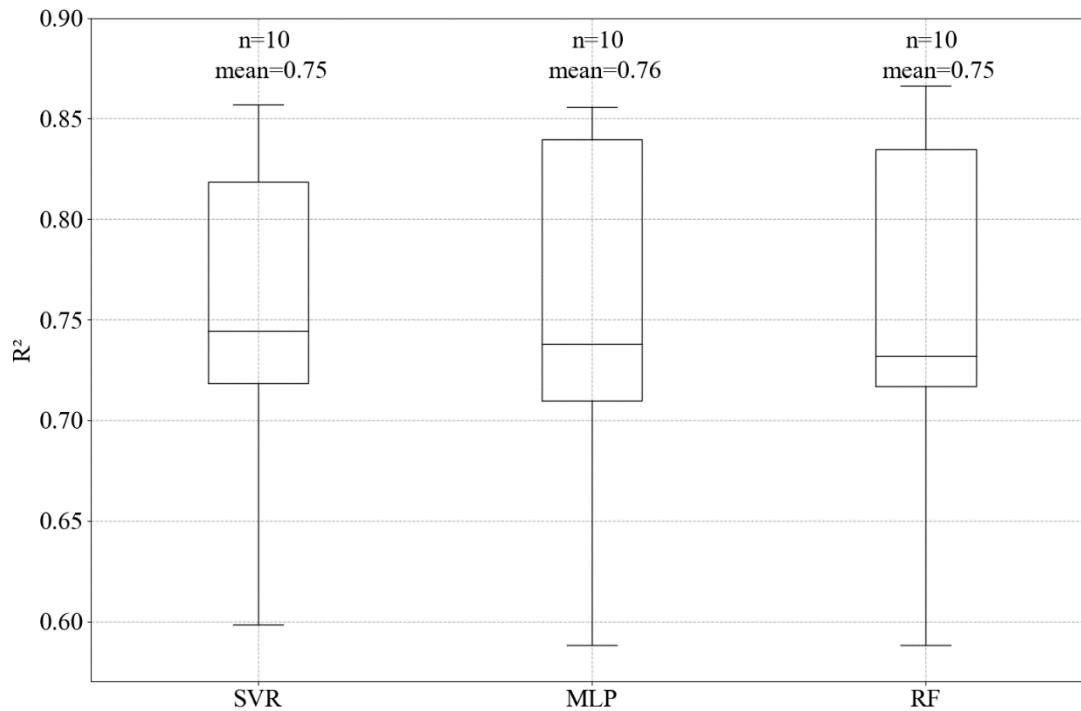


Figure 4.4. Boxplot of accuracy in the 10 fold cross-validation training step for the SVR, MLP and RF models, showing the mean and the number of folds (n) or subsets in the training data used to define the best hyperparameters.

The algorithms gave a good performance for the training dataset and allowed a good generalization for the test dataset, as it can be seen from how close the predicted values are from those observed in Figure 4.5. Using all of the 211 features and the default hyperparameters, the results in the test data were not as good as those from the optimized models (Table 4.5), mainly due to overfitting, when the models are more complex than necessary and the fitting in the training dataset is affected by noise (Lee & Chung, 2019).

Considering the features used as inputs in each of the algorithms, the Recursive Feature Elimination was implemented by combining Ridge and SVR linear estimators and selecting a maximum number of 17 predictors. This generated the following result: ('SD', 'SST', 'Salinity', 'SD_-1', 'SST_-1', 'SST_-2', 'SST_-9', 'SST_-12', 'SST_-13', 'SST_-14', 'SST_-15', 'Salinity_-1', 'Chl_-1', 'Chl_-4', 'Chl_-5', 'Chl_-7', 'Chl_-8'), with the negative numbers in the codes (Table 4.2) representing the applied lag in days. The adj R^2 results, which are sensitive to the number of used predictors, showed improvement from 0.02 to 0.76 for MLP, while for SVR the result improved from 0.63 to 0.77 and from 0.15 to 0.74 for RF in the test dataset.

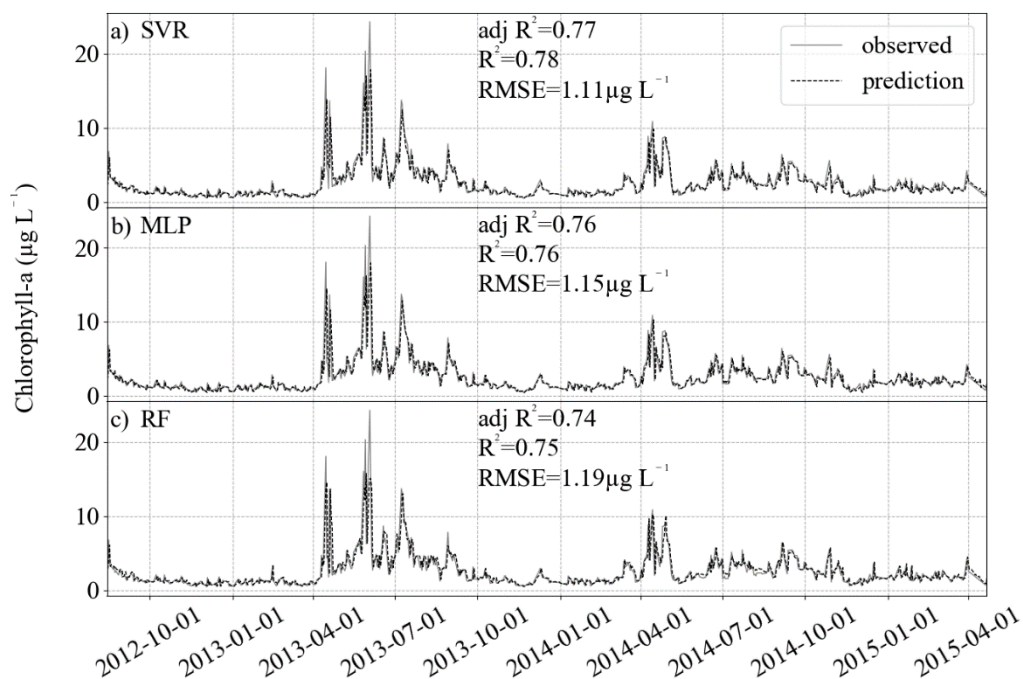


Figure 4.5: Results of prediction (black dashed) and comparison with the observed test dataset (grey solid). For the three algorithms, R^2 is higher than 0.7 and RMSE lower than $1.2 \mu\text{g L}^{-1}$. (a) SVR, (b) MLP and (c) RF.

For the independent validation, a chl-a dataset acquired by HPLC, the predictions had better RMSE and R^2 than the test datasets (Figure 4.6). Again, the higher values had limitations in prediction, but the lower variance compared with the training and testing datasets allowed for better evaluation indicators, with RMSE for all algorithms in the order of $0.3 \mu\text{g L}^{-1}$ and R^2 reaching approximately 0.90.

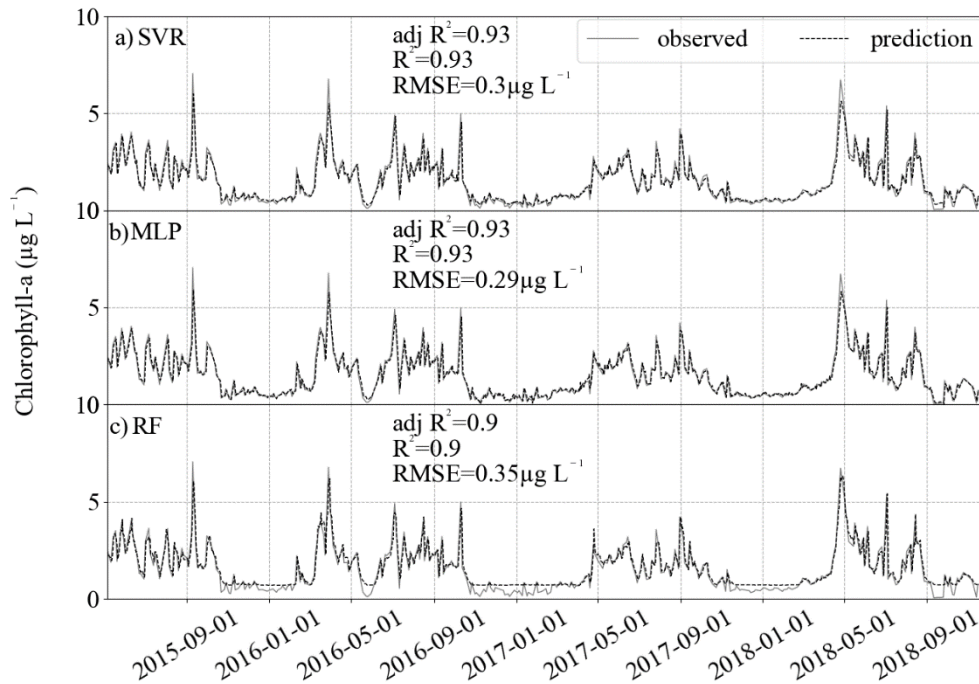


Figure 4.6: Results of prediction (black dashed) and comparison with the validation dataset (gray solid). For the three algorithms, R^2 is approximately 0.9 and RMSE lower than $0.3 \mu\text{g L}^{-1}$. (a) SVR, (b) MLP and (c) RF.

The iterative SARIMA parameters selection uses much more computer processing time compared with the GridSearchCV method in machine learning. The latter is a scale of seconds to minutes while the former hours to days. It took around two weeks to select the best p , q , P and Q parameters in the daily data considering a yearly seasonality. Fitting the test dataset with the SARIMA model gave the worst results when compared with the ML models (Figure 4.7).

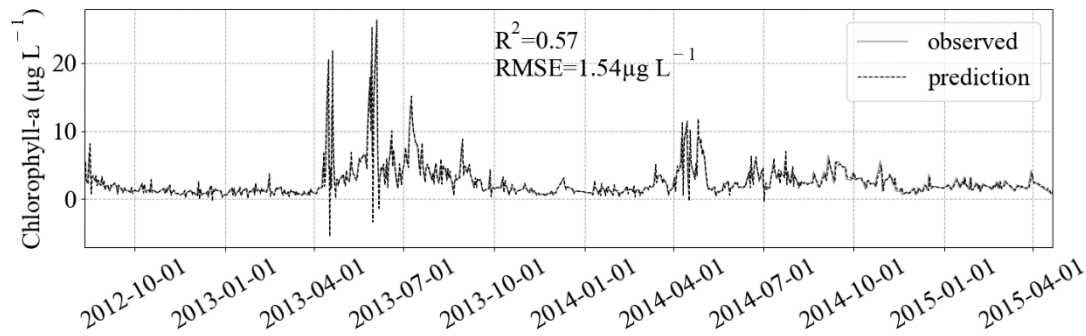


Figure 4.7: Result of SARIMA fit (black dashed) in the test dataset (grey solid). The better fit in extreme values is counter-balanced by the estimation of negative values, decreasing/increasing R^2 /RMSE compared to the ML models results.

4.4 DISCUSSION

Machine learning analysis was conducted on the Helgoland Roads time series to develop the best fit of chlorophyll-a concentrations over time using different parameters and their lagged correlates. For the three algorithms implemented, the model results were virtually equal in the evaluation metrics, presenting similar results in prediction, with slightly better values for the model SVR. For the time predictions, each of the three models' performances are acceptable with high R^2 values greater than 0.70 and RMSE lower than $1.5 \mu\text{g L}^{-1}$, $\approx 40\%$ smaller than the chlorophyll-a concentration standard deviation of $2.9 \mu\text{g L}^{-1}$. However, all of the algorithms were unable to predict extreme values (Figure 4.8). It was expected that a certain degree of decrease in accuracy would be incurred because of the difficulty in capturing and reproducing these extreme peaks (Rezaie-Balf et al., 2019). One hypothesis that would explain the underestimation of extreme values is the absence of predictive features, e.g., hydrodynamics can result in the transport of chlorophyll from other areas as an input event, even though salinity and wind parameters are reliable indicatives for current and wave dynamics in the German Bight (Schloen et al., 2017). As these events do not present as a temporal pattern, the ML models do not recognize the influence on the target.

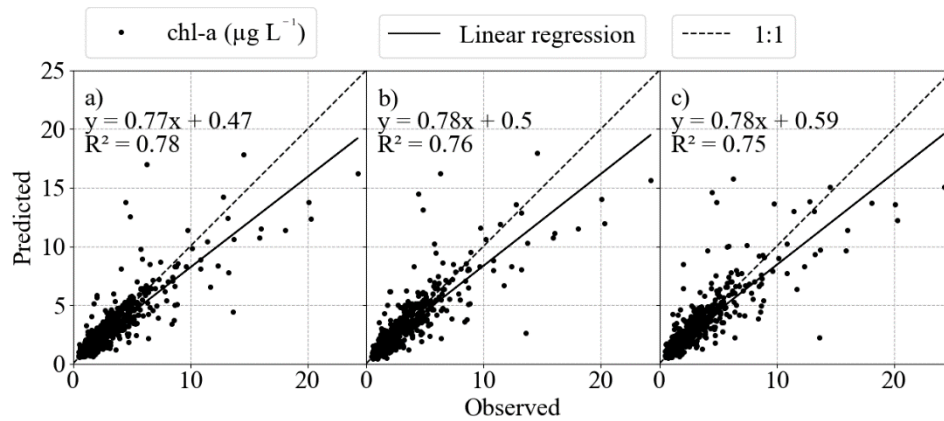


Figure 4.8: Cross-plots of the modeled and observed chlorophyll values in (a) SVR, (b) MLP and (c) RF. It is possible to notice the deviation in extreme values, showing the limitation of the ML models in deal with these data values.

Because each algorithm is based on different algebraic assumptions and procedures, they can result in different predictions. Between SVR and MLP, Park et al. (2015) points to differences in the nonlinear equalization performance and the structural risk minimization principle of SVR being more effective than the empirical risk minimization principle of neural networks in terms of minimizing error. According to Chen et al. (2015), in MLP the method for determining global solutions is difficult to converge because of its inherent algorithm design and model parameters are more complex than SVR, whereas the SVR has ready access to global optimal solutions, obtained by solving a linearly constrained quadratic programming problem (Park et al., 2015). Between SVR and RF, as we saw, the linear base model gave good results. There is the possibility of a linear dependency that is better captured by SVR, probably a result from the linear interpolation in the preprocessing step of this study. The feature selection and tuning of hyperparameters was extremely important and improved the results substantially. This was noticeable in the adj R^2 results for default and optimized models. Analysing the 17 features used in SVR and described in the results section, the algorithm considered SST, lagged SST, lagged chlorophyll, salinity and Secchi depth to reach the best results presented in this work. It is important to point that ML is a data-driven approach, but it is possible to make inferences about the selected features. The number of selected features was a response of balancing bias and variance in the learning algorithms (Munson & Caruana, 2009). For this study, we noticed the choice of SST as an important feature, probably representing the seasonal patterns in the chlorophyll target. Better R^2 , adj R^2 and RMSE results in the independent

validation dataset are possibly due to less variability and absence of extreme values, and shows the good generalization that the ML models are capable of. All of the good results, for both the test and independent validation data, show the better prediction power of the three ML algorithms evaluated in this study. Comparing with the classical SARIMA model, the univariate and linear background did not achieve the results needed for it to outperform the ML models. Compared with the ML literature, studies such as (Luo et al., 2019) and (Liu et al., 2019) achieved results of R^2 ranging from 0.50 to 0.80, analysing shorter time series of chl-a in lakes. The authors of Blaun et al. (2018) predicted variations of chlorophyll-a in different sites of the North Sea using generalized additive models (GAM) and the R^2 results ranged from 0.15 to 0.63. In Irwin and Finkel (2008), using GAM to predict chl-a in a spatial approach for the North Atlantic, got the best result for R^2 at 0.83. All of these values show how variable different methods performances in predicting chlorophyll can be, not necessarily meaning one method is better than the other, but more adaptive. ML models proved their generalization capacity and high accuracy.

4.5 CONCLUSIONS

In this work, we evaluated three machine learning algorithms in a regression task. Support vector regressor presented a slightly better performance, with the advantage that it used less computational time, and generated chlorophyll concentration predictions with 0.78 correlation to the observed data, in comparison to 0.76 and 0.75 for MLP and RF, respectively. Moreover, the root mean square error was approximately $1.1 \mu\text{g L}^{-1}$ for the test dataset and less than one for the independent validation data, which is approximately 38% percent smaller than the standard deviation of $2.9 \mu\text{g L}^{-1}$. This study demonstrates the ability of machine learning models to use environmental in situ time series to predict the chlorophyll concentration with significant accuracy (R^2), higher than 70%, and the importance of tuning hyperparameters and defining the best predictors (feature selection). Most chlorophyll-a prediction studies are conducted in fresh water environments or using satellite data and limited time series, so this work can be considered a step toward the use of machine learning algorithms in marine areas based on long-term time series. Being aware of the limitations presented in this study, in future works it would be interesting to work with irregular sampled time series, improve the method for feature selection, ensemble results of different ML and classical statistical models, and evaluate the forecasting power of these models in the short and long term. Besides, the use of

deep learning approaches has become more and more common, and in many cases, they are outperforming the traditional ML algorithms, with the cost of higher computer processing times.

4.6 ACKNOWLEDGMENTS

We acknowledge the present and past crews of the research vessels Aade and Ellenbogen of the Biologische Anstalt Helgoland (BAH) for their unfailing provision of samples. We also thank Kristine Carstens, Silvia Peters, Ursula Ecker and all colleagues of time series group and those who were instrumental in the analysis of samples during the last decades. We thank the NOAA Physical Sciences Laboratory and Deutsche Wetterdienst for providing climate and meteorological data.

4.7 SUPPLEMENTARY MATERIAL

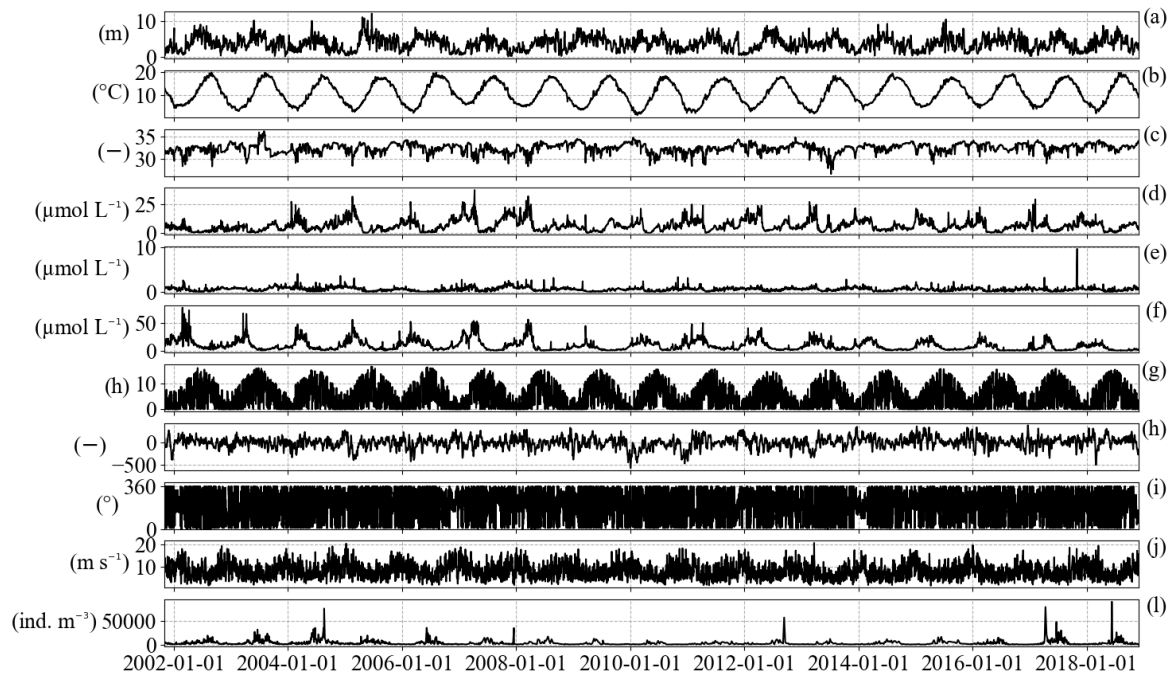


Figure 4.9: Time series of parameters used to predict chlorophyll-a concentration: (a) Secchi disk depth, in meters (m); (b) Sea Surface Temperature, in degrees Celsius ($^{\circ}\text{C}$); (c) Salinity (-); (d) Silicate ($\mu\text{mol L}^{-1}$); (e) Phosphate ($\mu\text{mol L}^{-1}$); (f) Nitrate ($\mu\text{mol L}^{-1}$); (g) Sunlight duration, in hours (h); (h) NAO index (-); (i) Wind Direction, in degrees ($^{\circ}$); (j) Wind Speed, in meters per second (m s^{-1}); and (l) Total zooplankton abundance, individuals per cubic meter (ind. m^{-3}).

5 Chapter 5

General Discussion and Conclusions

5.1 SYNTHESIS OF RESEARCH AND GENERAL DISCUSSION

The primary objective of this thesis was to estimate and investigate changes in the German Bight primary production associated with an increase in temperature, using the Chl-*a* concentration as a surrogate and applying various analytical tools and data sources. These objectives were achieved from different perspectives (i.e. from temporal to spatial analysis) and with classical and innovative analytical tools. Furthermore, the analysis of the surface Chl-*a* indicated that temperature plays a crucial role in its variability, not necessarily through direct influence but primarily through indirect effects. This finding offers insight into how and which processes should be investigated in more detail to mitigate the negative effects of warming. The questions presented in Chapter 1 that guided this thesis are reiterated, and the following answers are drawn:

Q1. How do SSTs and land surface temperatures correlate from global to local scales. What are the differences in trends and seasonal variability that could be implicated in various responses to ecological systems related to these spatial scales?

Reanalysis data offered by the Hadley MetOffice, land surface temperatures, and two long-term ecological time series, the HR and SR, were used to answer this question. Because HRTS and SR time series data are widely used for climate and ecological assessments, it was necessary to evaluate these two local sites in the context of the larger geographical regions, especially in the context of the warming of the North Sea and the temperatures of the North Atlantic. Correlations indicated that the two local stations were more correlated with the land temperatures and the North Sea and less correlated with the North Atlantic and overall Northern Hemisphere temperatures. This result answered the question of whether both sites can be considered representative of the overall North Sea temperature.

The SST anomalies were mainly negative, with a slight trend until the late 1980s for the North Atlantic, North Sea, HR, and SR, and mostly positive, with a larger positive trend afterwards (1991–2019). This finding aligns with a similar evolution found in the European

and German surface air temperature anomalies. To determine whether this phenomenon was only related to the Northern Atlantic or North Sea, we searched for other shelf seas comparable with the focus region, and the same was found for the YS. The SST anomalies in the North Atlantic, North Sea, HR, and SR revealed that the temperature density distribution clearly shifted to higher temperatures in the later years in these areas. Overall, the surface temperature seasonal variability and, concomitantly, the seasonal amplitude shifted considerably, becoming lower in winter and higher in autumn, manifesting mainly as a reduction of the definite seasonality at the open water site at Helgoland and the shallow Wadden Sea site of Sylt.

The NAO analysis found a positive trend towards a positive NAO, that is, more frequent westerly winds and warmer temperatures in winter in Europe (Trigo et al., 2002). Relating the findings in Chapter 2 with the results in Chapter 3 demonstrates the role of the NAO winter mean in the Chl-a variability. The positive NAO trends are related to the increase in westerly winds, increasing the Atlantic inflow into the German Bight and restricting coastal and riverine waters close to shallower areas due to the Ekman transport. Xu et al. (2020) also described this result based on a model simulation, corroborating the results of Chapters 2 and 3.

Q2. What are the current trends (from 1998 to 2020) and spatial variability of the surface Chl-a concentration in the German Bight?

Comparing the GlobColour remote-sensing product with a long-term in situ HPLC Chl-a concentration time series from 2004 to 2020 provided a coefficient of correlation of 0.6 and an RMSE of 1.09 mg m^{-3} . The distribution of Chl-a anomalies in both datasets was not significantly different, but the remote-sensing data overestimated values in low concentrations. Overall, the remote-sensing data aligned well with the Chl-a variability and seasonality of the in situ data. The EOFs demonstrated that the dominant modes of the Chl-a variability are defined by the inter- and intra-annual variability of spring blooms. The interannual mode acts in the whole basin, whereas the intra-annual variability splits the German Bight into coastal, transitional, and offshore areas. The MCA determined the covariability between Chl-a and SST/MLD. The first mode of the Chl-a covariability corresponded to 45% of the explained variance for SST and 23% for the MLD. The covariability with SST was positive in shallower areas and negative in deeper areas, whereas, for the MLD, it was the opposite.

The overall trend of Chl-a was defined by 31% of the German Bight under significant negative trends, whereas only 4% was significantly positive. This overall trend agreed with the results described by Xu et al. (2020) and Kaiser et al. (2023). Xu et al. (2020) used model simulations and observed negative Chl-a trends from 1987 to 2012 in the German Bight, with

negative values in most offshore areas and positive values following the coast. Kaiser et al. (2023) observed values below the baseline defined by the long-term average of the primary production in offshore areas and values above the baseline near the coast during 2018, characterized by strong summer heat waves.

Q3. How applicable are ML algorithms to the prediction of the Chl-a concentration time series acquired in the German Bight, and what are the best predictors defined by ML analyses? Can ML predict and generalize the results to an independent dataset? Does ML outperform classical statistics?

Moreover, ML techniques constitute a set of tools belonging to the fields of computer science and artificial intelligence. The versatility of these techniques allows for their successful application in many fields of science and a great variety of problems. It was the first time that the HRTS was used as input for ML algorithms. The ML algorithms predicted Chl-a with significant accuracy (R^2), higher than 70% and a low RMSE ($1.1 \mu\text{g L}^{-1}$). The generalizability of ML was also tested, highly accurately predicting an independent validation Chl-a dataset not used in any part of the training or testing process.

The results of this thesis indicate that SST affects Chl-a, as observed in Chapter 3 in the spatial domain analysis and Chapter 4 in the data-driven analysis, which defined SST as one of the most crucial predictors of Chl-a. These results are indicative that primary production is likely to decrease in most of the German Bight. In Chapter 2, the evidence that SST has different seasonal variability (considering various spatial scales) defined a range of effects of positive SST trends, most related to indirect rather than direct effects of SST. Other variables should also be considered and connected with temperature dynamics (e.g. wind regimes, nutrient availability, spatial shifts related to migration to better habitats, and hydrodynamics linked to the Atlantic water inflow and changing the water mass characteristics of the German Bight).

5.2 CONCLUDING REMARKS AND SUMMARY

This thesis presents information regarding the spatial and temporal distributions of Chl-a, a surrogate for primary production, in the German Bight, using classical statistical analyses and new ML algorithms. The results from this thesis offer an updated perspective on trends and variability in primary production under the influence of an increase in SST, a consequence of climate change. The influence of temperature varies according to spatial scales, indicating that global scales are less correlated than regional and local scales. Various spatial and temporal scales control the Chl-a concentration dynamics in the German Bight, as demonstrated by EOFs. The use of ML algorithms was a new approach to Chl-a time series prediction and demonstrated the robust capacity of ML to be applied in ecological time series prediction.

The conclusions in each of the three research chapters (Chapters 2, 3 and 4) are summarized below.

1. Evaluations and observed changes in variability (seasonal and interannual) cannot be ignored in temperature considerations because they are part of the significant changes occurring in temperature that affect ecological systems.
2. The assessment of Chl-a variability reveals that seasonal variations are dominant in the German Bight, regulated by two observed phytoplankton blooms. The nonseasonal variability is also defined by the interannual and intra-annual variability of the spring blooms, dominated by non-seasonal forcings, such as wind variability connected to NAO and the inflow of Atlantic water types that are warmer and poorer in nutrients from the English Channel and freshwater rivers.
3. This work demonstrates the ability of ML models to use environmental in situ time series to predict Chl-a concentration with significant accuracy while also defining the best predictors. This work is a step towards using ML algorithms in marine areas based on long-term time series.

Based on the results, primary production is affected by the constant positive trends in temperature. The decreasing trend in primary production, as observed in the majority of the German Bight, can cause a disturbance in food webs, also affecting the CO₂ fixation by marine organisms, a critical process of the biogeochemical cycle and climate regulation. The results of this thesis provide a new perspective on the direct and indirect effects of temperature increases on primary production in the German Bight.

5.3 FUTURE WORK

This work provides fundamental results and associated conclusions concerning the state of primary production variability in the German Bight. In addition to contributing to previous work, the combination of in situ and remote-sensing data could also be used to provide results in the water column. The use of long-term HRTS monitoring data is a strength of this study, and the data could be used with ML tools to improve the statistical and mechanistic models used to derive Chl-a.

A work that was initiated but not continued during this thesis was the simulation of past conditions (hindcast) of the HRTS. Hindcasting HRTS Chl-a could determine the influence of various regimes occurring in the German bight (e.g. the control of nutrient runoff by rivers in Europe, the great salinity in the North Sea, and the sharp temperature increase at the end of the 1980s). The use of GAMs to hindcast the HRTS Chl-a is a future work that could facilitate understanding the long-term behaviour of Chl-a before and after the SST regime change at the end of the 1980s, as described in detail in Chapter 2 of this thesis.

A form of data assimilation could be used to improve the remote-sensing data. Considering the algorithms used to derive Chl-a from reflectance in coastal waters, each coastal region presents its own particularities, making it necessary to adapt the global algorithms. The use of machine learning proved to be a promising tool, and the forecast of Chl-a should be considered in the short and long terms on temporal and spatial scales. Understanding the influence of global warming on the primary production in the ocean is a prerequisite for mitigating and preparing for the observed primary production decrease in the German Bight. Integrating in situ and remote sensing with mechanistic and ML statistical model simulations can improve forecasts. Combining available in situ vertical Chl-a data from the German Bight with remote-sensing surface Chl-a products could offer more insight regarding the trends and variability of Chl-a and primary production. With the steady increase in temperature due to climate change and planned increase in multi-use and especially offshore energy in the German Bight, this work can be used as a baseline to evaluate the future effects of environmental change and offshore structures on primary production.

6 References

- Addicott, J. F., Aho, J. M., Antolin, M. F., Padilla, D. K., Richardson, J. S., & Soluk, D. A. (1987). Ecological Neighborhoods: Scaling Environmental Patterns. *Oikos*, 49(3), 340. <https://doi.org/10.2307/3565770>
- Ainsworth, T. D., Hurd, C. L., Gates, R. D., & Boyd, P. W. (2020). How do we overcome abrupt degradation of marine ecosystems and meet the challenge of heat waves and climate extremes? *Global Change Biology*, 26(2), 343–354. <https://doi.org/10.1111/gcb.14901>
- Alheit, J., Licandro, P., Coombs, S., Garcia, A., Giráldez, A., Santamaría, M. T. G., Slotte, A., & Tsikliras, A. C. (2014). Reprint of “Atlantic Multidecadal Oscillation (AMO) modulates dynamics of small pelagic fishes and ecosystem regime shifts in the eastern North and Central Atlantic”. *Journal of Marine Systems*, 133, 88–102. <https://doi.org/10.1016/j.jmarsys.2014.02.005>
- Alheit, J., Möllmann, C., Dutz, J., Kornilovs, G., Loewe, P., Mohrholz, V., & Wasmund, N. (2005). Synchronous ecological regime shifts in the central Baltic and the North Sea in the late 1980s. *ICES Journal of Marine Science*, 62(7), 1205–1215. <https://doi.org/10.1016/J.ICESJMS.2005.04.024>
- Alvera-Azcárate, A., Van der Zande, D., Barth, A., Troupin, C., Martin, S., & Beckers, J. M. (2021). Analysis of 23 Years of Daily Cloud-Free Chlorophyll and Suspended Particulate Matter in the Greater North Sea. *Frontiers in Marine Science*, 8, 707632. <https://doi.org/10.3389/FMARS.2021.707632/BIBTEX>
- Amorim, F. de L. L. de, Wiltshire, K. H., Lemke, P., Carstens, K., Peters, S., Rick, J., Gimenez, L., & Scharfe, M. (2023). Investigation of marine temperature changes across temporal and spatial Gradients: Providing a fundament for studies on the effects of warming on marine ecosystem function and biodiversity. *Progress in Oceanography*, 216, 103080. <https://doi.org/10.1016/J.POCEAN.2023.103080>
- Androsov, A., Fofonova, V., Kuznetsov, I., Danilov, S., Rakowsky, N., Harig, S., Brix, H., & Wiltshire, K. H. (2019). FESOM-C v.2: coastal dynamics on hybrid unstructured meshes. *Geoscientific Model Development*, 12(3), 1009–1028. <https://doi.org/10.5194/gmd-12-1009-2019>

REFERENCES

- Arias-Ortiz, A., Serrano, O., Masqué, P., Lavery, P. S., Mueller, U., Kendrick, G. A., Rozaimi, M., Esteban, A., Fourqurean, J. W., Marbà, N., Mateo, M. A., Murray, K., Rule, M. J., & Duarte, C. M. (2018). A marine heatwave drives massive losses from the world's largest seagrass carbon stocks. *Nature Climate Change*, 8(4), 338–344. <https://doi.org/10.1038/s41558-018-0096-y>
- Asch, R. G., Stock, C. A., & Sarmiento, J. L. (2019). Climate change impacts on mismatches between phytoplankton blooms and fish spawning phenology. *Global Change Biology*, 25(8), 2544–2559. <https://doi.org/10.1111/gcb.14650>
- A Sea of Color and Wind (2020). Retrieved December 5, 2023, from <https://earthobservatory.nasa.gov/images/146556/a-sea-of-color-and-wind>
- Baker, K. G., Robinson, C. M., Radford, D. T., McInnes, A. S., Evenhuis, C., & Doblin, M. A. (2016). Thermal performance curves of functional traits aid understanding of thermally induced changes in diatom-mediated biogeochemical fluxes. *Frontiers in Marine Science*, 3(APR), 179676. <https://doi.org/10.3389/FMARS.2016.00044/BIBTEX>
- Balkoni, A., Guignard, M. S., Boersma, M., & Wiltshire, K. H. (2023). Evaluation of different averaging methods for calculation of ratios in nutrient data. *Fundamental and Applied Limnology*, 196(3–4), 195–203. <https://doi.org/10.1127/FAL/2023/1487>
- Baracchini, T., Chu, P. Y., Šukys, J., Lieberherr, G., Wunderle, S., Wüest, A., & Bouffard, D. (2020). Data assimilation of in situ and satellite remote sensing data to 3D hydrodynamic lake models: a case study using Delft3D-FLOW v4.03 and OpenDA v2.4. *Geoscientific Model Development*, 13(3), 1267–1284. <https://doi.org/10.5194/gmd-13-1267-2020>
- Barceló, C., Ciannelli, L., Olsen, E. M., Johannessen, T., & Knutsen, H. (2016). Eight decades of sampling reveal a contemporary novel fish assemblage in coastal nursery habitats. *Global Change Biology*, 22(3), 1155–1167. <https://doi.org/10.1111/gcb.13047>
- Barnard, P. L., Dugan, J. E., Page, H. M., Wood, N. J., Hart, J. A. F., Cayan, D. R., Erikson, L. H., Hubbard, D. M., Myers, M. R., Melack, J. M., & Iacobellis, S. F. (2021). Multiple climate change-driven tipping points for coastal systems. *Scientific Reports*, 11(1), 15560. <https://doi.org/10.1038/s41598-021-94942-7>
- Barton, A. D., Greene, C. H., Monger, B. C., & Pershing, A. J. (2003). The Continuous Plankton Recorder survey and the North Atlantic Oscillation: Interannual- to Multidecadal-

REFERENCES

- scale patterns of phytoplankton variability in the North Atlantic Ocean. *Progress in Oceanography*, 58(2–4), 337–358. <https://doi.org/10.1016/J.POCEAN.2003.08.012>
- Bauer, J. E., Cai, W. J., Raymond, P. A., Bianchi, T. S., Hopkinson, C. S., & Regnier, P. A. G. (2013). The changing carbon cycle of the coastal ocean. *Nature* 2013 504:7478, 504(7478), 61–70. <https://doi.org/10.1038/nature12857>
- Beaugrand, G. (2004). The North Sea regime shift: Evidence, causes, mechanisms and consequences. *Progress in Oceanography*, 60(2–4), 245–262. <https://doi.org/10.1016/J.POCEAN.2004.02.018>
- Beaugrand, G. (2009). Decadal changes in climate and ecosystems in the North Atlantic Ocean and adjacent seas. *Deep Sea Research Part II: Topical Studies in Oceanography*, 56(8–10), 656–673. <https://doi.org/10.1016/J.DSR2.2008.12.022>
- Beaugrand, G., Edwards, M., Brander, K., Luczak, C., & Ibanez, F. (2008). Causes and projections of abrupt climate-driven ecosystem shifts in the North Atlantic. *Ecology Letters*, 11(11), 1157–1168. <https://doi.org/10.1111/J.1461-0248.2008.01218.X>
- Beaugrand, G., Harlay, X., & Edwards, M. (2014). Detecting plankton shifts in the North Sea: A new abrupt ecosystem shift between 1996 and 2003. *Marine Ecology Progress Series*, 502, 85–104. <https://doi.org/10.3354/MEPS10693>
- Beaugrand, G., & Ibanez, F. (2004). Monitoring marine plankton ecosystems. II: Long-term changes in North Sea calanoid copepods in relation to hydro-climatic variability. *Marine Ecology Progress Series*, 284, 35–47. <https://doi.org/10.3354/MEPS284035>
- Beaugrand, G., Reid, P. C., Ibañez, F., Lindley, J. A., & Edwards, M. (2002). Reorganization of North Atlantic marine copepod biodiversity and climate. *Science*, 296(5573), 1692–1694. https://doi.org/10.1126/SCIENCE.1071329/SUPPL_FILE/1071329S4_THUMB.GIF
- Becherer, J., Burchard, H., Carpenter, J. R., Graewe, U., & Merckelbach, L. M. (2022). The Role of Turbulence in Fueling the Subsurface Chlorophyll Maximum in Tidally Dominated Shelf Seas. *Journal of Geophysical Research: Oceans*, 127(8), e2022JC018561. <https://doi.org/10.1029/2022JC018561>
- Becker, G. A., Dick, S., & Dippner, J. W. (1992). Hydrography of the German bight. *Marine Ecology Progress Series*, 9–18.

REFERENCES

- Becker, G. A., Giese, H., Isert, K., König, P., Langenberg, H., Pohlmann, Th., & Schrum, C. (1999). Mesoscale structures, fluxes and water mass variability in the German Bight as exemplified in the KUSTOS- experiments and numerical models. *Deutsche Hydrografische Zeitschrift* 1999 51:2, 51(2), 155–179. <https://doi.org/10.1007/BF02764173>
- Behrenfeld, M. J., Boss, E., Siegel, D. A., Shea, D. M., Behrenfeld, M. J., Boss, E., Siegel, D. A., & Shea, D. M. (2005). Carbon-based ocean productivity and phytoplankton physiology from space. *Global Biogeochemical Cycles*, 19(1), 1–14. <https://doi.org/10.1029/2004GB002299>
- Behrenfeld, M. J., O'Malley, R. T., Siegel, D. A., McClain, C. R., Sarmiento, J. L., Feldman, G. C., Milligan, A. J., Falkowski, P. G., Letelier, R. M., & Boss, E. S. (2006). Climate-driven trends in contemporary ocean productivity. *Nature* 2006 444:7120, 444(7120), 752–755. <https://doi.org/10.1038/nature05317>
- Beusekom, J. E. E., & Diel-Christiansen, S. (2009). Global change and the biogeochemistry of the North Sea: The possible role of phytoplankton and phytoplankton grazing. *International Journal of Earth Sciences*, 98(2), 269–280. <https://doi.org/10.1007/S00531-007-0233-8/METRICS>
- Beutler, M., Wiltshire, K. H., Meyer, B., Moldaenke, C., Lüring, C., Meyerhöfer, M., Hansen, U. P., & Dau, H. (2002). A fluorometric method for the differentiation of algal populations in vivo and in situ. *Photosynthesis Research*, 72(1), 39–53. <https://doi.org/10.1023/A:1016026607048/METRICS>
- Billé, R., Chabason, L., Drankier, P., Molenaar, E. J., & Rochette, J. (2016). Making Regional Seas Programmes, Regional Fishery Bodies and Large Marine Ecosystem Mechanisms Work Better Together. Retrieved 1 February 2024, from www.unep.org/regionalseas
- Bindoff, N., Cheung, W., Kairo, J. G., Aristegui, J., Guinder, V., Hallberg, R., Hilmi, N., Jiao, N., Karim, M., Levin, L., O'Donoghue, S. H., Purca, S., Rinkevich, B., Suga, T., Tagliabue, A., Williamson, P., Acar, S., Alava, J. J., Allison, E., & Whalen, C. (2019). Changing Ocean, Marine Ecosystems, and Dependent Communities (09 SROCC Ch05 FINAL-1) (pp. 447–588).
- Blankenship, R. E. (2008). Molecular Mechanisms of Photosynthesis. *Molecular Mechanisms of Photosynthesis*, 1–321. <https://doi.org/10.1002/9780470758472>

REFERENCES

- Blauw, A. N., Benincà, E., Laane, R. W. P. M., Greenwood, N., & Huisman, J. (2018). Predictability and environmental drivers of chlorophyll fluctuations vary across different time scales and regions of the North Sea. *Progress in Oceanography*, 161, 1–18. <https://doi.org/10.1016/J.POCEAN.2018.01.005>
- Blondeau-Patissier, D., Gower, J. F. R., Dekker, A. G., Phinn, S. R., & Brando, V. E. (2014). A review of ocean color remote sensing methods and statistical techniques for the detection, mapping and analysis of phytoplankton blooms in coastal and open oceans. *Progress in Oceanography*, 123, 123–144. <https://doi.org/10.1016/J.POCEAN.2013.12.008>
- Boersma, M., Grüner, N., Signorelli, N. T., Montoro González, P. E., Peck, M. A., & Wiltshire, K. H. (2016). Projecting effects of climate change on marine systems: is the mean all that matters? *Proceedings of the Royal Society B: Biological Sciences*, 283(1823). <https://doi.org/10.1098/RSPB.2015.2274>
- Bopp, L., Resplandy, L., Orr, J. C., Doney, S. C., Dunne, J. P., Gehlen, M., Halloran, P., Heinze, C., Ilyina, T., Séférian, R., Tjiputra, J., & Vichi, M. (2013). Multiple stressors of ocean ecosystems in the 21st century: Projections with CMIP5 models. *Biogeosciences*, 10(10), 6225–6245. <https://doi.org/10.5194/BG-10-6225-2013>
- Borics, G., Várbíró, G., & Padisák, J. (2013). Disturbance and stress: Different meanings in ecological dynamics? *Hydrobiologia*, 711(1), 1–7. <https://doi.org/10.1007/S10750-013-1478-9/METRICS>
- Botkin, D. B., Saxe, H., Araújo, M. B., Betts, R., Bradshaw, R. H. W., Cedhagen, T., Chesson, P., Dawson, T. P., Etterson, J. R., Faith, D. P., Ferrier, S., Guisan, A., Hansen, A. S., Hilbert, D. W., Loehle, C., Margules, C., New, M., Sobel, M. J., & Stockwell, D. R. B. (2007). Forecasting the Effects of Global Warming on Biodiversity. *BioScience*, 57(3), 227–236. <https://doi.org/10.1641/B570306>
- Box, G. E. P., Jenkins, G. M., Reinsel, G. C., & Ljung, G. M. (2016). *JOURNAL OF TIME SERIES ANALYSIS BOOK REVIEW TIME SERIES ANALYSIS: FORECASTING AND CONTROL, 5TH EDITION*, by. J. Time. Ser. Anal, 37, 709–711. <https://www.wiley.com/en-us/Time+Series+Analysis%3A+Forecasting+and+Control%2C+5th+Edition-p-9781118675021>

REFERENCES

- Boyce, D. G., Lewis, M. R., & Worm, B. (2010). Global phytoplankton decline over the past century. *Nature* 2010 466:7306, 466(7306), 591–596. <https://doi.org/10.1038/nature09268>
- Boyd, P. W., Rynearson, T. A., Armstrong, E. A., Fu, F., Hayashi, K., Hu, Z., Hutchins, D. A., Kudela, R. M., Litchman, E., Mulholland, M. R., Passow, U., Strzepek, R. F., Whittaker, K. A., Yu, E., & Thomas, M. K. (2013). Marine Phytoplankton Temperature versus Growth Responses from Polar to Tropical Waters – Outcome of a Scientific Community-Wide Study. *PLOS ONE*, 8(5), e63091. <https://doi.org/10.1371/JOURNAL.PONE.0063091>
- Boyer, J. N., Kelble, C. R., Ortner, P. B., & Rudnick, D. T. (2009). Phytoplankton bloom status: Chlorophyll a biomass as an indicator of water quality condition in the southern estuaries of Florida, USA. *Ecological Indicators*, 9(6), S56–S67. <https://doi.org/10.1016/J.ECOLIND.2008.11.013>
- Breiman, L. (2001). Random forests. *Machine Learning*, 45(1), 5–32. <https://doi.org/10.1023/A:1010933404324/METRICS>
- Bretherton, C. S., Smith, C., & Wallace, J. M. (1992). An Intercomparison of Methods for Finding Coupled Patterns in Climate Data. *Journal of Climate*, 5(6), 541–560. [https://doi.org/10.1175/1520-0442\(1992\)005<0541:AIOMFF>2.0.CO;2](https://doi.org/10.1175/1520-0442(1992)005<0541:AIOMFF>2.0.CO;2)
- Brownlee, J. (2020). How to Develop Multivariate Multi-Step Time Series Forecasting Models for Air Pollution - *MachineLearningMastery.com*. Retrieved 24 July 2020, from <https://machinelearningmastery.com/how-to-develop-machine-learning-models-for-multivariate-multi-step-air-pollution-time-series-forecasting/>
- Brunner, L., Schaller, N., Anstey, J., Sillmann, J., & Steiner, A. K. (2018). Dependence of Present and Future European Temperature Extremes on the Location of Atmospheric Blocking. *Geophysical Research Letters*, 45(12), 6311–6320. <https://doi.org/10.1029/2018GL077837>
- Bryndum-Buchholz, A., Tittensor, D. P., Blanchard, J. L., Cheung, W. W. L., Coll, M., Galbraith, E. D., Jennings, S., Maury, O., & Lotze, H. K. (2019). Twenty-first-century climate change impacts on marine animal biomass and ecosystem structure across ocean basins. *Global Change Biology*, 25(2), 459–472. <https://doi.org/10.1111/GCB.14512>

REFERENCES

- Buitinck, L., Louppe, G., & Blondel, M. (2013). API design for machine learning software: experiences from the scikit-learn project. *ECML/PKDD 2013 Workshop: Languages for Data Mining and Machine Learning*.
- Burson, A., Stomp, M., Akil, L., Brussaard, C. P. D., & Huisman, J. (2016). Unbalanced reduction of nutrient loads has created an offshore gradient from phosphorus to nitrogen limitation in the North Sea. *Limnology and Oceanography*, 61(3), 869–888. <https://doi.org/10.1002/LNO.10257>
- Burt, W. J., Thomas, H., Hagens, M., Pätsch, J., Clargo, N. M., Salt, L. A., Winde, V., & Böttcher, M. E. (2016). Carbon sources in the North Sea evaluated by means of radium and stable carbon isotope tracers. *Limnology and Oceanography*, 61(2), 666–683. <https://doi.org/10.1002/LNO.10243>
- Buschbaum, C., & Gutow, L. (2005). Mass occurrence of an introduced crustacean (*Caprella cf. mutica*) in the south-eastern North Sea. *Helgoland Marine Research*, 59(3), 252–253. <https://doi.org/10.1007/S10152-005-0225-7>
- Büttger, H., Nehls, G., & Witte, S. (2011). High mortality of Pacific oysters in a cold winter in the North-Frisian Wadden Sea. *Helgoland Marine Research*, 65(4), 525–532. <https://doi.org/10.1007/S10152-011-0272-1/FIGURES/6>
- Bzdok, D., Altman, N., & Krzywinski, M. (2018). Statistics versus machine learning. *Nature Methods*, 15(4), 233–234. <https://doi.org/10.1038/nmeth.4642>
- Cabré, A., Marinov, I., & Leung, S. (2015). Consistent global responses of marine ecosystems to future climate change across the IPCC AR5 earth system models. *Climate Dynamics*, 45(5–6), 1253–1280. <https://doi.org/10.1007/S00382-014-2374-3/METRICS>
- Chavez, F. P., Messié, M., & Pennington, J. T. (2010). Marine Primary Production in Relation to Climate Variability and Change, *Annual review of marine science*, 3, 227–260. <https://doi.org/10.1146/annurev.marine.010908.163917>
- Chegini, F., Holtermann, P., Kerimoglu, O., Becker, M., Kreuz, M., Klingbeil, K., Gräwe, U., Winter, C., & Burchard, H. (2020). Processes of Stratification and Destratification During An Extreme River Discharge Event in the German Bight ROFI. *Journal of Geophysical Research: Oceans*, 125(8), e2019JC015987. <https://doi.org/10.1029/2019JC015987>

REFERENCES

- Cheng, L., Foster, G., Hausfather, Z., Trenberth, K. E., & Abraham, J. (2022). Improved Quantification of the Rate of Ocean Warming. *Journal of Climate*, 35(14), 4827–4840. <https://doi.org/10.1175/JCLI-D-21-0895.1>
- Chen, W. H., Hsu, S. H., & Shen, H. P. (2005). Application of SVM and ANN for intrusion detection. *Computers & Operations Research*, 32(10), 2617–2634. <https://doi.org/10.1016/J.COR.2004.03.019>
- Cho, H., Choi, U. J., & Park, H. (2018). DEEP LEARNING APPLICATION TO TIME-SERIES PREDICTION OF DAILY CHLOROPHYLL-A CONCENTRATION. *WIT Transactions on Ecology and the Environment*, 215, 157–163. <https://doi.org/10.2495/EID180141>
- Chust, G., Allen, J. I., Bopp, L., Schrum, C., Holt, J., Tsiaras, K., Zavatarelli, M., Chifflet, M., Cannaby, H., Dadou, I., Daewel, U., Wakelin, S. L., Machu, E., Pushpadas, D., Butenschon, M., Artioli, Y., Petihakis, G., Smith, C., Garçon, V., ... Irigoien, X. (2014). Biomass changes and trophic amplification of plankton in a warmer ocean. *Global Change Biology*, 20(7), 2124–2139. <https://doi.org/10.1111/GCB.12562>
- Cloern, J. E., Abreu, P. C., Carstensen, J., Chauvaud, L., Elmgren, R., Grall, J., Greening, H., Johansson, J. O. R., Kahru, M., Sherwood, E. T., Xu, J., & Yin, K. (2016). Human activities and climate variability drive fast-paced change across the world's estuarine–coastal ecosystems. *Global Change Biology*, 22(2), 513–529. <https://doi.org/10.1111/GCB.13059>
- Cohen, D. (1967). Optimizing reproduction in a randomly varying environment when a correlation may exist between the conditions at the time a choice has to be made and the subsequent outcome. *Journal of Theoretical Biology*, 16(1), 1–14. [https://doi.org/10.1016/0022-5193\(67\)90050-1](https://doi.org/10.1016/0022-5193(67)90050-1)
- Collins, S. L. (1990). Effects of fire on community structure in tallgrass and mixed-grass prairie. *Fire in North American Tallgrass Prairies*, 81–98. <https://cir.nii.ac.jp/crid/1573668924927600256>
- Connell, J. H. (1978). Diversity in Tropical Rain Forests and Coral Reefs. *Science*, 199(4335), 1302–1310. <https://doi.org/10.1126/SCIENCE.199.4335.1302>
- Conversi, A., Umani, S. F., Peluso, T., Molinero, J. C., Santojanni, A., & Edwards, M. (2010). The Mediterranean Sea Regime Shift at the End of the 1980s, and Intriguing Parallelisms

REFERENCES

- with Other European Basins. *PLOS ONE*, 5(5), e10633. <https://doi.org/10.1371/JOURNAL.PONE.0010633>
- Cortes, C., Vapnik, V., & Saitta, L. (1995). Support-vector networks. *Machine Learning* 1995 20:3, 20(3), 273–297. <https://doi.org/10.1007/BF00994018>
- Cullen, J. J. (2011). The Deep Chlorophyll Maximum: Comparing Vertical Profiles of Chlorophyll a. *39(5)*, 791–803. <https://doi.org/10.1139/F82-108>
- Cushing, D. H. (1990). Plankton Production and Year-class Strength in Fish Populations: an Update of the Match/Mismatch Hypothesis. *Advances in Marine Biology*, 26(C), 249–293. [https://doi.org/10.1016/S0065-2881\(08\)60202-3](https://doi.org/10.1016/S0065-2881(08)60202-3)
- Daewel, U., & Schrum, C. (2017). Low-frequency variability in North Sea and Baltic Sea identified through simulations with the 3-D coupled physical-biogeochemical model ECOSMO. *Earth System Dynamics*, 8(3), 801–815. <https://doi.org/10.5194/ESD-8-801-2017>
- Dale, B. (2001). The sedimentary record of dinoflagellate cysts: looking back into the future of phytoplankton blooms. *Scientia Marina*, 65(S2), 257–272. <https://doi.org/10.3989/SCIMAR.2001.65S2257>
- Data, C. M. I. S. T. (2021). Product User Manual for multiparameter Copernicus In Situ TAC (PUM).
- Data GISS: GISS Surface Temperature Analysis (GISTEMP v4). (2022). Retrieved in 9 February 2022, from <https://data.giss.nasa.gov/gistemp/>
- De Boeck, H. J., Dreesen, F. E., Janssens, I. A., & Nijs, I. (2010). Climatic characteristics of heat waves and their simulation in plant experiments. *Global Change Biology*, 16(7), 1992–2000. <https://doi.org/10.1111/J.1365-2486.2009.02049.X>
- Dee, D. P., Balmaseda, M., Balsamo, G., Engelen, R., Simmons, A. J., & Thépaut, J. N. (2014). Toward a Consistent Reanalysis of the Climate System. *Bulletin of the American Meteorological Society*, 95(8), 1235–1248. <https://doi.org/10.1175/BAMS-D-13-00043.1>
- de Mello, C., Barreiro, M., Ortega, L., Trinchin, R., & Manta, G. (2022). Coastal upwelling along the Uruguayan coast: Structure, variability and drivers. *Journal of Marine Systems*, 230, 103735. <https://doi.org/10.1016/J.JMARSYS.2022.103735>

REFERENCES

- Desmit, X., Nohe, A., Borges, A. V., Prins, T., De Cauwer, K., Lagring, R., Van der Zande, D., & Sabbe, K. (2020). Changes in chlorophyll concentration and phenology in the North Sea in relation to de-eutrophication and sea surface warming. *Limnology and Oceanography*, 65(4), 828–847. <https://doi.org/10.1002/LNO.11351>
- Deutsche Wetterdienst (DWD) Climate Data Center (CDC): Daily Station Observations of Sunshine Duration in Hours for Germany. Retrieved in 26 April 2020, from <https://cdc.dwd.de/portal/>
- Deutsche Wetterdienst (DWD) Climate Data Center (CDC): Hourly Mean of Station Observations of Wind Speed ca. 10 m above Ground in m/s for Germany. Retrieved in 6 February 2020, from <https://cdc.dwd.de/portal/>
- Deutsche Wetterdienst (DWD) Climate Data Center (CDC): Hourly Station Observations of Wind Direction 10 m above Ground in Degree for Germany. Retrieved in 6 February 2020, <https://cdc.dwd.de/portal/>
- Dippner, J. W. (1997a). Long-term variability of a stochastic forced pelagic ecosystem model. *Environmental Modeling and Assessment*, 2(1–2), 37–42. <https://doi.org/10.1023/A:1019040806740/METRICS>
- Dippner, J. W. (1997b). Recruitment success of different fish stocks in the North Sea in relation to climate variability. *Deutsche Hydrografische Zeitschrift* 1997 49:2, 49(2), 277–293. <https://doi.org/10.1007/BF02764039>
- D’Odorico, P., Laio, F., Ridolfi, L., & Lerda, M. T. (2008). Biodiversity enhancement induced by environmental noise. *Journal of Theoretical Biology*, 255(3), 332–337. <https://doi.org/10.1016/J.JTBI.2008.09.007>
- Doerffer, R., & Fischer, J. (1994). Concentrations of chlorophyll, suspended matter, and gelbstoff in case II waters derived from satellite coastal zone color scanner data with inverse modeling methods. *Journal of Geophysical Research: Oceans*, 99(C4), 7457–7466. <https://doi.org/10.1029/93JC02523>
- Doerffer, R., & Schiller, H. (2007). The MERIS Case 2 water algorithm. *International Journal of Remote Sensing*, 28(3–4), 517–535. <https://doi.org/10.1080/01431160600821127>

REFERENCES

- Drinkwater, K. F. (2005). The response of Atlantic cod (*Gadus morhua*) to future climate change. *ICES Journal of Marine Science*, 62(7), 1327–1337. <https://doi.org/10.1016/J.ICESJMS.2005.05.015>
- Duarte, C. M., & Regaudie-de-Gioux, A. (2009). Thresholds of gross primary production for the metabolic balance of marine planktonic communities. *Limnology and Oceanography*, 54(3), 1015–1022. <https://doi.org/10.4319/LO.2009.54.3.1015>
- Dunstan, P. K., Foster, S. D., King, E., Risbey, J., O’Kane, T. J., Monselesan, D., Hobday, A. J., Hartog, J. R., & Thompson, P. A. (2018). Global patterns of change and variation in sea surface temperature and chlorophyll a. *Scientific Reports* 2018 8:1, 8(1), 1–9. <https://doi.org/10.1038/s41598-018-33057-y>
- du Pontavice, H., Gascuel, D., Reygondeau, G., Maureaud, A., & Cheung, W. W. L. (2020). Climate change undermines the global functioning of marine food webs. *Global Change Biology*, 26(3), 1306–1318. <https://doi.org/10.1111/GCB.14944>
- Durden, J. M., Luo, J. Y., Alexander, H., Flanagan, A. M., & Grossmann, L. (2017). Integrating “Big Data” into Aquatic Ecology: Challenges and Opportunities. *Limnology and Oceanography Bulletin*, 26(4), 101–108. <https://doi.org/10.1002/LOB.10213>
- Edwards, M., Beaugrand, G., Hays, G. C., Koslow, J. A., & Richardson, A. J. (2010). Multi-decadal oceanic ecological datasets and their application in marine policy and management. *Trends in Ecology & Evolution*, 25(10), 602–610. <https://doi.org/10.1016/J.TREE.2010.07.007>
- Edwards, M., Beaugrand, G., Reid, P. C., Rowden, A. A., & Jones, M. B. (2002). Ocean climate anomalies and the ecology of the North Sea. *Marine Ecology Progress Series*, 239, 1–10. <https://doi.org/10.3354/MEPS239001>
- Edwards, M., Reid, P., & Planque, B. (2001). Long-term and regional variability of phytoplankton biomass in the Northeast Atlantic (1960–1995). *ICES Journal of Marine Science*, 58(1), 39–49. <https://doi.org/10.1006/JMSC.2000.0987>
- Edwards, M., & Richardson, A. J. (2004). Impact of climate change on marine pelagic phenology and trophic mismatch. *Nature* 2004 430:7002, 430(7002), 881–884. <https://doi.org/10.1038/nature02808>

REFERENCES

- Ehrnsten, E., Norkko, A., Müller-Karulis, B., Gustafsson, E., & Gustafsson, B. G. (2020). The meagre future of benthic fauna in a coastal sea—Benthic responses to recovery from eutrophication in a changing climate. *Global Change Biology*, 26(4), 2235–2250. <https://doi.org/10.1111/GCB.15014>
- Eisner, L. B., Gann, J. C., Ladd, C., D. Cieciel, K., & Mordy, C. W. (2016). Late summer/early fall phytoplankton biomass (chlorophyll a) in the eastern Bering Sea: Spatial and temporal variations and factors affecting chlorophyll a concentrations. *Deep Sea Research Part II: Topical Studies in Oceanography*, 134, 100–114. <https://doi.org/10.1016/J.DSR2.2015.07.012>
- Emeis, K. C., van Beusekom, J., Callies, U., Ebinghaus, R., Kannen, A., Kraus, G., Kröncke, I., Lenhart, H., Lorkowski, I., Matthias, V., Möllmann, C., Pätsch, J., Scharfe, M., Thomas, H., Weisse, R., & Zorita, E. (2015). The North Sea — A shelf sea in the Anthropocene. *Journal of Marine Systems*, 141, 18–33. <https://doi.org/10.1016/J.JMARSYS.2014.03.012>
- European Environment Agency, (2022): Chlorophyll in transitional, coastal and marine waters in Europe. Retrieved 31 January 2024, from <https://www.eea.europa.eu/en/analysis/indicators/chlorophyll-in-transitional-coastal-and>
- Falkowski, P. G. (1984). Physiological responses of phytoplankton to natural light regimes. *Journal of Plankton Research*, 6(2), 295–307. <https://doi.org/10.1093/PLANKT/6.2.295>
- Falkowski, P. G., Barber, R. T., & Smetacek, V. (1998). Biogeochemical Controls and Feedbacks on Ocean Primary Production. *Science*, 281(5374), 200–206. <https://doi.org/10.1126/SCIENCE.281.5374.200>
- Falkowski, P. G., & Raven, J. A. (2007). *Aquatic photosynthesis*. 2nd Edition. Blackwell Science, London, UK, 484. <https://press.princeton.edu/books/paperback/9780691115511/aquatic-photosynthesis>
- Fellous, A., Wegner, K. M., John, U., Mark, F. C., & Shama, L. N. S. (2022). Windows of opportunity: Ocean warming shapes temperature-sensitive epigenetic reprogramming and gene expression across gametogenesis and embryogenesis in marine stickleback. *Global Change Biology*, 28(1), 54–71. <https://doi.org/10.1111/GCB.15942>
- Fernández-Tejedor, M., Velasco, J. E., & Angelats, E. (2022). Accurate Estimation of Chlorophyll-a Concentration in the Coastal Areas of the Ebro Delta (NW Mediterranean)

REFERENCES

- Using Sentinel-2 and Its Application in the Selection of Areas for Mussel Aquaculture. *Remote Sensing*, 14(20), 5235. <https://doi.org/10.3390/RS14205235/S1>
- Fettweis, M., Monbaliu, J., Baeye, M., Nechad, B., & Van den Eynde, D. (2012). Weather and climate induced spatial variability of surface suspended particulate matter concentration in the North Sea and the English Channel. *Methods in Oceanography*, 3–4, 25–39. <https://doi.org/10.1016/J.MIO.2012.11.001>
- Fichez, R., Jickells, T. D., & Edmunds, H. M. (1992). Algal blooms in high turbidity, a result of the conflicting consequences of turbulence on nutrient cycling in a shallow water estuary. *Estuarine, Coastal and Shelf Science*, 35(6), 577–592. [https://doi.org/10.1016/S0272-7714\(05\)80040-X](https://doi.org/10.1016/S0272-7714(05)80040-X)
- Field, C. B., Behrenfeld, M. J., Randerson, J. T., & Falkowski, P. (1998). Primary production of the biosphere: Integrating terrestrial and oceanic components. *Science*, 281(5374), 237–240. https://doi.org/10.1126/SCIENCE.281.5374.237/SUPPL_FILE/982246E_THUMB.GIF
- Flöder, S., & Sommer, U. (1999). Diversity in planktonic communities: An experimental test of the intermediate disturbance hypothesis. *Limnology and Oceanography*, 44(4), 1114–1119. <https://doi.org/10.4319/LO.1999.44.4.1114>
- Frajka-Williams, E., Beaulieu, C., & Ducez, A. (2017). Emerging negative Atlantic Multidecadal Oscillation index in spite of warm subtropics. *Scientific Reports* 2017 7:1, 7(1), 1–8. <https://doi.org/10.1038/s41598-017-11046-x>
- Franks, P. J. S. (1992). Sink or swim: Accumulation of biomass at fronts. *Marine Ecology Progress Series*, 82, 1–12. <https://doi.org/10.3354/MEPS082001>
- Friedland, K. D., Stock, C., Drinkwater, K. F., Link, J. S., Leaf, R. T., Shank, B. V., Rose, J. M., Pilskaln, C. H., & Fogarty, M. J. (2012). Pathways between Primary Production and Fisheries Yields of Large Marine Ecosystems. *PLOS ONE*, 7(1), e28945. <https://doi.org/10.1371/JOURNAL.PONE.0028945>
- Frölicher, T. L., & Laufkötter, C. (2018). Emerging risks from marine heat waves. *Nature Communications* 2018 9:1, 9(1), 1–4. <https://doi.org/10.1038/s41467-018-03163-6>

REFERENCES

- Fromentin, J. M., & Planque, B. (1996). Calanus and environment in the eastern North Atlantic. 2. Role of the North Atlantic Oscillation on *Calanus finmarchicus* and *C. helgolandicus*. *Marine Ecology Progress Series*, 134(1–3), 111–118. <https://doi.org/10.3354/MEPS134111>
- Fukutome, S., Frei, C., & Schär, C. (2003). Interannual Covariance between Japan Summer Precipitation and Western North Pacific SST. *Journal of the Meteorological Society of Japan. Ser. II*, 81(6), 1435–1456. <https://doi.org/10.2151/JMSJ.81.1435>
- Garcia, C. A. E., & Garcia, V. M. T. (2008). Variability of chlorophyll-a from ocean color images in the La Plata continental shelf region. *Continental Shelf Research*, 28(13), 1568–1578. <https://doi.org/10.1016/J.CSR.2007.08.010>
- Gardner, M. W., & Dorling, S. R. (1998). Artificial neural networks (the multilayer perceptron)—a review of applications in the atmospheric sciences. *Atmospheric Environment*, 32(14–15), 2627–2636. [https://doi.org/10.1016/S1352-2310\(97\)00447-0](https://doi.org/10.1016/S1352-2310(97)00447-0)
- Garnesson, P., Mangin, A., D'Andon, O. F., Demaria, J., & Bretagnon, M. (2019). The CMEMS GlobColour chlorophyll a product based on satellite observation: Multi-sensor merging and flagging strategies. *Ocean Science*, 15(3), 819–830. <https://doi.org/10.5194/OS-15-819-2019>
- GEBCO Bathymetric Compilation Group 2023 (2023). The GEBCO_2023 Grid - a continuous terrain model of the global oceans and land. NERC EDS British Oceanographic Data Centre NOC. <https://doi.org/10.5285/f98b053b-0cbc-6c23-e053-6c86abc0af7b>
- Giglio, D., Lyubchich, V., & Mazloff, M. R. (2018). Estimating Oxygen in the Southern Ocean Using Argo Temperature and Salinity. *Journal of Geophysical Research: Oceans*, 123(6), 4280–4297. <https://doi.org/10.1029/2017JC013404>
- Giménez, L. (2011). Exploring mechanisms linking temperature increase and larval phenology: The importance of variance effects. *Journal of Experimental Marine Biology and Ecology*, 400(1–2), 227–235. <https://doi.org/10.1016/J.JEMBE.2011.02.036>
- Giron-Nava, A., James, C. C., Johnson, A. F., Dannecker, D., Kolody, B., Lee, A., Nagarkar, M., Pao, G. M., Ye, H., Johns, D. G., & Sugihara, G. (2017). Quantitative argument for long-term ecological monitoring. *Marine Ecology Progress Series*, 572, 269–274. <https://doi.org/10.3354/MEPS12149>

REFERENCES

- Gittings, J. A., Raitzos, D. E., Krokos, G., & Hoteit, I. (2018). Impacts of warming on phytoplankton abundance and phenology in a typical tropical marine ecosystem. *Scientific Reports* 2018 8:1, 8(1), 1–12. <https://doi.org/10.1038/s41598-018-20560-5>
- Good, S., Fiedler, E., Mao, C., Martin, M. J., Maycock, A., Reid, R., Roberts-Jones, J., Searle, T., Waters, J., While, J., & Worsfold, M. (2020). The Current Configuration of the OSTIA System for Operational Production of Foundation Sea Surface Temperature and Ice Concentration Analyses. *Remote Sensing* 2020, Vol. 12, Page 720, 12(4), 720. <https://doi.org/10.3390/RS12040720>
- Gregg, W. W., Conkright, M. E., Ginoux, P., O'Reilly, J. E., & Casey, N. W. (2003). Ocean primary production and climate: Global decadal changes. *Geophysical Research Letters*, 30(15). <https://doi.org/10.1029/2003GL016889>
- Gregg, W. W., & Rousseaux, C. S. (2019). Global ocean primary production trends in the modern ocean color satellite record (1998–2015). *Environmental Research Letters*, 14(12), 124011. <https://doi.org/10.1088/1748-9326/AB4667>
- Gregory, B., Christophe, L., & Martin, E. (2009). Rapid biogeographical plankton shifts in the North Atlantic Ocean. *Global Change Biology*, 15(7), 1790–1803. <https://doi.org/10.1111/J.1365-2486.2009.01848.X>
- Greve, W., Reiners, F., Nast, J., & Hoffmann, S. (2004). Helgoland Roads meso- and macrozooplankton time-series 1974 to 2004: Lessons from 30 years of single spot, high frequency sampling at the only off-shore island of the North Sea. *Helgoland Marine Research*, 58(4), 274–288. <https://doi.org/10.1007/S10152-004-0191-5/FIGURES/8>
- Grime, J. P. (1973). Competitive Exclusion in Herbaceous Vegetation. *Nature* 1973 242:5396, 242(5396), 344–347. <https://doi.org/10.1038/242344a0>
- Gröger, M., Maier-Reimer, E., Mikolajewicz, U., Moll, A., & Sein, D. (2013). NW European shelf under climate warming: Implications for open ocean - Shelf exchange, primary production, and carbon absorption. *Biogeosciences*, 10(6), 3767–3792. <https://doi.org/10.5194/BG-10-3767-2013>
- Hackerott, S., Martell, H. A., & Eirin-Lopez, J. M. (2021). Coral environmental memory: causes, mechanisms, and consequences for future reefs. *Trends in Ecology & Evolution*, 36(11), 1011–1023. <https://doi.org/10.1016/J.TREE.2021.06.014>

REFERENCES

- Halpern, B. S., Walbridge, S., Selkoe, K. A., Kappel, C. V., Micheli, F., D'Agrosa, C., Bruno, J. F., Casey, K. S., Ebert, C., Fox, H. E., Fujita, R., Heinemann, D., Lenihan, H. S., Madin, E. M. P., Perry, M. T., Selig, E. R., Spalding, M., Steneck, R., & Watson, R. (2008). A global map of human impact on marine ecosystems. *Science*, 319(5865), 948–952. https://doi.org/10.1126/SCIENCE.1149345/SUPPL_FILE/HALPERN_SOM.PDF
- Harrison, W. G., & Cota, G. F. (1991). Primary production in polar waters: relation to nutrient availability. *Polar Research*, 10(1), 87–104. <https://doi.org/10.3402/POLAR.V10I1.6730>
- Harrison, W. G., Li, W. K. W., Harrison, W. G., & Li, W. K. W. (2008). Phytoplankton Growth and Regulation in the Labrador Sea: Light and Nutrient Limitation. *J. Northw. Atl. Fish. Sci.*, 39, 71–82. <https://doi.org/10.2960/J.v39.m592>
- Harvey, B. P., Marshall, K. E., Harley, C. D. G., & Russell, B. D. (2022). Predicting responses to marine heatwaves using functional traits. *Trends in Ecology & Evolution*, 37(1), 20–29. <https://doi.org/10.1016/J.TREE.2021.09.003>
- Hawkins, S. J., Southward, A. J., & Genner, M. J. (2003). Detection of environmental change in a marine ecosystem—evidence from the western English Channel. *Science of The Total Environment*, 310(1–3), 245–256. [https://doi.org/10.1016/S0048-9697\(02\)00645-9](https://doi.org/10.1016/S0048-9697(02)00645-9)
- Hayashida, H., Matear, R. J., & Strutton, P. G. (2020). Background nutrient concentration determines phytoplankton bloom response to marine heatwaves. *Global Change Biology*, 26(9), 4800–4811. <https://doi.org/10.1111/GCB.15255>
- Hayward, T. L., & Venrick, E. L. (1982). Relation between surface chlorophyll, integrated chlorophyll and integrated primary production. *Marine Biology*, 69(3), 247–252. <https://doi.org/10.1007/BF00397490/METRICS>
- Heath, M. R. (2005). Changes in the structure and function of the North Sea fish foodweb, 1973–2000, and the impacts of fishing and climate. *ICES Journal of Marine Science*, 62(5), 847–868. <https://doi.org/10.1016/J.ICESJMS.2005.01.023>
- Heath, M. R., Backhaus, J. O., Richardson, K., McKenzie, E., Slagstad, D., Beare, D., Dunn, J., Fraser, J. G., Gallego, A., Hainbucher, D., Hay, S., Jónasdóttir, S., Madden, H., Mardaljevic, J., & Schacht, A. (1999). Climate fluctuations and the spring invasion of the North Sea by *Calanus finmarchicus*. *Fisheries Oceanography*, 8(SUPPL. 1), 163–176. <https://doi.org/10.1046/J.1365-2419.1999.00008.X>

REFERENCES

- Henson, S. A., Dunne, J. P., & Sarmiento, J. L. (2009). Decadal variability in North Atlantic phytoplankton blooms. *Journal of Geophysical Research: Oceans*, 114(C4). <https://doi.org/10.1029/2008JC005139>
- Henson, S. A., Sarmiento, J. L., Dunne, J. P., Bopp, L., Lima, I., Doney, S. C., John, J., & Beaulieu, C. (2010). Detection of anthropogenic climate change in satellite records of ocean chlorophyll and productivity. *Biogeosciences*, 7(2), 621–640. <https://doi.org/10.5194/BG-7-621-2010>
- Henson, S., Cole, H., Beaulieu, C., & Yool, A. (2013). The impact of global warming on seasonality of ocean primary production. *Biogeosciences*, 10(6), 4357–4369. <https://doi.org/10.5194/BG-10-4357-2013>
- Hickel, W., Mangelsdorf, P., & Berg, J. (1993). The human impact in the German Bight: Eutrophication during three decades (1962-1991). *Helgoländer Meeresuntersuchungen*, 47(3), 243–263. <https://doi.org/10.1007/BF02367167/METRICS>
- Hinder, S. L., Hays, G. C., Edwards, M., Roberts, E. C., Walne, A. W., & Gravenor, M. B. (2012). Changes in marine dinoflagellate and diatom abundance under climate change. *Nature Climate Change* 2012 2:4, 2(4), 271–275. <https://doi.org/10.1038/nclimate1388>
- Holliday, P., Kennedy, J., Kent, E. C., Marsh, R., Hughes, S. L., Sherwin, T., & Berry, D. I. (2008). MCCIP Annual Report Card 2007-2008 Scientific Review-Sea Temperature Topic Sea Temperature Organisation(s) represented.
- Holt, J., Hughes, S., Hopkins, J., Wakelin, S. L., Penny Holliday, N., Dye, S., González-Pola, C., Hjøllø, S. S., Mork, K. A., Nolan, G., Proctor, R., Read, J., Shammon, T., Sherwin, T., Smyth, T., Tattersall, G., Ward, B., & Wiltshire, K. H. (2012). Multi-decadal variability and trends in the temperature of the northwest European continental shelf: A model-data synthesis. *Progress in Oceanography*, 106, 96–117. <https://doi.org/10.1016/J.POCEAN.2012.08.001>
- Hornik, K., Stinchcombe, M., & White, H. (1989). Multilayer feedforward networks are universal approximators. *Neural Networks*, 2(5), 359–366. [https://doi.org/10.1016/0893-6080\(89\)90020-8](https://doi.org/10.1016/0893-6080(89)90020-8)
- Humboldt, A. von, & Bonpland, A. (1805). *Analysis of the geography of plants*.

REFERENCES

- Hunter-Cevera, K. R., Neubert, M. G., Olson, R. J., Solow, A. R., Shalapyonok, A., & Sosik, H. M. (2016). Physiological and ecological drivers of early spring blooms of a coastal phytoplankter. *Science*, 354(6310), 326–329. https://doi.org/10.1126/SCIENCE.AAF8536/SUPPL_FILE/AAF8536-HUNTER-CEVERA-SM.PDF
- Huot, Y., Babin, M., Bruyant, F., Grob, C., Twardowski, M. S., & Claustre, H. (2007a). Does chlorophyll a provide the best index of phytoplankton biomass for primary productivity studies? *Biogeosciences Discussions*, 4(2), 707–745. <https://doi.org/10.5194/BGD-4-707-2007>
- Huot, Y., Babin, M., Bruyant, F., Grob, C., Twardowski, M. S., & Claustre, H. (2007b). Relationship between photosynthetic parameters and different proxies of phytoplankton biomass in the subtropical ocean. *Biogeosciences*, 4(5), 853–868. <https://doi.org/10.5194/BG-4-853-2007>
- Hurrell, J. W., Kushnir, Y., Ottersen, G., & Visbeck, M. (Eds.). (2003). *The North Atlantic Oscillation: Climatic Significance and Environmental Impact*. 134. <https://doi.org/10.1029/GM134>
- Hurrell, J. W., Kushnir, Y., & Visbeck, M. (2001). The North Atlantic Oscillation. *Science*, 291(5504), 603–605. <https://doi.org/10.1126/SCIENCE.1058761>
- Hussain, Md. M., & Mahmud, I. (2019). pyMannKendall: a python package for non parametric Mann Kendall family of trend tests. *Journal of Open Source Software*, 4(39), 1556. <https://doi.org/10.21105/JOSS.01556>
- Huthnance, J. M. (1991). Physical oceanography of the North Sea. *Ocean and Shoreline Management*, 16(3–4), 199–231. [https://doi.org/10.1016/0951-8312\(91\)90005-M](https://doi.org/10.1016/0951-8312(91)90005-M)
- IPCC. (2018). *Global warming of 1.5°C: An IPCC special report on the impacts of global warming of 1.5°C above pre-industrial levels and related global greenhouse gas emission pathways, in the context of strengthening the global response to the threat of climate change, sustainable development, and efforts to eradicate poverty*. Intergovernmental Panel on Climate Change. Retrieved from <https://www.ipcc.ch/sr15/>
- IPCC. (2019). Summary for policymakers. In H.-O. Pörtner, D. C. Roberts, V. Masson-Delmotte, P. Zhai, M. Tignor, E. Poloczanska, K. Mintenbeck, A. Alegría, M. Nicolai, A.

REFERENCES

- Okem, J. Petzold, B. Rama, & N. M. Weyer (Eds.), IPCC special report on the ocean and cryosphere in a changing climate. Intergovernmental Panel on Climate Change. Retrieved from <https://www.ipcc.ch/srocc/>
- Irwin, A. J., & Finkel, Z. V. (2008). Mining a Sea of Data: Deducing the Environmental Controls of Ocean Chlorophyll. *PLOS ONE*, 3(11), e3836. <https://doi.org/10.1371/JOURNAL.PONE.0003836>
- Jahnke, R. A. (2010). Global Synthesis I. In K.-K. Liu, L. Atkinson, R. Quiñones, & L. Talaue-McManus (Eds.), *Carbon and Nutrient Fluxes in Continental Margins: A Global Synthesis* (pp. 597–615). Springer Berlin Heidelberg. https://doi.org/10.1007/978-3-540-92735-8_16
- Jorda, G., Marbà, N., Bennett, S., Santana-Garcon, J., Agusti, S., & Duarte, C. M. (2019). Ocean warming compresses the three-dimensional habitat of marine life. *Nature Ecology & Evolution* 2019 4:1, 4(1), 109–114. <https://doi.org/10.1038/s41559-019-1058-0>
- Kaiser, D., Voynova, Y. G., & Brix, H. (2023). Effects of the 2018 European heatwave and drought on coastal biogeochemistry in the German Bight. *Science of The Total Environment*, 892, 164316. <https://doi.org/10.1016/J.SCITOTENV.2023.164316>
- Kara, A. B., Rochford, P. A., & Hurlburt, H. E. (2000). An optimal definition for ocean mixed layer depth. *Journal of Geophysical Research: Oceans*, 105(C7), 16803–16821. <https://doi.org/10.1029/2000JC900072>
- Keller, S., Maier, P. M., Riese, F. M., Norra, S., Holbach, A., Börsig, N., Wilhelms, A., Moldaenke, C., Zaake, A., & Hinz, S. (2018). Hyperspectral Data and Machine Learning for Estimating CDOM, Chlorophyll a, Diatoms, Green Algae and Turbidity. *International Journal of Environmental Research and Public Health* 2018, Vol. 15, Page 1881, 15(9), 1881. <https://doi.org/10.3390/IJERPH15091881>
- Kemp, W. M., Testa, J. M., Conley, D. J., Gilbert, D., & Hagy, J. D. (2009). Temporal responses of coastal hypoxia to nutrient loading and physical controls. *Biogeosciences*, 6(12), 2985–3008. <https://doi.org/10.5194/BG-6-2985-2009>
- Kendall, M. G. (1975). *Rank Correlation Measures*; Charles Griffin Book Series. Oxford University Press: London, UK.
- Kennedy, J. J., Rayner, N. A., Smith, R. O., Parker, D. E., & Saunby, M. (2011a). Reassessing biases and other uncertainties in sea surface temperature observations measured in situ since

REFERENCES

- 1850: 1. Measurement and sampling uncertainties. *Journal of Geophysical Research: Atmospheres*, 116(D14). <https://doi.org/10.1029/2010JD015218>
- Kennedy, J. J., Rayner, N. A., Smith, R. O., Parker, D. E., & Saunby, M. (2011b). Reassessing biases and other uncertainties in sea surface temperature observations measured in situ since 1850: 2. Biases and homogenization. *Journal of Geophysical Research: Atmospheres*, 116(D14), 14104. <https://doi.org/10.1029/2010JD015220>
- Kerimoglu, O., Hofmeister, R., Maerz, J., Riethmüller, R., & Wirtz, K. W. (2017). The acclimative biogeochemical model of the southern North Sea. *Biogeosciences*, 14(19), 4499–4531. <https://doi.org/10.5194/BG-14-4499-2017>
- Kerimoglu, O., Voynova, Y. G., Chegini, F., Brix, H., Callies, U., Hofmeister, R., Klingbeil, K., Schrum, C., & Van Beusekom, J. E. E. (2020). Interactive impacts of meteorological and hydrological conditions on the physical and biogeochemical structure of a coastal system. *Biogeosciences*, 17(20), 5097–5127. <https://doi.org/10.5194/BG-17-5097-2020>
- Kjellström, E., Nikulin, G., Strandberg, G., Bøssing Christensen, O., Jacob, D., Keuler, K., Lenderink, G., Van Meijgaard, E., Schär, C., Somot, S., Lund Sørland, S., Teichmann, C., & Vautard, R. (2018). European climate change at global mean temperature increases of 1.5 and 2 °C above pre-industrial conditions as simulated by the EURO-CORDEX regional climate models. *Earth System Dynamics*, 9(2), 459–478. <https://doi.org/10.5194/ESD-9-459-2018>
- Kraberg, A., Kieb, U., Peters, S., & Wiltshire, K. H. (2019). An updated phytoplankton checklist for the Helgoland Roads time series station with eleven new records of diatoms and dinoflagellates. *Helgoland Marine Research*, 73(1), 1–22. <https://doi.org/10.1186/S10152-019-0528-8/FIGURES/3>
- Krasnopolsky, V., Nadiga, S., Mehra, A., & Bayler, E. (2018). Adjusting neural network to a particular problem: Neural network-based empirical biological model for chlorophyll concentration in the upper ocean. *Applied Computational Intelligence and Soft Computing*, 2018. <https://doi.org/10.1155/2018/7057363>
- Kröncke, I., Dippner, J. W., Heyen, H., & Zeiss, B. (1998). Long-term changes in macrofaunal communities off Norderney (East Frisia, Germany) in relation to climate variability. *Marine Ecology Progress Series*, 167, 25–36. <https://doi.org/10.3354/MEPS167025>

REFERENCES

- Kwiatkowska, E. J., & Fargion, G. S. (2003). Application of machine-learning techniques toward the creation of a consistent and calibrated global chlorophyll concentration baseline dataset using remotely sensed ocean color data. *IEEE Transactions on Geoscience and Remote Sensing*, 41(12 PART I), 2844–2860. <https://doi.org/10.1109/TGRS.2003.818016>
- Lavergne, T., Macdonald Sørensen, A., Kern, S., Tonboe, R., Notz, D., Aaboe, S., Bell, L., Dybkjær, G., Eastwood, S., Gabarro, C., Heygster, G., Anne Killie, M., Brandt Kreiner, M., Lavelle, J., Saldo, R., Sandven, S., & Pedersen, L. T. (2019). Version 2 of the EUMETSAT OSI SAF and ESA CCI sea-ice concentration climate data records. *Cryosphere*, 13(1), 49–78. <https://doi.org/10.5194/TC-13-49-2019>
- Lee, J., Wang, W., Harrou, F., & Sun, Y. (2020). Wind Power Prediction Using Ensemble Learning-Based Models. *IEEE Access*, 8, 61517–61527. <https://doi.org/10.1109/ACCESS.2020.2983234>
- Lee, S., & Chung, J. Y. (2019). The Machine Learning-Based Dropout Early Warning System for Improving the Performance of Dropout Prediction. *Applied Sciences* 2019, Vol. 9, Page 3093, 9(15), 3093. <https://doi.org/10.3390/APP9153093>
- Lemenkova, P. (2019). Processing Oceanographic Data by Python Libraries Numpy, Scipy and Pandas. *Aquatic Research*, 73–91. <https://doi.org/10.3153/AR19009>
- Lenert, M. C., & Walsh, C. G. (2018). Balancing Performance and Interpretability: Selecting Features with Bootstrapped Ridge Regression. *AMIA Annual Symposium Proceedings*, 2018, 1377. [/pmc/articles/PMC6371276/](https://pubmed.ncbi.nlm.nih.gov/312767276/)
- Lenssen, N. J. L., Schmidt, G. A., Hansen, J. E., Menne, M. J., Persin, A., Ruedy, R., & Zyss, D. (2019). Improvements in the GISTEMP Uncertainty Model. *Journal of Geophysical Research: Atmospheres*, 124(12), 6307–6326. <https://doi.org/10.1029/2018JD029522>
- Lenz, M., da Gama, B. A. P., Gerner, N. V., Gobin, J., Gröner, F., Harry, A., Jenkins, S. R., Kraufvelin, P., Mummelthei, C., Sareyka, J., Xavier, E. A., & Wahl, M. (2011). Non-native marine invertebrates are more tolerant towards environmental stress than taxonomically related native species: Results from a globally replicated study. *Environmental Research*, 111(7), 943–952. <https://doi.org/10.1016/J.ENVRES.2011.05.001>

REFERENCES

- Lima, F. P., & Wetthey, D. S. (2012). Three decades of high-resolution coastal sea surface temperatures reveal more than warming. *Nature Communications* 2012 3:1, 3(1), 1–13. <https://doi.org/10.1038/ncomms1713>
- Liu, X., Feng, J., & Wang, Y. (2019). Chlorophyll a predictability and relative importance of factors governing lake phytoplankton at different timescales. *Science of The Total Environment*, 648, 472–480. <https://doi.org/10.1016/J.SCITOTENV.2018.08.146>
- Lo, A. W., Siah, K. W., & Wong, C. H. (2019). Machine Learning With Statistical Imputation for Predicting Drug Approvals. *Harvard Data Science Review*, 1(1). <https://doi.org/10.1162/99608F92.5C5F0525>
- Lohmann, G., & Wiltshire, K. H. (2012). Winter atmospheric circulation signature for the timing of the spring bloom of diatoms in the North Sea. *Marine Biology*, 159(11), 2573–2581. <https://doi.org/10.1007/S00227-012-1993-7/METRICS>
- Longhurst, A. R., & Glen Harrison, W. (1989). The biological pump: Profiles of plankton production and consumption in the upper ocean. *Progress in Oceanography*, 22(1), 47–123. [https://doi.org/10.1016/0079-6611\(89\)90010-4](https://doi.org/10.1016/0079-6611(89)90010-4)
- Longhurst, A., Sathyendranath, S., Platt, T., & Caverhill, C. (1995). An estimate of global primary production in the ocean from satellite radiometer data. *Journal of Plankton Research*, 17(6), 1245–1271. <https://doi.org/10.1093/PLANKT/17.6.1245>
- Los, F. J., Villars, M. T., & Van der Tol, M. W. M. (2008). A 3-dimensional primary production model (BLOOM/GEM) and its applications to the (southern) North Sea (coupled physical–chemical–ecological model). *Journal of Marine Systems*, 74(1–2), 259–294. <https://doi.org/10.1016/J.JMARSYS.2008.01.002>
- Lotze, H. K., Lenihan, H. S., Bourque, B. J., Bradbury, R. H., Cooke, R. G., Kay, M. C., Kidwell, S. M., Kirby, M. X., Peterson, C. H., & Jackson, J. B. C. (2006). Depletion degradation, and recovery potential of estuaries and coastal seas. *Science*, 312(5781), 1806–1809. https://doi.org/10.1126/SCIENCE.1128035/SUPPL_FILE/LOTZE.SOM.PDF
- Lotze, H. K., Tittensor, D. P., Bryndum-Buchholz, A., Eddy, T. D., Cheung, W. W. L., Galbraith, E. D., Barange, M., Barrier, N., Bianchi, D., Blanchard, J. L., Bopp, L., Büchner, M., Bulman, C. M., Carozza, D. A., Christensen, V., Coll, M., Dunne, J. P., Fulton, E. A., Jennings, S., ... Worm, B. (2019). Global ensemble projections reveal trophic amplification

REFERENCES

- of ocean biomass declines with climate change. *Proceedings of the National Academy of Sciences of the United States of America*, 116(26), 12907–12912. https://doi.org/10.1073/PNAS.1900194116/SUPPL_FILE/PNAS.1900194116.SAPP.PDF
- Luo, W., Zhu, S., Wu, S., & Dai, J. (2019). Comparing artificial intelligence techniques for chlorophyll-a prediction in US lakes. *Environmental Science and Pollution Research*, 26(29), 30524–30532. <https://doi.org/10.1007/S11356-019-06360-Y/METRICS>
- MacArthur, R. H., Levin, S. A., MacArthur, S. A. L., & Recipient, A. (1992). The Problem of Pattern and Scale in Ecology: The Robert H. MacArthur Award Lecture. *Ecology*, 73(6), 1943–1967. <https://doi.org/10.2307/1941447>
- Mackas, D. L., Denman, K. L., & Abbott, M. R. (1985). Plankton patchiness: biology in the physical vernacular. *Bulletin of Marine Science*, 37(2), 652–674.
- Mackenzie, B. R., & Schiedek, D. (2007). Daily ocean monitoring since the 1860s shows record warming of northern European seas. *Global Change Biology*, 13(7), 1335–1347. <https://doi.org/10.1111/J.1365-2486.2007.01360.X>
- Mackenzie, F. T., Andersson, A. J., Lerman, A., & Ver, L. M. (2005). Boundary exchanges in the global coastal margin: implications for the organic and inorganic carbon cycles. *The Sea*, 13, 193–225.
- Madeira, D., Narciso, L., Cabral, H. N., & Vinagre, C. (2012). Thermal tolerance and potential impacts of climate change on coastal and estuarine organisms. *Journal of Sea Research*, 70, 32–41. <https://doi.org/10.1016/J.SEARES.2012.03.002>
- Mann, H. B. (1945). Nonparametric Tests Against Trend. *Econometrica*, 13(3), 245. <https://doi.org/10.2307/1907187>
- Mann, M. E., Steinman, B. A., Brouillette, D. J., & Miller, S. K. (2021). Multidecadal climate oscillations during the past millennium driven by volcanic forcing. *Science*, 371(6533), 1014–1019. https://doi.org/10.1126/SCIENCE.ABC5810/SUPPL_FILE/ABC5810_MANN_SM.PDF
- Mao, H., Meng, J., Ji, F., Zhang, Q., & Fang, H. (2019). Comparison of Machine Learning Regression Algorithms for Cotton Leaf Area Index Retrieval Using Sentinel-2 Spectral Bands. *Applied Sciences* 2019, Vol. 9, Page 1459, 9(7), 1459. <https://doi.org/10.3390/APP9071459>

REFERENCES

- Margalef, R. (1973). Information theory in ecology. In *La teoría de la información en Ecología*. Real Academia de Ciencias y Artes de Barcelona.
- Marrari, M., Piola, A. R., & Valla, D. (2017). Variability and 20-year trends in satellite-derived surface chlorophyll concentrations in large marine ecosystems around South and Western central America. *Frontiers in Marine Science*, 4(NOV), 303758. <https://doi.org/10.3389/FMARS.2017.00372/BIBTEX>
- Marshall, D. J., & Burgess, S. C. (2015). Deconstructing environmental predictability: seasonality, environmental colour and the biogeography of marine life histories. *Ecology Letters*, 18(2), 174–181. <https://doi.org/10.1111/ELE.12402>
- Martínez-López, B., & Zavala-Hidalgo, J. (2009). Seasonal and interannual variability of cross-shelf transports of chlorophyll in the Gulf of Mexico. *Journal of Marine Systems*, 77(1–2), 1–20. <https://doi.org/10.1016/J.JMARSYS.2008.10.002>
- McKinney, W., Perktold, J., & Seabold, S. (2011). Time series analysis in python with statsmodels. *Jarrodmillman Com*, 96–102.
- Merchant, C. J., Embury, O., Bulgin, C. E., Block, T., Corlett, G. K., Fiedler, E., Good, S. A., Mittaz, J., Rayner, N. A., Berry, D., Eastwood, S., Taylor, M., Tsushima, Y., Waterfall, A., Wilson, R., & Donlon, C. (2019). Satellite-based time-series of sea-surface temperature since 1981 for climate applications. *Scientific Data*, 6(1). <https://doi.org/10.1038/S41597-019-0236-X>
- Meyerjürgens, J., Badewien, T. H., Garaba, S. P., Wolff, J. O., & Zielinski, O. (2019). A state-of-the-art compact surface drifter reveals pathways of floating marine litter in the German Bight. *Frontiers in Marine Science*, 6(FEB), 436473. <https://doi.org/10.3389/FMARS.2019.00058/BIBTEX>
- Mieruch, S., Freund, J. A., Feudel, U., Boersma, M., Janisch, S., & Wiltshire, K. H. (2010). A new method of describing phytoplankton blooms: Examples from Helgoland Roads. *Journal of Marine Systems*, 79(1–2), 36–43. <https://doi.org/10.1016/J.JMARSYS.2009.06.004>
- Moll, A. (1997). Modeling primary production in the North Sea. *Oceanography*, 10(1), 24–26. <https://doi.org/10.5670/OCEANOLOG.1997.41>

REFERENCES

- Morel, A., Claustre, H., & Gentili, B. (2010). The most oligotrophic subtropical zones of the global ocean: Similarities and differences in terms of chlorophyll and yellow substance. *Biogeosciences*, 7(10), 3139–3151. <https://doi.org/10.5194/BG-7-3139-2010>
- Morice, C. P., Kennedy, J. J., Rayner, N. A., Jones, P. D., Morice, C. :, Kennedy, J. J., Rayner, N. A., & Jones, P. D. (2012). Quantifying uncertainties in global and regional temperature change using an ensemble of observational estimates: The HadCRUT4 data set. *Journal of Geophysical Research: Atmospheres*, 117(D8), 8101. <https://doi.org/10.1029/2011JD017187>
- Munson, M. A., & Caruana, R. (2009). On feature selection, bias-variance, and bagging. *Lecture Notes in Computer Science (Including Subseries Lecture Notes in Artificial Intelligence and Lecture Notes in Bioinformatics)*, 5782 LNAI(PART 2), 144–159. https://doi.org/10.1007/978-3-642-04174-7_10/COVER
- Neumann, A., van Beusekom, J. E. E., Eisele, A., Emeis, K. C., Friedrich, J., Kröncke, I., Logemann, E. L., Meyer, J., Naderipour, C., Schückel, U., Wrede, A., & Zettler, M. L. (2021). Macrofauna as a major driver of benthic-pelagic exchange in the southern North Sea. *Limnology and Oceanography*, 66(6), 2203–2217. <https://doi.org/10.1002/LNO.11748>
- Nye, J. A., Baker, M. R., Bell, R., Kenny, A., Kilbourne, K. H., Friedland, K. D., Martino, E., Stachura, M. M., Van Houtan, K. S., & Wood, R. (2014). Ecosystem effects of the Atlantic Multidecadal Oscillation. *Journal of Marine Systems*, 133, 103–116. <https://doi.org/10.1016/J.JMARSYS.2013.02.006>
- Olden, J. D., Lawler, J. J., & Poff, N. L. (2008). Machine Learning Methods Without Tears: A Primer for Ecologists. *The Quarterly Review of Biology*, 83(2), 171–193. <https://doi.org/10.1086/587826>
- Olita, A., Ribotti, A., Sorgente, R., Fazioli, L., & Perilli, A. (2011). SLA-chlorophyll-a variability and covariability in the Algero-Provençal Basin (1997-2007) through combined use of EOF and wavelet analysis of satellite data. *Ocean Dynamics*, 61(1), 89–102. <https://doi.org/10.1007/S10236-010-0344-9/METRICS>
- Ooi, K. S., Chen, Z. Y., Poh, P. E., & Cui, J. (2022). BOD5 prediction using machine learning methods. *Water Supply*, 22(1), 1168–1183. <https://doi.org/10.2166/WS.2021.202>

REFERENCES

- Ostle, C., Paxman, K., Graves, C. A., Arnold, M., Artigas, L. F., Atkinson, A., Aubert, A., Baptie, M., Bear, B., Bedford, J., Best, M., Bresnan, E., Brittain, R., Broughton, D., Budria, A., Cook, K., Devlin, M., Graham, G., Halliday, N., ... McQuatters-Gollop, A. (2021). The Plankton Lifeform Extraction Tool: A digital tool to increase the discoverability and usability of plankton time-series data. *Earth System Science Data*, 13(12), 5617–5642. <https://doi.org/10.5194/ESSD-13-5617-2021>
- Pahlevan, N., Smith, B., Schalles, J., Binding, C., Cao, Z., Ma, R., Alikas, K., Kangro, K., Gurlin, D., Hà, N., Matsushita, B., Moses, W., Greb, S., Lehmann, M. K., Ondrusek, M., Oppelt, N., & Stumpf, R. (2020). Seamless retrievals of chlorophyll-a from Sentinel-2 (MSI) and Sentinel-3 (OLCI) in inland and coastal waters: A machine-learning approach. *Remote Sensing of Environment*, 240, 111604. <https://doi.org/10.1016/J.RSE.2019.111604>
- Park, Y., Cho, K. H., Park, J., Cha, S. M., & Kim, J. H. (2015). Development of early-warning protocol for predicting chlorophyll-a concentration using machine learning models in freshwater and estuarine reservoirs, Korea. *Science of The Total Environment*, 502, 31–41. <https://doi.org/10.1016/J.SCITOTENV.2014.09.005>
- Pauly, D., & Christensen, V. (1995). Primary production required to sustain global fisheries. *Nature* 1995 374:6519, 374(6519), 255–257. <https://doi.org/10.1038/374255a0>
- Pauly, D., Christensen, V., Guénette, S., Pitcher, T. J., Sumaila, U. R., Walters, C. J., Watson, R., & Zeller, D. (2002). Towards sustainability in world fisheries. *Nature* 2002 418:6898, 418(6898), 689–695. <https://doi.org/10.1038/nature01017>
- Pedregosa, F., Michel, V., Grisel, O., Blondel, M., Prettenhofer, P., Weiss, R., Vanderplas, J., Cournapeau, D., Pedregosa, F., Varoquaux, G., Gramfort, A., Thirion, B., Grisel, O., Dubourg, V., Passos, A., Brucher, M., Perrot, M., & Duchesnay, É. (2011). Scikit-learn: Machine Learning in Python. *The Journal of Machine Learning Research*, 12, 2825–2830. <https://doi.org/10.5555/1953048.2078195>
- Perkins, S. E., & Alexander, L. V. (2013). On the Measurement of Heat Waves. *Journal of Climate*, 26(13), 4500–4517. <https://doi.org/10.1175/JCLI-D-12-00383.1>
- Perry, A. L., Low, P. J., Ellis, J. R., & Reynolds, J. D. (2005). Ecology: Climate change and distribution shifts in marine fishes. *Science*, 308(5730), 1912–1915. https://doi.org/10.1126/SCIENCE.1111322/SUPPL_FILE/PERRY.SOM.REVISED.PDF

REFERENCES

- Petersen, W., Wehde, H., Krasemann, H., Colijn, F., & Schroeder, F. (2008). FerryBox and MERIS – Assessment of coastal and shelf sea ecosystems by combining in situ and remotely sensed data. *Estuarine, Coastal and Shelf Science*, 77(2), 296–307. <https://doi.org/10.1016/J.ECSS.2007.09.023>
- Peterson, D. L., & Parker, V. T. (1998). Dimensions of scale in ecology, resource management, and society. *Ecological Scale: Theory and Applications*, 499, 503–507.
- Philippart, C. J. M., Van Aken, H. M., Beukema, J. J., Bos, O. G., Cadée, G. C., & Dekker, R. (2003). Climate-related changes in recruitment of the bivalve *Macoma balthica*. *Limnology and Oceanography*, 48(6), 2171–2185. <https://doi.org/10.4319/LO.2003.48.6.2171>
- Phung, V. H., & Rhee, E. J. (2019). A High-Accuracy Model Average Ensemble of Convolutional Neural Networks for Classification of Cloud Image Patches on Small Datasets. *Applied Sciences* 2019, Vol. 9, Page 4500, 9(21), 4500. <https://doi.org/10.3390/APP9214500>
- Pierce, D. W., Barnett, T. P., AchutaRao, K. M., Gleckler, P. J., Gregory, J. M., & Washington, W. M. (2006). Anthropogenic Warming of the Oceans: Observations and Model Results. *Journal of Climate*, 19(10), 1873–1900. <https://doi.org/10.1175/JCLI3723.1>
- Pikitch, E. K., Santora, C., Babcock, E. A., Bakun, A., Bonfil, R., Conover, D. O., Dayton, P., Doukakis, P., Fluharty, D., Heneman, B., Houde, E. D., Link, J., Livingston, P. A., Mangel, M., McAllister, M. K., Pope, J., & Sainsbury, K. J. (2004). Ecosystem-based fishery management. *Science*, 305(5682), 346–347. <https://doi.org/10.1126/SCIENCE.1098222/ASSET/4DBF3890-C9B0-436C-99FF-2B5A809287E6/ASSETS/SCIENCE.1098222.FP.PNG>
- Pingree, R. (2005). North Atlantic and North Sea Climate Change: curl up, shut down, NAO and Ocean Colour. *Journal of the Marine Biological Association of the United Kingdom*, 85(6), 1301–1315. <https://doi.org/10.1017/S0025315405012488>
- Planque, B., & Fromentin, J. M. (1996). Calanus and environment in the Eastern North Atlantic. I. Spatial and temporal patterns of *C. finmarchicus* and *C. helgolandicus*. *Marine Ecology Progress Series*, 134(1–3), 101–109. <https://doi.org/10.3354/MEPS134101>
- Platt, T., Sathyendranath, S., Longhurst, A., Wilson, T. R. S., Woods, J., Takahashi, T., Eglinton, G., Elderfield, H., Whitfield, M., & Williams, P. J. Le. B. (1997). Remote sensing

REFERENCES

- of primary production in the ocean: promise and fulfilment. *Philosophical Transactions of the Royal Society of London. Series B: Biological Sciences*, 348(1324), 191–202. <https://doi.org/10.1098/rstb.1995.0061>
- Pörtner, H. O. (2002). Climate variations and the physiological basis of temperature dependent biogeography: systemic to molecular hierarchy of thermal tolerance in animals. *Comparative Biochemistry and Physiology Part A: Molecular & Integrative Physiology*, 132(4), 739–761. [https://doi.org/10.1016/S1095-6433\(02\)00045-4](https://doi.org/10.1016/S1095-6433(02)00045-4)
- Pörtner, H. O., Bock, C., & Mark, F. C. (2017). Oxygen- and capacity-limited thermal tolerance: bridging ecology and physiology. *Journal of Experimental Biology*, 220(15), 2685–2696. <https://doi.org/10.1242/JEB.134585>
- Pörtner, H.-O., Roberts, D. C., Alegría, A., Nicolai, M., Okem, A., Petzold, J., Rama, B., & Weyer, N. M. (2019). *The Ocean and Cryosphere in a Changing Climate A Special Report of the Intergovernmental Panel on Climate Change Edited by.*
- Pozo-Vázquez, D., Esteban-Parra, M. J., Rodrigo, F. S., & Castro-D íez, Y. (2001). A study of NAO variability and its possible non-linear influences on European surface temperature. *Climate Dynamics*, 17(9), 701–705. <https://doi.org/10.1007/S003820000137/METRICS>
- Pramlall, S., Jackson, J. M., Konik, M., & Costa, M. (2023). Merged Multi-Sensor Ocean Colour Chlorophyll Product Evaluation for the British Columbia Coast. *Remote Sensing*, 15(3). <https://doi.org/10.3390/RS15030687>
- Raabe, T., & Wiltshire, K. H. (2009). Quality control and analyses of the long-term nutrient data from Helgoland Roads, North Sea. *Journal of Sea Research*, 61(1–2), 3–16. <https://doi.org/10.1016/J.SEARES.2008.07.004>
- Racault, M. F., Sathyendranath, S., & Platt, T. (2014). Impact of missing data on the estimation of ecological indicators from satellite ocean-colour time-series. *Remote Sensing of Environment*, 152, 15–28. <https://doi.org/10.1016/J.RSE.2014.05.016>
- Rayner, N. A., Parker, D. E., Horton, E. B., Folland, C. K., Alexander, L. V., Rowell, D. P., Kent, E. C., & Kaplan, A. (2003). Global analyses of sea surface temperature, sea ice, and night marine air temperature since the late nineteenth century. *Journal of Geophysical Research: Atmospheres*, 108(D14), 4407. <https://doi.org/10.1029/2002JD002670>

REFERENCES

- Reid, P. C., Edwards, M., Beaugrand, G., Skogen, M., & Stevens, D. (2003). Periodic changes in the zooplankton of the North Sea during the twentieth century linked to oceanic inflow. *Fisheries Oceanography*, 12(4–5), 260–269. <https://doi.org/10.1046/J.1365-2419.2003.00252.X>
- Reise, K., Buschbaum, C., Büttger, H., Rick, J., & Wegner, K. M. (2017). Invasion trajectory of Pacific oysters in the northern Wadden Sea. *Marine Biology*, 164(4), 1–14. <https://doi.org/10.1007/S00227-017-3104-2/FIGURES/6>
- Rezaie-Balf, M., Kisi, O., & Chua, L. H. C. (2019). Application of ensemble empirical mode decomposition based on machine learning methodologies in forecasting monthly pan evaporation. *Hydrology Research*, 50(2), 498–516. <https://doi.org/10.2166/NH.2018.050>
- Rick, J. J., Romanova, T., & Wiltshire, K. H. (2017). Hydrochemistry time series at List Reede, Sylt, Germany, in 2014. PANGAEA. <https://doi.org/10.1594/PANGAEA.873549>
- Rick, J. J., Romanova, T., & Wiltshire, K. H. (2020a). Hydrochemistry time series at List Reede, Sylt, Germany, in 2015 (Version 2). PANGAEA. <https://doi.org/10.1594/PANGAEA.918018>
- Rick, J. J., Romanova, T., & Wiltshire, K. H. (2020b). Hydrochemistry time series at List Reede, Sylt, Germany, in 2016 (Version 2). PANGAEA. <https://doi.org/10.1594/PANGAEA.918023>
- Rick, J. J., Romanova, T., & Wiltshire, K. H. (2020c). Hydrochemistry time series at List Reede, Sylt, Germany, in 2017. PANGAEA. <https://doi.org/10.1594/PANGAEA.918024>
- Rick, J. J., Romanova, T., & Wiltshire, K. H. (2020d). Hydrochemistry time series at List Reede, Sylt, Germany, in 2018. PANGAEA. <https://doi.org/10.1594/PANGAEA.918025>
- Rick, J. J., Romanova, T., & Wiltshire, K. H. (2020e). Hydrochemistry time series at List Reede, Sylt, Germany, in 2019. PANGAEA. <https://doi.org/10.1594/PANGAEA.918026>
- Rick, J. J., van Beusekom, J., Romanova, T., & Wiltshire, K. H. (2017). Long-term physical and hydrochemical measurements at Sylt Roads LTER (1973-2013), Wadden Sea, North Sea, links to data sets. PANGAEA. <https://doi.org/10.1594/PANGAEA.150032>
- Rieger, N., Corral, Á., Olmedo, E., & Turiel, A. (2021). Lagged Teleconnections of Climate Variables Identified via Complex Rotated Maximum Covariance Analysis. *Journal of Climate*, 34(24), 9861–9878. <https://doi.org/10.1175/JCLI-D-21-0244.1>

REFERENCES

- Righetti, D., Vogt, M., Gruber, N., Psomas, A., & Zimmermann, N. E. (2019). Global pattern of phytoplankton diversity driven by temperature and environmental variability. *Science Advances*, 5(5), 6253–6268. https://doi.org/10.1126/SCIADV.AAU6253/SUPPL_FILE/AAU6253_SM.PDF
- Robinson, C. T., & Minshall, G. W. (1986). Effects of Disturbance Frequency on Stream Benthic Community Structure in Relation to Canopy Cover and Season. *Journal of the North American Benthological Society*, 5(3), 237–248. <https://doi.org/10.2307/1467711>
- Rodwell, M. J., Rowell, D. P., & Folland, C. K. (1999). Oceanic forcing of the wintertime North Atlantic Oscillation and European climate. *Nature* 1999 398:6725, 398(6725), 320–323. <https://doi.org/10.1038/18648>
- Root, T. L., Price, J. T., Hall, K. R., Schneider, S. H., Rosenzweig, C., & Pounds, J. A. (2003). Fingerprints of global warming on wild animals and plants. *Nature* 2003 421:6918, 421(6918), 57–60. <https://doi.org/10.1038/nature01333>
- Rubinetti, S., Fofonova, V., Arnone, E., & Wiltshire, K. H. (2023). A Complete 60-Year Catalog of Wind Events in the German Bight (North Sea) Derived From ERA5 Reanalysis Data. *Earth and Space Science*, 10(10), e2023EA003020. <https://doi.org/10.1029/2023EA003020>
- Saberioon, M., Brom, J., Nedbal, V., Souček, P., & Císař, P. (2020). Chlorophyll-a and total suspended solids retrieval and mapping using Sentinel-2A and machine learning for inland waters. *Ecological Indicators*, 113, 106236. <https://doi.org/10.1016/J.ECOLIND.2020.106236>
- Sabine, C. L., Feely, R. A., Gruber, N., Key, R. M., Lee, K., Bullister, J. L., Wanninkhof, R., Wong, C. S., Wallace, D. W. R., Tilbrook, B., Millero, F. J., Peng, T. H., Kozyr, A., Ono, T., & Rios, A. F. (2004). The oceanic sink for anthropogenic CO₂. *Science*, 305(5682), 367–371. https://doi.org/10.1126/SCIENCE.1097403/SUPPL_FILE/SABINE.SOM.PDF
- Sarker, S., Lemke, P., & Wiltshire, K. H. (2018). Does ecosystem variability explain phytoplankton diversity? Solving an ecological puzzle with long-term data sets. *Journal of Sea Research*, 135, 11–17. <https://doi.org/10.1016/J.SEARES.2018.02.002>

REFERENCES

- Sarker, S., & Wiltshire, K. H. (2017). Phytoplankton carrying capacity: Is this a viable concept for coastal seas? *Ocean & Coastal Management*, 148, 1–8. <https://doi.org/10.1016/J.OCECOAMAN.2017.07.015>
- Sathyendranath, S., Brewin, R. J. W., Ciavatta, S., Jackson, T., Kulk, G., Jönsson, B., Vicente, V. M., & Platt, T. (2023). Ocean Biology Studied from Space. *Surveys in Geophysics*, 44(5), 1287–1308. <https://doi.org/10.1007/S10712-023-09805-9/FIGURES/7>
- Saulquin, B., Gohin, F., & Fanton d'Andon, O. (2019). Interpolated fields of satellite-derived multi-algorithm chlorophyll-a estimates at global and European scales in the frame of the European Copernicus-Marine Environment Monitoring Service. *Journal of Operational Oceanography*, 12(1), 47–57. <https://doi.org/10.1080/1755876X.2018.1552358>
- Scharfe, M., & Wiltshire, K. H. (2019). Modeling of intra-annual abundance distributions: Constancy and variation in the phenology of marine phytoplankton species over five decades at Helgoland Roads (North Sea). *Ecological Modelling*, 404, 46–60. <https://doi.org/10.1016/J.ECOLMODEL.2019.01.001>
- Schloen, J., Stanev, E. V., & Grashorn, S. (2017). Wave-current interactions in the southern North Sea: The impact on salinity. *Ocean Modelling*, 111, 19–37. <https://doi.org/10.1016/J.OCEMOD.2017.01.003>
- Schrum, C. (1997). Thermohaline stratification and instabilities at tidal mixing fronts: results of an eddy resolving model for the German Bight. *Continental Shelf Research*, 17(6), 689–716. [https://doi.org/10.1016/S0278-4343\(96\)00051-9](https://doi.org/10.1016/S0278-4343(96)00051-9)
- Schulzweida, U. (2022). CDO User Guide. Zenodo. <https://doi.org/10.5281/zenodo.7112925>
- Shama, L. N. S., Mark, F. C., Strobel, A., Lokmer, A., John, U., & Mathias Wegner, K. (2016). Transgenerational effects persist down the maternal line in marine sticklebacks: gene expression matches physiology in a warming ocean. *Evolutionary Applications*, 9(9), 1096–1111. <https://doi.org/10.1111/EVA.12370>
- Shamshirband, S., Jafari Nodoushan, E., Adolf, J. E., Abdul Manaf, A., Mosavi, A., & Chau, K. wing. (2019). Ensemble models with uncertainty analysis for multi-day ahead forecasting of chlorophyll a concentration in coastal waters. *Engineering Applications of Computational Fluid Mechanics*, 13(1), 91–101. <https://doi.org/10.1080/19942060.2018.1553742>

REFERENCES

- Shang, S., Wu, J., Huang, B., Lin, G., Lee, Z., Liu, J., & Shang, S. (2014). A new approach to discriminate dinoflagellate from diatom blooms from space in the East China Sea. *Journal of Geophysical Research: Oceans*, 119(7), 4653–4668. <https://doi.org/10.1002/2014JC009876>
- Sharples, J., Mayor, D. J., Poulton, A. J., Rees, A. P., & Robinson, C. (2019). Shelf Sea Biogeochemistry: Nutrient and carbon cycling in a temperate shelf sea water column. *Progress in Oceanography*, 177, 102182. <https://doi.org/10.1016/J.POCEAN.2019.102182>
- Shin, Y., Kim, T., Hong, S., Lee, S., Lee, E., Hong, S. W., Lee, C. S., Kim, T. Y., Park, M. S., Park, J., & Heo, T. Y. (2020). Prediction of Chlorophyll-a Concentrations in the Nakdong River Using Machine Learning Methods. *Water* 2020, Vol. 12, Page 1822, 12(6), 1822. <https://doi.org/10.3390/W12061822>
- Siegismund, F., & Schrum, C. (2001). Decadal changes in the wind forcing over the North Sea. *Climate Research*, 18(1/2), 39–45. <http://www.jstor.org/stable/24861556>
- Silva, E., Counillon, F., Brajard, J., Korosov, A., Pettersson, L. H., Samuelsen, A., & Keenlyside, N. (2021). Twenty-One Years of Phytoplankton Bloom Phenology in the Barents, Norwegian, and North Seas. *Frontiers in Marine Science*, 8, 746327. <https://doi.org/10.3389/FMARS.2021.746327/BIBTEX>
- Simpson, J. H., & Sharples, J. (2012). *Introduction to the physical and biological oceanography of shelf seas*. Cambridge University Press.
- Skov, H., & Prins, E. (2001). Impact of estuarine fronts on the dispersal of piscivorous birds in the German Bight. *Marine Ecology Progress Series*, 214, 279–287. <https://doi.org/10.3354/MEPS214279>
- Slatkin, M. (1974). Hedging one's evolutionary bets. *Nature* 1974 250:5469, 250(5469), 704–705. <https://doi.org/10.1038/250704b0>
- Solga, M. J., Harmon, J. P., & Ganguli, A. C. (2014). Timing is Everything: An Overview of Phenological Changes to Plants and Their Pollinators. *Natural Areas Journal*, 34(2), 227–234. <https://doi.org/10.3375/043.034.0213>
- Sommer, U., & Lengfellner, K. (2008). Climate change and the timing, magnitude, and composition of the phytoplankton spring bloom. *Global Change Biology*, 14(6), 1199–1208. <https://doi.org/10.1111/J.1365-2486.2008.01571.X>

REFERENCES

- Stanev, E. V., Al-Nadhairi, R., Staneva, J., Schulz-Stellenfleth, J., & Valle-Levinson, A. (2014). Tidal wave transformations in the German Bight. *Ocean Dynamics*, 64(7), 951–968. <https://doi.org/10.1007/S10236-014-0733-6/TABLES/5>
- Steele, J. H. (2004). Regime shifts in the ocean: reconciling observations and theory. *Progress in Oceanography*, 60(2–4), 135–141. <https://doi.org/10.1016/J.POCEAN.2004.02.004>
- Steele, J. H., & Baird, I. E. (1961). RELATIONS BETWEEN PRIMARY PRODUCTION, CHLOROPHYLL AND PARTICULATE CARBON. *Limnology and Oceanography*, 6(1), 68–78. <https://doi.org/10.4319/LO.1961.6.1.0068>
- Steinacher, M., Joos, F., Frölicher, T. L., Bopp, L., Cadule, P., Cocco, V., Doney, S. C., Gehlen, M., Lindsay, K., Moore, J. K., Schneider, B., & Segschneider, J. (2010). Projected 21st century decrease in marine productivity: A multi-model analysis. *Biogeosciences*, 7(3), 979–1005. <https://doi.org/10.5194/BG-7-979-2010>
- Stenseth, N. C., Ottersen, G., Hurrell, J. W., & Belgrano, A. (2005). Marine Ecosystems and Climate Variation: The North Atlantic: A Comparative Perspective. *Marine Ecosystems and Climate Variation: The North Atlantic A Comparative Perspective*, 1–266. <https://doi.org/10.1093/ACPROF:OSO/9780198507499.001.0001>
- Stock, C. A., Dunne, J. P., & John, J. G. (2014). Drivers of trophic amplification of ocean productivity trends in a changing climate. *Biogeosciences*, 11(24), 7125–7135. <https://doi.org/10.5194/BG-11-7125-2014>
- Storch, H. von, & Zwiers, F. W. (1999). *Statistical Analysis in Climate Research*. Cambridge University Press. <https://doi.org/DOI:10.1017/CBO9780511612336>
- Strasser, M., Reinwald, T., & Reise, K. (2001). Differential effects of the severe winter of 1995/96 on the intertidal bivalves *Mytilus edulis*, *Cerastoderma edule* and *Mya arenaria* in the Northern Wadden Sea. *Helgoland Marine Research*, 55(3), 190–197. <https://doi.org/10.1007/s101520100079>
- Su, J., Tian, T., Krasemann, H., Schartau, M., & Wirtz, K. (2015). Response patterns of phytoplankton growth to variations in resuspension in the German Bight revealed by daily MERIS data in 2003 and 2004. *Oceanologia*, 57(4), 328–341. <https://doi.org/10.1016/J.OCEANO.2015.06.001>

REFERENCES

- Sun, Y., Li, J., Liu, J., Chow, C., Sun, B., & Wang, R. (2015). Using causal discovery for feature selection in multivariate numerical time series. *Machine Learning*, 101(1–3), 377–395. <https://doi.org/10.1007/S10994-014-5460-1/TABLES/6>
- Sverdrup, H. U. (1953). On conditions for the vernal blooming of phytoplankton. *ICES Journal of Marine Science*, 18(3), 287–295. <https://doi.org/10.1093/ICESJMS/18.3.287>
- TAE, (2023): Classical Statistics vs Machine Learning. Retrieved 28 January 2024, from <https://www.tutorialandexample.com/classical-statistics-vs-machine-learning#>
- Tang, W., Li, Z., & Cassar, N. (2019). Machine Learning Estimates of Global Marine Nitrogen Fixation. *Journal of Geophysical Research: Biogeosciences*, 124(3), 717–730. <https://doi.org/10.1029/2018JG004828>
- Terauchi, G., Tsujimoto, R., Ishizaka, J., & Nakata, H. (2014). Preliminary assessment of eutrophication by remotely sensed chlorophyll-a in Toyama Bay, the Sea of Japan. *Journal of Oceanography*, 70(2), 175–184. <https://doi.org/10.1007/S10872-014-0222-Z/METRICS>
- Thomas, M. K., Kremer, C. T., Klausmeier, C. A., & Litchman, E. (2012). A global pattern of thermal adaptation in marine phytoplankton. *Science*, 338(6110), 1085–1088. https://doi.org/10.1126/SCIENCE.1224836/SUPPL_FILE/THOMAS.SM.TABLE.S6.CSV
- Thomas, R. W., & Dorey, S. W. (1967). PROTECTED OCEANOGRAPHIC REVERSING THERMOMETER COMPARISON STUDY1. *Limnology and Oceanography*, 12(2), 361–363. <https://doi.org/10.4319/LO.1967.12.2.0361>
- Thornton, D. C. O. (2012). Primary production in the ocean. *Advances in Photosynthesis–Fundamental Aspects*. Intech, Rijeca, Croatia, 563–588.
- Thresher, R. E., Koslow, J. A., Morison, A. K., & Smith, D. C. (2007). Depth-mediated reversal of the effects of climate change on long-term growth rates of exploited marine fish. *Proceedings of the National Academy of Sciences of the United States of America*, 104(18), 7461–7465. <https://doi.org/10.1073/PNAS.0610546104/ASSET/6C4E287D-FFF5-44CE-BEB3-5DFB4E2D5232/ASSETS/GRAPHIC/ZPQ0160760330003.JPEG>
- Tian, T., Su, J., Flöser, G., Wiltshire, K., & Wirtz, K. (2011). Factors controlling the onset of spring blooms in the German Bight 2002–2005: Light, wind and stratification. *Continental Shelf Research*, 31(10), 1140–1148. <https://doi.org/10.1016/J.CSR.2011.04.008>

REFERENCES

- Topcu, D., Behrendt, H., Brockmann, U., & Claussen, U. (2011). Natural background concentrations of nutrients in the German Bight area (North Sea). *Environmental Monitoring and Assessment*, 174(1–4), 361–388. <https://doi.org/10.1007/S10661-010-1463-Y/METRICS>
- Trenberth, K. E., & Shea, D. J. (2006). Atlantic hurricanes and natural variability in 2005. *Geophysical Research Letters*, 33(12), 12704. <https://doi.org/10.1029/2006GL026894>
- Trigo, R. M., Osborn, T. J., & Corte-Real, J. M. (2002). The North Atlantic Oscillation influence on Europe: climate impacts and associated physical mechanisms. *Climate Research*, 20(1), 9–17. <https://doi.org/10.3354/CR020009>
- Tsai, C. F., & Hsiao, Y. C. (2010). Combining multiple feature selection methods for stock prediction: Union, intersection, and multi-intersection approaches. *Decision Support Systems*, 50(1), 258–269. <https://doi.org/10.1016/J.DSS.2010.08.028>
- van Aken, H. M. (2008). Variability of the water temperature in the western Wadden Sea on tidal to centennial time scales. *Journal of Sea Research*, 60(4), 227–234. <https://doi.org/10.1016/J.SEARES.2008.09.001>
- van Beusekom, J. E. E., Brockmann, U. H., Hesse, K.-J., Hickel, W., Poremba, K., & Tillmann, U. (1999). The importance of sediments in the transformation and turnover of nutrients and organic matter in the Wadden Sea and German Bight. *Deutsche Hydrografische Zeitschrift* 1999 51:2, 51(2), 245–266. <https://doi.org/10.1007/BF02764176>
- van Beusekom, J. E. E., Carstensen, J., Dolch, T., Grage, A., Hofmeister, R., Lenhart, H., Kerimoglu, O., Kolbe, K., Pätsch, J., Rick, J., Rönn, L., & Ruiters, H. (2019). Wadden sea eutrophication: Long-term trends and regional differences. *Frontiers in Marine Science*, 6(JUL), 428870. <https://doi.org/10.3389/FMARS.2019.00370/BIBTEX>
- Van Leeuwen, S., Tett, P., Mills, D., & Van Der Molen, J. (2015). Stratified and nonstratified areas in the North Sea: Long-term variability and biological and policy implications. *Journal of Geophysical Research: Oceans*, 120(7), 4670–4686. <https://doi.org/10.1002/2014JC010485>
- Weijerman, M., Lindeboom, H., & Zuur, A. F. (2005). Regime shifts in marine ecosystems of the North Sea and Wadden Sea. *Marine Ecology Progress Series*, 298, 21–39. <https://doi.org/10.3354/MEPS298021>

REFERENCES

- Wiltshire, K. H. (2009). 10 Pigment Applications in Aquatic Systems. Practical Guidelines for the Analysis of Seawater, 191.
- Wiltshire, K. H., Boersma, M., Carstens, K., Kraberg, A. C., Peters, S., & Scharfe, M. (2015). Control of phytoplankton in a shelf sea: Determination of the main drivers based on the Helgoland Roads Time Series. *Journal of Sea Research*, 105, 42–52. <https://doi.org/10.1016/J.SEARES.2015.06.022>
- Wiltshire, K. H., & Dürselen, C. D. (2004). Revision and quality analyses of the Helgoland Reede long-term phytoplankton data archive. *Helgoland Marine Research*, 58(4), 252–268. <https://doi.org/10.1007/S10152-004-0192-4/TABLES/7>
- Wiltshire, K. H., Kraberg, A., Bartsch, I., Boersma, M., Franke, H. D., Freund, J., Gebühr, C., Gerds, G., Stockmann, K., & Wichels, A. (2010). Helgoland roads, North Sea: 45 years of change. *Estuaries and Coasts*, 33(2), 295–310. <https://doi.org/10.1007/S12237-009-9228-Y/METRICS>
- Wiltshire, K. H., & Manly, B. F. J. (2004). The warming trend at Helgoland Roads, North Sea: Phytoplankton response. *Helgoland Marine Research*, 58(4), 269–273. <https://doi.org/10.1007/S10152-004-0196-0/FIGURES/3>
- Xu, X., Lemmen, C., & Wirtz, K. W. (2020). Less Nutrients but More Phytoplankton: Long-Term Ecosystem Dynamics of the Southern North Sea. *Frontiers in Marine Science*, 7, 539528. <https://doi.org/10.3389/FMARS.2020.00662/BIBTEX>
- Xu, Y., Chant, R., Gong, D., Castelao, R., Glenn, S., & Schofield, O. (2011). Seasonal variability of chlorophyll a in the Mid-Atlantic Bight. *Continental Shelf Research*, 31(16), 1640–1650. <https://doi.org/10.1016/J.CSR.2011.05.019>
- Yang, J., Gong, P., Fu, R., Zhang, M., Chen, J., Liang, S., Xu, B., Shi, J., & Dickinson, R. (2013). The role of satellite remote sensing in climate change studies. *Nature Climate Change* 2013 3:10, 3(10), 875–883. <https://doi.org/10.1038/nclimate1908>
- Yang, J., Löder, M. G. J., Wiltshire, K. H., & Montagnes, D. J. S. (2021). Comparing the Trophic Impact of Microzooplankton during the Spring and Autumn Blooms in Temperate Waters. *Estuaries and Coasts*, 44(1), 189–198. <https://doi.org/10.1007/S12237-020-00775-4/METRICS>

REFERENCES

- Zhang, Z., Qiu, B., Klein, P., & Travis, S. (2019). The influence of geostrophic strain on oceanic ageostrophic motion and surface chlorophyll. *Nature Communications* 2019 10:1, 10(1), 1–11. <https://doi.org/10.1038/s41467-019-10883-w>
- Zhao, C., Maerz, J., Hofmeister, R., Röttgers, R., Wirtz, K., Riethmüller, R., & Schrum, C. (2019). Characterizing the vertical distribution of chlorophyll a in the German Bight. *Continental Shelf Research*, 175, 127–146. <https://doi.org/10.1016/J.CSR.2019.01.012>